



HAL
open science

Study on the origin of $1/f$ in bulk acoustic wave resonators

Santunu Ghosh

► **To cite this version:**

Santunu Ghosh. Study on the origin of $1/f$ in bulk acoustic wave resonators. Acoustics [physics.class-ph]. Université de Franche-Comté, 2014. English. NNT : 2014BESA2046 . tel-01126865

HAL Id: tel-01126865

<https://theses.hal.science/tel-01126865>

Submitted on 6 Mar 2015

HAL is a multi-disciplinary open access archive for the deposit and dissemination of scientific research documents, whether they are published or not. The documents may come from teaching and research institutions in France or abroad, or from public or private research centers.

L'archive ouverte pluridisciplinaire **HAL**, est destinée au dépôt et à la diffusion de documents scientifiques de niveau recherche, publiés ou non, émanant des établissements d'enseignement et de recherche français ou étrangers, des laboratoires publics ou privés.

SPIM

Thèse de Doctorat

UFC

école doctorale **sciences pour l'ingénieur et microtechniques**
UNIVERSITÉ DE FRANCHE-COMTÉ

Contribution à l'étude des origines du bruit en $1/f$ dans les résonateurs à onde acoustique de volume

Study on the origin of $1/f$ noise in bulk acoustic wave resonators

■ **SANTUNU GHOSH**

SPIM

Thèse de Doctorat

UFC

école doctorale **sciences pour l'ingénieur et microtechniques**
UNIVERSITÉ DE FRANCHE-COMTÉ

THÈSE

de l'Université de Franche-Comté

pour obtenir le grade de

DOCTEUR

Discipline : **Sciences pour l'Ingénieur**

Contribution à l'étude des origines du bruit en $1/f$ dans les résonateurs à onde acoustique de volume

Study on the origin of $1/f$ noise in bulk acoustic wave resonators
par

Santunu GHOSH

Institut FEMTO-ST

Soutenue le 17 octobre 2014 devant le jury composé de :

Rapporteurs :	L. BELLON	Chargé de Recherche, HDR, Labo. de Physique, ENS, Lyon
	O. LLOPIS	Directeur de Recherche CNRS, LAAS, Toulouse
Examineurs :	G. CIBIEL	Dr., Ingénieur CNES, Toulouse
	M. DEVEL	Professeur des Universités, FEMTO-ST, ENSMM, Besançon
	J. IMBAUD	Maître de Conférences, FEMTO-ST, ENSMM, Besançon
	F. STHAL	Professeur des Universités, FEMTO-ST, ENSMM, Besançon

During the journey of my 3 years PhD thesis research in an exciting and one of the most challenging topics in recent time, on the investigation of the origin of $1/f$ in BAW quartz crystal resonators, I have gained many things to learn and understand and predict. But at the edge of the journey of my PhD thesis I would like to mention a quote:

“Learn from yesterday, live for today, hope for tomorrow. The important thing is to not stop questioning.”

— Albert Einstein, Relativity: The Special and the General Theory

Acknowledgements:

I would like to say a special word of thanks to the members of the examination board:

Dr. Olivier LLOPIS, Directeur de Recherche in CNRS-LAAS, Toulouse, France, MOST group (Microondes et Opto-microondes pour Systèmes de Télécommunications) (Reviewer).

Dr. Ludovic Bellon, Chargé de Recherche CNRS, Habilitation à Diriger des Recherches, in the Laboratoire de Physique at ENS Lyon, France (Reviewer).

Dr. Gilles Cibiel, Centre National d'Etudes Spatiales, Microwave & Time Frequency Dept., Toulouse, France, (Examinator).

My PhD thesis not only represents a systematic research in physics and engineering but it also represents a wonderful working relationship and interactions with scientists, students, technician and professors with different academic and cultural background. During these three years, since October 1, 2011, I felt home at ENSMM (Ecole Nationale Supérieure de Mécaniques et des Microtechniques) and my experience in ENSMM is shortly amazing. This thesis is the result of many experiences I have encountered at FEMTO-ST Institute from lots of remarkable individuals whom I wish to acknowledge.

First and foremost I want to thank my PhD supervisor Prof. Fabrice Sthal. It has been an honor to be his PhD student to work at the Time and Frequency department in FEMTO-ST Institute. I appreciate all of his contributions of time, ideas, and funding to make my PhD experience. The joy and enthusiasm he has for his research was contagious and motivational for me, even during tough times in the PhD pursuit. He has always made himself available to clarify my doubts despite his busy schedules and I consider it as a great opportunity to do my doctoral program under his guidance and to learn from his research expertise. Thank you very much Fabrice for all of your help and support and I am grateful for the excellent example you have provided as a successful engineer and professor.

I want to thank my co-supervisor Prof. Michel Devel and Dr. Joel Imbaud and the collaborator Emeritus Prof. Roger Bourquin. Michel Devel is someone you will instantly like and never forget once you meet him. He's the one of the talented advisors and smartest people I know. I hope that I could be as lively, enthusiastic, and energetic as Michel and to someday be able to command an audience as well as he can. Michel has been supportive and has given me the freedom to pursue various projects without objection. He has also provided many insightful discussions about the research. I want to thank Dr. Joel Imbaud for his important contribution for the experiments in my thesis. My sincere thanks goes to Prof. Roger Bourquin for his scientific advice

and knowledge and many insightful discussions and theoretical and experimental contribution in my PhD thesis.

I am extremely grateful to P. H. Handel for his fundamental theory and for his valuable discussion and for sharing his ideas with us on $1/f$ noise for quartz crystal resonators. He is one of the most experienced and wisest researchers in the world in the domain of $1/f$ noise. I want to thank Dr. Ludovic Bellon for his presentation and important scientific discussion with us. I want to thank technician Cedric Vuillemin and Ahmed Bakir for their contribution to measure $1/f$ noise in my PhD thesis. I want to thank Philippe Abbe for helping me for the low temperature experiments. I want to thank the previous director of the time and Frequency Department Prof. Bernard Dulmet for allowing me as a PhD student and I also want to thank our recent director Dr. Vincent Giordano and the managing staff for providing the different facilities.

A special thanks to my parents Debesh Ghosh, Shamali Ghosh and my brother Suman Ghosh, my grandmother and my other relative Nishir Ghosh for their love and encouragement and their contribution cannot be expressed by words. I would also like to thank all of my friends who supported me in different aspects, and incited me to strive towards my goal, especially to Ashim Roy, Avik Ram Mondal, Sanando Bandopadhyay, Raj Narayan Dhara, Nandish Calchand. I want to thank my special friend Roselei Bilas for her valuable help in my difficult situation during these years. Thanks to all of you once again.

Table of contents:

Acknowledgements:.....	iii
Table of contents:.....	v
List of captions:.....	ix
List of tables:.....	xiii
Introduction:.....	1
Chapter 1: General Overview	3
1. Piezoelectricity.....	3
1.1. General constitutive equations of piezoelectricity.....	5
1.2. Voigt's notations.....	7
1.3. Simplifications for the trigonal crystallographic class	8
1.4. Electromechanical coupling factor	8
2. Crystal characteristics	9
2.1. Quartz crystal.....	9
2.2. Crystals Homeotypic to Quartz (LGS, LGT and GaPO ₄).....	20
2.3. Materials constants comparison.....	23
3. Crystal resonators and oscillators	26
3.1. Crystal resonators	26
3.2. Crystal Oscillators	31
3.3. Noise and stabilities in the time and frequency domains	33
4. Conclusions.....	36
5. References.....	37
Chapter 2: Bibliography of 1/f noise models	41
1. 1/f noise by summing Lorentzians	42
1.1. Schottky's theory and its derivatives.....	42
1.2. F.K Du Pré's theory.....	43
1.3. Dutta, Dimon and Horn's theory	44

1.4.	F. N. Hooge and P. A. Bobbert's theory.....	45
2.	$1/f$ noise from the fluctuations of time intervals between pulses.....	46
3.	$1/f$ noise and self-organized criticality.....	47
4.	$1/f$ noise in quartz crystal resonators by using statistical mechanics: Michel Planat's Model.....	48
5.	A possible explanation for the absence of observation of lower cut-off.....	50
6.	Other interesting models of $1/f$ noise.....	52
7.	Conclusions.....	52
8.	References.....	53
Chapter 3: Investigation of Quantum $1/f$ noise.....		55
1.	On some of Handel's theories concerning $1/f$ noise.....	55
1.1.	Handel's theory of quantum $1/f$ noise in electronic devices.....	55
1.2.	Criticisms of Handel's theory.....	60
1.3.	Handel's theory of quantum $1/f$ noise for piezoelectric quartz crystal resonators.....	62
2.	Calculation of β'	68
2.1.	Handel's evaluation of the order of magnitude of β'	68
2.2.	Points of concern in Handel's model as concerns the evaluation of β'	68
2.3.	Our calculation of β'	70
3.	Volume dependence in Handel's model of quartz crystal resonator noise.....	70
3.1.	Acoustic volume estimation.....	72
3.2.	Application of the models to experimental measurements.....	73
3.3.	Size dependence.....	76
4.	Attempts to compute the average circular frequency present in Handel's theory of quantum $1/f$ noise for BAW quartz resonators thanks to molecular dynamics.....	79
4.1.	Simulation details.....	79
4.2.	Estimation of the average angular frequency.....	82
5.	Conclusions.....	86
6.	References.....	88
APPENDIX A: example of LAMMPS input script.....		92

Chapter 4: Investigation of $1/f$ Noise With The help of Fluctuation-Dissipation Theorem	95
1. Fluctuation-Dissipation Theorem (FDT)	95
1.1. Callen-Welton form of the FDT	96
1.2. Callen-Greene form of the FDT	96
1.3. Kubo's form of the FDT	98
2. Investigation of $1/f$ Noise with the help of the FDT	100
2.1. Evaluation of the contribution of thickness fluctuations to frequency noise.....	100
2.2. Tentative physical explanation of the internal friction coefficient ϕ	104
3. Conclusions	108
4. References.....	109
Chapter 5: Experimental observations.....	111
1. Resonator Realization	111
1.1. Crystal block and blank cutting	111
1.2. Final 5 MHz SC-cut resonators	113
1.3. Resonator parameters.....	113
2. Resonator noise measurements	116
2.1. Measurement set-up.....	116
2.2. Noise results	120
3. Low temperature measurements	122
3.1. Cryogenic set-up.....	122
3.2. Measurement results	124
4. Exploration of $1/f$ noise origin using time measurements.....	127
4.1. Time measurement setup	127
4.2. Results	128
4.3. Mathematical treatments.....	130
5. Conclusions.....	132
6. References.....	134
Conclusion and perspectives:.....	137

Conclusion.....	137
Perspectives.....	139
References	141

List of captions:

<i>Fig.1.1: Schematic diagram of charge separation inside a piezoelectric crystal under the influence of external mechanical stress [2].....</i>	<i>3</i>
<i>Fig.1.2: Direct and converse piezoelectric effect [3].</i>	<i>4</i>
<i>Fig. 1.3: The forces on the faces of a cube located inside a stressed body [4].</i>	<i>5</i>
<i>Fig.1.4: Phase diagram of Silica (SiO₂) [2].</i>	<i>9</i>
<i>Fig.1.5: The quartz lattice (from http://volga.eng.yale.edu/sohrab/grouppage/pics/SiO2bulksupercell.jpg). Si atoms/ions are in red, Oxygen atoms/ions in blue, iono-covalent bounds in black.</i>	<i>10</i>
<i>Fig. 1.6: Left-Handed and Right-handed quartz [2].</i>	<i>12</i>
<i>Fig.1.7: Inclusion detection and seed localization with white light [10].</i>	<i>13</i>
<i>Fig.1.8: X-ray topography of Y-cut plates.</i>	<i>14</i>
<i>Fig.1.9: Value of the IR transmission versus wavelength expressed in cm⁻¹ (left) and α parameters (at 3410, 3500 and 3580 cm⁻¹) versus inverted wavelength of crystal bar (right) [10].</i>	<i>16</i>
<i>Fig.1.10: Description of the axis of quartz and X, Y, and Z rotational cuts [12].</i>	<i>16</i>
<i>Fig.1.11: Zero temperature-coefficient quartz cuts [2].</i>	<i>17</i>
<i>Fig. 1.12: Schematic representation of various cuts in the quartz crystal [12].</i>	<i>18</i>
<i>Fig.1.13: Schematic diagram of quartz AT cut [13].</i>	<i>18</i>
<i>Fig.1.14: Schematic diagram of quartz SC cut.</i>	<i>19</i>
<i>Fig.1.15: Temperature dependent resonant frequency of langasite, gallium phosphate and quartz BAW resonators [14].</i>	<i>20</i>
<i>Fig.1.16: Crystal structure of Langasite. (a) a1-a2 plane and (b) a1-c plane are viewed from [001] and [120], respectively. (c) four kinds of cation of cation polyhedra [15].</i>	<i>21</i>
<i>Fig.1.17: Gallium orthophosphate (GaPO₄) crystal.</i>	<i>23</i>
<i>Fig.1.18: Model of temperature-frequency curve of AT cut [27].</i>	<i>27</i>
<i>Fig.1.19: Frequency-Temperature characteristics of AT-cut for different values of θ. [2].</i>	<i>27</i>
<i>Fig.1.20: Typical frequency-temperature characteristics of SC-cut, third overtone, for different values of θ. $\Delta\theta$ varies from -1' to 8' from $\theta = 34^\circ$, [27].</i>	<i>28</i>
<i>Fig.1.21: Equivalent electrical circuit [27].</i>	<i>28</i>
<i>Fig.1.22: Resonance and phase curves [27].</i>	<i>30</i>
<i>Fig.1.23: Load capacitance in series[27].</i>	<i>31</i>
<i>Fig.1.24: Classical circuit of a crystal oscillator [2].</i>	<i>31</i>
<i>Fig.1.25: Time domain stability of the fractional frequency change (in ppm) over time (days), starting from a point of calibration. Zoom in the figure shows the short term time domain stability or the fractional frequency change over time (seconds) and its relationship to aging [12].</i>	<i>32</i>
<i>Fig.1.26: Exemple of short term time domain stability curve: RMS of averaged relative frequency fluctuations, for specific averaging times. [12].</i>	<i>33</i>
<i>Fig.1.27: Samples divided into time steps by an interval τ to get the average value of $y(t)$ [32].</i>	<i>34</i>
<i>Fig.2.1: Spectral density observed by J.B. Johnson(1925) [1]. The vertical scale represents the observed noise power density divided by the theoretical shot noise power density; the horizontal scale is the frequency in Hz.</i>	<i>41</i>
<i>Fig.2.2: Log power spectral density plot with respect to log frequency [4].</i>	<i>43</i>

Fig.3.1: Geometric definition of a plano-convex resonator.	72
Fig.3.2: $S_y(1 \text{ Hz})$ as a function of the volume between the electrodes of the resonator for experimental points from various authors.	76
Fig.3.3: $Q^4 \cdot S_y$ as a function of the volume between the electrodes of the resonator, experimental points from various authors + straight line for Handel's prediction with $\beta = 1 \text{ cm}^{-3}$	77
Fig.3.4: $Q^4 \cdot S_y$ as a function of the acoustic volume of the resonator (given by (3.55) for plano-convex resonators and (3.65) for plano-plano resonators), experimental points from various authors + straight line for Handel's prediction with $\beta = 1 \text{ cm}^{-3}$	77
Fig.3.5: Phonon dispersion curves for α -quartz, i.e. eigenfrequencies (in THz) as a function of one of the vibration wave vector reduced coordinate, following paths along several cristallographic directions, starting from the center of the Brillouin zone (Γ), going in the 1120 direction (ΓK), then in the 1210 direction (KM), or in the 0001 direction (ΓA) Left: Circles are experimental values and solid lines represent the results of our calculations for 6.5 million time steps in LAMMPS. Right: Circles are experimental values and solid lines represent the results of the quasi-harmonic calculations of Gonze et al. [50].....	83
Fig.3.6: α -quartz phonon density of states vs frequency (in THz), for 6.5M time steps in LAMMPS.	84
Fig.3.7: α -quartz phonon density of states vs frequency (in THz), as digitized from Fig. 1 of Ref. [38], which is recalled in the insert.	84
Fig.3.8: Experimental X-VDOS of α -quartz (room temperature) compared to the calculated X-VDOS (with the CASTEP code) and the true VDOS (as measured by neutron inelastic scattering). The areas underneath the curves are normalized to the same surface. (Fig. 1 from [51]).....	85
Fig.4.1: Resonator design.....	100
Fig.4.2: Variations of $S_y(\omega)$ in log-log scale.	102
Fig.4.3: Behavior of $S_y(\omega)$ for various values of φ for a thickness oscillation mode with $\omega r = c_{22}/\rho h^2 \approx 6 \cdot 10^6 \text{ rad/s}$. The transition frequency between the $1/\omega$ regime and the white noise regime is proportional to φ . At low frequencies $S_y(\omega)$ is also proportional to φ , whereas at resonance and above the influence of φ can be completely neglected with respect to the traditional $\eta_{22}\omega c_{22}$ viscoelastic damping term.	103
Fig.4.4: Motion of a pinned dislocation loop under the influence of externally applied stress (A. Granato and K. Lucke, "Theory of mechanical damping due to dislocations", J. Appl. Phys. Vol. 27, No-583, 1956. (page.584)).	105
Fig.4.5: The stress-amplitude dependence of the decrement (A. Granato and K. Lucke, "Theory of mechanical damping due to dislocations", J. Appl. Phys. Vol. 27, No-583, 1956. (page.584)).	106
Fig.5.1: Quartz C2 crystal block.	112
Fig.5.2: Quartz crystal bars and their positions in the crystal.....	112
Fig.5.3: SC-cut plates obtained in the quartz crystal bar.....	112
In bar 11 to 14, the position of all resonators is known along the bar. Resonators from bar 1 to 11 are not precisely localized along the bar.	112
Fig.5.4: Quartz resonator.....	113
Fig.5.5: X-ray topography of the resonator in its (300) vibration mode [5].	113
Fig.5.6: Motional resistances of measured resonators.....	114
Fig.5.7: Resonant frequency of the measured resonators.....	115
Fig.5.8: Turnover temperature of the measured resonators.....	115
Fig.5.9: Unloaded quality factor of the measured resonators.....	116

<i>Fig.5.10: Resonator noise measurement set-up</i>	117
<i>Fig.5.11: Typical phase noise measurement</i>	118
<i>Fig.5.12: Transfer function: a) amplitude b) phase</i>	119
<i>Fig.5.13: Noise measurements from resonator cut in bar 14 [2]</i>	120
<i>Fig.5.14: Noise measurements from resonators [8]</i>	121
<i>Fig.5.15: General construction of the cryogenic system [15]</i>	122
<i>Fig.5.16: Schematic diagram of the pulse tube cryocooler [16]</i>	123
<i>Fig.5.17: Resonator impedance measurements [15]</i>	124
<i>Fig.5.18: Resonator noise as a function of Q-factor of the resonators for different modes of vibration (Temperature 4K).</i>	125
<i>Fig.5.19: Resonator noise as a function of Q-factor of the resonators for anharmonic modes of C300 (Temperature 4K).</i>	126
<i>Fig.5.20: Resonator noise as a function of Q-factor of the resonators for overtone modes of C300</i>	127
<i>Fig.5.21: Time measurement setup [8]</i>	127
<i>Fig.5.22: a) Synchronization signal, b) Attenuation of resonator a, c) Zoom on a maximum value of resonator a</i>	129
<i>Fig.5.23: Attenuation signal of resonator h</i>	130
<i>Fig.5.24: Residuals of the fit (in mV) as a function of the number of the residual for resonator a (top left), b(top right), f (bottom left), g (bottom right). The upper (or lower) envelope could be described by piecewise linear functions giving some hint at solid friction, as discussed in the conclusions</i>	132
<i>Fig.5.25: Zoom of Fig.5.24. Zoom on the residuals of the fit as a function of the number of the residual used in the figure, for resonator f</i>	132

List of tables:

Table 1.1: Most important crystallographic forms in quartz.....	12
Table 1.2: Chemical impurities measured in the crystal block.....	15
Table 1.3: Material properties of α -Quartz, GaPO ₄ , LGS, LGT.....	24
Table 1.4: Values of the expansion coefficients of α -Quartz, GaPO ₄ , LGS, LGT (given at 25 °C).....	24
Table 1.5: Values of the piezoelectric and dielectric constants of α -Quartz, GaPO ₄ , LGS, LGT (given at 25 °C).....	25
Table 1.6: Values of the elastic constants of α -Quartz, GaPO ₄ , LGS, LGT (given at 25 °C).....	25
Table 1.7: Values of the temperature coefficient of elastic constants of α -Quartz, GaPO ₄ , LGS and LGT (given at 25 °C).	25
Table 1.8: Correspondence between noise types, power spectral densities and Allan variance (f_h is the high cut-off frequency) [31].	36
Table 3.1: Comparison of the short-term stability in terms of Allan standard deviation σ_{y_floor} of a SC-cut, 5 MHz and 3 rd OT resonator.	75
Table 3.2: Resonator parameters from [35] and [36] used to draw Fig.3.4. Q factor of resonators from [36] have been found more precisely in [37].	78
Table 3.3: Parameter set for quartz BKS potential.	81
Table 3.4: Average frequency for different time steps.	86
Table 5.1: Theoretical values of resonant frequencies of the designed resonator for A, B and C modes (overtones and anharmonic modes of C300 modes (Temperature = 4 K)).	124
Table 5.2: Q -factor at cryogenic temperature of selected resonators (a to l in Fig.5.14).....	125
Table 5.3: Resonators selected for time measurements.	128
Table 5.4: Loaded Q -factor measured from the logarithmic decrement of weakly damped oscillations, for several very good and not so good resonators.....	131

Introduction:

From last few decades, frequency control technology has been the heart of modern day electronics due to its huge area of applications in communication systems, computers, navigation systems or military defense. Frequency control devices provide high frequency stabilities and spectral purities in the short-term stability domain. However, improvement of the performance of these devices, in terms of frequency stability on the long term, remains a big challenge for researchers.

Frequency control systems are often made with ultra-stable oscillators (USO) using quartz crystals or atomic clocks in which quartz crystals provide the short term stability while the atomic part provides the accuracy. Hence, piezoelectric quartz crystals are the backbone of most of the frequency control systems due to some important features such as, availability of zero temperature coefficient cut, stress compensated cut, low loss, high Q , abundance in nature and low cost. Indeed, following John R. Vig, we may question “What would happen if all the quartz crystal stop vibrating?” [1], since then, the entire communication systems would be disabled, and all the computers would stop working... Furthermore, the number of users of such systems has been growing so rapidly that engineers keep trying to reduce the channel spacing in a given frequency band. Hence, the frequency tolerance of the communication systems should be tighter for both transmitters and receivers. Reducing noise in order to increase the short term stability and avoid unwanted switching between channels is thus very desirable. It is commonly admitted that the fundamental limitation to this short-term stability is due to flicker frequency noise in the quartz resonators. For more than fifty years many researchers have tried to find the physical origin of this inherent flicker noise, but till now there is no effective model to predict the origin and amplitude of flicker noise so that it is still an important fundamental problem for the current generation.

This work is directed to investigate the physical origin of quantum $1/f$ noise (or pink noise where the spectral density of frequency fluctuation is inversely proportional to the frequency). Numerous scientists have proposed models on the origin of $1/f$ noise for different types of physical systems. But in their model, effective means to improve the frequency stability of the quartz crystal resonators cannot be found (except maybe in some of P. H. Handel’s papers). Hence, providing a physical model of good but not perfect piezoelectric resonators in order to get better fabrication yields, better frequency stability and higher spectral purity for space application, navigation and military defense systems is the main objective of this PhD thesis.

Recently, several other piezoelectric materials than quartz have been considered for applications at high temperatures (several hundred °C). In most cases, researchers and engineers are trying to reduce the flicker noise of ultra-stable oscillators or MEMS made with these new synthetic materials arbitrarily by using electric or electronic circuits instead of trying to find the fundamental physical origin of the flicker noise applicable for the whole class of material. However, this kind of task has been a formidable challenge for more than fifty years, because one needs to deal with many different aspects of physics (classical, quantum, statistical, ...) and engineering. The goal of this PhD thesis was nonetheless to tackle this subject, with the help of a pluridisciplinary team of supervisors, in a pluridisciplinary institute of research. The progresses we have been able to do theoretically and experimentally are discussed in details in this document.

In this manuscript, the first chapter recalls the basic crystallography, quartz crystal cuts, impurities in quartz and definitions of time and frequency domain needed to explore ultra-stable resonators and oscillators. The second chapter is devoted to a summary of the different theories and models on flicker frequency noise based on the different physical and mathematical background. Then, the third chapter concerns our studies on Handel's quantum $1/f$ noise model, which although criticized by many, is still the only one that provides an estimation of the floor amplitude of $1/f$ noise that is not invalidated by experimental data. In the fourth chapter, another approach, based on the fluctuation-dissipation theorem, is used in order to put numerical constraints on a model of $1/f$ noise caused by an internal (or structural) dissipation proportional to the amplitude and not to the speed. The last chapter is devoted to experimental results. An ultra-stable resonator used during this study is described. Phase noise measurements on several batches of resonators are given. Measurements of resonator parameters have been done at low temperature in order to correlate them with noise results. Another approach with a procedure that use transient pseudo periodic oscillations and put to their limits the capacities of presently available digital oscilloscopes, is presented, in order to assess rapidly the quality of various resonators.

Chapter 1: General Overview

1. Piezoelectricity

Piezoelectricity is the consequence of the linear interaction between the mechanical deformation and the electrical polarization of matter. Piezo is derived from the Greek word piezin and means “to press”. Piezoelectricity in piezoelectric crystals is due to the fact that an external mechanical stress which deforms the crystal lattice causes a separation of the centers of gravity of the positive and negative charges. This charge separation then generates a net dipole in each primitive unit cell of the crystal (Fig.1.1). As a result a dielectric polarization appears which changes the macroscopic electric field in the material (Fig. 1.2, upper part). This is known as the direct piezoelectric effect. In direct piezoelectric effect, the change of electric polarization is proportional to the strain.

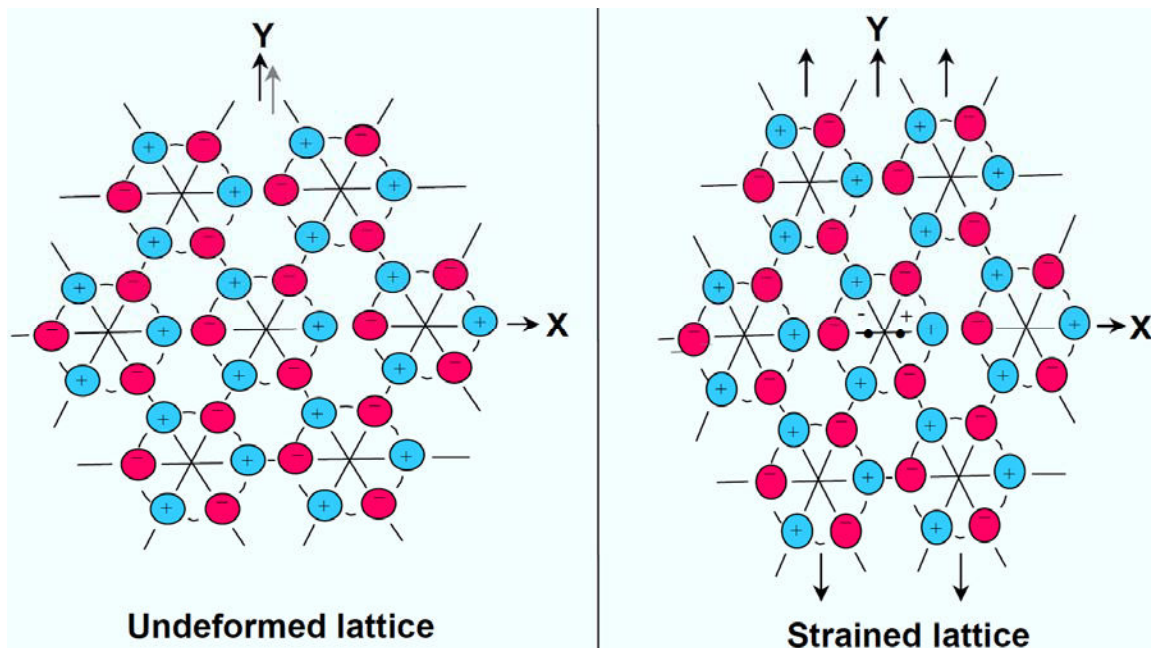


Fig.1.1: Schematic diagram of charge separation inside a piezoelectric crystal under the influence of external mechanical stress [2].

In converse piezoelectric effect, a piezoelectric crystal becomes strained under the influence of an external electric field (Fig.1.2, bottom part). Under a force F , a polarization P will appear inside the crystal. Thus displacements x will occur.

1.1. General constitutive equations of piezoelectricity

To understand the elastic constants and piezoelectric equations as described by L. E. Halliburton et al. (1985) [4], let us consider a cube with side length l inside the solid with the origin of orthogonal coordinate system located at the center of the volume element (Fig. 1.3).

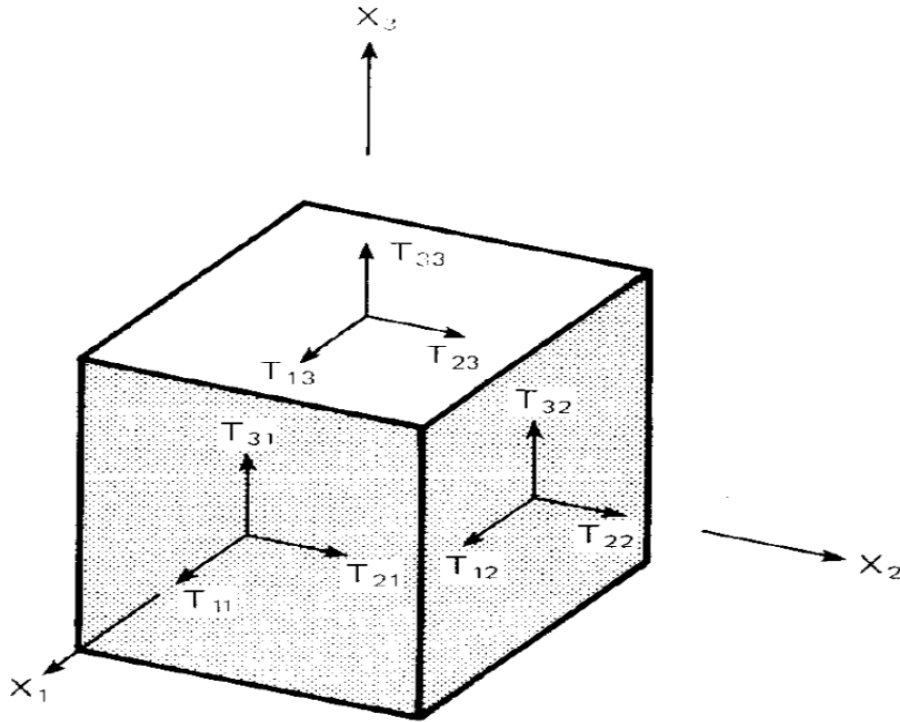


Fig. 1.3: The forces on the faces of a cube located inside a stressed body [4].

Here Cauchy's stress tensor¹ is represented by the symbol T and strain is represented by the symbol S . Under the application of a complex stress the point with initial coordinates x_1, x_2, x_3 is displaced to the position $x_1 + u_1, x_2 + u_2, x_3 + u_3$. The components of the strain tensor are given by:

$$S_{ij} = \frac{1}{2} \left(\frac{\partial u_i}{\partial x_j} + \frac{\partial u_j}{\partial x_i} \right) \quad (1.1)$$

Then Hooke's law is given by^{2 3}:

$$T_{ij} = c_{ijkl} S_{kl} \quad (1.2)$$

or

$$S_{ij} = s_{ijkl} T_{kl} \quad (1.3)$$

where c_{ijkl} is the elastic stiffness tensor and s_{ijkl} the elastic compliance tensor. Both of them are fourth rank tensors. Hooke's law is a linear approximation, valid for small strains (with respect to 1) and in the absence of any other multiphysics effect.

¹ The j^{th} component of the stress vector is given by $\Sigma_j = \sum_{i=1}^3 n_i T_{ij}$, with n_i the i^{th} component of the vector normal to the surface on which the stress acts.

² Here we adopt the usual convention that repeated indices are summed, e.g. $T_{ij} = \sum_{k=1}^3 \sum_{l=1}^3 c_{ijkl} S_{kl}$.

³ In reality, even in the elastic regime and in the absence of any electric or magnetic excitation, there can be nonlinear elastic terms or anelastic terms due to the fact that the response is not instantaneous.

Indeed, in direct piezoelectric effect, applied stress produces an additional electric polarization given by:

$$\Delta P_i = d_{ijk} T_{jk} \quad (1.4)$$

Since T and S are connected by Hooke's law, this can also be expressed as:

$$\Delta P_i = e_{ijk} S_{jk} \quad \text{with} \quad e_{ijk} = d_{imn} c_{mnjk}^E \quad (1.5)$$

The superscript E denotes whether the electric field has been held fixed during the measurement. Similarly, for the converse piezoelectric effect, crystal becomes (further) deformed under the application of an electric field:

$$\Delta S_{jk} = d_{ijk} E_i \quad (1.6)$$

or equivalently (in linear response theory):

$$\Delta T_{jk} = -e_{ijk} E_i \quad (1.7)$$

d_{ijk} and e_{ijk} represent the piezoelectric strain tensor and piezoelectric stress tensor respectively.

So the total (small) strain experienced by the crystal, in these conditions, is the sum of two contributions, one due to the applied stress and the other due to the applied field via piezoelectric effect:

$$S_{ij} = s_{ijkl}^E T_{kl} + d_{kij} E_k \quad (1.8)$$

Similarly the total polarization is given by:

$$P_i = d_{ikl} T_{kl} + \varepsilon_0 \chi_{ik}^T E_k \quad (1.9)$$

where χ_{ik}^T corresponds to the electric susceptibility, measured under constant stress T , of the material under consideration.

Then, the dielectric displacement is obtained by adding $\varepsilon_0 E_i$ to the left hand side of (1.9) and $\varepsilon_0 \delta_{ik} E_k$ to the right hand side of (1.9)⁴:

$$D_i = d_{ikl} T_{kl} + \varepsilon_{ik}^T E_k \quad (1.10)$$

Alternatively, one can choose strain and electric field as independent thermodynamic variables. The characteristic equations then become:

$$T_{ij} = c_{ijkl}^E S_{kl} - e_{kij} E_k \quad (1.11)$$

$$D_i = e_{ikl} S_{kl} + \varepsilon_{ik}^S E_k \quad (1.12)$$

where superscript S means that the strain has been held fixed during the measurement of the permittivity ε_{ik}^S .

Thanks to thermodynamic considerations (equality of second derivatives of the thermodynamic functions with respect to different thermodynamic variables whatever the order of

⁴ We recall that in SI units, the absolute electric permittivity is related to the susceptibility by $\varepsilon_{ik}^T = \varepsilon_0 (\delta_{ik} + \chi_{ik}^T)$.

derivation), it can be shown that stress and strain tensors are symmetric, so that $d_{ijk} = d_{ikj}$ and $e_{ijk} = e_{ikj}$, that c^E and s^E must also be symmetric with respect to the interchange of the first and second pair of indices, that ε^T and ε^S must be symmetric. Furthermore, it can be shown that⁵ $c_{ijmn}^E s_{mnpq}^E = \delta_{ip} \delta_{jq}$ and that⁶ $\varepsilon_{ik}^T - \varepsilon_{ik}^S = d_{imn} e_{kmn} = e_{imn} d_{kmn}$.

1.2. Voigt's notations

Due to all the symmetry relations, a lot of coefficients are equal, hence a more compact matrix notations is possible (Voigt's notations). Hence a pair of symmetric indices jk running from 1 to 3 is replaced by a single index α running from 1 to 6:

jk	11	22	33	23 or 32	13 or 31	12 or 21
α	1	2	3	4	5	6

Hence stress and strain tensors become 1×6 matrices, while piezoelectric tensors become 3×6 matrices, stiffness and compliance become 6×6 matrices and dielectric permittivity becomes a 3×3 matrix. However, due to the equivalence of indices 4, 5 and 6 to 2 different pairs of indices jk , one must be careful not losing factors of 2. It is therefore usually defined that:

$$\boxed{S_\alpha = 2^p S_{jk}, d_{i\alpha} = 2^p d_{ijk} \text{ and } s_{\alpha\beta}^E = 2^p s_{ijkl}^E} \quad (1.13)$$

with p the number of Greek indices equal to either 4, 5 or 6 or equivalently to the number of pair(s) of roman indices that are not equal⁷.

This means that:

$$\begin{aligned} T_1 &= T_{11}, T_2 = T_{22}, T_3 = T_{33}, T_4 = T_{23}, T_5 = T_{13}, T_6 = T_{12} \\ S_1 &= S_{11}, S_2 = S_{22}, S_3 = S_{33}, S_4 = 2S_{23}, S_5 = 2S_{13}, S_6 = 2S_{12} \\ s_{12}^E &= s_{1122}^E, s_{35}^E = 2s_{3331}^E, s_{45}^E = 4s_{2331}^E. \\ e_{122} &= e_{12}, e_{231} = e_{25}, d_{122} = d_{12}, 2d_{231} = d_{25} \end{aligned}$$

Using these notations, we have:

$$\begin{cases} T_\alpha = c_{\alpha\beta}^E S_\beta - e_{i\alpha} E_i \\ D_i = e_{i\beta} S_\beta + \varepsilon_{ij}^S E_j \end{cases} \text{ or } \begin{cases} S_\alpha = s_{\alpha\beta}^E T_\beta + d_{i\alpha} E_i \\ D_i = d_{i\beta} T_\beta + \varepsilon_{ij}^T E_j \end{cases} \quad (1.14)$$

In this linear approximation, the first set of constitutive relations in the above equations can thus be written, for any anisotropic material in any coordinate system, as:

⁵ E.g. by $T_{ij} = c_{ijmn}^E S_{mn} - e_{kij} E_k = c_{ijmn}^E (s_{mnpq}^E T_{pq} + d_{kmn} E_k) - e_{kij} E_k$

⁶ E.g. by $d_{ikl} T_{kl} + \varepsilon_{ik}^T E_k = d_{imn} (c_{mnpq}^E S_{pq} - e_{kmn} E_k) + \varepsilon_{ik}^T E_k = e_{ipq} S_{pq} + \varepsilon_{ik}^S E_k$

⁷ With this notation, we have $S_{jk} T_{kj} = S_\alpha T_\alpha$ (but not $S_{jk} S_{kj} = S_\alpha S_\alpha$ or $T_{jk} T_{kj} = T_\alpha T_\alpha$ as with Mandel's notation)

$$\begin{bmatrix} T_1 \\ T_2 \\ T_3 \\ T_4 \\ T_5 \\ T_6 \\ D_1 \\ D_2 \\ D_3 \end{bmatrix} = \begin{bmatrix} c_{11} & c_{12} & c_{13} & c_{14} & c_{15} & c_{16} & -e_{11} & -e_{21} & -e_{31} \\ c_{21} & c_{22} & c_{23} & c_{24} & c_{25} & c_{26} & -e_{12} & -e_{22} & -e_{32} \\ c_{31} & c_{32} & c_{33} & c_{34} & c_{35} & c_{36} & -e_{13} & -e_{23} & -e_{33} \\ c_{41} & c_{42} & c_{43} & c_{44} & c_{45} & c_{46} & -e_{14} & -e_{24} & -e_{34} \\ c_{51} & c_{52} & c_{53} & c_{54} & c_{55} & c_{56} & -e_{15} & -e_{25} & -e_{35} \\ c_{61} & c_{62} & c_{63} & c_{64} & c_{65} & c_{66} & -e_{16} & -e_{26} & -e_{36} \\ e_{11} & e_{12} & e_{13} & e_{14} & e_{15} & e_{16} & \varepsilon_{11} & \varepsilon_{12} & \varepsilon_{13} \\ e_{21} & e_{22} & e_{23} & e_{24} & e_{25} & e_{26} & \varepsilon_{21} & \varepsilon_{22} & \varepsilon_{23} \\ e_{31} & e_{32} & e_{33} & e_{34} & e_{35} & e_{36} & \varepsilon_{31} & \varepsilon_{32} & \varepsilon_{33} \end{bmatrix} \begin{bmatrix} S_1 \\ S_2 \\ S_3 \\ S_4 \\ S_5 \\ S_6 \\ E_1 \\ E_2 \\ E_3 \end{bmatrix} \quad (1.15)$$

1.3. Simplifications for the trigonal crystallographic class

In our case, we will be interested by materials in the 32 trigonal class. Taking into account this additional symmetries, the dielectric matrix is given by:

$$\begin{pmatrix} \varepsilon_{11} & 0 & 0 \\ 0 & \varepsilon_{11} & 0 \\ 0 & 0 & \varepsilon_{33} \end{pmatrix} \quad (1.16)$$

The piezoelectric stress matrix is given by:

$$\begin{pmatrix} e_{11} & -e_{11} & 0 & e_{14} & 0 & 0 \\ 0 & 0 & 0 & 0 & -e_{14} & -e_{11} \\ 0 & 0 & 0 & 0 & 0 & 0 \end{pmatrix} \quad (1.17)$$

and the elastic stiffness by (with $c_{66} = (c_{11} - c_{12})/2$):

$$\begin{pmatrix} c_{11} & c_{12} & c_{13} & c_{14} & 0 & 0 \\ c_{12} & c_{11} & c_{13} & -c_{14} & 0 & 0 \\ c_{13} & c_{13} & c_{33} & 0 & 0 & 0 \\ c_{14} & -c_{14} & 0 & c_{44} & 0 & 0 \\ 0 & 0 & 0 & 0 & c_{44} & c_{14} \\ 0 & 0 & 0 & 0 & c_{14} & c_{66} \end{pmatrix} \quad (1.18)$$

It can then be proved that the compliance matrix $\overline{s^E} = [\overline{c^E}]^{-1}$ is of the same form than the elastic stiffness matrix except that $s_{66} = 2(s_{11} - s_{12})$ and that piezoelectric strain matrix $\overline{d} = \overline{e} \cdot {}^t[\overline{s^E}]$ is of the same form than the piezoelectric stress matrix, except that $d_{26} = -2d_{11}$.

1.4. Electromechanical coupling factor

Electromechanical coupling factor (or coefficient), k , is a numerical measure of the conversion efficiency between electrical and acoustic energy in piezoelectric materials. It can be determined as the ratio between the mechanical energy provided to the material and its part converted in electrical energy, and this, in a case of given strain and given electric field:

$$k^2 = \frac{\text{obtained electrical energy}}{\text{mechanical energy provided}} = \frac{\text{obtained mechanical energy}}{\text{electrical energy provided}} \quad (1.19)$$

where the second equality comes from the equivalence between the direct and the converse piezoelectric effects.

k is generally expressed using piezoelectric coefficients [5]:

$$(k_{KL})^2 = \frac{[e_{Kj}l_j][l_i e_{iL}]}{(c_{KL}^E)(l_i \epsilon_{ij}^S l_j)} \quad (1.20)$$

with l_i the wave vector directions.

2. Crystal characteristics

2.1. Quartz crystal

The chemical formula of Silica (SiO_2) consists of two elements, oxygen and silicon. Silica crystallizes into a number of different structures among which quartz, tridymite and cristobalite are the most common whereas the crystalline polymorphs coesite, stishovite and keatite are rare [6] (Fig.1.4). Only one allotrope of silica, low quartz commonly known as alpha quartz, has application in frequency control systems. Alpha quartz is a member of the 32 point group that exists in two chiral varieties: left- handed alpha quartz ($P3_121$ space group) and right-handed quartz ($P3_221$ space group).

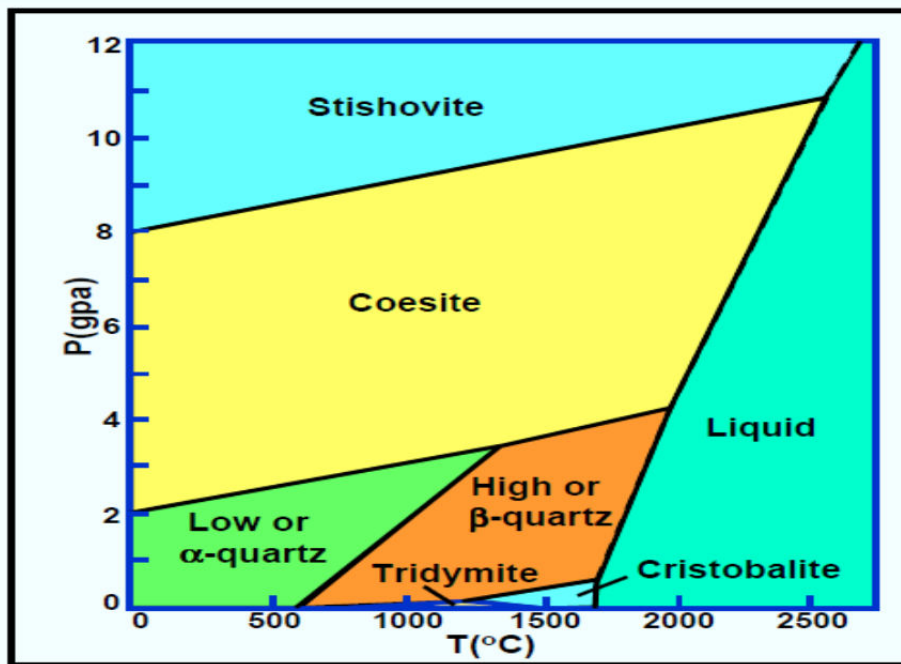


Fig.1.4: Phase diagram of Silica (SiO_2) [2].

2.1.1. Quartz Crystallography

2.1.1.1. DEFINITIONS OF THE CRYSTALLOGRAPHIC AND CARTESIANS AXES

Normally alpha quartz can be viewed as rigid SiO_4 tetrahedra connected at their corners by flexible Si-O-Si articulations [6]. The four oxygen atoms surround a silicon atom⁸ where the Si-O long bond distance is 1.612 Å and Si-O short bond is 1.606 Å. The angle O-Si-O is 109° , while the angle Si-O-Si is 144.2° (Fig.1.5) [7].

⁸ The chemical bonds between oxygen and silicon are partly (doubly) covalent, partly ionic, so that one can either use the words ions or atoms to designate the entities forming the crystal.

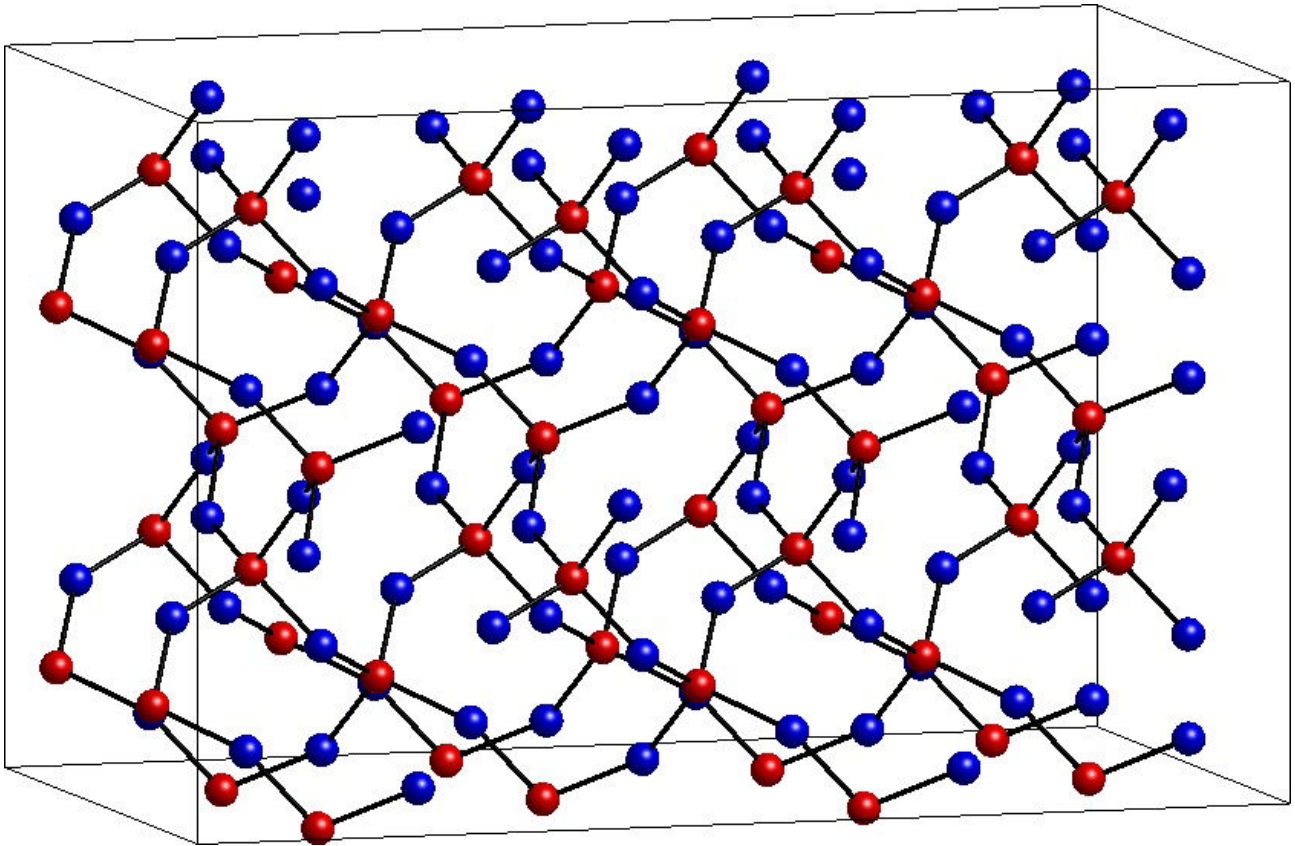


Fig.1.5: The quartz lattice (from <http://volga.eng.yale.edu/sohrab/grouppage/pics/SiO2bulksupercell.jpg>). Si atoms/ions are in red, Oxygen atoms/ions in blue, iono-covalent bounds in black.

In fact, due to the 32 symmetry class, the basic structural unit of quartz is a group of three connected SiO_4 tetrahedra. However, since oxygen atoms are shared among two silicon atoms and therefore each account for $\frac{1}{2}$, the crystallographic primitive unit cell chemical formula is Si_3O_6 . Hence, in crystallographic databases, one can find the coordinates of these 9 entities in a Cartesian frame that can however differ from a database to another⁹.

The coordination system of the alpha quartz can then be defined as a single axis of threefold symmetry known as trigonal axis c (or optical axis¹⁰) and the three axes of twofold symmetry (a_1 , a_2 , and a_3), known as diagonal axes (or electrical axes), perpendicular to the trigonal axis [8]. The major axis of quartz growth is c axis and it is taken parallel to Z axis (called optical axis) having positive arbitrary direction, in an orthogonal XYZ coordinate system. A quartz crystal having 6 sides has three separate possible X axes and three separate corresponding Y axes. The X axis (called electrical) conventionally adopted lies along one of the three equivalent a axes and is chosen so that the piezoelectric constant d_{11} is positive for right handed quartz (cf. IEEE Standard on

⁹ For our molecular dynamics simulations that will be described in a subsequent chapter, we used the free-access Mincryst database to get input coordinates (<http://database.iem.ac.ru/mincryst/index.php>).

¹⁰ It is called optical axis because quartz being trigonal, it is uniaxial. Hence, a light beam propagating in the direction of the optical axis is not split (ordinary index $n_o = \sqrt{\epsilon_{11}(\lambda)} = 1.54422$ for $\lambda \approx 590$ nm) while a beam propagating perpendicularly to this axis is split into two beams of complementary polarization, according to a birefringence $n_e - n_o = 0.00910$ ($n_e = \sqrt{\epsilon_{33}(\lambda)} = 1.55332$).

piezoelectricity ANSI/IEEE Std 176-1987, table 5). The Y axis (called mechanical axis¹¹) is chosen to form right handed coordinate system for both left and right-hand alpha quartz. The Y axes are perpendicular to the prism faces ($\{10\bar{1}0\}$ family of crystallographic planes) and X axes bisect the angles of the adjacent prisms (and would be perpendicular to the $\{2\bar{1}\bar{1}0\}$ family of crystallographic planes).¹²

2.1.1.2. LEFT AND RIGHT HANDED QUARTZ

When a linearly polarized light beam is transmitted along the optic axis then a rotation of the direction of polarization occurs and the amount of the rotation is in first approximation proportional to the path length in quartz¹³. The direction of rotation can be used to understand the difference between left and right-handed alpha quartz. For the dextrorotary alpha quartz, the rotation of the plane of polarization is clockwise if the rotation is observed towards the source of light and the rotation is anti-clockwise for the levorotary alpha quartz¹⁴. This comes from the fact that, in a quartz crystal, the Si and O ions can be viewed as forming parallel, corkscrew-like chains or helices.

In quartz crystal the orientation of the x and s faces¹⁵ with respect to the prism faces give a way of differentiation between left and right handed alpha quartz (Fig. 1.6). The different faces correspond to different crystal lattice planes. They can be related to different forms, and accordingly the whole crystal can be viewed as the intersection of these forms. Table 1.1 lists the most important crystallographic forms in quartz.

¹¹ If a mechanical stress is applied to opposite faces perpendicular to the mechanical axis, along that axis ($T_{22} = T_2 \neq 0$), equal and opposite net charges appear on opposite surfaces perpendicular to the electric axis ($P_1 \neq 0$), (direct piezoelectric effect). Conversely, if a time varying potential difference is applied to opposite faces perpendicular to the electric axes ($E_1 \neq 0$), then the crystal vibrates along the corresponding mechanical axis (inverse piezoelectric effect).

¹² Even with the directions of the axes fixed, the origin of the frame still remains to be fixed...

¹³ According to http://en.wikipedia.org/wiki/Optical_rotation, this effect was first observed in 1811 in quartz (!) by French physicist François Arago, whereas John Herschel realized in 1822 that 2 crystals images from one another through a mirror symmetry, would rotate the polarization by the same amount but in opposite directions.

¹⁴ A dextrorotary substance (crystal or solution) makes the polarization direction turn clockwise around the propagation direction as seen by an observer that receives light, while a levorotary substance makes it turn anticlockwise. This should normally not be mistaken with right or left handedness since these are normally two variants of a property of a non-linearly polarized propagating electromagnetic wave for which two conventions exist (e.g. clockwise rotation as seen from the source or from the detector). For a right-handed circularly polarized wave the polarization vector makes a complete turn clockwise after propagation on a distance equal to the wavelength, which is usually not the case for the propagation of a linearly polarized wave in a dextrorotary substance.

¹⁵ "The typical s-face is a rhomb, whereas an x-face is usually either a triangle or - when it is bordering an s-face - a trapezoid. (...) If an x- or s-face is present at the left side of an r-face, the quartz is called left-handed (or left quartz, for short). If an x- or s-face is present at the right side of an r-face, the quartz is called right-handed (or right quartz, for short)" (cf. http://www.quartzpage.de/crs_intro.html).

Table 1.1: Most important crystallographic forms in quartz.

Form	Symbol
Positive Rhombohedron	r
Negative Rhombohedron	z
Hexagonal Prism	m
Trigonal Bipyramid	s
Positive Trapezohedron	x

Right handed quartz is the usual characteristic of the synthetic quartz that can be found on the sale market.

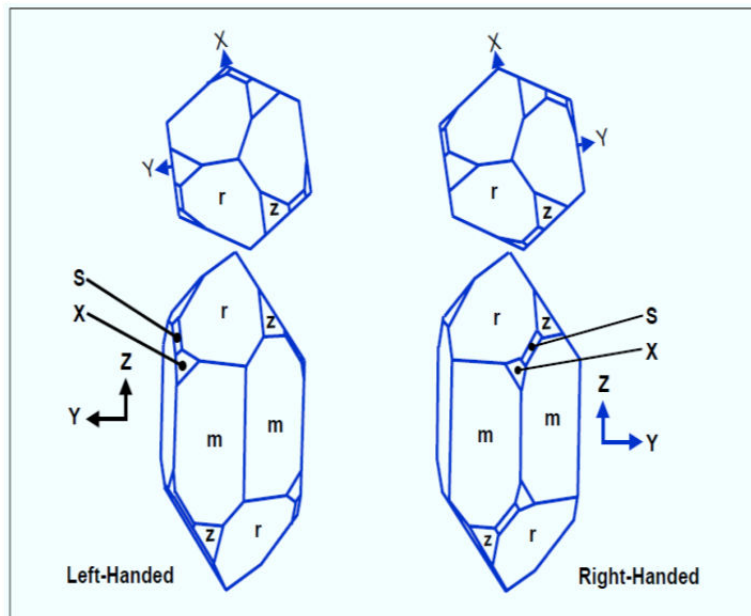


Fig. 1.6: Left-Handed and Right-handed quartz [2].

2.1.1.3. TWINNING AND PHASE TRANSITIONS

Both optical and electrical twins occur in alpha quartz. The orientation of left and right handed quartz crystal depends on the orientation of the seed crystal. The synthetic quartz produced is generally right-handed quartz, whereas in natural quartz both left and right handed properties are equally distributed. The material in which left and right-handed forms are mixed is known as optically twinned or Brazil twinned material and it can't be used to manufacture resonators. The electrically twinned or Dauphiné material is one in which the material has same handedness, but the material contains a region in which the orientation of electrical axis is reversed, as a result piezoelectric effect is reduced. In electrical twinning the breaking of Si-O bond is not needed, rather the slight displacements of Si-O bonds are required and these types of material are also not suitable for making good resonators. Polarized light and etching techniques can be used to identify the optical and electrical twinning.

When alpha quartz is heated above 573°C at 1 atmosphere pressure, then alpha quartz changes into the hexagonal beta quartz. If the material is cooled down below 573°C temperature then it will again be reverted into alpha quartz but the material will be electrically twinned. Similarly an application of large mechanical stress can induce twinning in the material. So, at the time of the processing of resonators it is necessary to avoid mechanical and thermal shocks on the material.

2.1.1.4. STRUCTURAL DEFECTS

Exhaustive lists of quartz defects can be found in the literature [7], [8]. In this paragraph, we just give the characteristics measured for the very high quality quartz crystal that was used to build the quartz resonators measured during this PHD thesis (see chapter 5). It is representative of the very high quality of the recent synthetic quartz crystals. Inclusions, dislocations and surface defects are the dominant structural defects in quartz crystals [7].

The IEC-758 standard defines the inclusion density by cm^3 [9]. This standard takes into account several sizes of inclusions. In the best grade (Ia), the number of inclusions must be equal or lower than 3, 2, 1 and 1, respectively in the 10-30 μm , 30-70 μm , 70-100 μm and above 100 μm size classes. Fig.1.7 shows the quartz crystal block illuminated with a white light beam. The big inclusions are clearly visible (single light spots). Most of them are located near the seed of the crystal block (horizontal white bar in the middle of the crystal). They are not taken into account because this part of the crystal is not used. Finally, the number of inclusions above 10 μm corresponds to the Grade Ia standard.

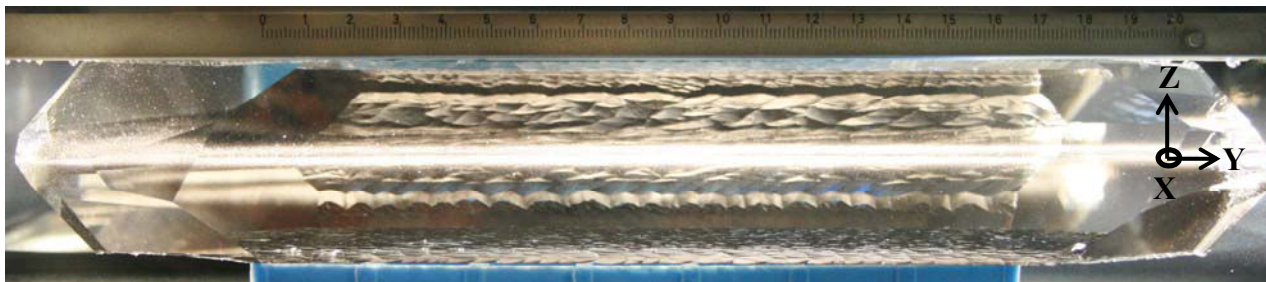


Fig.1.7: Inclusion detection and seed localization with white light [10].

Concerning dislocations, X-ray topography is usually used to observe the residual dislocations inside the crystal. This topography is done in thin plates (“blanks”) cut perpendicularly to the Y-axis (see § 2.1.2 in this chapter for the quartz cuts), which corresponds to the longest dimension of the crystal block (Fig.1.7). Fig.1.8 presents the results obtained in two such plates (the cutting of these plates is detailed in chapter 5). The length of exposure of the photos is about 5h30 with an X-ray vertical beam given by a generator of 45 kV with 25 mA.

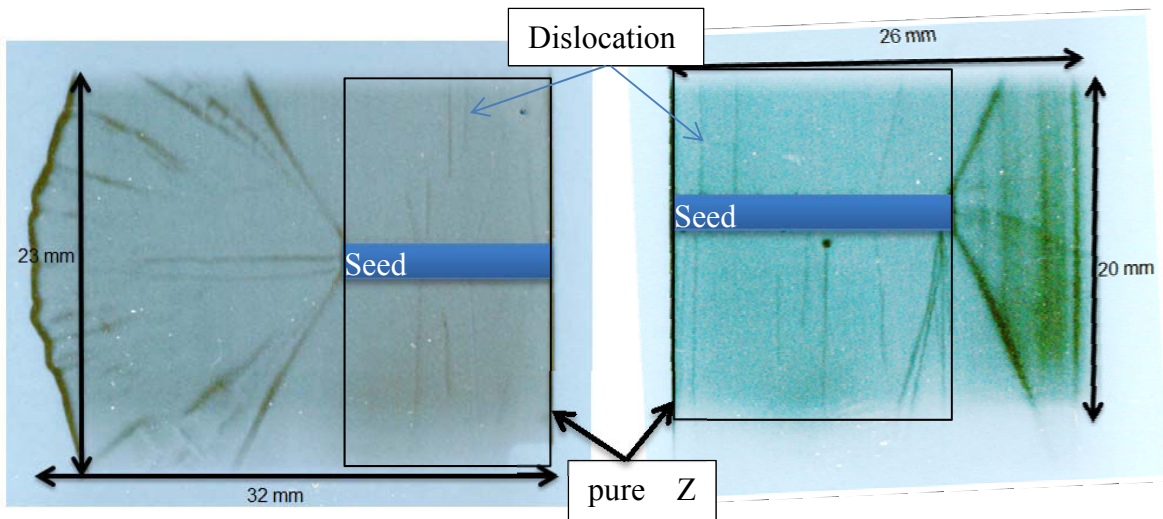


Fig.1.8: X-ray topography of Y-cut plates.

The number of dislocations, observed inside the black square zone with seed excluded, is visible. It is about 1 to 3 per cm^2 which corresponds to a very high quality quartz crystal.

Surface defects occur principally due to the polishing of the convex face of the resonator. This process step may be done differently by the manufacturers with which we have worked and is covered by confidentiality agreements. However, since we are concerned by noise in bulk acoustic wave oscillators, we will disregard surface defects in the following hence supposing that their effect is negligible compared to the effect of the bulk defects.

In quartz minerals, one can also find traces of other elements than Si and O, e.g. H, Li, Al, Na, Ti, Fe, ... [7]. These elements cause distortions in the quartz structure so that the optical properties can change and quartz which should normally be transparent to visible light, can get colored. Hence the distribution of some kinds of impurities can be detected with a good resolution by cathodoluminescence¹⁶.

Chemical impurities of our crystal block have been measured by an inductively coupled plasma mass spectrometry technique (ICP-MS method). This method is a type of mass spectrometry which is capable of detecting metals and several non-metals at concentrations as low as one part in 10^{12} (part per trillion). This is achieved by ionizing the sample with inductively coupled plasma and then using a mass spectrometer to separate and quantify those ions. These measurements have been done by colleagues from the LCABIE (LCABIE, IPREM, UMR CNRS 5254, Université de Pau et des Pays de l'Adour, Pau, France). Analyses were performed with an ICPMS 7500ce from Agilent technologies (Tokyo, Japan). A certified reference material, the NIST 612 (National Institute of Standards and Technology, USA), was chosen to validate optimized working conditions, due to its low concentrations in some analyzed elements. About 3 grams of quartz samples were used for

¹⁶ In cathodoluminescence, high-energy electron beams ("cathode rays") induce short-lived luminescence effects that can be captured on ordinary film

analysis. The preparation procedure was composed of three steps: cleaning, dissolution and analysis. Table 1.2 presents the results of two samples from the triangular crystal parts in the front and end of the block. The impurities rates are very low and seem homogeneous along the crystal block. The Li concentration is similar in both samples. The concentrations of Al, Na, Li and K, lower than 0.1 $\mu\text{g/g}$, correspond to a very high quality of the crystal even though the Ca concentration varies between 0.2 to 0.5 $\mu\text{g/g}$. The Fe concentration (lower than 1 $\mu\text{g/g}$) seems to be more important at the front of the block and requires more investigations to confirm this difference.

Table 1.2: Chemical impurities measured in the crystal block.

(in ppmw)	Front block	End block
Li	0.09 ± 0.03	0.1 ± 0.02
Na	< 0.07	< 0.05
Mg	< 0.0004	< 0.0003
Al	< 0.03	< 0.02
K	< 0.06	0.058 ± 0.001
Ca	0.22 ± 0.02	0.45 ± 0.03
Fe	0.98 ± 0.02	< 0.0001

Furthermore, fundamental resonant frequencies of vibration of quartz crystal are sensitive to infrared beam with low energy (typically between 10^{-21} and 10^{-19} Joules equivalent to 10 meV to 1 eV). This kind of measurements is used to define the intrinsic quality factor of the crystal [8]. The infrared measurements have been achieved with a Fourier transform infrared (FTIR) spectrometer (Nicolet Magna 750). With IR transmission measurements at room temperature, the absorption parameter α is defined according to the IEC758 standard [9], by reference with the transmission at 3800 cm^{-1} . The expression for α is given by the following equation, where d is the thickness of the sample (generally chosen perpendicular to the Y-axis) expressed in cm and T is the transmission in percent:

$$\alpha_n = \frac{1}{d} \ln \frac{T_{3800}}{T_n} \quad (1.21)$$

Measurement of the IR absorption rate along a quartz bar are usually performed to check the homogeneity of the areas Z along the Y axis of the bar by scanning the sample at a constant wavelength (3500 cm^{-1}) from the seed to outwards. It requires the polishing of the Z surfaces. In our experiment, the diameter of the IR beam is about 8 mm. Measurements are performed every 8 mm

along the 70 mm of the bar. The thickness of the bar is equal to 14 mm. The Z-faces of sample have been polished with 5 μm abrasive grains. As an example, Fig.1.9 presents the α parameter of one of the quartz bars.

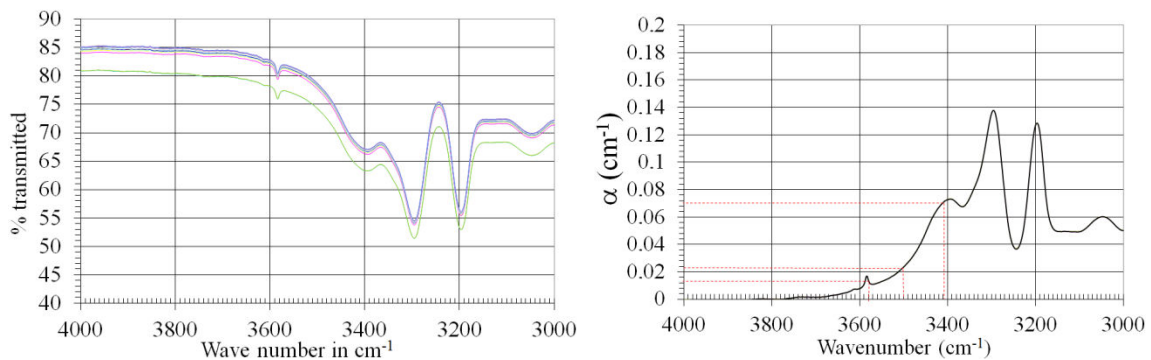


Fig.1.9: Value of the IR transmission versus wavelength expressed in cm^{-1} (left) and α parameters (at 3410, 3500 and 3580 cm^{-1}) versus inverted wavelength of crystal bar (right) [10].

The value of α_{3500} is close to 0.023. This value corresponds to a class which is the best one defined in IEC758 standard [9]. The expected quality factor computed from an empirical relationship [11] gives a Q-value of about $2.8 \cdot 10^6$ for a resonator working at 5 MHz. This value is in good agreement with those measured for the ultra-stable quartz resonators used in Chapter 5.

2.1.2. Quartz crystal cuts

A small piece of quartz material is obtained by cutting the crystal at specific angles to the various axes. In frequency control the different cuts are used to produce different kinds of performances according to the temperature sensibility (cf. §3.1.1), and different physical and electrical parameters of the resonators. Cuts are defined by the two rotation angles θ and ϕ around the X and Z crystallographic axis respectively. There are cuts along the crystallographic axis, such as X-cut and Y-cut crystal (Fig.1.10). In X-cut, the prism face should be normal to the X axis. The advantage of this cut is that it produces relatively large voltage under compression. However, there is a decrease in frequency when temperature increases. For the Y cut resonator, the prism face of the crystal should be normal to the Y axis and the advantage of this cut is that it exhibits positive temperature coefficient.

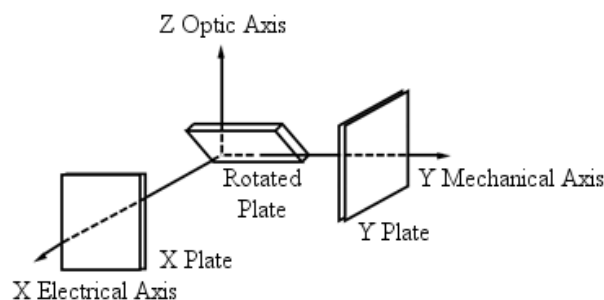


Fig.1.10: Description of the axis of quartz and X, Y, and Z rotational cuts [12].

Formerly, searchers and engineers were usually interested by zero temperature-coefficient cuts in which temperature coefficient lies along the locus of the zero temperature (Fig.1.11). In this figure, blue and dash lines represent cut angles where first order temperature coefficient of the frequency is equal to zero. This kind of cuts has usually two-letter names, where “T” in the name represents the temperature-coefficient cut. AT cut was the first temperature compensated cut discovered.

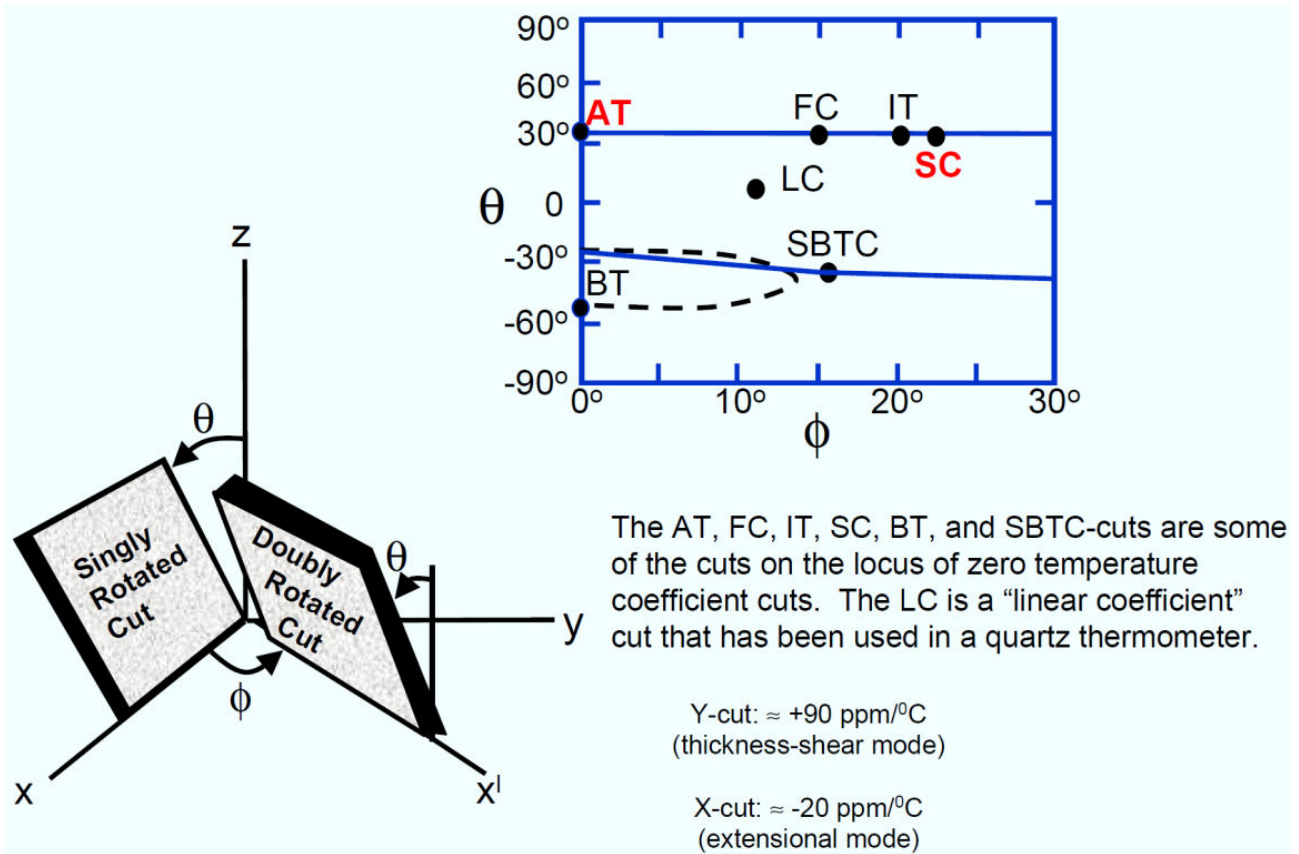


Fig.1.11: Zero temperature-coefficient quartz cuts [2].

The FT, BT and CT are other different zero temperature compensated cuts, used in past for some special properties before discovering SC cut (Fig. 1.12).

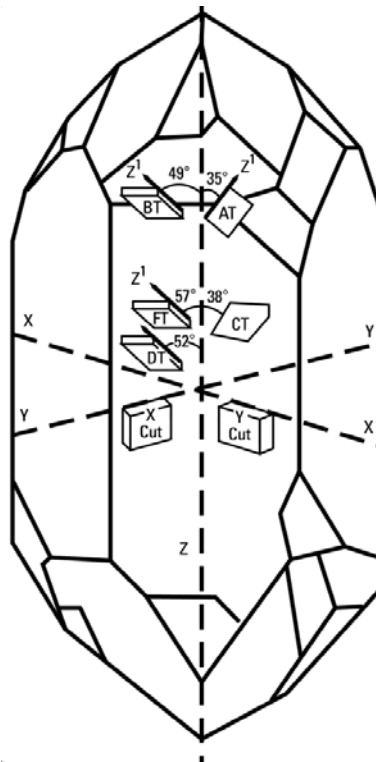


Fig. 1.12: Schematic representation of various cuts in the quartz crystal [12].

2.1.2.1. AT CUT:

AT cut is the most popular cut in industry because it has very good performance over a wide temperature range. For AT cut, the rotation θ of the Z-axis around the X axis is equal to $35^{\circ}15'$ and it is known as temperature compensated cut (Fig.1.13). AT cut is used for electronic instruments where oscillators are required to run in the range 500 kHz to 500 MHz. AT cut are used for TCXO (Temperature Compensated Crystal Oscillator). For AT cut necessary tolerance is $\pm 30''$. Inflection temperature of AT cut is 25°C .

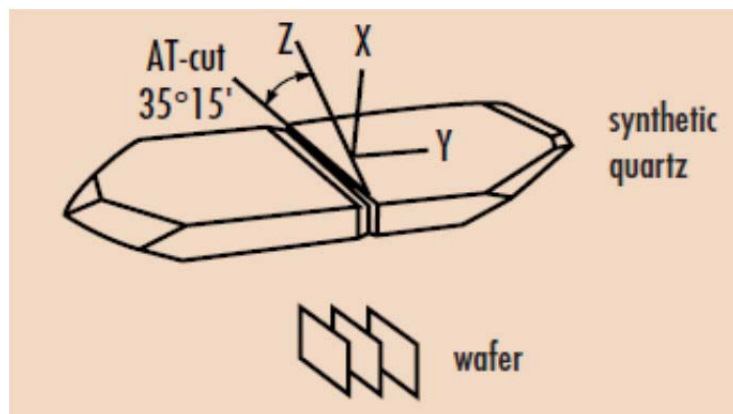


Fig.1.13: Schematic diagram of quartz AT cut [13].

2.1.2.2. SC CUT:

SC cut or stress compensated cut, was defined theoretically in 1976 by Earl Eer Nisse and confirmed through experiment by Jack Kusters, in 1977, in an attempt to find a thickness shear mode with low sensitivity to thermal and mechanical stress and better aging. This cut needs a

double rotation, with X-axis rotation φ is approximately 21.93° and Z-axis rotation θ is equal to 34.11° (Fig.1.14)¹⁷ with a tolerance of $\pm 10''$. The SC cut has 2 quasi-thickness shear modes, the C mode which has classic cubic thermal coefficient and the B mode which has a steep positive slope operating approximately +10% higher in frequency than the C mode. The SC cut oscillator has the capability to trap out the B mode if the operation of the C mode is only desired. SC cut resonators are generally operated within the frequency range 0.5 to 200 MHz.

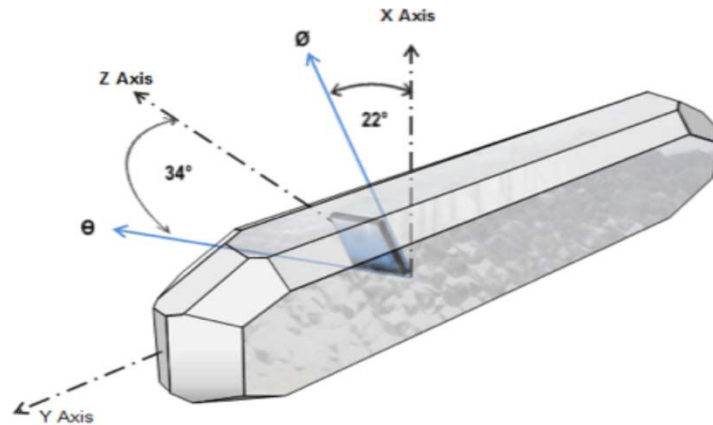


Fig.1.14: Schematic diagram of quartz SC cut.

SC cut oscillators are usually used for OCXO (Oven Controlled Crystal Oscillator) applications since it has a low temperature turn over point ($70\sim 85^\circ\text{C}$) which corresponds to a null slope of the frequency-temperature curve (see §3.1.1). The inflection temperature of SC cut is around 93°C .

The advantages of SC cut are:

- Thermal transient compensated allows faster warm up OCXO.
- Static and dynamic behaviors of frequency vs temperature allows higher stability OCXO and MCXO (Microcomputer-Compensated Crystal Oscillators).
- Lower motional capacitance (cf. § 3.1.2).
- Higher Q factor.
- Higher frequency times thickness constant¹⁸.
- Lower phase noise and better short term stability.
- Higher operating temperature.
- Lower acceleration sensitivity.
- Improved thermal stability.
- Improved thermal stress.

¹⁷ It means that the X axis rotates by an angle φ around the Z axis and that the Z axis rotate by an angle θ around the X axis

¹⁸ The resonant frequencies are generally found to be inversely proportional to thickness

But much higher cost due to the difficulty of the two cutting angles is the big disadvantage of SC-cut quartz.

2.2. Crystals Homeotypic to Quartz (LGS, LGT and GaPO₄)

During the last two decades, a new group of materials isomorphous with quartz has been developed and studied for high temperature piezoelectric crystal devices [14]. Traditional piezoelectric materials such as quartz are widely used for high precision frequency control systems and sensor based applications. However, at normal pressure and 573°C, the trigonal α -quartz will transform into hexagonal β -quartz, thus limiting the temperature at which quartz crystal devices can be used. Crystals homeotypic to quartz such as Langasite (LGS), Langanite (LGN), Langatate (LGT), Berlinite (AlPO₄), Gallium Orthophosphate (GaPO₄) are promising candidates for high temperature applications, since their phase transition temperature or melting point is far higher than 573°C (Fig.1.15). Furthermore, their piezoelectric and electromechanical coupling constants are higher than those of quartz, they also exhibit temperature compensated cuts for various modes of vibration and they have lower acoustic attenuations than quartz and higher quality factor for AT and SC-cut than quartz.

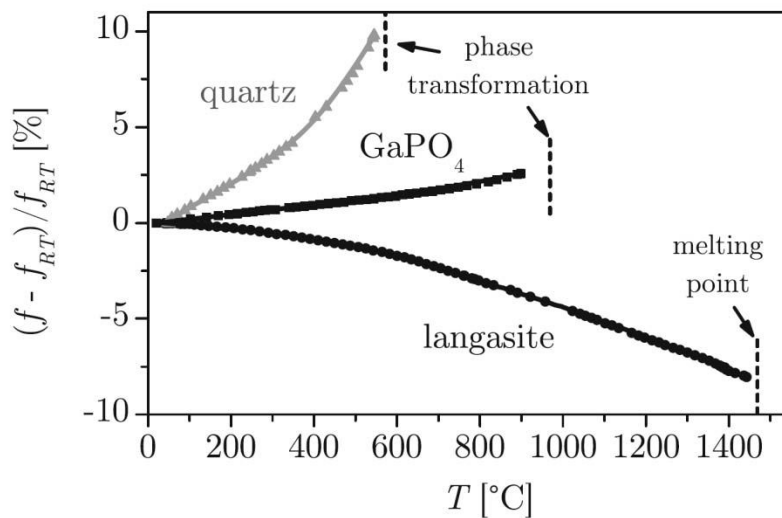


Fig.1.15: Temperature dependent resonant frequency of langasite, gallium phosphate and quartz BAW resonators [14].

2.2.1. Langasite (La₃Ga₅SiO₁₄)

The lanthanum gallium silicate was first developed in Russia from a joint research of the Moscow State University (MSU) and the Institute of Crystallography of the Russian Academy of Sciences. The Langasite family crystals have been developed for their possible applications as a bulk acoustic wave (BAW) and surface acoustic wave (SAW) devices with a high coupling and a better temperature-frequency behavior. For, the langasite family, crystal growth [15], [16], crystal structure [14], [15], [16], [17], [18], piezoelectricity [15], [17], [18], [19] structural perfections and acoustic properties [20], dielectric properties [19], [21], electrical properties [16], elastic properties

[19], magnetic properties [21] have been studied and compared with quartz. The interesting characteristic of langasite is its high temperature performance because it has no phase transition up to the melting point at 1475°C. Furthermore, the piezoelectric factor d_{11} of langasite is 2.7 times greater than that of quartz, so this allows to make piezo sensors with significantly higher sensitivity.

The langasite family crystal structure has the same trigonal symmetry than quartz with spacegroup P321 and is isostructural to $\text{CaGa}_2\text{Ge}_4\text{O}_{14}$ [22]. Langasite is a piezoelectric material according to its composition, that is, La, Ga and silicate minerals with structural group $\text{A}_3\text{BC}_3\text{D}_2\text{O}_{14}$, where A and B represents a decahedral site coordinated by eight oxygen ions, and an octahedral site coordinated by six oxygen ions, respectively; while C and D represent tetrahedral sites coordinated by four oxygen ions, with the size of D site being smaller than that of the C site. In case of Langasite, La^{3+} occupies the A sites, Ga^{3+} occupies sites B, C and half of the D sites and Si^{4+} occupies the half of the D sites as shown in Fig.1.16.

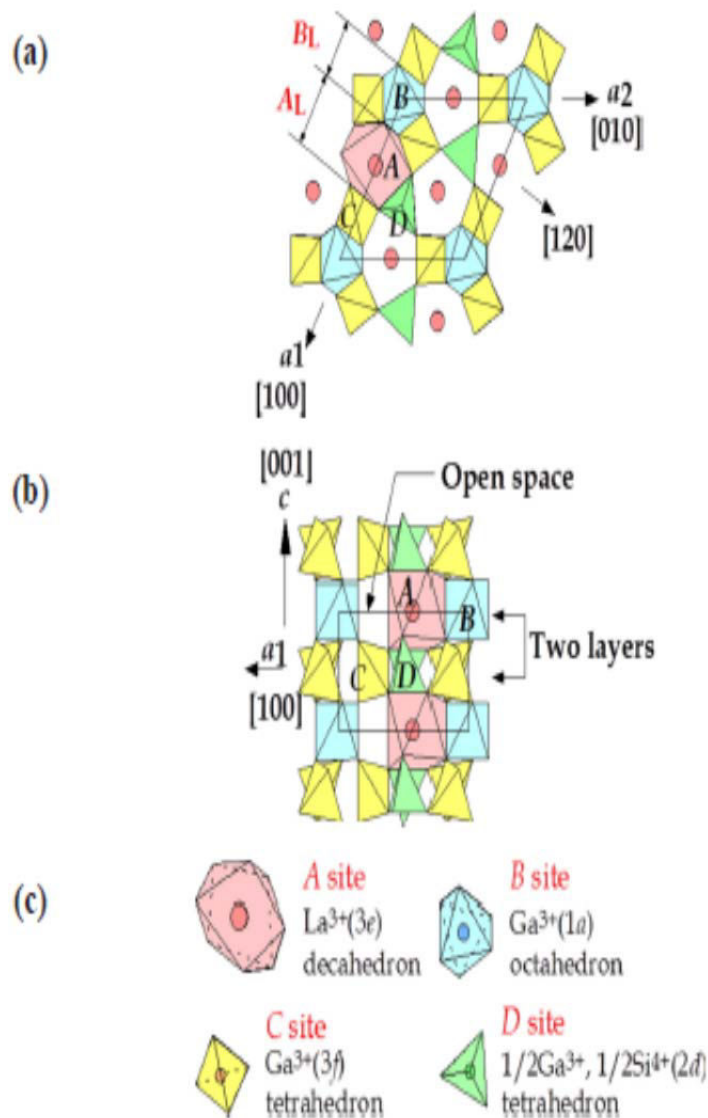


Fig.1.16: Crystal structure of Langasite. (a) a_1 - a_2 plane and (b) a_1 - c plane are viewed from $[001]$ and $[120]$, respectively. (c) four kinds of cation of cation polyhedra [15].

2.2.2. Langatate ($La_3Ga_{5.5}Ta_{0.5}O_{14}$)

Langatate (LGT) is another synthetic piezoelectric crystal homeotypic to quartz, with chemical composition $La_3Ga_{5.5}Ta_{0.5}O_{14}$. It has exciting properties, such as its higher piezoelectric coupling, structural stability up to 1400°C and presence of temperature compensated acoustic wave orientations, which have drawn the attention of sensor and frequency control communities as a possible alternative to quartz. The advantages of langatate are:

- 1) no Langatate phase transitions at normal pressure, up to the melting temperature 1450°C.
- 2) It has no pyroelectric effect.
- 3) Langatate has very small hysteresis loss.
- 4) High electromechanical coupling factor.
- 5) Steady-state value of piezoelectric constant d_{11} in a temperature range up to 600 °C (less than 5% change up to 450 °C).
- 6) High electrical resistivity.

Its piezoelectric properties [23], [24] dielectric and elastic properties [23], piezoelectric coupling factor [25] have been studied for high temperature applications in acoustic waves sensors or timing, and frequency control. Y cut oscillators are usually used for OCXO applications.

2.2.3. Gallium orthophosphate ($GaPO_4$)

Gallium Orthophosphate is a quartz homeotypic piezoelectric crystal with a high sensitivity and a thermal stability up to 970°C. The number of formula units per unit cell is 3, the same as in quartz, but due to the alternate sequence of *Ga* and *P* there is a doubling of the unit cell dimension in the c-direction, compared with quartz (Fig.1.17). The detailed crystal structure and temperature dependence of gallium orthophosphate was studied by H. Nakae et al. [26].

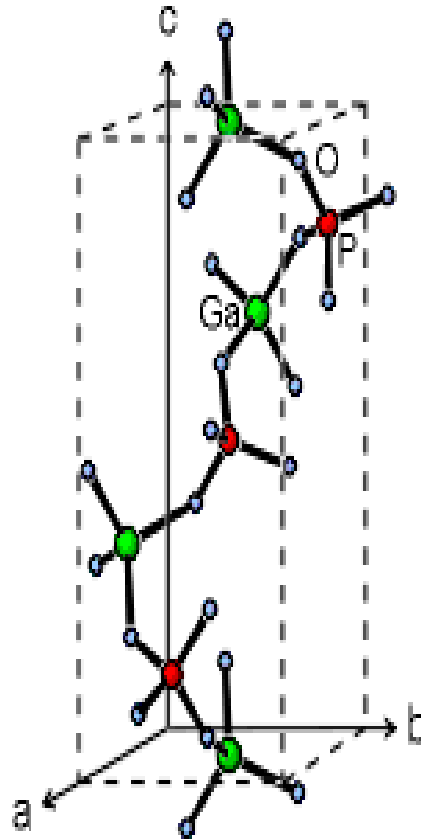


Fig.1.17: Gallium orthophosphate (GaPO_4) crystal.

There exist two enantiomorphous structures of GaPO_4 with the alpha-quartz space group $P3_121$ and $P3_221$, yielding the (structural) right-handed and left-handed varieties. The lattice parameters are $a = 4.901 \text{ \AA}$ and $c = 11.048 \text{ \AA}$ at room temperature. GaPO_4 is not ferroelectric so it has no Curie temperature and it does not show any pyroelectric effect. Gallium orthophosphate exhibits electromechanical coupling factors and longitudinal piezoelectric coefficients higher than those of quartz. GaPO_4 is usually used for direct piezoelectric applications (accelerometers, force sensors), bulk acoustic wave applications (VCXOs – voltage controlled crystal oscillators –, OCXOs, chemical sensors, biosensors), surface acoustic wave applications (wireless identification system, remote control sensors). Y-16° cut oscillators are usually used in OCXO applications.

2.3. Materials constants comparison

A comparison of the material properties of alpha quartz, LGT, LGS and GAPO_4 (LGT and LGS main properties from AXTAL, www.AXTAL.com, and GaPO_4 properties from www.piezocryst.com) are given in the following tables.

Table 1.3 to Table 1.7 respectively present the general properties, the expansion coefficients, the piezoelectric and dielectric constants, the elastic moduli and the temperature coefficient of those elastic moduli for α -Quartz, GaPO_4 , LGS and LGT.

Table 1.3: Material properties of α -Quartz, GaPO₄, LGS, LGT.

Material	SiO ₂	GaPO ₄	La ₃ Ga ₅ SiO ₁₄	La ₃ Ga _{5,5} Ta _{0,5} O ₁₄
Crystal space group	32	32	32	32
Melting point (°C)	1650	1670	1470	1510
Curie temperature (°C)	573 $\alpha \rightarrow \beta$	933 $\alpha \rightarrow \beta_{cristo}$	No phase transition	No phase transition
Lattice parameter (Å)	a = b = 4.913 c = 5.406	a = b = 4.901 c = 11.048	a = b = 8.1685 c = 5.0920	a = b = 8.2470 c = 5.1303
Density (kg/m ³)	2648.6	3570	5742.4	6126
Moh's Hardness	7.0	5.5	6.5	6.4
Electromechanical coupling factor % X-cut vibrating according Y axis	10.9	14.5	16.6	16.7

Table 1.4: Values of the expansion coefficients of α -Quartz, GaPO₄, LGS, LGT (given at 25 °C).

Material	SiO ₂	GaPO ₄	La ₃ Ga ₅ SiO ₁₄	La ₃ Ga _{5,5} Ta _{0,5} O ₁₄
$\alpha_{11}^{(1)}$ (10 ⁻⁶ K ⁻¹)	13.71	12.78	5.68	6.17
$\alpha_{33}^{(1)}$ (10 ⁻⁶ K ⁻¹)	7.48	3.69	4.08	3.93
$\alpha_{11}^{(2)}$ (10 ⁻⁹ K ⁻²)	6.5	10.6	5.43	4.77
$\alpha_{33}^{(2)}$ (10 ⁻⁹ K ⁻²)	2.9	5	5.43	4.01
$\alpha_{11}^{(3)}$ (10 ⁻¹² K ⁻³)	-1.9	-16.1	-	-
$\alpha_{33}^{(3)}$ (10 ⁻¹² K ⁻³)	-1.5	-5.4	-	-

Table 1.5: Values of the piezoelectric and dielectric constants of α -Quartz, GaPO₄, LGS, LGT (given at 25 °C).

Material	SiO ₂	GaPO ₄	La ₃ Ga ₅ SiO ₁₄	La ₃ Ga _{5.5} Ta _{0.5} O ₁₄
d_{11} (10 ⁻¹² C/N)	2.31	4.5	-6.36	-6.54
d_{14} (10 ⁻¹² C/N)	-0.726	1.9	5.85	5.30
e_{11} (Cm ⁻²)	0.171	0.209	-0.456	-0.456
e_{14} (Cm ⁻²)	0.0406	0.107	0.150	0.094
$\varepsilon_{11}^T/\varepsilon_0$	4.428	6.1	18.99	19
$\varepsilon_{33}^T/\varepsilon_0$	4.634	6.6	50.44	78.95

Table 1.6: Values of the elastic constants of α -Quartz, GaPO₄, LGS, LGT (given at 25°C).

Material	SiO ₂	GaPO ₄	La ₃ Ga ₅ SiO ₁₄	La ₃ Ga _{5.5} Ta _{0.5} O ₁₄
C_{11}^E (10 ¹⁰ Nm ⁻²)	8.674	6.658	18.873	18.852
C_{12}^E (10 ¹⁰ Nm ⁻²)	0.699	2.181	10.459	10.788
C_{13}^E (10 ¹⁰ Nm ⁻²)	1.191	2.487	9.624	10.336
C_{14}^E (10 ¹⁰ Nm ⁻²)	1.791	0.391	1.414	1.351
C_{33}^E (10 ¹⁰ Nm ⁻²)	10.72	10.213	26.151	26.18
C_{44}^E (10 ¹⁰ Nm ⁻²)	5.794	3.766	5.39	5.11
C_{66}^E (10 ¹⁰ Nm ⁻²)	3.99	2.238	4.207	4.032

Table 1.7: Values of the temperature coefficient of elastic constants of α -Quartz, GaPO₄, LGS and LGT (given at 25 °C).

Material	SiO ₂	GaPO ₄	La ₃ Ga ₅ SiO ₁₄	La ₃ Ga _{5.5} Ta _{0.5} O ₁₄
$T^{(1)}C_{11}^E$ (10 ⁻⁶ K ⁻¹)	-48.5	-44.1	-54.6	78.3
$T^{(1)}C_{12}^E$ (10 ⁻⁶ K ⁻¹)	-3000	-226.7	-104.6	165.5
$T^{(1)}C_{13}^E$ (10 ⁻⁶ K ⁻¹)	-550	-57.6	-73.1	-111.4
$T^{(1)}C_{14}^E$ (10 ⁻⁶ K ⁻¹)	101	507.2	-351	-359.6
$T^{(1)}C_{33}^E$ (10 ⁻⁶ K ⁻¹)	-160	-127.5	-101.3	-102.2
$T^{(1)}C_{44}^E$ (10 ⁻⁶ K ⁻¹)	-177	-0.4	-66.1	21.6

$T^{(1)}C_{66}^E (10^{-6} K^{-1})$	178	44.9	7.51	-43.6
$T^{(2)}C_{11}^E (10^{-9} K^{-2})$	-107	-28.5	-72.3	-273.6
$T^{(2)}C_{12}^E (10^{-9} K^{-2})$	-3050	-70.8	-25.2	313.9
$T^{(2)}C_{13}^E (10^{-9} K^{-2})$	-1150	41.3	-64.9	-557.7
$T^{(2)}C_{14}^E (10^{-9} K^{-2})$	-48	280.6	212	1604.8
$T^{(2)}C_{33}^E (10^{-9} K^{-2})$	-275	-18.3	-63.2	-107.7
$T^{(2)}C_{44}^E (10^{-9} K^{-2})$	-216	-43.8	-74.2	-11.98
$T^{(2)}C_{66}^E (10^{-9} K^{-2})$	118	-7.9	-131	-901.4
$T^{(3)}C_{11}^E (10^{-12} K^{-3})$	-70	-59.4	-	-
$T^{(3)}C_{12}^E (10^{-12} K^{-3})$	-1260	-205.7	-	-
$T^{(3)}C_{13}^E (10^{-12} K^{-3})$	-750	-109.9	-	-
$T^{(3)}C_{14}^E (10^{-12} K^{-3})$	-590	-99.9	-	-
$T^{(3)}C_{33}^E (10^{-12} K^{-3})$	-250	-134.8	-	-
$T^{(3)}C_{44}^E (10^{-12} K^{-3})$	-216	-37.1	-	-
$T^{(3)}C_{66}^E (10^{-12} K^{-3})$	21	11.9	-	-

3. Crystal resonators and oscillators

3.1. Crystal resonators

A resonator is a device which produces electromagnetic or mechanical oscillations at resonant frequency by using the property of piezoelectricity. A crystal resonator can have many modes of vibration. Generally, only one of these modes is important for a particular application in communication systems. Resonators are usually used to generate the waveform with a specific frequency or as a selector to select a specific frequency from many other frequencies.

3.1.1. Frequency temperature characteristics of a quartz resonator

The temperature characteristics of AT and SC cut are represented by 3rd order polynomials. The amount of frequency variation due to the crystal temperature coefficients depends on the crystal cut. The relative change in frequency is described by:

$$\frac{\Delta f}{f} = A_i \Delta T + C_i \Delta T^3 \quad (1.22)$$

with $\Delta T = T - T_i$, where T_i is the inflection temperature.

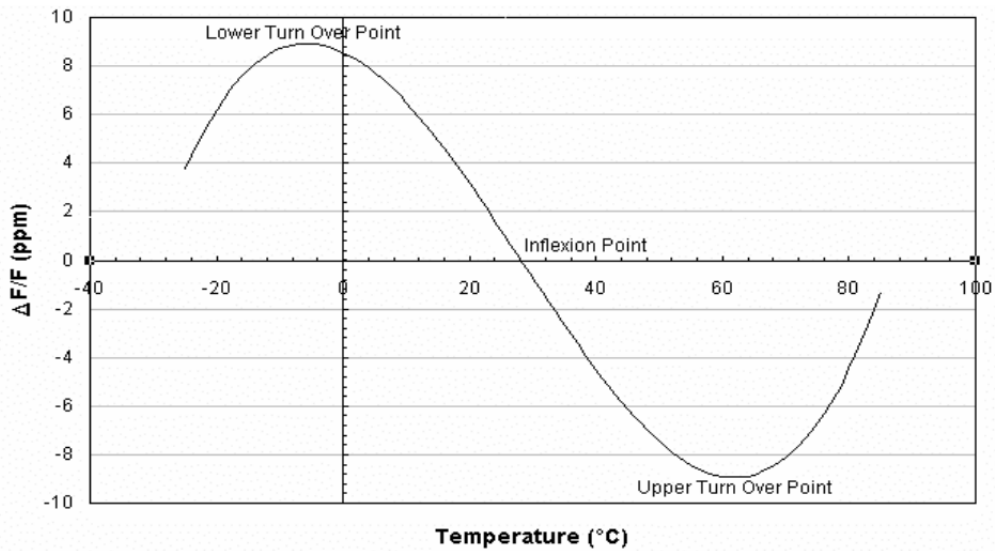


Fig.1.18: Model of temperature-frequency curve of AT cut [27].

In the equation (1.22), T_i varies between +25°C and +35°C for AT cut crystal and from +85°C to +95°C for SC cut, depending on the dimensions of the crystal. The frequency-temperature characteristics is primarily dependent on the cut angle, because in equation (1.22), the quantity A_i changes with θ , while C_i is almost constant.

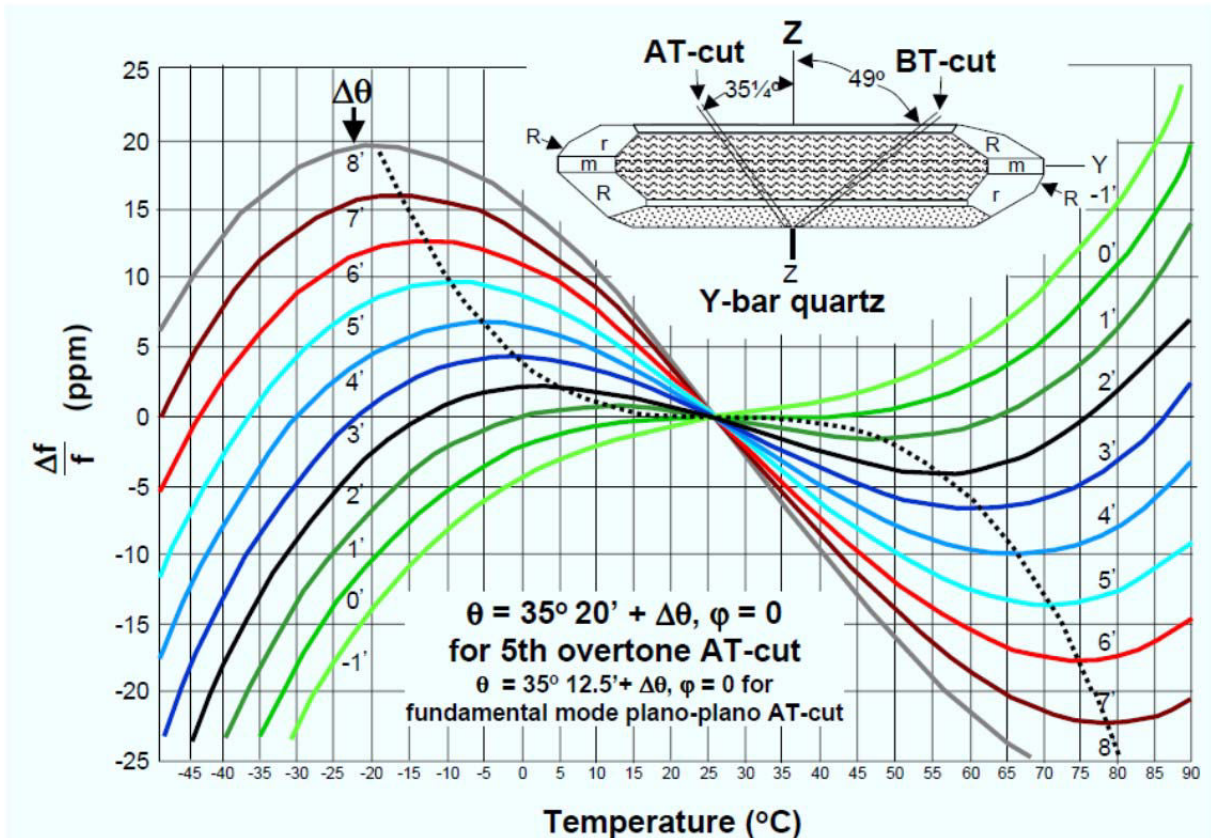


Fig.1.19: Frequency-Temperature characteristics of AT-cut for different values of θ . [2].

Note the different scale between Fig.1.19 and Fig.1.20, the SC-cut presents a very low dependency of frequency against temperature. So, this is a big advantage of SC cut over AT cut.

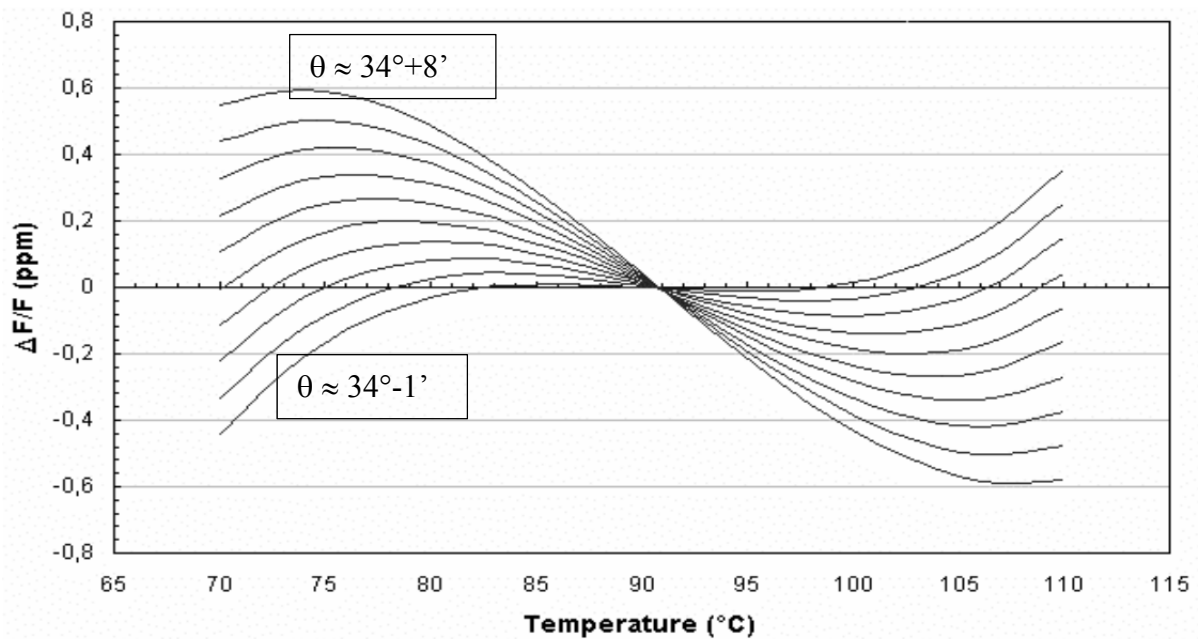


Fig.1.20: Typical frequency-temperature characteristics of SC-cut, third overtone, for different values of θ . $\Delta\theta$ varies from $-1'$ to $8'$ from $\theta = 34^\circ$, [27].

3.1.2. Equivalent circuit of crystal resonator:

The electrical equivalent circuit provides the link between the physical properties of crystal and the oscillator. The electrical parameters are:

C_0 = Shunt capacitance (capacitance between the electrodes, crystal holder, leads).

C = Motional capacitance which represents the mechanical elasticity.

L = Motional inductance which represents the mechanical inertia.

R = Motional resistance which represents the mechanical losses.

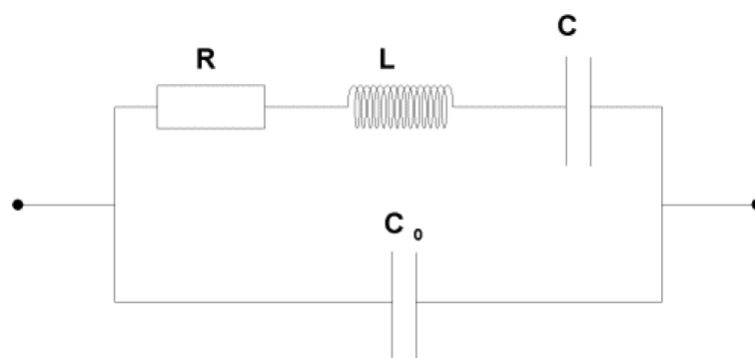


Fig.1.21: Equivalent electrical circuit [27].

Physically, a piezoelectric resonator is not exactly equal to its equivalent circuit. This is just an approximation valid in the vicinity of a resonant frequency that gives another way to express the relation of the current through the resonator as a function of the frequency by using a schema instead of the analytical expression. If we consider a portion of surface S of an infinite plate (AT

cut, thickness $2h$), having its faces coated by thin electrodes, the current is given, without approximation, by [28]:

$$I = jC_0\omega V + I_1 \quad (1.23)$$

$$I_1 = j\omega \frac{e_{26}^2 S}{2h} \frac{\sin(qh)}{\bar{c}_{66}qh\cos(qh) - \frac{e_{26}^2}{\varepsilon_{22}h} \sin(qh)} V \quad (1.24)$$

where

$$C_0 = \frac{\varepsilon_{22}S}{2h} \quad (1.25)$$

and

$$q = \omega \sqrt{\frac{\rho}{\bar{c}_{66}}} \quad (1.26)$$

where ρ is the density of the material.

and

$$\bar{c}_{66} = c_{66}^E + \frac{e_{26}^2}{\varepsilon_{22}^S} \quad (1.27)$$

\bar{c}_{66} is a so-called ‘‘stiffened’’ constants [29]. It is not a true elastic constant since it is defined only for plane wave and it depends on the propagation direction. Hence, here, the coefficients are expressed in the coordinate axes of the AT cut (rotated coefficients). The resonant frequency ω_r is found by solving:

$$\cotan(qh) = \frac{e_{26}^2}{\bar{c}_{66}\varepsilon_{22}qh} \quad (1.28)$$

At a frequency ω near ω_r the current I_1 can be approximated to the first order in $\omega - \omega_r$ by:

$$\frac{I_1}{V} = 2j\omega_r \frac{e_{26}^2 S}{h} \frac{1}{n^2\pi^2\bar{c}_{66}\left(1 - \frac{\omega}{\omega_r}\right)} \quad (1.29)$$

Where n is the overtone rank.

One then obtains an expression of the current which is of the same form than the current through a dipole consisting of a series circuit LC in parallel with a capacitance C_0 with:

$$C = \frac{4e_{26}^2 S}{n^2\pi^2\bar{c}_{66}h} \quad (1.30)$$

$$L = \frac{\rho h^3}{e_{26}^2 S} \quad (1.31)$$

To take into account the (small) damping in the material, one can simply replace \bar{c}_{66} by $\bar{c}_{66} \left(1 + \frac{j\eta_{66}\omega}{\bar{c}_{66}}\right)$ where η_{66} is the viscoelastic coefficient. In this case C become complex and is equivalent to the preceding capacitance in series with a resistance R equal to:

$$R = \frac{n^2\pi^2\eta_{66}h}{4e_{26}^2 S} \quad (1.32)$$

This results in the approximate equivalent circuit depicted in Fig.1.21. Let us insist on the fact that this modeling is valid only near the resonant (series) frequency:

$$f_r = f_s = \frac{1}{2\pi\sqrt{LC}} \quad (1.33)$$

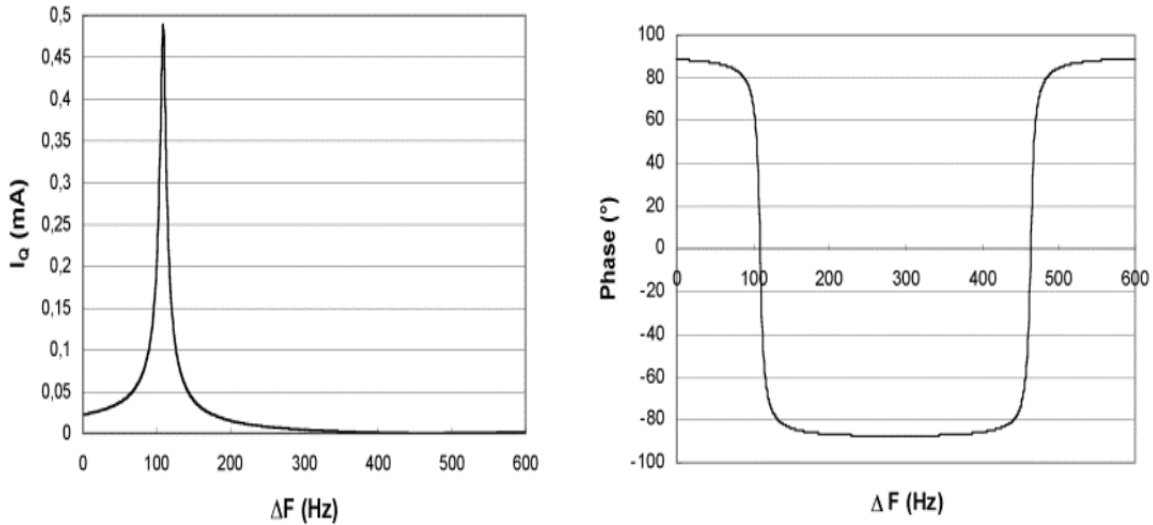


Fig.1.22: Resonance and phase curves [27].

When a crystal operates at series resonance then it looks like purely resistive and the reactances of the inductor and capacitor are equal. A series resonant circuit is characterized by the angular frequency ω_s and its quality factor Q given by:

$$\omega_s^2 = \frac{1}{LC}, Q = \frac{L\omega_s}{R} = \frac{1}{RC\omega_s} \quad (1.34)$$

where the quality factor (Q) is usually defined as:

$$Q \equiv 2\pi \frac{\text{Energy stored during a cycle}}{\text{Energy loss during a cycle}} \quad (1.35)$$

Q is inversely proportional to the linewidth of resonance. Classically, higher Q means higher frequency stability and higher accuracy capability of a resonator.

With a load capacitance in series to the crystal (Fig.1.23), the resonance frequency is shifted according to:

$$f_{LS} \approx f_s \left(1 + \frac{C}{2(C_0 + C_L)}\right) \quad (1.36)$$

and the resistance at resonance is given by:

$$R_{LS} = R \left(1 + \frac{C_0}{C_L}\right)^2 \quad (1.37)$$

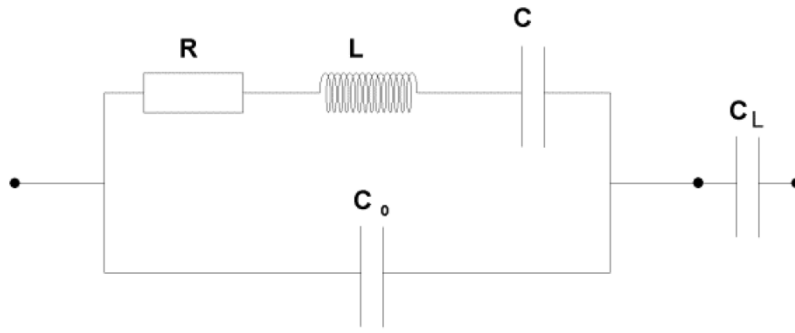


Fig.1.23: Load capacitance in series[27].

3.2. Crystal Oscillators

An electronic oscillator can be characterized as a device for producing a periodic oscillating signal such as sine wave or square wave. An oscillator produces AC signal of specific frequency from a DC power source. A simple harmonic oscillator circuit consists of an active amplifier and passive feedback network. If the output of the feedback amplifier can be used as a signal with suitable amplitude and phase then sustained oscillations can occur [6]. (Fig.1.24). Usually, the frequency of the main loop can be tuned by a voltage using a varicap diode in a small range (typically 1 or 2 Hz maximum at 5 MHz). Finally, an output amplifier is used as a buffer to get the final voltage level of the output.

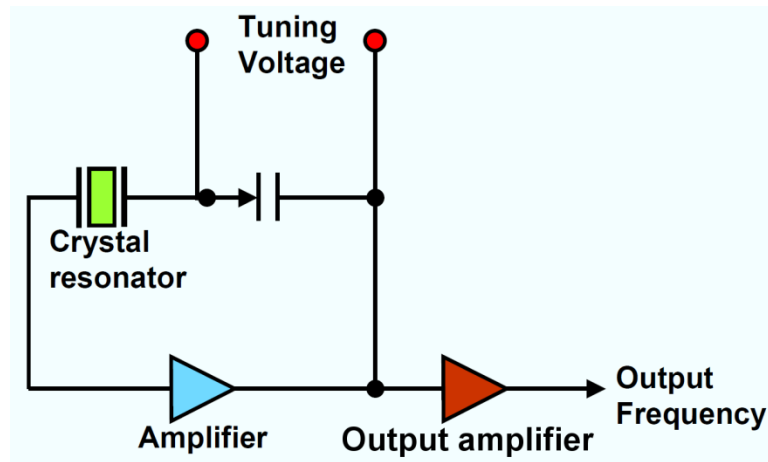


Fig.1.24: Classical circuit of a crystal oscillator [2].

If the amplifier network has a voltage gain A and the feedback network has a feedback ratio β , then in order to sustain oscillations, one must have $A\beta = 1$. Both A and β are complex functions of angular frequency and can be written as $|A|e^{j\Phi_A}$ and $|\beta|e^{j\Phi_\beta}$ where Φ_A and Φ_β are the phase shifts of the amplifier and feedback network respectively. Then the conditions for sustained oscillations are:

$$|A(\omega_r)||\beta(\omega_r)| = 1 \tag{1.38}$$

and

$$\Phi_A(\omega_r) + \Phi_\beta(\omega_r) = 2N\pi \tag{1.39}$$

where N is an integer.

These conditions (1.38-1.39) are called Barkhausen criterion. Equation (1.39) shows that, at the frequency of oscillation, the closed loop phase shift must be an integer multiple of 2π . When the system is initially closed, the only signal in the circuit is noise. The component of the noise which satisfies the phase condition for oscillation propagates around the loop with increasing amplitude. Amplitude continues to increase until the amplifier gain is reduced by nonlinearities or by an automatic gain control (AGC). For the real world oscillators [30]:

1. It is necessary that for small signal: $A\beta(\omega) > 1$
2. For large signal gain saturation: $|A\beta|(\omega) = 1$
3. The frequency of oscillation is determined by the phase condition: $\arg[A\beta(\omega)] = 0$

3.2.1. Long-term and short term stabilities

A gradual change in frequency over days or months is known as aging or long term stability. This occurs for various reasons such as the change of crystal coefficients of elasticity due to creation or diffusion of defects, or when the crystal is subjected to stress or when trapped gasses escape. Aging occurs at a relatively constant rate per decade for each crystal (Fig.1.25).

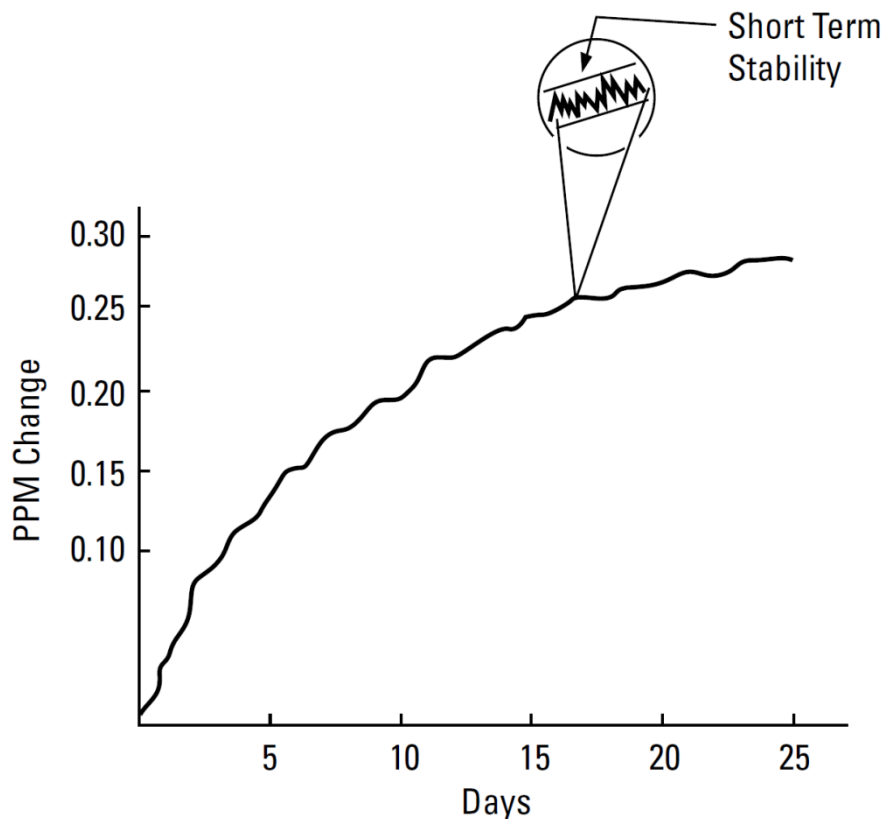


Fig.1.25: Time domain stability of the fractional frequency change (in ppm) over time (days), starting from a point of calibration. Zoom in the figure shows the short term time domain stability or the fractional frequency change over time (seconds) and its relationship to aging [12].

Therefore, to maintain an accurate frequency, adjustments should continuously be made to remove these effects. In general, frequency of an oscillator can be varied by a few cycles by slight change of phase in the feedback signal by using an adjustable capacitor. For example, a 10 MHz

oscillator with an adjustment range of 20 Hz can be corrected for 9 or 10 years of aging at a 10^{-10} per day rate.

Short term Root Mean Square (*RMS*) frequency variations are a measure of the frequency fluctuations or phase noise. This can be defined as the standard deviation of the fractional frequency fluctuations for a specific averaging time (typically $\tau = 1$ s for short term stability). This means that a time window τ is used to measure the value of $\delta f/f$, then the *RMS* value is computed from many time windows. Shorter or longer averaging times may be required to assess the accuracy for a given application. The manufacturers of high performance oscillators usually measure averages over 10^{-4} to 10^2 s and represent the results in log-log scale (Fig.1.26).

As detailed in the next paragraph, time domain stability is related to frequency domain measurements through the power spectral density of frequency fluctuations.

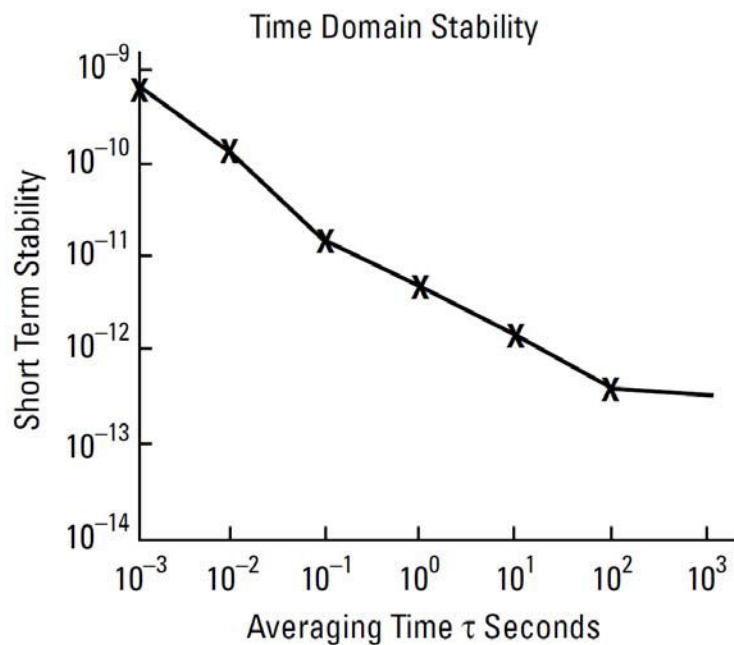


Fig.1.26: Example of short term time domain stability curve: *RMS* of averaged relative frequency fluctuations, for specific averaging times. [12].

3.3. Noise and stabilities in the time and frequency domains

3.3.1. Noise in time domain

Let us consider the sinusoidal voltage delivered by a real oscillator [31]:

$$v(t) = V_0[1 + \alpha(t)]\cos[2\pi f_0 t + \varphi(t)] \quad (1.40)$$

where:

- V_0 is the nominal peak voltage amplitude,
- $\alpha(t)$ is the amplitude noise (around nominal amplitude V_0),
- f_0 is the nominal frequency,

- $\varphi(t)$ is the phase noise (around nominal phase $2\pi f_0 t$).

For ultra-stable systems, low noise conditions are considered and the amplitude noise is always neglected ($|\alpha| = 0$ and $|\varphi| \ll 1$). To study the phase noise of an oscillator, two random quantities are used:

- 1) Phase time: $x(t) = \frac{\varphi(t)}{2\pi f_0}$ where $\varphi(t)$ (phase noise) and $x(t)$ (jitter) are instantaneous
- 2) Fractional frequency fluctuation: $y(t) = \frac{f(t)-f_0}{f_0} = \frac{\Delta f(t)}{f_0} = \frac{\dot{\varphi}(t)}{2\pi f_0} = \dot{x}(t)$

Then $y(t)$ is averaged over successive time intervals τ starting at regularly spaced instants (Fig.1.27).

$$\bar{y}_k = \frac{1}{\tau} \int_{t_k}^{t_k+\tau} y(t) dt = \frac{x(t_k+\tau) - x(t_k)}{\tau} \quad (1.41)$$

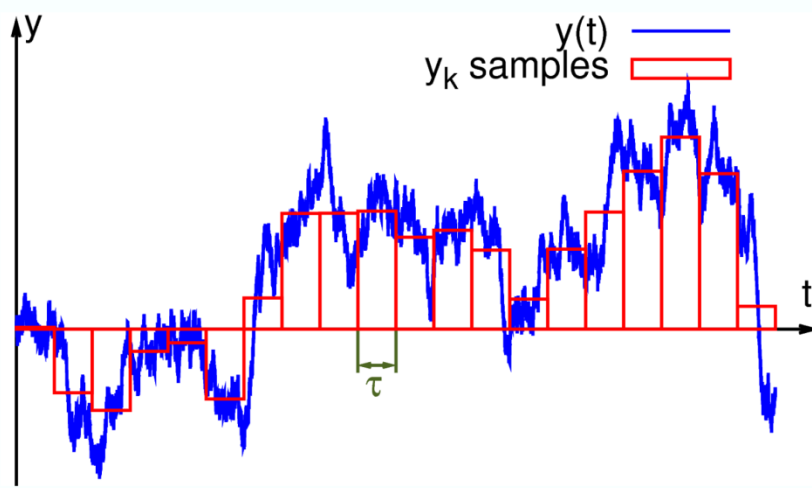


Fig.1.27: Samples divided into time steps by an interval τ to get the average value of $y(t)$ [32].

The definition of the true variance is given by:

$$I^2(\tau) = \langle (\bar{y}_k - \langle \bar{y}_k \rangle)^2 \rangle \quad (1.42)$$

Thus, the estimation of the true variance for N samples, is given by:

$$\sigma^2(N, \tau) = \frac{1}{N-1} \sum_{i=1}^N \left(\bar{y}_i - \frac{1}{N} \sum_{j=1}^N \bar{y}_j \right)^2 \quad (1.43)$$

In the Time & Frequency domain, the Allan variance is usually used. It is in fact the 2 samples variance and it is given by:

$$\sigma_y^2(\tau) = \langle \sigma^2(2, \tau) \rangle = \langle \sum_{i=1}^2 \left(\bar{y}_i - \frac{1}{2} \sum_{j=1}^2 \bar{y}_j \right)^2 \rangle = \frac{1}{2} \langle (\bar{y}_2 - \bar{y}_1)^2 \rangle \quad (1.44)$$

Thus, Allan deviation is given by:

$$\sigma_y(\tau) = \sqrt{\sigma_y^2(\tau)} = \sqrt{\frac{1}{2} \langle (\bar{y}_2 - \bar{y}_1)^2 \rangle} \quad (1.45)$$

3.3.2. Noise in frequency domain

For a stationary process, the IEEE norm [31] states that “The measure of frequency instability is the (one-sided) spectral density of normalized frequency fluctuations, $S_y(f)$, given by:

$$S_y(f) = y_{rms}^2(f) \frac{1}{BW} \quad (1.46)$$

- $y_{rms}(f)$ is the measured root mean squared (rms) value of normalized frequency fluctuations in a band of Fourier frequencies containing frequency f
- BW is the width of this frequency band in Hz

For sufficiently narrow Fourier frequency bands (such that $S_y(f)$ is approximately constant over the bandwidth), we have:

$$\lim_{T \rightarrow \infty} \frac{1}{T} \int_{-T/2}^{+T/2} |y(t)|^2 dt \equiv y_{rms}^2 = \int_0^\infty S_y(f) df \approx \sum_{k=1}^\infty S_y(f_k) BW = \sum_{k=1}^\infty y_{rms}^2(f_k) \quad (1.47)$$

Similarly, for the amplitude and phase one-sided spectral densities, we have:

$$S_a(f) = a_{rms}^2(f) \frac{1}{BW} \text{ and } S_\varphi(f) = \varphi_{rms}^2(f) \frac{1}{BW} \quad (1.48)$$

However, manufacturers prefer the quantity $\mathcal{L}(f)$ (dBc/Hz) instead of $S_\varphi(f)$. $\mathcal{L}(f)$ (pronounced “*ell of f*”) is the ratio of the power in one sideband due to phase modulation (PM) by noise (for a 1 Hz bandwidth) to the total signal power (carrier plus sidebands). $\mathcal{L}(f)$ can be defined as:

$$\mathcal{L}(f) = \frac{1}{2} S_\varphi(f) \quad (1.49)$$

In decibels, $\mathcal{L}(f) = S_\varphi(f) - 3 \text{ dB}$

Due to Fourier transform properties, the power spectral densities $S_x(f)$ and $S_y(f)$ are given by:

$$S_x(f) = \frac{1}{(2\pi f_0)^2} S_\varphi(f) \quad (1.50)$$

$$S_y(f) = \frac{f^2}{f_0^2} S_\varphi(f) \quad (1.51)$$

Experimental practice shows that, besides long-term frequency drifts, the frequency of a high-quality frequency source can be perturbed by a superposition of independent noise processes, which can be adequately represented by random fluctuations having the following one-sided power spectral density of phase fluctuations:

$$S_\varphi(f) = \sum_{i=0}^{-4} b_i f^i \quad (1.52)$$

This power law model can be applied to $S_x(f)$ and $S_y(f)$. The five common power-law noise processes in precision oscillators are:

$$S_y(f) = \sum_{\alpha=-2}^{+2} h_\alpha f^\alpha \quad (1.53)$$

$$S_y(f) = h_{-2}f^{-2} + h_{-1}f^{-1} + h_0 + h_1f + h_2f^2 \quad (1.54)$$

(Random-walk FM) (Flicker FM) (White FM) (Flicker PM) (White PM)

with FM =Frequency Modulation and PM = phase modulation.

3.3.3. Relationship between time and frequency stabilities

When one of the five common power-law noise processes, is a good approximation, the corresponding Allan variance can be calculated by [31]:

$$\sigma_y^2(\tau) = 2 \int_0^\infty h_\alpha f^\alpha \frac{\sin^4(\pi f \tau)}{(\pi f \tau)^2} df \quad (1.55)$$

Table 1.8 presents the correspondence between noise types, PSD and Allan variance.

Table 1.8: Correspondence between noise types, power spectral densities and Allan variance (f_h is the high cut-off frequency) [31].

$S_y(f)$	$S_\varphi(f)$	$S_y \leftrightarrow S_\varphi$	$\sigma_y^2(\tau)$	Noise type	Origin
h_2f^2	b_0	$h_2 = \frac{b_0}{v_0^2}$	$\frac{3h_2f_h}{4\pi^2} \tau^{-2}$	White PM	Environment
h_1f	$b_{-1}f^{-1}$	$h_1 = \frac{b_{-1}}{v_0^2}$	$\frac{[1.04 + 3\ln(2\pi f_h \tau)]h_1}{4\pi^2} \tau^{-2}$	Flicker PM	Resonator
h_0	$b_{-2}f^{-2}$	$h_0 = \frac{b_{-2}}{v_0^2}$	$\frac{h_0}{2} \tau^{-1}$	White FM	Thermal noise
$h_{-1}f^{-1}$	$b_{-3}f^{-3}$	$h_{-1} = \frac{b_{-3}}{v_0^2}$	$2\ln(2)h_{-1}$	Flicker FM	Electronic noise
$h_{-2}f^{-2}$	$b_{-4}f^{-4}$	$h_{-2} = \frac{b_{-4}}{v_0^2}$	$\frac{2\pi^2h_{-2}}{3} \tau$	Random walk FM	External white noise

4. Conclusions

During this PHD thesis, we were mainly concerned by flicker of frequency noise, that can be modeled by a process with a power spectral density of frequency fluctuations proportional to the inverse of the difference between the instantaneous frequency and the resonance frequency. From Table 1.8, we can see that such processes have a constant Allan variance which is therefore a good characteristic of the process. In the remaining chapters, we will explore how the intrinsic floor for this variance could be linked to the relative amounts of defects in the material of the resonator or to the quantum fluctuations of the cross-sections for 2 or 3 phonons interaction processes.

5. References

- [1] J. R. Vig and Arthur Ballato, "Frequency control devices", Ultrasonic Instruments and Devices, Academic Press, Inc., 1999.
- [2] John R. Vig, "Quartz crystal resonators and oscillators ", For Frequency Control and Timing Applications, A tutorial, January 2000, (page 3-2).
- [3] J. Tichý et al., "Fundamentals of piezoelectric sensorics", Springer-Verlag Berlin Heidelberg, 2010, (page2).
- [4] L. E. Halliburton, Joel J. Martin, Dale R. Koehler, "Precision frequency control Volume-2", Academic Press Inc., 1985.
- [5] B. Auld, "Acoustic fields and waves in solids: Volume 1", John Wiley & Sons, Inc, 1973.
- [6] D. Salt, "Quartz crystal devices", Van Nostrand Reinhold (UK) Co. Ltd, 1987.
- [7] J.C. Brice, "Crystals for quartz resonators", Rev. Mod. Phys., vol. 57, no. 1, pp. 105-146, 1985.
- [8] J.J. Boy, PHD thesis, University of Franche-Comté, 1994.
- [9] International Electrotechnical Commission, "Synthetic quartz crystal – Specifications and guide to the use ", 758@CEI, 1993.
- [10] J. Imbaud, J.J. Boy, J.P. Romand, J. Frayret, D. Piccheda, G. Cibiel and F. Sthal, "Analyzes of very high-Q quartz crystal aimed to high quality 5 MHz resonators achievement", 24th European Frequency and Time Forum, Noordwijk, NL, 13-16 April, pp. 1-7, 2010.
- [11] B. Sawyer, "International Round Robin in Infrared Alpha on Measurements on Slices of Synthetic Quartz", IEEE Trans. Ultrason. Ferroelec. Freq. Contr., vol. 41, no. 4, pp. 467-472, 1994.
- [12] Fundamentals of Quartz Oscillators, HP® Application Note 200-2, H. Electronic Counters Series (page.5), <http://www.leapsecond.com/pdf/an200-2.pdf>.
- [13] http://www.jauch.de/ablage/med_00000818_1327049076_Quartz%20Crystal%20Theory%20007.pdf (page.3).
- [14] H. Fritze, "High-temperature piezoelectric crystals and devices", J. Electroceram, vol. 26, no. 1-4, pp.122-161, 2011.
- [15] H. Ohsato, T. Iwataki, H. Morikoshi, "Mechanism of Piezoelectricity for Langasite Based on the Framework Crystal Structure", Trans. Electr. Electron. Mater. vol. 13, no. 2, pp. 51-59, 2012.

- [16] H. Takeda, J. Yamaura, T. Hoshina and T. Tsusumi, "Growth, structure and electrical properties of aluminum substituted langasite family crystals", IOP Conf. Series: Materials Science and Engineering, vol. 18, 2011.
- [17] H. Iwataki, H. Ohsato, K. Tanaka, H. Morikoshi, J. Sato, K. Kwasaki, "Mechanism of the piezoelectricity of Langasite based on the crystal structures" Journal of the European Ceramic Society, vol. 21, no. 9, pp. 1409-1412, 2001.
- [18] N. Araki, H. Ohsato, K. Kakimoto, T. Kuribayashi, Y. Kudoh, H. Morikoshi, "Origin of piezoelectricity for langasite $A_3Ga_5SiO_{14}$ ($A = La$ and Nd) under high pressure", Journal of the European Ceramic Society, vol. 27, no. 13-15, pp. 4099-4102, 2007.
- [19] M. Adachi, T. Kimura, W. Miyamoto, Z. Chen and A. Kawabata, "Dielectric, Elastic and Piezoelectric Properties of $La_3Ga_5SiO_{14}$ (LANGASITE) Single Crystals", Journal of the Korean Physical Society, vol. 32, pp. S1274-S1277, 1998.
- [20] D. V. Roshchupkin, D. V. Irzhak, E. D. Roshchupkina, and O. A. Buzanov", "Investigation of Structural Perfection and Acoustic Properties of $La_3Ga_5SiO_{14}$ Crystals by High Resolution X-Ray Diffraction, Topography, and Microfluorescence Analysis", Crystallography Reports, vol. 49, no. S1, pp. S80-S88, 2004.
- [21] K. Marty, P. Bordet, V. Simonet, M. Loire, R. Ballou, C. Darie, J. Kljun, P. Bonville, O. Isnard, P. Lejay, B. Zawilski and C. Simon, "Magnetic and dielectric properties in the langasite-type compounds : $A_3BFe_3D_2O_{14}$ with $A=Ba, Sr, Ca$, $B=Ta, Nb, Sb$ and $D=Ge, Si$ ", Phys. Rev. B, vol. 81, no. 5, 054416, 2010.
- [22] B. V. Mill, A. V. Buntashin, G. G. Khodzhabagyan, E. L. Belokoneba and N. V. Belov, "Modified rare earth gallates of $CaGa_2Ge_4O_{14}$ structure", Doklady Akademii Nauk USSR, vol. 264, no. 4, pp. 1385-1389, 1982.
- [23] P. M. Davulis and M. P. Da Cunha, "A full set of langatate high-temperature acoustic wave constants: elastic, piezoelectric, dielectric constants up to $900^\circ C$ ", IEEE Trans. Ultrason. Ferroelectr. Freq. Control, vol. 60, no. 4, pp. 824-833, 2013.
- [24] G. Sreenivasulu, L. Y. Fetisov, Y. K. Fetisov, and G. Srinivasan, "Piezoelectric single crystal langatate and ferromagnetic composites: Studies on low-frequency and resonance magnetoelectric effects", Appl. Phys. Lett., vol. 100, no. 5, 052901, 2012.
- [25] A. Khan and A. Ballato, "Piezoelectric coupling factor calculations for plates of langatate driven in simple thickness modes by lateral-field-excitation", IEEE Trans. Ultrason. Ferroelectr. Freq. Control, vol. 49, no. 7, pp. 922-928, 2002.

- [26]H. Nakae, K. Kihara, M. Okuno, S. Hirano, “The crystal structure of the quartz-type form of GaPO₄ and its temperature dependence”, *Zeitschrift für Kristallographie*. vol. 210, no. 10, pp. 746-753, 1995.
- [27]N. Gufflet, “Quartz Crystal Resonators- Brief overview”, KVG Quartz Crystal Technology. <http://www.kvg-gmbh.de/en/home.html>.
- [28]J. A. Lewis, “The effect of driving electrode shape on the electrical properties of piezoelectric crystals”, *Bell System Technical Journal*, vol. 40, no. 5, pp. 1259-1280, 1961.
- [29]D. Royer, E. Dieulesaint, “Elastic waves in solid 1”, Springer-Verlag, Berlin Heidelberg, 2000.
- [30]E. Rubiola, “Phase noise and frequency stability in oscillators“, Cambridge University Press, November 2008.
- [31]IEEE, “IEEE Standard Definitions of Physical Quantities for Fundamental Frequency and Time Metrology -- Random Instabilities”, in *IEEE STD 1139-2008: IEEE*, 2008, pp. 1-35.
- [32]F. Vernotte, “Variance Measurements”, *Proc. Joint conference of the IEEE International Frequency Control Symposium (IFCS) and European frequency and time forum (EFTF)*, San Francisco, CA, 1-5 May 2011, pp. 845-849, 2011.

Chapter 2: Bibliography of $1/f$ noise models

In 1921, C.A. Hartman attempted to verify Schottky's formula (1918) of shot noise spectral density for the current originating from electron motion inside a vacuum tube but he failed. However in 1926, J. B. Johnson successfully measured white noise spectrum and in addition with that he also measured an unexpected "flicker noise" in the low frequency range [1] as shown in Fig.2.1. Schottky later explained that this flicker noise might appear due to fluctuations of electron emission rate by the cathode due to molecule adsorption on this cathode.

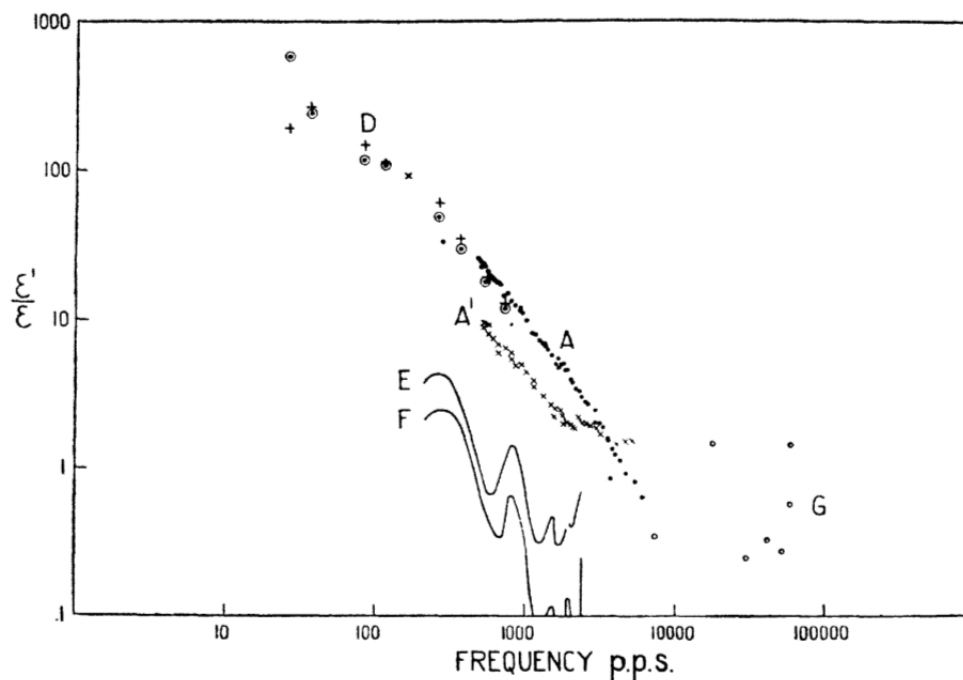


Fig.2.1: Spectral density observed by J.B. Johnson(1925) [1]. The vertical scale represents the observed noise power density divided by the theoretical shot noise power density; the horizontal scale is the frequency in Hz.

After this unexpected discovery of $1/f$ noise by Johnson, it has been seen that this strange noise is present in the response of many electric and electronic devices and even in natural phenomena like earthquakes, thunderstorms, rate of the Nile over the last 2000 years, annual thickness of glacial varves (clay deposits formed from the yearly runoff from a receding glacier) [2] or in biological systems like heart beats, blood pressure etc... Searchers in these various fields have therefore tried to find a common mathematical framework that they could apply to their particular case. In the following, we shall first review the models that find $1/f$ PSD as suitably weighted sums of Lorentzians for several different distributions of characteristic relaxation rate or time. Then, we give account of other models that might be pertinent to our study of $1/f$ noise in quartz oscillators.

1. 1/f noise by summing Lorentzians

1.1. Schottky's theory and its derivatives

In 1926, W. Schottky gave a mathematical explanation [3] to understand the $1/f^\alpha$ noise in vacuum tubes. He assumed that the fluctuations in the number of electrons released from the cathode, due to surface trapping by foreign atoms/molecules of a given kind, adsorbed at t_0 , are supposed to be governed by a simple exponential law:

$$N(t, t_0) = \begin{cases} N_0 e^{-\lambda(t-t_0)}, & t \geq t_0 \\ 0, & t < t_0 \end{cases} \quad (2.1)$$

where λ is the relaxation rate.

Using the fact that the Fourier transform of $N(t, t_0)$ is given by:

$$\int_{-\infty}^{+\infty} N(t, t_0) e^{-i\omega t} dt = \frac{N_0}{\lambda + i\omega} e^{-i\omega t_0} \quad (2.2)$$

one can show that the power spectral density for independent adsorption times and for a given relaxation rate, is Lorentzian:

$$S^{(\lambda)}(\omega) = \lim_{T \rightarrow \infty} \frac{1}{T} \langle \left| \int_{-\infty}^{+\infty} \sum_k N(t, t_k) e^{-i\omega t} dt \right|^2 \rangle = \frac{N_0^2}{\lambda^2 + \omega^2} \lim_{T \rightarrow \infty} \frac{1}{T} \langle \left| \sum_k e^{-i\omega t_k} \right|^2 \rangle = \frac{N_0^2 n}{\lambda^2 + \omega^2} \quad (2.3)$$

where the triangular bracket denotes the statistical ensemble average and n represents the average pulse rate i.e. the number of pulse characteristic times t_k during an interval of time Δt , divided by Δt , when $\Delta t \rightarrow \infty$.

The above expression of the power spectral density (PSD) is constant near $f=0$ and nearly proportional to $1/f^2$ for large f .

If there are multiple relaxation rates λ uniformly distributed between λ_1 and λ_2 then, the total PSD is given by the following ‘‘sum’’ of Lorentzians [4], [5]:

$$S(\omega) = \int_{\lambda_1}^{\lambda_2} S^{(\lambda)}(\omega) \frac{d\lambda}{(\lambda_2 - \lambda_1)} \quad (2.4)$$

$$S(\omega) = \frac{N_0^2 n}{\omega(\lambda_2 - \lambda_1)} \left[\tan^{-1} \left(\frac{\lambda_2}{\omega} \right) - \tan^{-1} \left(\frac{\lambda_1}{\omega} \right) \right] \approx \begin{cases} \frac{N_0^2 n}{\lambda_1 \lambda_2}, & 0 < \omega \ll \lambda_1 \ll \lambda_2 \\ \frac{N_0^2 n \pi}{2\omega(\lambda_2 - \lambda_1)}, & \lambda_1 \ll \omega \ll \lambda_2 \\ \frac{N_0^2 n}{\omega^2}, & \lambda_1 \ll \lambda_2 \ll \omega \end{cases} \quad (2.5)$$

Hence, if $\lambda_1 \ll \omega \ll \lambda_2$, one obtains fluctuations in the number of electrons released from the cathode with a $1/f$ PSD:

$$S(\omega) \approx \frac{N_0^2 n \pi}{2(\lambda_2 - \lambda_1)} \times \frac{1}{\omega} \quad (2.6)$$

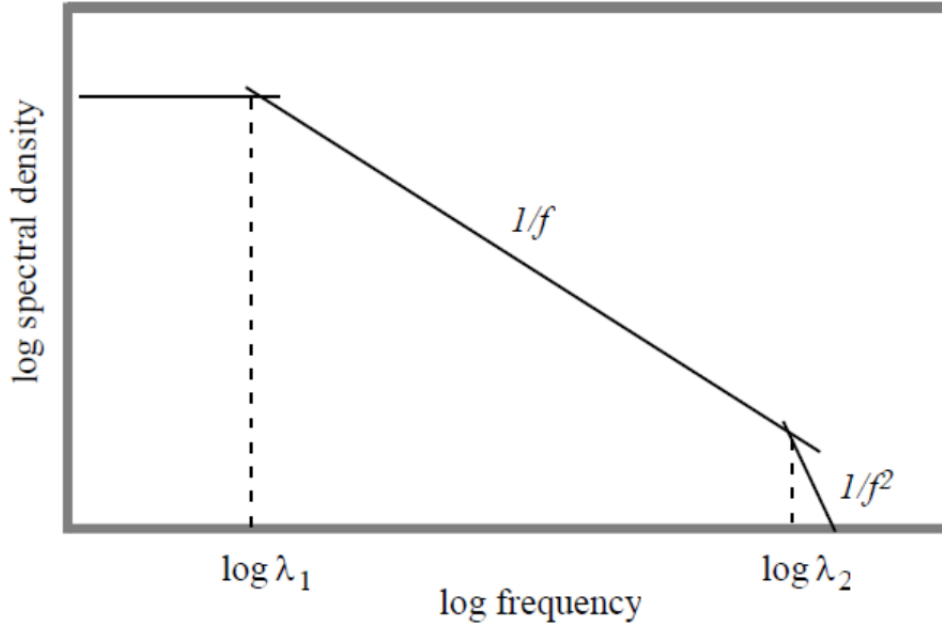


Fig.2.2: Log power spectral density plot with respect to log frequency [4].

Alternatively, if the relaxation rate is distributed according to a law:

$$dP(\lambda) = \frac{A}{\lambda^\beta} d\lambda, \quad \lambda_1 < \lambda < \lambda_2 \quad (2.7)$$

the PSD is then given by [4], [6]:

$$S(\omega) \propto \int_{\lambda_1}^{\lambda_2} \frac{1}{\lambda^2 + \omega^2} \frac{d\lambda}{\lambda^\beta} = \frac{1}{\omega^{1+\beta}} \int_{\lambda_1/\omega}^{\lambda_2/\omega} \frac{1}{1+x^2} \frac{dx}{x^\beta} \quad (2.8)$$

Hence, in the limit $\lambda_1 \ll \omega \ll \lambda_2$, we have:

$$S(\omega) \propto \frac{1}{\omega^{1+\beta}} \quad (2.9)$$

Thus, we get the family of colored noises and with $\beta = 0$, we get $1/f$ noise.

1.2. F.K Du Pré's theory

In 1950, F. K. Du Pré [7] proposed a theory for flicker noise by summing Lorentzians with an exponential distribution of relaxation times due to a thermally activated process with a distribution of activation energy that would vary little around its maximum.

He started from Schottky's expression of the mean square noise current per unit frequency interval, for a given characteristic time $\tau=1/\lambda$ [3]:

$$\langle i^2 \rangle_{Av} \propto \frac{\tau I^2}{1+\tau^2 \omega^2} \quad (2.10)$$

where I is the average current and τ is the average time spent by an atom/molecule on the surface of the cathode.

Du Pré modified Schottky's theory to predict the frequency and temperature dependence correctly at the same time. He assumed first that the temperature dependence of the relaxation time is given by:

$$\tau = \tau_0 \exp\left(\frac{Q}{k_B T}\right) \quad (2.11)$$

where, Q is the diffusion activation energy. Then he supposed that there could be a certain spread in the values of the diffusion activation energy at the different points of the surface barrier given by a distribution $f(Q)$. Then, Eq. (2.10) can be written as.

$$\langle i^2 \rangle_{Av} \propto \int_0^\infty f(Q) \frac{\tau l^2}{1+\tau^2 \omega^2} dQ = \left(\frac{l^2}{\omega}\right) \int_0^\infty f(Q) \frac{\tau \omega}{1+\tau^2 \omega^2} dQ \quad (2.12)$$

The expression $\frac{\tau \omega}{1+\tau^2 \omega^2}$ possesses a sharp maximum for $\tau = \tau_m$ such that $\tau_m \omega = 1$. This corresponds to a diffusion activation energy given by $Q_m = -k_B T \ln(\tau_0 \omega)$. Du Pré then assumed that $f(Q)$ varies relatively little in a range of the order of $k_B T$ around Q_m . As a result:

$$\langle i^2 \rangle_{Av} \propto \left(\frac{l^2}{\omega}\right) f(Q_m) \int_0^\infty \frac{\tau \omega}{1+\tau^2 \omega^2} dQ \quad (2.13)$$

Since $\tau_m \omega = 1$, $\tau \omega = \tau/\tau_m = \exp((Q - Q_m)/k_B T)$, the change of variable $z = \tau \omega$ gives:

$$\langle i^2 \rangle_{Av} \propto \left(\frac{l^2}{\omega}\right) k_B T f(Q_m) \int_{\exp(-Q_m/k_B T)}^\infty \frac{1}{1+z^2} dz \quad (2.14)$$

Assuming $Q_m \gg k_B T$ gives:

$$\langle i^2 \rangle_{Av} \propto \left(\frac{l^2}{\omega}\right) T f[-k_B T \ln(\tau_0 \omega)] \quad (2.15)$$

Thanks to the \ln in its argument, the value of the function f depends very weakly on ω . Hence the main dependence is $1/\omega$ over several decades, provided f varies little over an interval of several $k_B T$ around Q_m .

1.3. Dutta, Dimon and Horn's theory

In 1979, P. Dutta et al. proposed a theory of $1/f$ noise based on the concept of summing the Lorentzian spectrum in metals [8]. Their model has been developed on the basis of three basic assumptions:

- 1) The noise arises from random fluctuation with characteristic times that are thermally activated.
- 2) The resistance is linearly coupled to the fluctuating quantity with a coupling constant that is non-singular at long wavelengths.
- 3) All samples studied are inhomogeneous.

Their derivation begins exactly as that of Du Pré, but integrates a Taylor expansion of f around Q_m instead of just taking $f(Q_m)$ out of the integral. They obtain:

$$S_v(\omega, T) \propto \frac{k_B T}{\omega} \left[f(Q_m) + \sum_{n=1}^\infty \frac{\mathcal{G}_n}{(2n)!} \left(\frac{\pi k_B T}{2}\right)^2 \frac{d^{2n}}{dQ^{2n}} f(Q) \Big|_{Q=Q_m} \right] \quad (2.16)$$

where $Q_m = -k_B T \ln(\tau_0 \omega)$ and \mathcal{G}_n is the n^{th} Euler number. The conclusion is the same as that of Du Pré, but the interval of validity of the approximation can be evaluated more precisely.

1.4. F. N. Hooge and P. A. Bobbert's theory

In 1997, F. N. Hooge and P. A. Bobbert calculated the correlation function of approximate $1/f$ noise and studied how it could be derived from summing Lorentzians [9]. They started from the consideration that even if pure $1/f$ noise can not exist down to $f = 0$, since the variance of the process $\int_0^{f_h} (A/f) df$ would be infinite, it is nonetheless reasonable to consider some process X that would have a noise power spectral density experimentally undistinguishable from A/f on a wide interval $[f_l, f_h]$. Furthermore, they supposed that below f_l the spectrum would be white and that above f_h the spectral power density would decrease as $1/f^2$. With a ratio $f_h/f_l \sim 10^{10}$, they could estimate that around 90% of the variance was in the interval $[f_l, f_h]$.

Considering the summation of Lorentzians with a wide range of relaxation times between τ_1 and τ_2 , with a statistical distribution given by:

$$g(\tau) d\tau = \frac{1}{\ln\left(\frac{\tau_2}{\tau_1}\right)} \frac{1}{\tau} d\tau \quad (2.17)$$

gives:

$$S_X(f) = \overline{X^2} \int_{\tau_1}^{\tau_2} g(\tau) \frac{4\tau}{1+\tau^2\omega^2} d\tau = \frac{4\overline{X^2}}{\omega \ln\left(\frac{\tau_2}{\tau_1}\right)} \int_{\omega\tau_1}^{\omega\tau_2} \frac{1}{1+\tau^2\omega^2} d(\tau\omega) \quad (2.18)$$

As in the previous paragraphs, the value of the integral in the above equation is $\frac{\pi}{2}$ for $1/\tau_2 \ll \omega \ll 1/\tau_1$, so that the power spectrum of the summed Lorentzians is:

$$S_X(f) = \frac{\overline{X^2}}{\ln\left(\frac{\tau_2}{\tau_1}\right)} \frac{1}{f} \quad (2.19)$$

Hence, a sum of Lorentzians spectra gives rise to $1/f$ noise in the frequency range between $f_l = 1/2\pi\tau_2$ and $f_h = 1/2\pi\tau_1$, provided the distribution of relaxation times is given by Eq. (2.17) and no transitions are allowed between processes with different relaxation times.

Hooge and Bobbert then proved that the correlation function of limited $1/f$ noise is:

$$\psi(t) = \overline{X^2} \frac{\ln\left(\frac{\tau_2}{t}\right)}{\ln\left(\frac{\tau_2}{\tau_1}\right)} \quad \tau_1 < t < \tau_2 \quad (2.20)$$

Finally, they proved that such a correlation function in $-\ln(t)$ can also be found for a process consisting of a random series of pulses with a power time dependence in $t^{-1/2}$, such as the process introduced by Schönberg to find a $1/f$ spectrum thanks to Carson's theorem (H. Schönfeld, Z. Naturf., vol. 10a, pp. 291, 1955).

Unfortunately, for this physical explanation, in 2002, C. M. van Vliet showed that the claim that a $1/f$ spectrum could be associated with a sum of pulses arising from a one-dimensional collective random walk stochastic diffusion process, is fallacious [10].

2. 1/f noise from the fluctuations of time intervals between pulses

In 1998, B. Kaulakys and T. Meškauskas made the observation that for a signal composed of a sequence of random pulses of identical shapes, the shape of the pulses mainly influences the high frequency part of the power spectral density while fluctuations of the pulse amplitude result in white or Lorentzian but not 1/f noise. Hence they considered a sequence of Dirac impulsions $I(t) = \sum_k \delta(t - t_k)$, with random increments of the time intervals between pulses:

$$\tau_k = \tau_{k-1} - \gamma(\tau_{k-1} - \bar{\tau}) + \sigma \varepsilon_k \quad (2.21)$$

with $\tau_k = t_k - t_{k-1}$, γ the rate of relaxation to the average time interval between pulses $\bar{\tau}$ and σ is the standard deviation of white noise and $\{\varepsilon_k\}$ is a sequence of uncorrelated normally distributed random variables ε_k with zero expectation and unit variance. Their model could e.g. describe a flow of identical objects such as electrons, photons, or cars!

In their paper, Kaulakys and Meškauskas prove that the power spectral density of the current is then given by a 1/f law:

$$S(f) = 2\bar{I} \frac{\Psi(0)}{f}, \quad f_1 < f < f_2, f_\tau \quad \text{with } \Psi(0) = \frac{1}{2\pi} \int_{-\infty}^{+\infty} \langle \exp(i\theta \tau_k) \rangle d\theta \quad (2.22)$$

where $\bar{I} = 1/\bar{\tau}$ is the average current of pulses, $\langle \rangle$ is an averaging over the distributions of the time intervals between pulses τ_k , which coincides with the usual average on all the realizations of the process and f_1, f_2, f_τ are characteristic frequencies which expression depends on the distribution of τ_k considered.

For example, for a Gaussian distribution of time intervals between pulses:

$$\Psi(0) = \frac{1}{\sqrt{2\pi}\sigma_\tau} \exp(-\bar{\tau}^2/2\sigma_\tau^2) \quad (2.23)$$

Kaulakys and Meškauskas find that the power spectrum is then given by:

$$S(f) = \frac{\bar{I}^2 \alpha_H}{f}, \quad f_1 < f < f_2, f_\tau \quad (2.24)$$

with α_H is a dimensionless quantity similar to the Hooge parameter.

$$\alpha_H = \frac{2}{\sqrt{\pi}} K e^{-K^2}, \quad \text{with } K = \frac{\bar{\tau}}{\sqrt{2}\sigma_\tau} = \frac{\bar{\tau}\sqrt{\gamma}}{\sigma} \quad (2.25)$$

The interesting feature of the Gaussian model is that it allows calculating the analytical approximate forms for the frequencies at which a transition between two kinds of noise is observed. The Gaussian model gives (after some lengthy derivation detailed in the paper) 1/f noise for only one relaxation rate γ , in an adjustable frequency range $f_1 < f < f_2$ and $f \ll f_\tau$ (with $f_1 = \gamma^{3/2}/\pi\sigma$, $f_2 = 2\gamma^{1/2}/\pi\sigma$ and $f_\tau = 1/2\pi\bar{\tau}$). They also find a Lorentzian power spectrum density $S(f) = 2\bar{I} \frac{\sigma^2}{\tau^2 \gamma^2} \frac{1}{1+(\pi f \sigma^2 / \bar{\tau} \gamma^2)^2}$ for $f < f_1$ and thus white noise for $f \ll f_0$, with $f_0 = \bar{\tau} \gamma^2 / \pi \sigma^2$. As a consequence, this Gaussian model does not present any physical divergence for small frequencies.

3. $1/f$ noise and self-organized criticality

In 1987, P. Bak *et al.* got inspiration from the fact that power-law temporal or spatial correlations extend over several decades in self-similar temporal and/or spatial fractal structures. They introduced the notion of locally minimally stable (and maximally sensitive) states [12]¹⁹. Under a small perturbation those states redistribute their “energy” on local neighbors which themselves do the same if their energy is above some critical value, triggering some avalanche process with a characteristic time much faster than the build-up time of energy. A cluster of minimally stable states is then defined dynamically as the spatial region over which a small local perturbation will propagate. In numerical simulations, the system is randomly initialized with some energies much bigger than the critical energy. Then it evolves until all the energies are below the critical value. The dynamics is then probed by the measurement of the state resulting from a small local random perturbation. They found power-law distributions of the $1/f^\alpha$ type for avalanche sizes and durations respectively. This introduced the concept of Self-Organized Criticality (SOC) where the lack of characteristic length leads directly to a lack of characteristic time for the resulting fluctuations, without any need for a “fine tuning” of the parameters of the model!

The analogy was made with a sand pile with slopes so steep that a single sand grain addition can trigger a collapse of the pile until the average slope reaches a critical value where the system is barely stable with respect to the addition of new sand grains.

However, in 1999, P. De Los Rios and Y. Zhang argued that for such systems, the α exponent is seldom close to 1 and that it depends strongly on the dimensionality of the system. Moreover, power-law time correlations corresponds to power-law (long-range) spatial correlations, for which they claim that there is no evidence in most systems exhibiting $1/f$ noise. To remedy these problems, they added two new ingredients [13] to the model developed by Bak *et al.*: they added the energy only on one side of the lattice, defining implicitly a preferred propagation direction and added some dissipation during the (non-linear since there is a threshold) redistribution of energy on neighboring sites. With this model, they showed numerically that they got a $1/f$ power spectrum on several decades in 1D and 2D with the same other conditions, thus hinting towards the independence of such behavior on the actual dimensionality of the system. They also pointed out the fact that the $1/f$ power spectrum for the whole lattice comes from the superposition of local (measured and not imposed as in sum of Lorentzians theories!) power spectra that are far from $1/f$ spectra.

¹⁹ According to the statistics on the APS web site, this paper has been cited more than 2860 times at the time of this writing.

In 2001, studying fluctuations with a $1/f$ PSD in oscillatory combustion regimes, V. N. Skokov *et al.* proposed a mathematical model for the origin of flicker spectrum fluctuations at the interaction of phase transitions in distributed systems to interpret their experimental data on flame front fluctuations in combustion of a porous wick impregnated with spirits [14]. They made the observation that the absence of a lower temporal scale for flicker could be due to the fact that the system is in the vicinity of a critical phase transition. Hence they proposed that self-organization of a critical state in their system may be the consequence of the intersection and interaction of a subcritical non-equilibrium phase transition and a supercritical one, namely the boiling-up of an ignitable matter before its combustion front could lead to stochastic oscillations of the reaction front with a $1/f^\alpha$ (with α significantly different from 1) power spectrum experimentally and theoretically.

4. $1/f$ noise in quartz crystal resonators by using statistical mechanics: Michel Planat's Model

In 2003, M. Planat proposed a model based on quantum statistical thermodynamics to explain the $1/f$ noise in quartz crystal resonators [15]. In this paper, M. Planat considered the case of a population of massless bosons (phonons) with degenerate energy levels, nhf , with h being Planck's constant and n a positive integer. This may be interpreted physically by the fact that, in Debye's approximation the dispersion relation is linear ($2\pi f = |k|c$, with k the pseudo wave vector and c the celerity of the corresponding sound wave). Hence the allowed frequencies are integer multiples of a fundamental frequency since, due to the confinement of the waves in an interval of length L , in that direction the wave vectors are integer multiples of $2\pi/L$. According to M. Planat, the degree of degeneracy of the energy level nhf is equal to the number of unrestricted partitions of the integer n i.e. the number of different ways to calculate n as a sum of integers. The explicit consideration of this degeneration in the partition function per mode (instead of it being implicitly included in the density of modes as in the standard formulation) introduced changes in the standard calculation of the spectral density of thermal phonons, which eventually lead M. Planat to a hyperbolic fluctuation spectrum at low frequencies.

Indeed, under this approach, the natural logarithm of the partition function per mode is written:

$$\ln(\tilde{Z}(f, T)) = -\sum_{n \geq 1} \ln(1 - \exp(-\beta h n f)) \quad (2.26)$$

with $\beta = 1/k_B T$, instead of:

$$\ln(\tilde{Z}(f, T)) = -\ln(1 - \exp(-\beta h n f)) \quad (2.27)$$

in standard Planck (photons) or Einstein-Debye (phonons) approaches. Nonetheless, in both cases, the internal energy per mode can be calculated by:

$$\tilde{E}(f, T) = -\frac{\partial \ln \tilde{Z}}{\partial \beta} \quad (2.28)$$

and the fluctuation of the internal energy per mode by (Gibbs (1902) and Einstein (1904 and 1909) [16]):

$$\tilde{\varepsilon}^2(f, T) = \langle (\tilde{E} - \langle \tilde{E} \rangle)^2 \rangle = -\frac{\partial^2 \ln \tilde{Z}}{\partial \beta^2} \quad (2.29)$$

M. Planat then used the standard spectral density of modes $D(f)$ to define the spectral density of energy:

$$u(f, T) = D(f)\tilde{E}(f, T) \quad (2.30)$$

and the power spectral density (PSD) of the energy fluctuations:

$$S_u(f, T) = D(f)\tilde{\varepsilon}^2(f, T) \quad (2.31)$$

and the PSD of the relative fluctuations of energy:

$$\frac{S_u(f, T)}{u^2(f, T)} = \frac{1}{D(f)} \frac{\varepsilon^2(f, T)}{\tilde{E}^2(f, T)} = \frac{1}{D(f)} \frac{\frac{\partial^2 \ln \tilde{Z}}{\partial \beta^2}}{\left(\frac{\partial \ln \tilde{Z}}{\partial \beta}\right)^2} \quad (2.32)$$

As in the standard approach for phonons in an isotropic crystal, M. Planat took a spectral density of modes equal to:

$$D(f) = \frac{12\pi V}{c_{ph}^3} f^2 \quad (2.33)$$

with V the volume of the crystal and $\frac{3}{c_{ph}^3} = \frac{1}{c_L^3} + \frac{1}{c_{T1}^3} + \frac{1}{c_{T2}^3}$, where c_L, c_{T1}, c_{T2} are the velocities of the longitudinal (L) and transverse (T_1, T_2) modes respectively.

In the standard approach, the complete calculation can be carried out analytically (by casting Eqs. (2.26), (2.30), (2.31), and (2.33) in Eq. (2.32)) and we find:

$$\frac{S_u(f, T)}{u^2(f, T)} = \frac{c_{ph}^3}{12\pi V} \frac{\exp\left(\frac{hf}{k_B T}\right)}{f^2} \quad (2.34)$$

which is proportional to $1/f^2$ at low frequencies.

Using his partition function (Eq. (2.26)) instead of the standard one, M. Planat found, in the limit of low frequencies, and after a mathematical proof using advanced notions of number theory:

$$\left[\frac{S_u(f, T)}{u^2(f, T)} \right]_{LF} = \frac{9hc_{ph}^3}{4\pi^3 V} \frac{1}{k_B T f} = \frac{A_{ph}}{V f} \quad (2.35)$$

The transition to the spectral density of relative fluctuations of frequency was then obtained by considering the $1/Q^4$ law proposed by P. Handel (*cf.* [17] and next chapter). The resulting formula is:

$$S_y(f) = \frac{S_\omega(f)}{\omega^2} = \frac{1}{Q^4} \frac{A_{ph}}{V f} = \frac{h_{-1}}{f} \quad (2.36)$$

where Q is the unloaded quality factor of the resonator.

The floor of the short-term stability is then classically given by Allan's standard deviation:

$$\sigma_{y_floor} = \sqrt{2 \ln(2) S_y(1Hz)} \quad (2.37)$$

However, the order of magnitude for σ_{y_floor} obtained from M. Planat's formula, in the case of a 5 MHz SC-cut resonator, using the volume under the electrodes, is 5×10^{-12} . This limit is far exceeded by the experimental results of the best resonators [18], [19] and [20].

In our opinion, this problem may be due to the fact that in his model, Planat used the standard density of modes. Thus, the modes corresponding to frequencies of the type nf with n integer are counted both in the partition function and in the density of modes.

Using an adapted density of modes with only the lowest frequency in each direction may avoid this double counting and lower the theoretical limit for the spectral power density of noise, but the $1/f$ behavior would probably disappear to give the standard $1/f^2$ behavior at low frequencies, so that we did not try to find the modified density of modes.

5. A possible explanation for the absence of observation of lower cut-off

Since $1/f$ noise cannot extend to infinitely small frequencies (otherwise the total power would diverge), experimentalists have tried to find a lower frequency cut-off value for this regime. However, most of the time this quest remained elusive, even for an observation period of 300 years of weather data [21]! In 2013, Markus Niemann *et al.* [22] proposed an explanation for this phenomenon by making a connection between power-law intermittency and $1/f$ noise. They used weak ergodicity breaking to explain the absence of observed cut-off frequency for $1/f$ by the fact that, the cut-off frequency f_c is nearly equal to the inverse of the observation time and got back an integrable power spectral density.

To illustrate their findings, they considered a two-state model with states up $I(t) = I_0$ and down $I(t) = -I_0$. After waiting a random time τ_i in any state, the particle chooses the next state to be up or down with equal probability. The waiting times in each of these states are supposed to be independently, identically distributed random variables with Probability Density Function (PDFs) with long tails $\psi(\tau) \propto \tau^{-(1+\alpha)}$ with $0 < \alpha < 1$. In their numerical experiment, for a given α , the waiting times were generated according to $\tau = c_\alpha X^{-1/\alpha}$, with X a random number uniformly distributed between 0 and 1 and c_α chosen so that $\langle n(1) \rangle \approx 10\,000$, with $n(t)$ the number of completed waiting times up to time t and $\langle \rangle$ the ensemble average (10 000 realizations of times series in their case). Then, for a given measurement time t , they defined the power spectrum by:

$$S_t(\omega) = [\tilde{I}_t(\omega)\tilde{I}_t^*(\omega)]/t, \text{ with } \tilde{I}_t(\omega) = \int_0^t I(t')\exp(-i\omega t')dt' \quad (2.38)$$

A plot of $\langle S_t(\omega) \rangle$ for various values of the measurement time t clearly matches their theoretical result that²⁰:

$$\langle S_t(\omega) \rangle \approx \frac{2I_0^2 \cos(\frac{\alpha\pi}{2})}{\Gamma(1+\alpha)} \frac{t^{\alpha-1}}{|\omega|^{2-\alpha}} \text{ as } \omega \rightarrow 0 \quad (2.39)$$

Furthermore, from Eq. (2.38), we get $S_t(0) = \left| \int_0^t I(t') dt' \right|^2 / t \equiv |\bar{I}|^2 t$ for a single realization and $\langle S_t(0) \rangle = I_0^2(1-\alpha)t$ for the ensemble average²¹. Niemann et al. then define a crossover circular frequency ω_c by the approximation that $\langle S_t(\omega) \rangle$ is constant between 0 and ω_c and equal to Eq. (2.39) for $\omega > \omega_c$. Hence,

$$\frac{2I_0^2 \cos(\frac{\alpha\pi}{2})}{\Gamma(1+\alpha)} \frac{t^{\alpha-1}}{|\omega_c|^{2-\alpha}} = \langle S_t(\omega_c) \rangle = \langle S_t(0) \rangle = I_0^2(1-\alpha)t \implies \omega_c = \frac{1}{t} \frac{2 \cos(\frac{\alpha\pi}{2})}{(1-\alpha)\Gamma(1+\alpha)} \quad (2.40)$$

The crossover frequency is thus inversely proportional to the measurement time: the measurement itself sets the time scale for the crossover since there is no time scale in the dynamics of the process²²! This means that for such intermittent power-law processes it is not useful to increase the measurement time to try to see the crossover frequency since it will decrease with the increase of the measurement time. Furthermore, this resolves the nonintegrability paradox, since the amplitude of the power spectrum itself decreases with time:

$$\begin{aligned} \int_0^\infty \langle S_t(\omega) \rangle d\omega &\approx I_0^2(1-\alpha)t\omega_c + \int_{\omega_c}^\infty \frac{2I_0^2 \cos(\frac{\alpha\pi}{2})}{\Gamma(1+\alpha)} \frac{t^{\alpha-1}}{|\omega|^{2-\alpha}} d\omega \\ &= \frac{2-\alpha}{1-\alpha} \left[I_0^2(1-\alpha) \right]^{1-\alpha} \left(\frac{2I_0^2 \cos(\frac{\alpha\pi}{2})}{\Gamma(1+\alpha)} \right)^{1/(\alpha-2)} \end{aligned} \quad (2.41)$$

Hence $\int_0^\infty \langle S_t(\omega) \rangle d\omega$ indeed turns out to be finite and measurement time independent.

Finally, we point out that Niemann et al. proposed two tests to experimentalists to check whether or not measured data (or numerical simulation data) is compatible with intermittency-caused $1/f^{2-\alpha}$ noise with $0 < \alpha \leq 1$:

- The first one is to check that $\langle S_t(\omega) \rangle$ indeed decays as $t^{\alpha-1}$ with the measurement time t .
- The second one is to compare the distribution of frequency averaged spectrum $M = \frac{1}{N} \sum_{i=1}^N \frac{S_t(\omega_i)}{\langle S_t(\omega_i) \rangle}$ (with N large enough), with a normalized Mittag-Leffler distribution Y_α (see e.g. http://en.wikipedia.org/wiki/Mittag-leffler_distribution).

²⁰ $\Gamma(t) = \int_0^\infty x^{t-1} e^{-x} dx$ is the function that generalizes the factorial since $\Gamma(t+1) = t\Gamma(t)$ and $\Gamma(1) = 1$.

²¹ For the non ergodic processes considered by Niemann *et al.* the time average of a quantity remains a random variable in the infinite time limit and is thus not equal to its ensemble average.

²² Furthermore $1/t$ appears as the frequency resolution of the discrete Fourier transform used in spectral analysis.

6. Other interesting models of $1/f$ noise

- In 1980, B. Pellegrini showed that the flicker noise arises in islands, of any size (from a few nm to several μm), which are enclosed by a potential-energy barrier or which, especially for the smallest volumes, present an energy well for the carriers [23]. This model was later improved in several papers, see, e.g. [24] and references therein.
- In 1983, E. Marinari *et al.* proposed a model of $1/f$ power spectrum from one-dimensional random walks in random environments [25].
- In 2007, Erland and Greenwood proposed a general mathematical construction of reversible Markov chains which leads to $1/\omega^\alpha$ noise with α between 0.5 and 1.5 [26].
- In 2007, K. A. Kazakov gave a new model of flicker noise by considering the quantum fluctuations of coulomb potential [27].
- In 2011, T. Prevenslik proposed another quantum theory of flicker noise, in the case of nanowires [28].

7. Conclusions

Many mathematical models have been proposed to explain the origin of $1/f^\alpha$ noise with $0.5 < \alpha < 1.5$. However, exact $1/f$ noise is still pretty much controversial since very few papers propose a way to compute the amplitude of the $1/f$ noise for a particular system. Furthermore, there are even fewer papers providing a specific model suitable for quartz ultra-stable oscillators compared to what exists for electronic devices. We shall see in the next two chapters two possible route towards this goal, namely Handel's quantum theory of $1/f$ noise and the study of the hysteretic motion of dislocations using the Fluctuation-Dissipation theorem.

8. References

- [1] J. B. Johnson, “The Schottky effect in low frequency circuits”, *Phys. Rev.*, vol. 26, no. 1, pp. 71-85, 1925.
- [2] W. H. Press, “Flicker noises in astronomy and elsewhere”, *Comments Astrophys.*, vol. 7, no 4, pp. 103-119, 1978.
- [3] W. Schottky, “Small shot-effect and flicker-effect”, *Phys. Rev. Lett.*, vol. 28, no. 1, pp. 74-103, 1926. (errata in *Phys. Rev.*, vol. 28, no. 6, pp. 1131-1131, 1926).
- [4] E. Milotti, “ $1/f$ noise: a pedagogical review”, unpublished (but cited more than 50 times!...), <http://arxiv.org/abs/physics/0204033>, 2002.
- [5] J. Bernamont, “Fluctuations in the resistance of thin films”, *Proc. Phys. Soc.*, vol. 49, pp. 138-139, 1937.
- [6] A. R. Butz, “A theory of $1/f$ noise”, *J. Stat. Phys.*, vol. 4, no. 2-3, pp. 199-216, 1972.
- [7] F. K. Du Pré, “A suggestion regarding the spectral density of flicker noise”, *Phys. Rev. Lett.*, vol. 78, no. 5, pp. 615-615, 1950.
- [8] P. Dutta, P. Dimon and P. M. Horn, “Energy scales for noise processes in metals”, *Phys. Rev. Lett.*, vol. 43, no. 9, pp. 646-649, 1979.
- [9] F. N. Hooge and P. A. Bobbert, “On the correlation function of $1/f$ noise”, *Physica B*, vol. 239, no. 3-4, pp. 223-230, 1997.
- [10] C. M. van Vliet, “Random walk and $1/f$ noise”, *Physica A*, vol. 303, pp. 421-426, 2002.
- [11] B. Kaulakys and T. Meškauskas, “Modeling of $1/f$ noise”, *Phys. Rev. E*, vol. 58, no. 6, pp. 7013-7019, 1998.
- [12] P. Bak, C. Tang and K. Wiesenfeld, “Self-Organized Criticality: An Explanation of $1/f$ Noise”, *Phys. Rev. Lett.*, vol. 59, no. 4, pp. 381-384, 1987.
- [13] P. De Los Rios and Y. Zhang, “Universal $1/f$ Noise from Dissipative Self-Organized Criticality Models”, *Phys. Rev. Lett.*, vol. 82, no. 3, pp. 472-475, 1999.
- [14] V. N. Skokov, A. V. Reshetnikov, V. P. Koverda, A. V. Vinogradov, “Self-organized criticality and $1/f$ -noise at interacting nonequilibrium phase transitions”, *Physica A*, vol. 293, no. 1-2, pp. 1-12, 2001.
- [15] M. Planat, “Thermal $1/f$ noise from the theory of partitions: application to a quartz resonator”, *Physica A*, vol. 318, pp. 371–386, 2003.
- [16] F. E. Irons, “Reappraising Einstein’s 1909 application of fluctuation theory to planckian radiation”, *Am. J. Phys.*, vol. 72, no. 8, pp. 1059–1067, August 2004.
- [17] P. H. Handel, “Nature of $1/f$ frequency fluctuations in quartz crystal resonators”, *Solid State Electronics*, vol. 22, pp. 875–876, 1979.

- [18] J. R. Norton, “Performance of ultrastable quartz oscillators using BVA resonators”, in Proc. European Frequency and Time Forum, Munich, Germany, pp. 457–465, 1994.
- [19] F. L. Walls, “The quest to understand and reduce $1/f$ noise in amplifiers and BAW quartz oscillators”, in Proc. European Frequency and Time Forum, Besançon, France, pp. 227-243, 1995.
- [20] P. Salzenstein, A. Kuna, L. Sojdr, and J. Chauvin, “Significant step in ultra-high stability quartz crystal oscillators”, *Elec. Lett.*, vol. 46, no. 21, pp. 1433–1434, 2010.
- [21] B. B. Mandelbrot and J. R. Wallis, “Some long-run properties of geophysical records”, *Water Resour. Res.*, vol. 5, no. 2, pp. 321-340, 1969.
- [22] M. Niemann, H. Kantz, and E. Barkai, “Fluctuations of $1/f$ noise and the low-frequency cutoff paradox”, *Phys. Rev. Lett.*, vol. 110, no. 14, pp. 140603, 5 pages, 2013.
- [23] B. Pellegrini, “New theory of flicker noise”, *Phys. Rev. B*, vol. 22, no. 10, pp. 4684-4691, 1980.
- [24] B. Pellegrini, “Semiconductor noise”, *Phys. Rev. B*, vol. 38, no. 12, pp. 8269-8278, 1988.
- [25] E. Marinari, G. Parisi, D. Ruelle, P. Windey, “Random Walk in a Random Environment and $1/f$ Noise”, *Phys. Rev. Lett.*, vol. 50, no. 17, pp. 1223-1225, 1983.
- [26] S. Erland, P. E. Greenwood, “Constructing $1/\omega^{\alpha}$ noise from reversible Markov chains”, *Phys. Rev. E*, vol. 76, no. 3, pp. 031114 (13 pages), 2007.
- [27] K. A. Kazakov, “Quantum fluctuations of Coulomb potential as a source of Flicker noise: the influence of a heat bath”, *J. Phys. A: Math. Theor.*, vol. 40, no. 20, pp. 5277-5296, 2007.
- [28] T. Prevenslik, “ $1/f$ noise in nanowires by quantum mechanics”, unpublished, 2012.
(<http://www.nanoqed.org/resources/2012/Noise.pdf>)

Chapter 3: Investigation of Quantum 1/f noise

1. On some of Handel's theories concerning 1/f noise

1.1. *Handel's theory of quantum 1/f noise in electronic devices*

During the last few decades lots of papers have been published on the theory of quantum 1/f noise. In 1975, P. H. Handel devised a quantum theory of 1/f noise [1], [2], [3], [4] in electronic devices by assuming that the origin of 1/f noise is due to the intrinsic current fluctuations during the quantum interaction of the current carriers with some scattering electromagnetic field (which for one current carrier can be due solely to the interaction with the other current carriers). Indeed, in these conditions, some change of speed of current carriers may occur, which must be accompanied by the emission of one or several photon(s) (so-called Bremsstrahlung process). The differential cross-section for the emission of a low energy photon has the peculiarity of being inversely proportional to that (small) energy ϵ (hence frequency since $\epsilon = hf$ for a photon) [4]²³. Handel then first proved [1] that this translates into DC current fluctuations with a power spectral density similar to the phenomenological expression of Hooge, then that the power spectral density of the phase fluctuations of an electric AC current also has a 1/f spectrum [2]²⁴. Paper [3] essentially reviews the physical meaning, accuracy and limits of application of the approximations done in [1].

Since paper [2] uses results of paper [1], we shall summarize both of these papers at the same time to illustrate the claim by Handel, that **the intrinsic quantum 1/f noise²⁵ is due to quantum beats between two quantum waves. The first one is attached to the current carriers that contributes to the nominal frequency of the signal. The second one corresponds to the quantum of current carriers that have emitted low energy photons in Bremsstrahlung processes one at a time and independently.** Indeed, according to this mechanism, the individual current carriers that have emitted a Bremsstrahlung photon contribute to frequencies with small differences to the nominal frequency and therefore to the fluctuations of the nominal frequency. In paper [2], P. H. Handel assumes that, in the presence of a harmonic signal of circular frequency ω_0 ,

²³ This means that the amount of energy radiated through these low-energy photons is the same in any frequency interval of given bandwidth df , down to $f = 0$, so that a logarithmically divergent number of photon are emitted in the low energy limit.

²⁴ In fact, if one takes into account both real and virtual multi-photon processes, one does not find exactly 1/f but $1/f^{1-\alpha A}$, where $\alpha = 2\pi e^2 / (4\pi\epsilon_0)hc \approx 1/137$ is the so-called fine structure constant of quantum electrodynamics and $A \approx \frac{8}{3\pi} \left(\frac{v}{c}\right)^2 \sin^2 \frac{\theta_0}{2}$, with $v \ll c$ the speed of the current carrier and $\theta_0 \ll 1$ the change of direction of this speed during the emission. Hence $\alpha A \ll 1$. This little change is nonetheless very important it renders convergent the otherwise logarithmically divergent spectral integral.

²⁵ Being intrinsic to the motion of charge carriers in an electric device, this contribution is supposed to always exist and be the lower limit for 1/f noise, since other contributions of different physical origins may also exist.

the state of a current carrier can be written as a mixture of pure quantum states, among which one can find states of the following form:

$$\Psi_0(\vec{r}, t) = a\{\exp[(i/\hbar)(\vec{p}_1 \cdot \vec{r} - E_1 t)] + \exp[(i/\hbar)(\vec{p}_2 \cdot \vec{r} - E_2 t)]\} \quad (3.1)$$

where, $E_2 - E_1 = \hbar\omega_0$. This kind of split states generates a current $\vec{j}_0 = \frac{\hbar}{2mi}(\Psi_0^+ \nabla \Psi_0 - \Psi_0 \nabla \Psi_0^+)$ of circular frequency ω_0 . However, the interaction of the wave function (3.1) with the quantized electromagnetic field gives rise to low-frequency photon emission or absorption. As a result, the current carrier wave function must be complemented by a coherent superposition of waves with slightly different energies:

$$\Psi(\vec{r}, t) = a\{\exp[(i/\hbar)(\vec{p}_1 \cdot \vec{r} - E_1 t)] + \exp[(i/\hbar)(\vec{p}_2 \cdot \vec{r} - E_2 t)]\} + \int_{\epsilon_0}^{\epsilon_1} b_\epsilon \{\exp[(i/\hbar)(\vec{p}'_1 \cdot \vec{r} - (E_1 - \epsilon)t)] + \exp[(i/\hbar)(\vec{p}'_2 \cdot \vec{r} - (E_2 - \epsilon)t)]\} a_\epsilon^+ \frac{d\epsilon}{\sqrt{\epsilon}} \quad (3.2)$$

where ϵ_0 is either the soft-photon detection threshold or the lower-frequency limit of the electric-current-noise spectral measurement, $\epsilon_1 \ll E_1, E_2$ is some arbitrary energy loss which must be weak enough not to change appreciably the momentum amplitude of the current carrier, b_ϵ is a relative amplitude connected to the differential emission cross-section for a photon of energy ϵ and a_ϵ^+ is the normed second quantization creation operator for this photon of energy ϵ , emitted in any direction²⁶:

$$a_\epsilon^+ = \frac{\sqrt{\hbar c}}{\epsilon} \int_0^{4\pi} f_\epsilon^*(\theta, \varphi) a_k^+ k^2 d\Omega_k, \text{ with } \int_0^{4\pi} |f_\epsilon^*(\theta, \varphi)|^2 d\Omega_k = 1 \text{ and } \epsilon/\hbar c = |\vec{k}| = k \quad (3.3)$$

$$\frac{b_\epsilon}{a} = (\alpha A)^{\frac{1}{2}} (\epsilon/\epsilon_0)^{\alpha A/2} e^{i\gamma(\epsilon)} \equiv \rho_\epsilon e^{i\gamma(\epsilon)}, \quad (3.4)$$

where $\alpha = e^2/(4\pi\epsilon_0)\hbar c \approx 1/137$ is the so-called fine structure constant of quantum electrodynamics and A is defined thanks to an approximate expression for the infrared exponent of the Bremsstrahlung photon emission differential cross-section for small four-momentum transfers (adapted from Eq. 2.34 of Ref. [4]):

$$A \approx \frac{8}{3\pi} \left(\frac{v}{c}\right)^2 \sin^2 \frac{\theta_0}{2} = \frac{2}{3\pi} \left(\frac{\Delta v}{c}\right)^2 \quad (3.5)$$

where v is the velocity norm of the current carrier before and after emission (small transfer!) and θ_0 is the change of direction of this speed during the transfer ($\Delta v = 2v \sin(\theta_0/2)$).

Now subtracting dc and dc/df noise currents from the total current calculated from this new wave function, the ac current contribution \vec{j}^\sim is given by²⁷:

²⁶ In the following formula, a_ϵ^+ is homogeneous to $1/\sqrt{\epsilon}$, while a_k^+ is homogeneous to $k^{-3/2}$.

²⁷ In paper [3], P. H. Handel states that the inclusion of an electromagnetic vector potential term into the definition of the current operator would add terms in the current (linear and quadratic in this vector potential) that can be neglected with respect to the leading $1/f$ term, because they are at least a factor $\alpha v/c$ smaller.

$$\vec{j}^- = \left(\frac{|a|^2}{m}\right) \{ \vec{p}_1 \exp[-i\omega_0 t + (i/\hbar)(\vec{p}_1 - \vec{p}_2) \cdot \vec{r}] + \vec{p}_2 \exp[i\omega_0 t - (i/\hbar)(\vec{p}_1 - \vec{p}_2) \cdot \vec{r}] \} \\ \times \left(1 + \int_{\epsilon_0}^{\epsilon_1} \rho_\epsilon \{ \exp[i\epsilon t/\hbar + i\gamma(\epsilon)] a_\epsilon^+ + \exp[-i\epsilon t/\hbar - i\gamma(\epsilon)] a_\epsilon \} \left(\frac{d\epsilon}{\sqrt{\epsilon}}\right) \right) \\ + \int_{\epsilon_0}^{\epsilon_1} \int_{\epsilon_0}^{\epsilon_1} \rho_\epsilon \rho_{\epsilon'} \exp[i(\epsilon' - \epsilon) t/\hbar + i\gamma(\epsilon') - i\gamma(\epsilon)] a_\epsilon a_{\epsilon'}^+ \left(\frac{d\epsilon}{\sqrt{\epsilon}}\right) \left(\frac{d\epsilon'}{\sqrt{\epsilon'}}\right) \right) \quad (3.6)$$

The (small) phase shift $\delta\varphi \ll \pi$ of this contribution with respect to $\omega_0 t + ((\vec{p}_1 - \vec{p}_2)/\hbar) \cdot \vec{r}$ can be detected either by coherent detection (multiplication by a quadrature carrier $A \sin(\omega_0 t)$ followed by low-pass filtering) or by envelop detection (addition of a quadrature carrier followed by rectification, low-pass filtering and subtraction of the constant). In both cases, the intensity of the detected signal will be proportional to $\delta\varphi$, with a proportionality constant named k_D by Handel. Replacing everywhere $\cos[\omega_0 t - (\vec{p}_1 - \vec{p}_2) \cdot \vec{r}]$ by $k_D \sin \varphi$ in the real part of Eq. (3.6), the expression of the detected current density is found to be:

$$\vec{J}_D = -k_D \left(\frac{|a|^2}{m}\right) (\vec{p}_1 - \vec{p}_2) \left\{ \int_{\epsilon_0}^{\epsilon_1} \rho_\epsilon \sin[\epsilon t/\hbar + \gamma(\epsilon)] (a_\epsilon^+ - a_\epsilon) \left(\frac{d\epsilon}{\sqrt{\epsilon}}\right) \right. \\ \left. + \int_{\epsilon_0}^{\epsilon_1} \int_{\epsilon_0}^{\epsilon_1} \rho_\epsilon \rho_{\epsilon'} \sin[(\epsilon' - \epsilon) t/\hbar + \gamma(\epsilon') - \gamma(\epsilon)] a_\epsilon a_{\epsilon'}^+ \left(\frac{d\epsilon}{\sqrt{\epsilon}}\right) \left(\frac{d\epsilon'}{\sqrt{\epsilon'}}\right) \right\} \quad (3.7)$$

The autocorrelation function of the detected current can then be calculated as:

$$\langle \langle \vec{J}_D^+(t) \vec{J}_D(t + \tau) \rangle \rangle_{av} = k_D^2 \frac{|a|^4}{m^2} (\vec{p}_1 - \vec{p}_2)^2 \times \\ \int_{\epsilon_0}^{\epsilon_1} \int_{\epsilon_0}^{\epsilon_1} \rho_\epsilon \rho_{\epsilon'} \langle \sin\left[\frac{\epsilon t}{\hbar} + \gamma(\epsilon)\right] \sin\left[\frac{\epsilon'}{\hbar}(t + \tau) + \gamma(\epsilon')\right] \rangle_{av} \langle a_\epsilon a_{\epsilon'}^+ \rangle \left(\frac{d\epsilon}{\sqrt{\epsilon}}\right) \left(\frac{d\epsilon'}{\sqrt{\epsilon'}}\right) \\ = k_D^2 \frac{|a|^4}{2m^2} (\vec{p}_1 - \vec{p}_2)^2 \int_{\epsilon_0}^{\epsilon_1} \rho_\epsilon^2 \cos\left(\frac{\epsilon\tau}{\hbar}\right) \frac{d\epsilon}{\epsilon} \quad (3.8)$$

Where the first $\langle \ \rangle$ is the quantum expectation value and $\langle \ \rangle_{av}$ is a time average.

According to the Wiener-Khintchine theorem²⁸, the power energy density of the detected current is therefore found to be²⁹:

$$\langle \vec{J}_D^+ \vec{J}_D \rangle_\epsilon = \frac{k_D^2 |a|^4}{2 m^2} (\vec{p}_1 - \vec{p}_2)^2 \frac{\rho_\epsilon^2}{\epsilon} \quad (3.9)$$

The power energy density of phase fluctuations is then defined and calculated by Handel as³⁰:

$$\langle (\delta\varphi)^2 \rangle_\epsilon = \frac{\langle \vec{J}_D^+ \vec{J}_D \rangle_\epsilon}{k_D^2 \langle \vec{j}^- \rangle^2} = \frac{(\vec{p}_1 - \vec{p}_2)^2}{2(\vec{p}_1 + \vec{p}_2)^2} \left[1 - \int_{\epsilon_0}^{\epsilon_1} \rho_\epsilon^2 \frac{d\epsilon}{\epsilon} \right]^{-2} \frac{\rho_\epsilon^2}{\epsilon} \quad (3.10)$$

By introducing the definition of $\rho_\epsilon = (\alpha A)^{\frac{1}{2}} (\epsilon/\epsilon_0)^{\alpha A/2}$, performing the integration and finally replacing the energies by frequencies, one finds that the power spectral density of phase fluctuations is given by:

²⁸ Cf. e.g. http://en.wikipedia.org/wiki/Wiener-Khintchine_theorem

²⁹ $\langle \vec{J}_D^+ \vec{J}_D \rangle_\epsilon = \int_{-\infty}^{+\infty} \langle \vec{J}_D^+(t) \vec{J}_D(t + \tau) \rangle_{av} \exp\left(-\frac{i\epsilon\tau}{\hbar}\right) d\tau/\hbar$
 $= k_D^2 \frac{|a|^4}{2m^2} (\vec{p}_1 - \vec{p}_2)^2 \int_{\epsilon_0}^{\epsilon_1} \rho_{\epsilon'}^2 \int_{-\infty}^{+\infty} \cos\left(\frac{\epsilon'\tau}{\hbar}\right) \exp\left(-i\left(\frac{\epsilon\tau}{\hbar}\right)\right) d\left(\frac{\tau}{\hbar}\right) \frac{d\epsilon'}{\epsilon'}$

³⁰ In Handel's paper, it is $[1 + \int_{\epsilon_0}^{\epsilon_1} \rho_\epsilon^2 \frac{d\epsilon}{\epsilon}]$ and not $[1 - \int_{\epsilon_0}^{\epsilon_1} \rho_\epsilon^2 \frac{d\epsilon}{\epsilon}]$ which surprises us.

$$S_{\varphi}(f) = \left(\frac{\alpha A}{2}\right) \frac{(\bar{p}_1 - \bar{p}_2)^2}{2(\bar{p}_1 + \bar{p}_2)^2} \left(\frac{f f_0}{f_1^2}\right)^{\alpha A} f^{-1} \quad (3.11)$$

Integrating over frequencies from f_0 to f_1 , we obtain a finite total equivalent phase dispersion:

$$\int_{f_0}^{f_1} S_{\varphi}(f) df = \left(\frac{1}{2}\right) \frac{(\bar{p}_1 - \bar{p}_2)^2}{2(\bar{p}_1 + \bar{p}_2)^2} (f_0/f_1)^{\alpha A} \left[1 - \left(\frac{f_0}{f_1}\right)^{\alpha A}\right] \quad (3.12)$$

Thus equation (3.11) shows that the spectral density of phase fluctuations is inversely proportional to the frequency i.e. $1/f$ spectrum.

According to Handel, $1/f$ noise similar to the equation (3.11) is obtained when the incoming particles are described by a density matrix which corresponds to incoherent mixture of states with a definite energy. This $1/f$ noise is an incoherent sum of $1/f$ noise contributions arising from all components of the density matrix. He suggested that, phase noise in a simple harmonic signal modifies the power spectrum of the current which carries the signal. On both sides of the δ function singularity present at the frequency of the harmonic signal, the power spectrum exhibits sidebands due to the random phase and frequency fluctuations which define phase noise.

P.H. Handel also suggests in [2] that the upper frequency limit f_1 is determined by the validity of the approximation $(\vec{p}'_{1,2} - \vec{p}_{1,2}) \cdot \vec{r} \ll \pi \hbar$. However, in the presence of negative feedback, the passage of the signal through the sample will be iterated over a closed loop, and $(\vec{p}' - \vec{p}) \cdot \vec{r}$ will lead to destructive self-interference, for which the condition $f \ll f_1$ is well satisfied. This results in a substantial reduction of $1/f$ phase noise generated by amplifiers or frequency multipliers, when feedback is included.

Since these 1975 papers, P. H. Handel has been applying his model to several physically different systems in numerous papers (see e.g. <http://www.umsl.edu/~handelp/QuantumBib.html>). On the same web site (<http://www.umsl.edu/~handelp/research.htm#res1>) he also summarizes his findings on quantum $1/f$ noise effects by writing that “These simple and fundamental effects explain $1/f$ noise as a universal infrared divergence phenomenon. According to this theory, any current I with infrared-divergent coupling to a system of infraquanta must exhibit $1/f$ noise with a spectral density of fractional fluctuations of $2\alpha/\pi f N$ (coherent quantum $1/f$ effect observed in large samples, devices or systems) or $2\alpha A/f N$ (conventional quantum $1/f$ effect observed in small devices or systems). Here N is the number of carriers in the sample used for the definition of the current I . For electric currents, taking the photons as infraquanta, we get a quantum $1/f$ noise contribution with $\alpha = 1/137$ the fine structure constant. Finally³¹, $\alpha A = (2\alpha/3\pi)(\Delta v/c)^2$ is the

³¹ We have taken the liberty to correct a typing error on Handel’s web site since, there, it is written $\alpha A = (2\alpha/3\pi)(\Delta v/e)^2$ (e instead of c).

infrared exponent, essentially the quadratic velocity change in the process considered, in units of the speed of light".³² Concerning experimental verifications, Handel states on the same web page that "The theory has been verified in many ways: $1/f$ noise was found experimentally to be caused by mobility fluctuations, not carrier concentration fluctuations, and the magnitude and temperature dependence was shown to agree with the measurements in submicron metal films and vacuum tubes. Furthermore, $1/f$ fluctuations in the rate of α -radioactive decay, predicted by the theory in 1975 have been verified experimentally, recently also for I^{131} -decay³³. Additional evidence comes from $1/f$ noise in frequency standards and in SQUIDS. Finally, the quantum $1/f$ noise theory has recently been most successful in explaining partition noise in vacuum tubes, and $1/f$ noise in transistors, pen junctions and infrared radiation detectors." We also note that this theory was favorably presented in several papers by Aldert van der Ziel, including his 1988 review [19] from which, we reproduce the conclusion:

"This project started as an attempt to verify or refute the predictions made by Handel's quantum $1/f$ noise theories; more particularly his theory of the Hooge parameter α_H . This is now practically complete, except for some more work on vacuum photodiodes, on BJTs and on ballistic devices. We see from Section V, that Handel's result, if properly applied to the device under test, agrees with our measurements in nearly all cases. Both the experimental numbers for the various α_H values and their agreement with Handel's predictions represent scientific information that should not be ignored.

Our project cannot check the validity or invalidity of Handel's derivation of his predictions for α_H . This is the domain of the theoreticians. They have every right to criticize the derivation and replace it by a better one. In the latter case, they should see to it that their prediction for α_H agrees with Handel's prediction for α_H , when the latter has been verified experimentally. Up to now this has not been done.

It is difficult for some scientists to understand how a theory that is in their opinion incorrect can give correct predictions. It must be emphasized that only experiment can decide whether a conclusion is correct or incorrect. In our situation experiments decided that the predictions were right, and I see no way to avoid this conclusion.

Since the accuracy of the measurements is ± 30 percent, correction factors close to unity cannot be detected."

³² We also note incidentally that section IV of Ref. [11] proposes a general "Sufficient Criterion for Fundamental $1/f$ Noise".

³³ There must be a typing mistake or a problem during the conversion to HTML here also.

1.2. Criticisms of Handel's theory

In the first papers in a series, it seems to us that P.H. Handel puts more the emphasis on physical ideas than mathematical rigorousness. Furthermore, the use of ad hoc units such that $c = 1, \hbar = 1$ or the use of CGS units does not facilitate the understanding of some formula through dimensions equation analysis. However, in subsequent papers, remarks or notes often provide more insights, explanations or corrections of small calculations mistakes. This may be a reason why, although Handel's theory has proved interesting as a guide for the optimization and study of several electronic devices, it has remained quite controversial over the years with strong opponents. See e.g. comments by Weissman in his 1988 review [7]³⁴. Some more recent comments (2010) by Weissman can also be found in http://en.wikipedia.org/wiki/Talk:Quantum_1/f_noise³⁵.

In 1986, L. B. Kiss and P. Heszler published a paper [8] in which they claim to prove the invalidity of Handel's model of $1/f$ noise: "On the basis of rigorous quantum electrodynamics we show that the value of the beating term is zero at any given time, consequently this hypothetical type of $1/f$ noise does not exist". Since this paper is quite short and is in our opinion wrong, we study it here.

For them, P. H. Handel starts from the idea that an electron Schrodinger field $\Psi_x(\vec{r}, t)$ emerging from a scattering event consists of two parts, a weak Bremsstrahlung part $\Psi_{Br}(\vec{r}, t)$, and a larger non-Bremsstrahlung part, $\Psi_{no}(\vec{r}, t)$. The Bremsstrahlung part, $\Psi_{Br}(\vec{r}, t)$ of the electron wave function is the sum of components $\Psi_{Br}^i(\vec{r}, t)$, describing the probabilities of different photon emission events during the scattering (i labels the different frequencies and polarizations that the emitted photon can have. Note that the remaining electron then has a lower frequency due to energy conservation):

$$\Psi_{Br}(\vec{r}, t) = \sum_i \Psi_{Br}^i(\vec{r}, t) \quad (3.13)$$

The probability density of the scattered electron is:

³⁴ "Some of the theories that try to find a fundamental explanation of the Hooge formula are well enough known to make it worthwhile to look at some of their particulars, despite the general argument against such theories as an explanation for $1/f$ noise. The theory of Handel (1980) and the related theory of Ngai (1980) both explain $1/f$ noise as arising from quantum beats between elastically scattered and weakly inelastically scattered carriers, with different inelastic scattering mechanisms used by the two theories. In order to obtain the low-frequency beats, however, monochromatic incident quantum waves are assumed—a completely unrealistic assumption in view of the fact that thermal frequencies are almost always 6-15 orders of magnitude greater than the frequencies in the observed $1/f$ range. Severe problems also arise for the theory when one remembers that the wave packet is localized within the sample, so that the beats, if any, integrate to zero."

³⁵ "The basic reasons that this "theory" cannot be correct are: 1. It treats the wave function of an electron which has some amplitude for having had a weakly inelastic scattering event as a coherent superposition of the scattered and unscattered components, with the noise coming from their interference. Of course, those components are actually entangled with different versions of the scatterer and therefore exist as an incoherent interference-free mixture (density matrix). 2. In almost every reported case, the characteristic noise times extend to much longer than the dwell time of the carrier in the device. That rules out not only the Handel idea but any other idea that treats the noise as coming from independent properties of individual mobile carriers."

$$\rho(r, t) = |\Psi_x(\vec{r}, t)|^2 \quad (3.14)$$

$$\rho(r, t) = |\Psi_{no}(\vec{r}, t)|^2 + \sum_i |\Psi_{Br}^i(\vec{r}, t)|^2 + \sum_i \Psi_{Br}^{i*}(\vec{r}, t) \Psi_{no}(\vec{r}, t) + \sum_i \Psi_{no}^*(\vec{r}, t) \Psi_{Br}^i(\vec{r}, t) \quad (3.15)$$

The cross terms $\Psi_{Br}^{i*}(\vec{r}, t) \Psi_{no}(\vec{r}, t)$ and $\sum_i \Psi_{no}^*(\vec{r}, t) \Psi_{Br}^i(\vec{r}, t)$ are beating (oscillating) in space and time because they are the products of frequency-shifted and non-shifted components. As we have seen in the previous paragraph, Handel then uses approximate results for the infrared contribution to the emission cross-section to show that the low-frequency power density spectrum of the third and fourth terms in the right-hand side of Eq. (3.15) is of $1/f$ -type.

Restricting themselves to one photon emission processes, Kiss and Heszler proposed alternatively that the exact wavefunction of the entire system should also include wavefunctions for photons of all types multiplying the corresponding parts for the electron:

$$\Psi_{sys}(\vec{r}, \vec{z}_1, \dots, \vec{z}_i, \dots, t) = \Psi_{no}(\vec{r}, t) \prod_k \Phi_0^k(\vec{z}_k, t) + \sum_i (\Psi_{Br}^i(\vec{r}, t) \Phi^i(\vec{z}_i, t) \prod_{j \neq i} \Phi_0^j(\vec{z}_j, t)) \quad (3.16)$$

Where $\Phi_0^k(z_k, t)$ is the vacuum wavefunction for type k photons that have not been irradiated and $\Phi^i(\vec{z}_i, t)$ is the wave function for an irradiated photon of type i (where \vec{z}_j is the space vector of a type j photon).

The electron probability density can then be calculated by integrating on the coordinates of all the photons, with $d\vec{z} = \prod_i d\vec{z}_i$:

$$\begin{aligned} \rho(\vec{r}, t) &= \int_{\prod_i v_i} |\Psi_{sy}(r, z_1, \dots, z_i, \dots, t)|^2 d\vec{z} \\ \rho(\vec{r}, t) &= \int_{\prod_i v_i} |\Psi_{no}(\vec{r}, t) \prod_k \Phi_0^k(\vec{z}_k, t)|^2 d\vec{z} + \int_v |\sum_i (\Psi_{Br}^i(\vec{r}, t) \Phi^i(\vec{z}_i, t) \prod_{j \neq i} \Phi_0^j(\vec{z}_j, t))|^2 d\vec{z} \\ &\quad + \int_{\prod_i v_i} (\Psi_{no}^*(\vec{r}, t) \prod_k \Phi_0^{k*}(\vec{z}_k, t) \sum_i (\Psi_{Br}^i(\vec{r}, t) \Phi^i(\vec{z}_i, t) \prod_{j \neq i} \Phi_0^j(\vec{z}_j, t))) d\vec{z} \\ &\quad + \int_{\prod_i v_i} (\Psi_{no}(\vec{r}, t) \prod_k \Phi_0^k(\vec{z}_k, t) \sum_i (\Psi_{Br}^{i*}(\vec{r}, t) \Phi^{i*}(\vec{z}_i, t) \prod_{j \neq i} \Phi_0^{j*}(\vec{z}_j, t))) d\vec{z} \end{aligned} \quad (3.17)$$

Using the following relations of the photon wavefunctions (according to them)

$$\int_v \Phi^{j*}(\vec{z}_j, t) \Phi^k(\vec{z}_k, t) d\vec{z}_j d\vec{z}_k = \delta_{jk} \text{ and presumably also } \int_v \Phi_0^{j*}(\vec{z}_j, t) \Phi_0^k(\vec{z}_k, t) d\vec{z}_j d\vec{z}_k = \delta_{jk},$$

Kiss and Heszler claimed that Eq. (3.17) would simplify into:

$$\begin{aligned} \rho(r, t) &= |\Psi_{no}(\vec{r}, t)|^2 + \sum_i |\Psi_{Br}^i(\vec{r}, t)|^2 + \Psi_{no}^*(\vec{r}, t) \sum_i \left\{ \Psi_{Br}^i(\vec{r}, t) \int_v \Phi_0^{i*}(\vec{z}_i, t) \Phi^i(\vec{z}_i, t) d^2 \vec{z}_i \right\} \\ &\quad + \Psi_{no}(\vec{r}, t) \sum_i \left\{ \Psi_{Br}^{i*}(\vec{r}, t) \int_v \Phi_0^i(\vec{z}_i, t) \Phi^{i*}(\vec{z}_i, t) d^2 \vec{z}_i \right\} \end{aligned} \quad (3.18)$$

Then, they claim that the 3rd and 4th terms of the above equation are corresponding to the 3rd and 4th term of the equation (3.15) and that since, according to them, $\int_v \Phi_0^j(\vec{z}_j, t) \Phi^{k*}(\vec{z}_k, t) d\vec{z}_j d\vec{z}_k = 0$, their 3rd and 4th term of the above equation become zero and

hence Handel's interference beating term does not exist physically. However (without even discussing the use of space-time functions for the photons), we note that in our opinions Eq. (3.18) is wrong because it should be:

$$\rho(r, t) = |\Psi_{no}(\vec{r}, t)|^2 + \sum_i |\Psi_{Br}^i(\vec{r}, t)|^2 + \Psi_{no}^*(\vec{r}, t) \sum_i \left\{ \Psi_{Br}^i(\vec{r}, t) \int_{v_i} \Phi_0^{i*}(\vec{z}_i, t) \Phi^i(\vec{z}_i, t) d\vec{z}_i \right\} \\ + \Psi_{no}(\vec{r}, t) \sum_i \left\{ \Psi_{Br}^{i*}(\vec{r}, t) \int_{v_i} \Phi_0^i(\vec{z}_i, t) \Phi^{i*}(\vec{z}_i, t) d\vec{z}_i \right\} \quad (3.19)$$

where we do not see why the remaining single integrals should be 0. Furthermore one can question whether their normalization relations should not be $\int_{v_i} \Phi_0^{j*}(\vec{z}_i, t) \Phi_0^k(\vec{z}_i, t) d\vec{z}_i = \delta_{jk}$, instead of the relation $\int_{v_i} \Phi_0^{j*}(\vec{z}_j, t) \Phi_0^k(\vec{z}_k, t) d\vec{z}_j d\vec{z}_k = \delta_{jk}$, they wrote in the paper. Then the conclusion of Kiss and Heszler does not seem firmly established for us. We also note that P. H. Handel published a detailed rebuttal of the paper of Kiss and Heszler [9].

Finally, we note that in 1987, Th. M. Neiuwenhuigen, D. Frenkel and N.G. van Kampen also published a paper [10] containing several physical and mathematical objections to Handel's theory of quantum $1/f$ noise, some of which seem much more serious than the above one. However, we do have demonstrations from Handel taking into account explicitly the correlations between bosons (photons, phonons,...) or fermions (electrons,...) e.g. in [11] in which one can find demonstrations of the conventional quantum $1/f$ effect and the coherent quantum $1/f$ effect³⁶, both in the second quantization framework and in an approximate semi-classical derivation. The problem is that the application of these formulae to frequency standards [12] and particularly the numerical estimates that can be computed for the hydrogen maser and Cs or Rb or laser clocks do not seem to convince the specialists.

1.3. Handel's theory of quantum $1/f$ noise for piezoelectric quartz crystal resonators

P. H. Handel has been applying these predictions to several physically different systems (see e.g. [6], [12], [13], [14]), among which quartz crystal resonators. Indeed, in the case of bulk acoustic wave resonators, the model proposed by Handel based on the "conventional quantum $1/f$

³⁶ Handel's predicts $1/f$ noise in any system whenever the cross section for scattering of particles exhibits an infrared divergence due to the generation of low-frequency excitations. Namely, the power spectral density of relative cross-section fluctuations in small devices or systems is given by (conventional quantum $1/f$ effect):

$$S_{\delta\sigma/\sigma}(f) = \frac{4\alpha(q/e)^2(\Delta v/c)^2}{3\pi f N}$$

while in bigger systems, coherence must be taken into account (coherent quantum $1/f$ effect) and the power spectral density of relative current density fluctuations is given by:

$$S_{\delta j/j}(f) = \frac{2\alpha}{\pi f N}$$

where N is the number of particles involved in the definition of the cross-section or the current density.

effect” is given in term of power spectral density of relative frequency fluctuations as follows (see [15] and all subsequent papers on that subject with Handel among the authors):

$$S_y(f) = \frac{\beta'V}{Q^4 f} \quad (3.20)$$

with V the active volume of the resonator (cm^3), Q the intrinsic quality factor of the resonator and β' a proportionality factor function of the physical parameters of the material that will be detailed (and numerically evaluated) below. The demonstration of this formula can be separated into three main steps.

1.3.1. Obtention of the power spectral density for the relative fluctuations of the number of interactions per unit time

For this part, we refer to e.g. [16] for a formal quantum derivation, to e.g. [13] or [14] for a semi-classical derivation by Handel and to [17] and [19] for a classical justification using Carson’s theorem³⁷ applied to the square root of the power dissipated, by van der Ziel.

The first step is to consider the disappearance of a phonon from the main mode f_0 of the resonator, due to an interaction supposed to be instantaneous (local in time $\delta(t - t_0)$). This elementary process leads to a sudden decrease hf_0 of the main mode total energy. The total fluctuation of the main mode energy therefore corresponds to the fluctuation in the number of phonons in that mode. Hence, the relative fluctuation of the power (P) is equal to the relative fluctuation in the number of interactions per unit time (Γ): ($\Delta\Gamma/\Gamma = \Delta P/P$). Two kinds of processes can occur. The first one, the three-phonon process is characterized by a number of interactions per second Γ' . It is characteristic of the non-harmonic part of the vibrations in a perfect crystal. In this case, a phonon of the main mode interacts with a thermal phonon to give another thermal phonon plus an energy amount of hf . At high temperatures, this process is dominant. The second one, the two-phonon process, characterized by Γ'' , involves the interaction of a phonon of the main mode with a primary defect of the resonator. This process gives a phonon in another mode and a defect having absorbed energy. This process is characteristic of a non-perfect crystal. This process is said to be the dominant one at very low temperature³⁸.

³⁷ Consider a realization of a series of random pulses $x_T(t) = \sum_{k=1}^K a_k f(t - t_k)$, with f a fixed pulse shape function of Fourier transform F and random amplitude a_k such that $\forall k, \langle a_k \rangle = \langle a \rangle$ the common mean pulse amplitude independent of the random t_k which are distributed uniformly in $[0, T]$. Its Fourier transform is given by $X_T(i\omega) = F(i\omega) \sum_{k=1}^K a_k \exp(-i\omega t_k)$ and its one-sided power spectral density by $S_X(\omega) = \lim_{T \rightarrow \infty} 2\langle |X_T(i\omega)|^2 \rangle / T$. It can then be demonstrated that:

$$S_X(\omega) = 2\nu \langle a^2 \rangle |F(i\omega)|^2 + 4\pi\nu^2 \langle a \rangle^2 |F(0)|^2 \delta(\omega) \quad (\text{Carson's theorem}),$$

with $\nu = \lim_{T \rightarrow \infty} K/T$, the average rate of pulse emission and $\langle a^2 \rangle = \lim_{T \rightarrow \infty} \sum_{k=1}^K \langle a_k^2 \rangle / K$ the mean-square of the pulse amplitudes.

³⁸ Here, we are considering not only intrinsic defects (since their number usually decreases exponentially with the inverse of T), but also extrinsic defects.

Total losses of the main mode per unit time are thus defined as the sum of both interaction rates of disappearance of a quantum of the main mode, following interaction with another phonon or a defect in the crystal: $\Gamma = \Gamma' + \Gamma''$. Furthermore, $\left| \frac{\delta\sigma}{\sigma} \right| = \left| \frac{\delta\Gamma}{\Gamma} \right|$ because the ratio Γ/σ , equal to the flux of phonon-phonon collisions and phonon-defect interactions, is considered constant because of the stability of the involved oscillators. Consequently the power spectral densities of relative fluctuations of cross-section, interaction rate, power are all the same.

According to Handel, the expression of the energy lost ΔE , in a unit frequency interval $\Delta f = 1$ Hz, due to the disappearance of phonon(s) from the main resonator mode is given by a law similar to Larmor's formula for Bremsstrahlung:

$$\frac{\Delta E}{\Delta f} = \frac{1}{4\pi\epsilon_0} \frac{2 \|\Delta\dot{\vec{P}}\|^2}{3c^3} \quad (3.21)$$

In order to try to demonstrate or at least justify this formula, we adopt the "elementary" derivation of his formula by Handel (see *e.g.* [13]) which starts from the classical Larmor formula (1897)³⁹ for the total electromagnetic power radiated in all the directions by a moving particle of charge q with acceleration a (Bremsstrahlung):

$$P = \frac{dE}{dt} = \frac{1}{4\pi\epsilon_0} \frac{2q^2 a^2}{3c^3} \quad (3.22)$$

P. H. Handel then makes an assumption that for a fluctuation event, there is an interaction of the particle with something else that changes its speed at a given time t . This gives rise to a supplementary acceleration of the form:

$$\vec{a}(t) = \Delta\vec{v}\delta(t) = \Delta\vec{v} \int_{-\infty}^{+\infty} e^{\pm i2\pi f t} df \quad (3.23)$$

Since the square of a Dirac delta has no meaning for a mathematician, Handel uses a trick to go further⁴⁰:

$$\begin{aligned} \int_{-\infty}^{+\infty} P dt &= \frac{1}{4\pi\epsilon_0} \frac{2q^2 \|\Delta\vec{v}\|^2}{3c^3} \int_{-\infty}^{+\infty} \int_{-\infty}^{+\infty} \int_{-\infty}^{+\infty} e^{-i2\pi f t} e^{-i2\pi f' t} df df' dt \\ &= \frac{1}{4\pi\epsilon_0} \frac{2q^2 \|\Delta\vec{v}\|^2}{3c^3} \int_{-\infty}^{+\infty} \int_{-\infty}^{+\infty} \left(\int_{-\infty}^{+\infty} e^{-i2\pi(f+f')t} dt \right) df' df \\ &= \int_{-\infty}^{+\infty} \frac{1}{4\pi\epsilon_0} \frac{2q^2 (\Delta\vec{v})^2}{3c^3} df \end{aligned} \quad (3.24)$$

This quantity is infinite, but it allows us first to recover Eq. (3.21)⁴¹, then to define a 1-sided spectral density of Bremsstrahlung energy radiated by a single charged particle due to a sudden speed change⁴².

³⁹ see *e.g.* Jackson - Classical electrodynamics (Wiley - 2001), paragraph 9.2 or http://en.wikipedia.org/wiki/Larmor_formula.

⁴⁰ We note incidentally that the total energy radiated by this suddenly accelerated charge (after the sudden change, if causality is to be respected...) is $\int_0^{+\infty} P dt$ and not $\int_{-\infty}^{+\infty} P dt!$...

⁴¹ $\Delta\dot{\vec{P}} = \Delta \left[\frac{d\vec{P}}{dt} \right] = \Delta \left[\frac{d}{dt} (\sum \vec{p}_i) \right] = \sum q_i \Delta\vec{v}_i$ with $\vec{p}_i = q_i \vec{\delta}_i$ and $\vec{v}_i = d\vec{\delta}_i / dt$, $\vec{\delta}_i$ being the difference of positions between the barycenter of positive charges (total q_i) and the barycenter of the negative charges (total $-q_i$) in unit cell i .

$$\frac{1}{4\pi\epsilon_0} \frac{4q^2 \|\Delta\vec{v}\|^2}{3c^3} = \frac{1}{4\pi\epsilon_0} \frac{4 \|\Delta\dot{\vec{P}}\|^2}{3c^3} \quad (3.25)$$

If we divide this quantity by hf , we get the 1-sided spectral number density of photon radiated by a single charged particle due to a sudden speed change *i.e.* the number of emitted photon in a unit frequency interval from the Bremsstrahlung process:

$$N_p = \frac{1}{4\pi\epsilon_0} \frac{4q^2 \|\Delta\vec{v}\|^2}{3c^3 hf} = \frac{\alpha A}{f}, \text{ with } A = \frac{2(q/e)^2 \|\Delta\vec{v}/c\|^2}{3\pi} \text{ and } \alpha = \frac{2\pi e^2}{(4\pi\epsilon_0)hc} \quad (3.26)$$

This is the general (approximate⁴³) formula for Handel's conventional quantum $1/f$ noise. The problem is then to relate the speed change of charge q to other measurable quantities, whose fluctuations constitutes the noise to evaluate. This process is specific to each class of physical systems to study.

In order to find this relation, in section V of paper [16], it is demonstrated that the (1-sided?) power spectral density of the relative fluctuation of the charge probability density $|\Psi|^2$ is:

$$S_{\delta|\Psi|^2/|\Psi|^2}(f) = 2 \frac{\alpha A}{(1+\alpha A \ln(f_1/f_0))^2 f} \approx 2 \frac{\alpha A}{f} \quad (3.27)$$

The origin of the extra factor 2 seems to be in the double product of the cross-correlation function in section IV of [16]. Since the number of particles having a sudden speed change per unit time is proportional to the amount of sudden crystal polarization change which is itself related to the change in the elastic energy of the piezoelectric crystal, hence to the number of phonons, the fluctuations of the phonon interaction rate in a given frequency interval due to the emission of photons in the same interval by the charge are considered equal by Handel⁴⁴. Thus, the 1-sided power density of phonon interaction rate Γ is given by⁴⁵:

$$S_{\delta\Gamma/\Gamma}(f) = \frac{4\alpha \|\Delta\dot{\vec{P}}\|^2}{3\pi f e^2 c^2} \quad (3.28)$$

Finally, we recall a remark put forward by Handel below Eq. (5.6) of [16], that "one will have to replace c by the speed of light in the medium considered" in all these formula.

Since, for time separated events, only one charge has a sudden change of speed, we have $\Delta\dot{\vec{P}} = q\Delta\vec{v}$. However, we stress that here \vec{P} is the total dielectric momentum and not the polarization vector (as stated in Handel's papers on $1/f$ noise in quartz resonators), as can be checked from dimensions.

⁴² This means that the energy spectrum of the emitted radiation is independent of frequency (at low frequencies compared with the inverse of the characteristic time for the speed change of the charges particle (of the scattering process)), or that the number of photon emitted per frequency band Δf is inversely proportional to $(\Delta E = hf\Delta n)$.

⁴³ If one realizes that the N_p computed here is nothing else than the quantity ρ_e^2/ϵ introduced in the first paragraph (see Eqs. (3.2), (3.4) and (3.5)), we can see that the semi-classical derivation given here recovers the quantum result up to a factor $(\epsilon/\epsilon_0)^{\alpha A}$ which is essentially 1, since $\alpha A \ll 1$.

⁴⁴ Here, we can question the fact that the rate of loss of a phonon (*i.e.* of an energy quantum from an eigenmode of vibration of the whole crystal) is directly connected to the rate of events occurring locally in the crystal at the position of the charged particle having a change of speed, but we must also keep in mind that there are statistical ensemble averages in the quantum derivation of these formula by Handel...

⁴⁵ One may wonder whether this should be $\langle \|\Delta\dot{\vec{P}}\|^2 \rangle$ instead of $\|\Delta\dot{\vec{P}}\|^2$, with an additional quantum expectation value or time average or statistical ensemble average...

1.3.2. Obtention of the $1/Q^4$ factor

The next step is to explain the factor $1/Q^4$ in Eq. (3.20). For this, we follow Ref. [18] and start from the differential equation of the classical forced harmonic oscillator with damping:

$$\frac{d^2x}{dt^2} + 2\gamma \frac{dx}{dt} + \omega_0^2 x = F(t) \quad (3.29)$$

Since, the resonance frequency is given by:

$$\omega_r^2 = \omega_0^2 - 2\gamma^2 \quad (3.30)$$

the fluctuations in the resonant frequency due to fluctuations in the damping coefficient can be computed by:

$$\omega_r \delta\omega_r = -2\gamma \delta\gamma \quad (3.31)$$

$$\frac{\delta\omega_r}{\omega_r} = -2 \left(\frac{\gamma}{\omega_r}\right)^2 \left(\frac{\delta\gamma}{\gamma}\right) = -\left(\frac{1}{2Q^2}\right) \left(\frac{\delta\gamma}{\gamma}\right) \quad (3.32)$$

where $Q = \frac{\omega_r}{2\gamma}$ is the quality factor. It then follows immediately that the spectral power density of frequency fluctuations is given by:

$$S_y(f) = S_{\delta\omega/\omega}(f) = \left\langle \left(\frac{\delta\omega_r}{\omega_r}\right)^2 \right\rangle_f = \left(\frac{1}{4Q^4}\right) \left\langle \left(\frac{\delta\gamma}{\gamma}\right)^2 \right\rangle_f \quad (3.33)$$

Since the damping coefficient γ is assumed to be proportional to the rate of interactions Γ leading to a loss of energy of the eigenmodes of the crystal, (*i.e.* the disappearance of phonons), which is itself inversely proportional to the loss event cross section, we get:

$$S_y(f) = \frac{1}{4Q^4} S_{\delta\gamma/\gamma}(f) = \frac{1}{4Q^4} S_{\delta\sigma/\sigma}(f) = \frac{1}{4Q^4} S_{\delta\Gamma/\Gamma}(f) \quad (3.34)$$

Finally, we note that since we use $Q = \omega_r/2\gamma$, viscous damping must be the dominant cause of damping in the vicinity of resonance and that this Q is an unloaded Q^{46} .

1.3.3. Detailed expression of the β factor

The final step consists in determining the coefficient of proportionality β' between $S_y(f)$ and $V/(Q^4 f)$ in Eq. (3.20). For this, we put Eq. (3.28) into Eq. (3.34) to get:

$$S_y(f) = \frac{1}{4Q^4} \frac{4\alpha \|\Delta\dot{\vec{P}}\|^2}{3\pi f e^2 c^2} \quad (3.35)$$

We must now relate $(\Delta\dot{\vec{P}})^2$ to measurable quantities. In order to do this, Handel⁴⁷ used the fact that the vibrational energy in a given mode of circular frequency $\langle\omega\rangle$ (corresponding to the average frequency of the thermal phonons that interacted with the main mode phonons to create the

⁴⁶ In Ref. [19], T. Parker found by studying numerous surface acoustic wave devices that the $1/f$ process is essentially the same for bulk and surface acoustic wave devices and that “the power spectral density of frequency fluctuations shows a clear power law dependence that is very close to $1/Q_u^4$, where Q_u is the unloaded Q . However, the observed dependence on loaded Q is weak.”

⁴⁷ *cf.* for example Eq. (2) of Ref. [15] (first paper in which it appears) which is the same as Eqs. (11) and (12) of Ref. [13] (a priori Handel’s most recent journal paper in which they appear).

dissipation) is twice⁴⁸ the kinetic energy of the corresponding crystal vibration eigenmode expressed thanks to a quantum harmonic oscillator in the corresponding normal coordinate (called “interacting resonator mode” by Handel):

$$W = n\hbar\langle\omega\rangle = 2\left(\frac{Nm}{2}\right)\left(\frac{dx}{dt}\right)^2 \quad (3.36)$$

with “ m the reduced mass of the elementary oscillating dipoles” and “ N their number in the resonator” as stated in all Handel’s papers in which this equation appears.⁴⁹

The time derivative of the total dipole momentum of the crystal is then introduced through the following identification:

$$\left(\frac{dx}{dt}\right) = \left(\frac{1}{Ne}\right)\frac{d(Nex)}{dt} = \left(\frac{1}{Ne}\right)\chi\left\|\dot{\vec{P}}\right\| \quad (3.37)$$

with e the charge of the elementary oscillating dipole and χ a polarization constant (stated as being of the order of unity, sometimes named ε or g (or even V in Eq. (5) of Ref. [20]) and never defined in Handel’s papers...). By inserting Eq. (3.37) into Eq. (3.36), we get:

$$W = n\hbar\langle\omega\rangle = \left(\frac{m}{Ne^2}\right)\chi^2\left\|\dot{\vec{P}}\right\|^2 \quad (3.38)$$

By differentiating this expression and setting $\Delta n = 1$, we can find the change of total dipole time derivative due to the loss of a single phonon:

$$\frac{\Delta n}{n} = 2\frac{\left\|\Delta\dot{\vec{P}}\right\|}{\left\|\dot{\vec{P}}\right\|} \text{ with } \Delta n = 1, \text{ gives } \left\|\Delta\dot{\vec{P}}\right\| = \frac{\left\|\dot{\vec{P}}\right\|}{2n} \quad (3.39)$$

Using (3.38), we then obtain:
$$\left\|\Delta\dot{\vec{P}}\right\|^2 = \frac{\hbar\langle\omega\rangle}{n} \times \frac{Ne^2}{4m\chi^2} \quad (3.40)$$

If we insert this result into Eq. (3.35), we get:

$$S_y(f) = \frac{1}{Q^4} \frac{\alpha\left\|\Delta\dot{\vec{P}}\right\|^2}{3\pi fe^2c^2} = \frac{1}{Q^4} \frac{\alpha}{3\pi fe^2c^2} \times \frac{\hbar\langle\omega\rangle}{n} \times \frac{Ne^2}{4m\chi^2} = \frac{\beta'V}{Q^4f} \quad (3.41)$$

with

$$\beta' = \frac{\left(\frac{N}{V}\right)\alpha\hbar\langle\omega\rangle}{12\pi nm\chi^2c^2} \quad (3.42)$$

The final expression of Handel can then be obtained by recalling that if $\hbar\langle\omega\rangle/k_B T \ll 1$ (which is valid in our case), then Planck’s distribution reduces to $n \approx k_B T/\hbar\langle\omega\rangle$:

$$\beta' = \frac{\left(\frac{N}{V}\right)\alpha(\hbar\langle\omega\rangle)^2}{12k_B T\pi\chi^2 mc^2} \quad (3.43)$$

⁴⁸ For a harmonic oscillator the kinetic and potential energies are equal.

⁴⁹ One could wonder how this could be related to some average of the values given by the diagonalization of the dynamic matrix in the quasi-harmonic approach...

Finally, for an arbitrary temperature, Handel generalizes the above expression by taking into account the loss of a main mode phonon through interaction with a defect (point-like or extended) which is the dominant term at low temperature and obtains (Refs. [13], [14], [20], [21],...):

$$\beta = \frac{\beta'[\Gamma'^2 + (\frac{\omega}{\langle\omega\rangle})^2 \Gamma'']}{\Gamma^2} \quad (3.44)$$

2. Calculation of β'

2.1. *Handel's evaluation of the order of magnitude of β'*

For the SC cut quartz resonators at their inversion temperature, interaction with defects can a priori be neglected with respect with 3-phonon processes. We therefore first recall the evaluation of the order of magnitude of the numerical value of β' as given by Eq. (3.43) done by Handel in several of his papers *e.g.* [13], [14] and [15].

The numerical values used by Handel in his calculations are:

- $\langle\omega\rangle \approx 10^8$ rad/s
- $T=300\text{K}$ $k_B T = 4 \times 10^{-14}$ erg (1 erg = $1\text{g}\cdot\text{cm}^2\cdot\text{s}^{-2} = 10^{-7}$ J)
- Polarization constant $\chi = 1$
- $N/V \approx 10^{22}$ cm^{-3}
- $\hbar \approx 10^{-27}$ erg·s (Planck's reduced constant)
- $\alpha \approx 1/137$ (fine structure constant)
- $m =$ mass of electron $\approx 10^{-27}$ g

Hence, Handel finds the following order of magnitude:

$$\beta' = \frac{(10^{22} \text{ cm}^{-3})(1/137)(10^{-27} \text{ erg}\cdot\text{s} \times 10^8 \text{ rad/s})^2}{12 \times (4 \times 10^{-14} \text{ erg}) \times 3.14 \times 10^{-27} \text{ g} \times 9 \times 10^{20} (\text{cm/s})^2} \approx 1 \text{ cm}^{-3}. \quad (3.45)$$

2.2. *Points of concern in Handel's model as concerns the evaluation of β'*

Nowadays, quartz oscillators are so good that they seem to tackle the limit set by Handel's model. Furthermore, the limit set by this model for oscillators made with other materials than quartz are desirable. Hence, it is important to evaluate β' more precisely. However, even if we accept Eq. (3.43) as is (which is questionable), several problems remain for an accurate evaluation of β' .

- The physical origin of the "polarization constant" χ in Eq. (3.36) is not clear. From Eq. (3.36), $\chi=P/Nex\dots$, with P being the total dipole of the quartz crystal (and not the polarization of the quartz crystal, as stated in some of the papers, which is not possible due to dimensionality constraints). How can it be connected to the quartz dielectric constant? However, we note that if we recall the remark that the speed of light in quartz should be

used instead of the speed of light in vacuum in Eq. (3.35), then a factor $n^2 = \varepsilon$ should be present in the denominator of (3.43) and one may wonder if it is the same as χ^2 or a new factor. We also note that setting a numerical value for this parameter is not evident since quartz is optically anisotropic.

- P. H. Handel used the mass of an electron ($m \approx 10^{-27}$ g) in his numerical calculation of β' , whereas he used $N/V \approx 10^{22}$ cm⁻³ which is approximately the volume density of unit cells in quartz!... How can we define properly this “reduced mass of the elementary oscillating dipoles”? Furthermore, is m the mass of an oscillating dipole or the effective mass associated to a crystal vibration mode? Shouldn't we use the (27×27) dynamic matrix approach? Shall we consider that the elementary oscillatory dipole used by Handel is constituted by a massive ion and a single (light) electron, so that the reduced mass is indeed the mass of the electron and the effect on the motion of the heavy ion due to the loss of a phonon or the Bremsstrahlung process can be neglected with respect to the amplitude of the sudden change of speed of the electron? Then what would be N exactly? The total number of silicon and oxygen ions or the number of crystallographic unit cells in the crystal (that we would have if the elementary dipole would be the quartz unit cell with 6 oxygen ions and 3 Si ions), or ...? We take the occasion to mention *en passant* that in the first paper [15] in which Eq. (3.43) appears, Walls et al. used $m \approx 2 \cdot 10^{-24}$ g in their numerical calculations below their Eq. (9), but nonetheless found $\beta' \approx 1$ cm⁻³ (also stating that $\langle \omega \rangle \approx 10^{11}$ rad/s, but using $\langle \omega \rangle \approx 10^8$ rad/s in the developed expression of the numerical calculation...).
- How should we define $\langle \omega \rangle$? The value $\langle \omega \rangle \approx 10^8$ rad/s used by Handel is never justified. Furthermore, since phonons from the main mode have a frequency (5 MHz) well below the average frequency of the thermal modes, is it possible that they interact efficiently with one another? Is there somewhere an expression of the 3-phonon process cross-section in a form simple enough so that we could use it as a weight to be able to compute the average as advocated by P. H. Handel in a reply mail to us?
- We note that contrarily to the electronic devices also studied by Handel, there is no electron “transit” inside quartz since it is an insulator. Hence, is the Bremsstrahlung radiation (also emitted by the surface electrons of the metallic electrodes that are “moved” by the piezoelectric field created by quartz at the surface of the electrodes (which creates the detected current)? The loss of a phonon may be seen has a sudden reduction in the amplitude

of the eigenmode for the whole crystal. Can we really consider that this can give rise to a local variation for a single particle?

2.3. Our calculation of β'

In our paper [22], we tried to calculate β' more precisely. However, considering the problems stated in the previous paragraph, we finally restricted ourselves to the evaluation of the value of $\langle\omega\rangle$ which would give $\beta' = 1 \text{ cm}^{-3}$ if we would take the mass of an SiO_2 pattern for m , the density of SiO_2 pattern for N/V and more precise values for the other parameters:

Since, $\text{SiO}_2 = \text{Si} + 2\text{O}$, the molar mass of a SiO_2 pattern can be computed thanks to:

$$M = 28.0855 + 2 \times 15.999305 = 60.0842 \text{ g/mol}$$

so that $m = 60.08 / (6.022 \cdot 10^{23}) \approx 9.96 \cdot 10^{-23} \text{ g}$

$$\frac{N}{V} = \frac{\rho N_A}{M} = \frac{2.648 \times 6.02214179 \times 10^{23}}{60.0842} / \text{cm}^3 = 2.654 \times 10^{22} / \text{cm}^3$$

where the density of quartz is

$$\rho = 2.648 \text{ g/cm}^3$$

$N_A = 6.022 \times 10^{23} \text{ mol}^{-1}$ is the Avogadro number

$k_B T$ at quartz turnover temperature 353 K (80°C) is:

$$k_B T = 1.38 \cdot 10^{-16} \times 353 = 4.87 \times 10^{-14} \text{ erg}$$

$$\hbar = 1.055 \cdot 10^{-27} \text{ erg} \cdot \text{s}$$

Speed of light $c = 3.00 \cdot 10^{10} \text{ cm/s}$

With these values, we find that we need to have $\langle\omega\rangle \approx \chi \times 2.8 \cdot 10^{10} \text{ rad/s}$ to have $\beta' = 1 \text{ cm}^{-3}$ ⁵⁰. By recalling that β' is proportional to $\langle\omega\rangle^2$ we can see that it is really very important to at least set an order of magnitude for $\langle\omega\rangle$ to have even a crude estimate of β' . We will turn to this again in the last section of this chapter.

3. Volume dependence in Handel's model of quartz crystal resonator noise

Though criticized by many [8], [10], Handel's quantum model for $1/f$ noise remains the only model giving a quantitative estimation of the level of intrinsic $1/f$ noise in quartz crystal resonators, compatible with the best experimental results. In our paper [23], we reconsider the volume dependence in this model. We first argue that an acoustic volume, representing the volume in which

⁵⁰ We left χ in the final result since it is also not known precisely.

the vibration energy is trapped, should be used instead of the geometrical volume between the electrodes. Then, we show that since there is an implicit dependence of the quality factor of the resonator with its thickness, the net effect of Handel's formula is not an increase of noise proportionally to the thickness of the resonator, as could be naively expected, but a net decrease when thickness increases. Finally, we show that a plot of $Q^4 S_y$ versus the acoustic volume, instead of the usual S_y plot, could be useful to compare the quality of acoustic resonators having very different resonance frequencies.

So far, ultra-stable oscillators (USO) using quartz crystal resonators remain the best solution to have the highest short-term stability in volumes of a few cm^3 which is very important for local time references in space applications (for example) since size and weight are important parameters. With low noise electronics at the state of the art, the fundamental limitation for this short-term stability is flicker frequency noise in the resonator (hereafter simply called $1/f$ noise). Until recently, the best short-term stability for a quartz crystal resonator was measured in 1994 by J. Norton, for a 5 MHz, SC cut, resonator, mounted in an electrode-less structure (BVA) [24]. The corresponding result in terms of Allan standard deviation was $3.74 \cdot 10^{-14}$ at $\tau = 10$ s.

Furthermore, two 10 MHz BVA, SC-cut quartz crystal oscillators were measured in 1999, by R. J. Besson, to have a $5 \cdot 10^{-14}$ at $\tau \approx 10$ s Allan standard deviation [25]. This seemed to be the ultimate limit that one could obtain for a quartz based oscillator in the short-term stability domain since, no more tangible solution had been found to improve the phase noise of the resonator itself.

Recently, better experimental results [26], [27] and [28] have reintroduced hopes that quartz crystal oscillators may still have a progression margin in the short-term stability domain and refueled the discussion about what is the main factor limiting the stability between the phase flicker noise in the electronics and the intrinsic noise of the quartz crystal.

P. H. Handel used the equation (3.20) for the power spectral density of relative frequency fluctuations. In this equation Q is the intrinsic quality factor of the resonator, V (in cm^3) is the volume of the resonant part inside the resonator, and β is the proportionality factor dependent on the physical parameters of the material, numerically estimated to be of the order of 1 cm^{-3} in quartz resonators as seen previously. We note first that this is supposed to represent the fundamental lower limit of noise spectral density at low frequencies, in the resonator, therefore in the oscillator. Second, we recall that A. van der Ziel was able to recover the same formula [15], except for the detailed expression of β , using semiclassical arguments. However, we should also note that a careful analysis of this detailed analytical expression of β and the way it is demonstrated by Handel

calls for more precise definitions of some of the quantities occurring in this expression, so as to have an explicit way to numerically evaluate them more precisely.

In formula (3.20), the volume V has been traditionally approximated by the volume between the electrodes [22], but then, the latest experimental results [28] seem to be below the prediction (considering $\beta = 1 \text{ cm}^{-3}$). Now, we try to show that a better estimation of the theoretical limit may be extracted from Handel's model, using the acoustic volume of the resonator, defined by the trapping of energy, instead of the volume between the electrodes. Additionally, the presence of the volume V in the numerator of (3.20), instead of in the denominator as naively expected from experimental facts, will be discussed.

3.1. Acoustic volume estimation

The acoustic volume estimation is carried out using Tiersten's model as *e. g.* in [29].

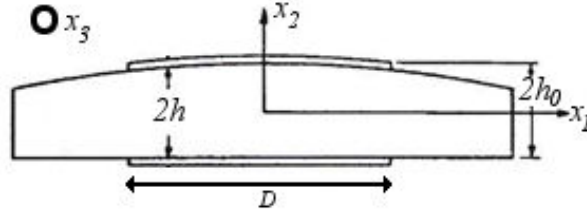


Fig.3.1: Geometric definition of a plano-convex resonator.

Because of the plano-convex shape of a resonator (Fig.3.1), the thickness $2h$ of the resonator at some off-axis point with coordinates (x_1, x_2, x_3) , is given by the following expression:

$$2h \approx 2h_0 \left[1 - \frac{(x_1^2 + x_2^2)}{4Rh_0} \right] \quad (3.46)$$

where h_0 is the maximum height of the resonator (on the x_2 axis) and R the curvature radius of the convex face. Furthermore, for stationary shear waves propagating in the x_2 direction, the amplitude of the mechanical displacement modes in the resonator can be approximated by [29]:

$$u_{nmp} \approx A \sin\left(\frac{n\pi x_2}{2h}\right) H_m(\sqrt{\alpha_n} x_1) H_p(\sqrt{\beta_n} x_3) \exp(-\alpha_n x_1^2/2 - \beta_n x_3^2/2) \exp(j\omega_{mnp} t) \quad (3.47)$$

with:

$$\alpha_n^2 = \frac{n^2 \pi^2 \hat{c}}{8R h_0^3 M'_n} \quad \text{and} \quad \beta_n^2 = \frac{n^2 \pi^2 \hat{c}}{8R h_0^3 P'_n} \quad (3.48)$$

where ω_{mnp} is the mode pulsation with $n = 1, 3, 5, \dots$ the overtone (OT) number, $m, p = 0, 2, 4, \dots$ the numbers of the anharmonic modes, label the different mode shapes in the plane of the resonator, H_m and H_p are Hermite polynomials, M'_n and P'_n are the dispersion constants and \hat{c} is the effective elastic constant associated to the propagation of this kind of mode.

For the 3rd overtone (OT 3), we consequently have:

$$u_{300} \approx A \sin\left(\frac{3\pi x_2}{2h}\right) \exp(-\alpha_3 x_1^2/2 - \beta_3 x_3^2/2) \exp(j\omega_{300} t) \quad (3.49)$$

with

$$\alpha_3^2 = \frac{9\pi^2 \hat{c}}{8Rh_0^3 M_3'} \text{ and } \beta_3^2 = \frac{9\pi^2 \hat{c}}{8Rh_0^3 P_3'} \quad (3.50)$$

The eigenfrequency ω_{300} is obtained from:

$$\omega_{300}^2 = \frac{9\pi^2 \hat{c}}{4h_0^2 \rho} \left[1 + \frac{1}{3\pi} \sqrt{\frac{2h_0}{R}} \left(\sqrt{\frac{M_3'}{\hat{c}}} + \sqrt{\frac{P_3'}{\hat{c}}} \right) \right] \quad (3.51)$$

The elastic energy in the resonator is approximately given by:

$$W_1 \approx \frac{A^2}{2} \hat{c} \left(\frac{3\pi}{2h_0} \right)^2 \iiint_V \cos^2 \left(\frac{3\pi x_2}{2h_0} \right) \exp(-\alpha_3 x_1^2 - \beta_3 x_3^2) dV \quad (3.52)$$

We then define the acoustic volume as the volume that would contain the same elastic energy, for a hypothetical wave that would have constant amplitude in the (x_1, x_3) plane, for a resonator with two plane electrodes ($1/R = 0$) of equivalent surface S_{eq} separated by a distance $2h_0$. For this hypothetical resonator, the trapped elastic energy would be:

$$W_2 \approx \frac{A^2}{2} \hat{c} \left(\frac{3\pi}{2h_0} \right)^2 \int_{-h_0}^{h_0} \cos^2 \left(\frac{3\pi x_2}{2h_0} \right) dx_2 \times S_{eq} \quad (3.53)$$

Thus:

$$W_1 = W_2 \Rightarrow V_{ac} = 2h_0 S_{eq} = 2h_0 \iint \exp(-\alpha_3 x_1^2 - \beta_3 x_3^2) dx_1 dx_3 \quad (3.54)$$

However, thanks to the Gaussian functions, as long as the electrodes diameter $D > 4/\text{Min}(\sqrt{\alpha_3}, \sqrt{\beta_3})$, their real outer shape is not important and the diameter can even be taken to be infinite. Using the fact that $\int_{-\infty}^{\infty} \exp(-\alpha x^2) dx = \sqrt{\pi/\alpha}$, we then find that:

$$V_{ac} = 2h_0 S_{eq} \approx 2h_0 \pi / \sqrt{\alpha_3 \beta_3} = \sqrt{32Rh_0^5 \sqrt{M_3' P_3'} / 9\hat{c}} \quad (3.55)$$

3.2. Application of the models to experimental measurements

As seen in [28], the best measured resonators are the 5 MHz BVA SC-cut, 3rd OT C-mode, manufactured by the Oscilloquartz S.A. Company (Swatch Group), based in Neuchatel, Switzerland. Since for SC-cut quartz resonators, the cut is defined by a double rotation ($\varphi = 22^\circ 45'$, $\theta = 34^\circ$), the relevant effective parameters are $\hat{c} \approx 34.6$ GPa, $M_3' \approx 57$ GPa and $P_3' \approx 67$ GPa [30]. In [31], a succinct geometrical description of the resonator is given which allows us to estimate the diameter of the resonant part of the resonator (around 20 mm) and the electrodes diameter D (about 11 mm). Using Stevens and Tiersten's results [29], we can relate the motional capacitance C_{mot} of the resonator, for the 3rd OT, to the thickness and curvature radius of the resonator:

$$C_{mot} = \frac{64\hat{e}_{26}^2}{9\pi^3 h_0 \hat{c}} \sqrt{\alpha_3 \beta_3} \left[\int_0^{D/2} \exp(-\alpha_3 x_1^2 / 2) dx_1 \int_0^{D/2} \exp(-\beta_3 x_3^2 / 2) dx_3 \right]^2 \quad (3.56)$$

With D the electrode diameter and $\hat{e}_{26} = -0.0576$ C/m² the effective piezoelectric constant.

Since, for the same specific kind of resonator that was used for the record measurement [28], the motional capacitance was measured to be 0.195 fF in [26], we have together with (3.51), a set of two nonlinear equations in h_0 and R . In order to solve them numerically, we compute initial

estimates of h_0 and R using first the fact that the thickness at the center of the resonator $2h_0$ is approximately given by $2h_0 \approx 3\lambda/2$.

In the present case, since the acoustic velocity for the 5 MHz thickness shear C-mode in a SC-cut quartz crystal is $\sqrt{\hat{c}/\rho} \approx 3613$ m/s ($\rho = 2650$ kg/m³), we find that $2h_0 \approx 1.084$ mm. Then, we use the fact that the electrodes diameter is always chosen big enough so that the two Gaussian integrals in (3.56) can be approximated by $\sqrt{\pi/2\alpha_3}$ and $\sqrt{\pi/2\beta_3}$ respectively. Thus:

$$C_{mot} \approx \frac{16\hat{e}_{26}^2}{9\pi h_0 \hat{c} \sqrt{\alpha_3 \beta_3}} = \frac{32\hat{e}_{26}^2}{\pi^2 (9\hat{c})^{3/2}} \sqrt{2h_0 R \sqrt{M'_3 P'_3}} \quad (3.57)$$

Accordingly, the initial value for R , can be estimated by:

$$R = \frac{1}{2h_0 \sqrt{M'_3 P'_3}} \left(\frac{\pi^2 (9\hat{c})^{3/2} C_{mot}}{32\hat{e}_{26}^2} \right)^2 \quad (3.58)$$

With $C_{mot} \approx 0.195$ fF, we find $R \approx 148$ mm. Then, by solving together (3.51) and (3.56) (with $D = 11$ mm), we refine our estimation to $2h_0 \approx 1.097$ mm and $R \approx 146.6 \pm 0.2$ mm (depending whether the integrations are performed for a square in Cartesian coordinates or for a disk in polar coordinates). This leads to $1/\sqrt{\alpha_3} \approx 1.38$ mm and $1/\sqrt{\beta_3} \approx 1.43$ mm. Using (3.55), we can now compute $V_{ac} = 6.81 \cdot 10^{-9}$ m³, whereas a direct numerical integration of (3.54) in polar coordinates, gives $V_{ac} = 6.80 \cdot 10^{-9}$ m³. In both cases, this is much smaller than the volume under the electrodes $V \approx 2h_0 \pi D^2/4 \approx 1.04 \cdot 10^{-7}$ m³.

Finally, we note, that if we would know the static capacitance C_0 of the same resonator, we could estimate D by adding the following formula [29]:

$$C_0 = \frac{\pi D^2}{4} \left(1 + \frac{(D/2)^2}{8Rh_0} \right) \frac{\epsilon_{22} + \hat{e}_{26}^2/\hat{c}}{2h_0} \quad (3.59)$$

to the set of nonlinear equations to solve. Conversely, using $\epsilon_{22} = 39.78 \cdot 10^{-12}$ F/m the permittivity constant corresponding to the x_2 direction in the SC-cut and $D = 11$ mm, we estimate $C_0 \approx 3.6$ pF.

One can then verify that the applicability condition $D > 4/\text{Min}(\sqrt{\alpha_3}, \sqrt{\beta_3})$ stated in the previous paragraph is indeed numerically verified in this case since $D = 11$ mm and $4/\text{Min}(\sqrt{\alpha_3}, \sqrt{\beta_3}) \approx 5.6$ mm. As argued in the previous paragraph, in contoured resonators, the energy trapping is quasi-independent of the electrodes dimension, provided they are big enough, though they influence the motional elements and the static capacitor of the Butterworth - van Dyke equivalent circuit. Indeed, for such a radius of curvature the energy density at the edge of the volume between the electrodes is at least $2 \cdot 10^6$ smaller than the energy density at the same height on the axis.

In order to use Handel's formula (3.20), we still need to compute the quality factor Q of this kind of resonator, which can be obtained using the following classical equation (*cf.* next chapter):

$$Q = \frac{\hat{c}}{2\pi f \hat{\eta}} \quad (3.60)$$

In our case, $\hat{\eta} \approx 3.95 \cdot 10^{-4} \text{ Ns/m}^2$ [32], which turns into an estimation of the maximum quality factor of about $2.79 \cdot 10^6$. This value corresponds well with the one given in [26] ($2.7 \cdot 10^6$).

We now turn to the experimental quantities that we could compare to Handel's $1/f$ noise threshold. The short-term stability is usually given in the time domain by the Allan variance [33], which is the variance of the difference of the average fractional frequencies measured for two consecutive samples of time length τ . It can be computed in the frequency domain by using the power spectral density of frequency fluctuations [34]:

$$\sigma_y^2(\tau) = \int_0^\infty S_y(f) \frac{2\sin^4(\pi f \tau)}{(\pi f \tau)^2} df \quad (3.61)$$

In the case of flicker frequency noise (which is the limiting resonator noise at low frequencies), the Allan standard deviation corresponding to the power spectral density (PSD) of relative frequency fluctuations $S_y(f) = S_y(1 \text{ Hz})/f$ turns out to be independent of τ and constitutes the floor of the noise at low frequencies (*cf.* end of chapter 1⁵¹). It is then given by the expression [34]:

$$\sigma_y(\tau) = \sqrt{2\ln(2)S_y(1\text{Hz})} \quad (3.62)$$

Table 3.1 presents the comparison between measurements and the results of Handel's model, considering both definitions of volume in (3.20) (and $\beta = 1 \text{ cm}^{-3}$). One can see that the limit set by Handel's model with $\beta = 1 \text{ cm}^{-3}$, is indeed below the experimental results if one uses the acoustic volume defined here, whereas it is not if one uses the geometrical volume between electrodes.

Table 3.1: Comparison of the short-term stability in terms of Allan standard deviation σ_{y_floor} of a SC-cut, 5 MHz and 3rd OT resonator.

Frequency (MHz)	5
Quality factor Q (10^6)	2.79
Volume under electrodes V_{el} (mm^3)	104.3
Acoustic volume V_{ac} (mm^3)	6.81
Volume ratio	15
$\sigma_{y_floor_Handel}$ (vol. under electrodes)	$4.89 \cdot 10^{-14}$
$\sigma_{y_floor_Handel}$ (acoustic vol.)	$1.25 \cdot 10^{-14}$
$\sigma_{y_floor_exp}$ [24] (oscillator measurement)	$3.75 \cdot 10^{-14}$
$\sigma_{y_floor_exp}$ [27] (oscillator measurement)	$2.5 \cdot 10^{-14}$

⁵¹ We recall that $S_y(1 \text{ Hz})$ is a notation for a numerical value (without dimension) and not the value of $S_y(f)$ for $f = 1 \text{ Hz}$, which is homogeneous to the inverse of a frequency, hence a time, for $1/f$ noise.

3.3. Size dependence

A point that can be a priori surprising with Handel's formula is the proportionality of $S_y(1\text{ Hz})$ with the volume. In Fig.3.2, we plotted experimental values for $S_y(1\text{ Hz})$ as a function of the volume V_{el} between the electrodes, using results from various publications [24], [25], [35] and [36], including those used by Handel to justify his model and recent results obtained for 5 MHz oscillators specially designed by FEMTO-ST for industrial partners. One can easily see that a linear increase of $S_y(1\text{ Hz})$ with V_{el} is NOT supported by the experimental results. This seems at first sight to be a very serious problem for Handel's theory, but if we look closer at (3.20), we see that there are other factors in this equation that may also depend on the geometrical dimensions of the resonator.

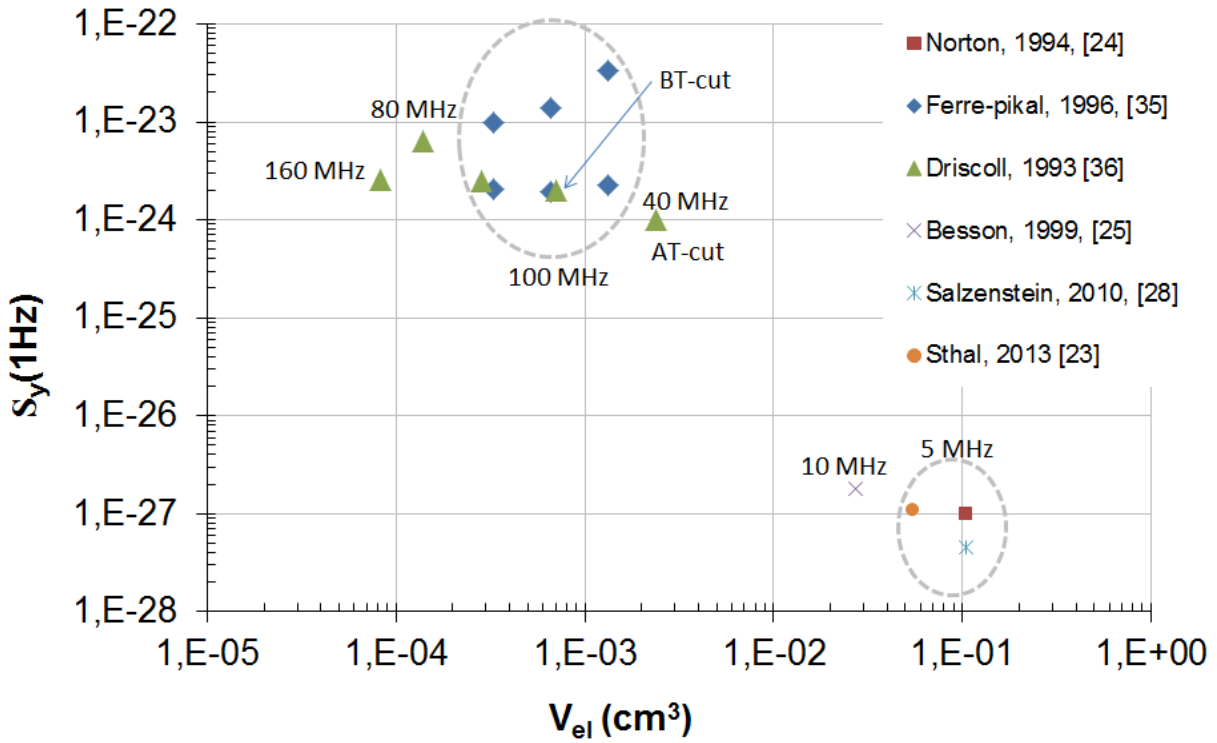


Fig.3.2: $S_y(1\text{ Hz})$ as a function of the volume between the electrodes of the resonator for experimental points from various authors.

Indeed, a plot of the $Q^4 S_y(1\text{ Hz})$ product for the same experiments, as a function of V_{el} (Fig.3.3), gives a very different trend: the volume dependence is now similar to that predicted by Handel in his model! This is due to the fact that Q^4 also depends on the dimensions of the resonator (particularly its thickness $2h_0$). This introduces a hidden dependence with the size of the resonator that we will study in more details below. However, several points seem to have a lower noise than the intrinsic limit supposedly set by Handel's model if one uses $\beta = 1\text{ cm}^{-3}$ as proposed in Handel's papers. At this point, one could either question this $\beta = 1\text{ cm}^{-3}$ value, as we did in paper [22], or use the above-defined acoustic volume, describing the volume in which elastic energy is confined, instead of the geometric volume between the electrodes.

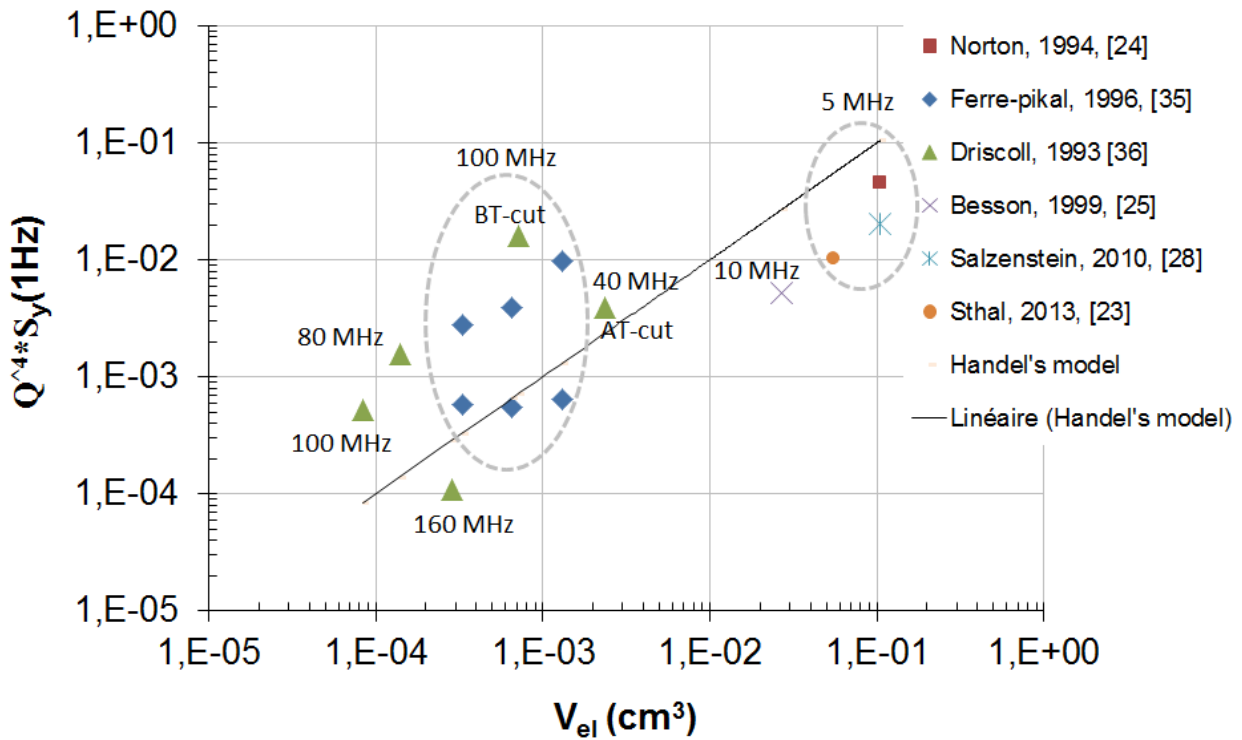


Fig.3.3: $Q^4 \cdot S_y$ as a function of the volume between the electrodes of the resonator, experimental points from various authors + straight line for Handel's prediction with $\beta = 1 \text{ cm}^{-3}$.

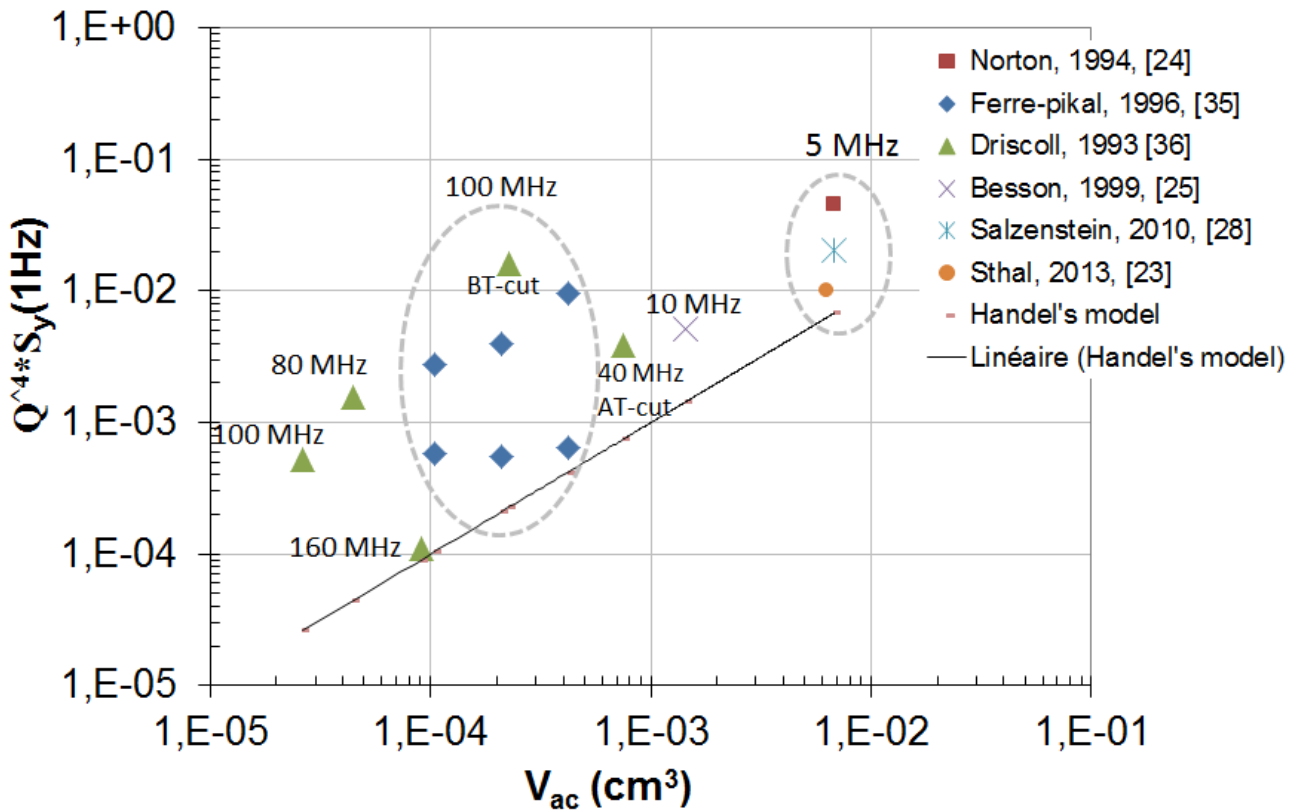


Fig.3.4: $Q^4 \cdot S_y$ as a function of the acoustic volume of the resonator (given by (3.55) for plano-convex resonators and (3.65) for plano-plano resonators), experimental points from various authors + straight line for Handel's prediction with $\beta = 1 \text{ cm}^{-3}$.

For plano-convex resonators, formula (3.55) was used instead of the volume between electrodes to draw Fig.3.4. However, higher frequency resonators have a plano-plano shape and we had to use another formula for the acoustic volume. According to [29] section III, the trapped energy mode shape can then be approximated by products of simple trigonometric functions in such resonators, the trapped energy W_1 is computed from the following equation:

$$W_1 \approx \frac{A^2}{2} \hat{c} \left(\frac{n\pi}{2h_0} \right)^2 \iiint_V \left[\cos \left(\frac{n\pi x_2}{2h_0} \right) \cos \left(\frac{\pi x_1}{2l} \right) \cos \left(\frac{\pi x_3}{2l} \right) \right]^2 dV \quad (3.63)$$

with l the half width of a square electrode. At this point, following Stevens and Tiersten, we consider that circular electrodes can be approximated by square electrodes with a width equal to the diameter of the real electrodes. Thus using (3.53), we find:

$$W_1 = W_2 \Rightarrow V_{ac} = 2h_0 S_{eq} = 2h_0 \int_{-l}^l \int_{-l}^l \left[\cos \left(\frac{\pi x_1}{2l} \right) \cos \left(\frac{\pi x_3}{2l} \right) \right]^2 dx_1 dx_3 \quad (3.64)$$

$$V_{ac} = 2h_0 S_{eq} \approx 2h_0 l^2 \approx V_{el}/4 \quad (3.65)$$

In the plano-plano case, the acoustic volume V_{ac} is simply proportional to the thickness of the resonator and to the area of the electrodes and equals a fourth of the volume between the electrodes. Data from [35] and [36], necessary to compute V_{ac} for these high frequency plano-plano resonators, are recalled in Table 3.2. We note that we only kept the best measurements from [35], in order to draw Fig.3.4.

Table 3.2: Resonator parameters from [35] and [36] used to draw Fig.3.4. Q factor of resonators from [36] have been found more precisely in [37].

Reference	[35]	[35]	[35]	[36]	[36]	[36]
Frequency (MHz)	100	100	100	80	100	160
Overtone	5	5	5	3	3	5
Crystal-Cut	SC	SC	SC	SC	SC	SC
Unloaded quality factor	$1.3 \cdot 10^5$	$1.3 \cdot 10^5$	$1.3 \cdot 10^5$	$1.25 \cdot 10^5$	$1.19 \cdot 10^5$	$1.25 \cdot 10^5$
Electrode diameter (mm)	2.16	3.05	4.32	1.63	1.40	2.54
Resonator Thickness (μm)	90	90	90	67.8	54.4	56.7

Looking at Fig.3.4, one can see that the line corresponding to Handel's model is now lower than all the experimental points. Furthermore, the proportionality of $Q^4 S_y$ with V_{ac} for the best resonators now seems reasonable. Finally this kind of $Q^4 S_y$ plot seems to be useful to compare the performance of resonators with various resonant frequencies.

Since the comparison of the previous graphs clearly shows that one should not forget that the quality factor depends on the physical dimensions of the resonator, we study in more details the thickness dependence of V/Q^4 . For that purpose, we recall that, in the expression (3.60) of the intrinsic quality factor of an acoustic resonator, $f \sim 1/h_0$ (cf. e.g. Eq. (3.51) for $h_0 \ll R$), hence $Q \sim h_0$. Given the h_0 dependence of Q and V , we then get for constant area electrodes, an inverse proportionality of S_y with h_0^3 if V is the volume between the electrodes, or $S_y \sim 1/h_0^{3/2}$, if V is the acoustic volume. In both cases, noise reduction should be enhanced by an increase of thickness. In high purity crystals, this trend seems to be confirmed by the fact that 5 MHz resonators ($2h \sim 1$ mm) have so far shown short-term stabilities below that of 10 MHz resonators ($2h \sim 0,5$ mm).

From the previous considerations, we showed how the intrinsic lower limit for $1/f$ noise limiting short term stability, set by Handel's model can be reconciled with the best latest experimental results, provided one uses the acoustic volume computed from Tiersten's model, instead of the volume between the electrodes. We also showed how Handel's model can be qualitatively very useful in order to compare the quality of oscillators of various resonant frequencies, thanks to the $Q^4 \cdot S_y$ plot. Furthermore, we showed how Handel's model is not in contradiction with the fact that usually thicker resonators exhibit less noise, despite an apparent proportionality of the noise with the volume of the resonator in this model.

4. Attempts to compute the average circular frequency present in Handel's theory of quantum $1/f$ noise for BAW quartz resonators thanks to molecular dynamics

As stated in a previous paragraph, we had some concerns about Handel's theory of quantum $1/f$ noise, one of them being the numerical evaluation of at least an order of magnitude for the average circular frequency of the 3-phonon interactions appearing in Eq. (3.43). Since this 3-phonon interactions come from non-harmonic terms in the quartz elastic energy, we decided to use molecular dynamics to compute the Phonon Density Of States (PDOS) for α -quartz using a realistic non harmonic interaction energy between the ions of quartz $PDOS_{NH}(\omega)$. Then by subtracting the density of states found in the harmonic approximation by Lee et al. [38] $PDOS_H(\omega)$, our goal was to concentrate on the effect of the non-harmonic terms and compute $\langle \omega \rangle$ thanks to:

$$\langle \omega \rangle = \frac{\int_0^\infty PDOS_{NH}(\omega)\omega d\omega}{\int_0^\infty PDOS_{NH}(\omega)d\omega} - \frac{\int_0^\infty PDOS_H(\omega)\omega d\omega}{\int_0^\infty PDOS_H(\omega)d\omega} \quad (3.66)$$

4.1. Simulation details

4.1.1. Introduction to molecular dynamics simulations

At the core of a classical Molecular Dynamics (MD) code, there is a method to solve Newton's equations for a collection of point-like particles in a given thermodynamic environment:

$$\forall i = 1, \dots, N \quad m_i \frac{d^2 \vec{r}_i}{dt^2} = -\vec{\nabla}_i V(\{\vec{r}_j\}_{j=1, \dots, N}) \quad (3.67)$$

where $V(\{\vec{r}_j\})$ is the potential energy functional which describes the physical interactions between the N particles (atoms, ions, molecules, rigid groups of atoms,...). However, several other steps must be taken for a good simulation:

- Choice of the units for the simulation (most code work with adimensioned quantities internally), selection of the type of particles used in the simulation and of the functional form of the potential energy between them, choice of the environmental conditions (which quantities will be considered constant (volume or pressure, total energy, entropy or temperature,...))
- Initialization of the time step Δt ⁵², positions, speeds and forces at initial time t_0 + initialization of the thermodynamic quantities to be computed through statistical means.
- Loop on the discretized instants (usually equidistant): computations of the positions, speeds and forces at t_{j+1} knowing them at previous instants (usually only values at t_j are used). The most widely used integrator is the Velocity Verlet Algorithm [39], [40], [41] (which is in fact a 3D version of a mid-point Runge-Kutta of order 2 algorithm)⁵³:
 - For j from 0 to j_{max} and i from 0 to N , estimate the speeds at $t_j + \Delta t/2$, then estimate the positions at $t_{j+1} = t_j + \Delta t$:

$$\vec{v}_i(t_j + \Delta t/2) = \vec{v}_i(t_j) + \vec{F}_i(t_j)\Delta t/(2m_i) + O[(\Delta t)^3] \quad (3.68)$$

$$\vec{r}_i(t_{j+1}) = \vec{r}_i(t_j + \Delta t) = \vec{r}_i(t_j) + \vec{v}_i(t_j + \Delta t/2)\Delta t + O[(\Delta t)^4] \quad (3.69)$$

- Compute the forces $\vec{F}_i(t_j + \Delta t)$, then the speeds at $t_j + \Delta t$:

$$\vec{v}_i(t_j + \Delta t) = \vec{v}_i(t_j + \Delta t/2) + \frac{\vec{F}_i(t_j + \Delta t)\Delta t}{2m_i} + O[(\Delta t)^3] \quad (3.70)$$

- Use some numerical procedure to enforce the thermodynamic constraints (*e.g.* Nosé-Hoover thermostat or barostat [42], [43]). These procedures need not necessarily be the same during a first period of time called “equilibration” in which the system relaxes towards a thermodynamic equilibrium situation and a second period of time (“production phase”), during which sums or accumulated to later compute time averages⁵⁴, standard deviations,...

⁵² Δt must be much smaller than the characteristic time of the fastest internal motion of the structure. Usually Δt is of the order of a femtosecond or less (!) except when some part(s) of the structure is(are) considered rigid.

⁵³ This algorithm uses only 3 arrays of $3N$ elements (positions, speeds and forces), and has errors smaller than traditional algorithm based on the direct use of Taylor expansions because the errors done on the estimations of the quantities at t_{j+1} are partially compensated by the error done at t_j . Furthermore, this algorithm is invariant by time reversal which improves the numerical accuracy of the total energy conservation, while numerical stability is improved by the fact that one never adds terms of order $(\Delta t)^2$ to terms of order $(\Delta t)^0$.

⁵⁴ Thanks to the ergodic hypothesis, time averages are used instead of statistical ensemble averages (averages on all the possible initial conditions that lead to an equilibrium situation respecting some set of thermodynamic constraints).

- Save results from time to time for offline treatment or to be able to restart the code in case of a power failure or computer crash.
- After end of loop, finalize the computation of all the statistical estimates, extract useful data from raw atomic trajectory information. Compute material properties of interest and visualize them.

Usually, most of the execution time is spent in the computation of the forces $-\vec{\nabla}_i V(\{\vec{r}_j\}_{j=1,\dots,N})$, hence various kinds of more or less phenomenological forms of potential are used to speed up the computations.

4.1.2. BKS Potential

The interionic potential energy functional used in our molecular dynamics simulation is called BKS potential according to the initials of the names of the authors of the paper in which it is parameterized [45] (van Beest, Kramer and van Santen). The BKS potential is the sum of a Coulomb potential plus a modified Buckingham potential which does not only account for the repulsion but also incorporates a $1/r^6$ dispersion-like term. It is given by:

$$U_{BKS}(\vec{r}_i) = \sum_{j>i} \frac{q_i q_j}{r_{ij}} + \sum_{j>i} \left[A_{ij} \exp(-b_{ij} r_{ij}) - \frac{C_{ij}}{r_{ij}^6} \right] \quad (3.71)$$

where r_{ij} is the distance between the ions i and j . The first term represents the long-range electrostatic interaction between i and j determined by the species-dependent effective charges q_i and q_j . The second term represents the short-range interaction in a Buckingham-type form where A_{ij} , b_{ij} and C_{ij} are the constants derived from fitting to Hartree-Fock ab-initio calculations and selected empirical measurements. The parameter set for BKS potential suitable for quartz is recalled in Table 3.3. We note that a version of the BKS potential improved for simulations at high pressures has been proposed Farow and Probert in Ref. [45], but we shall not need this version here since we are interested only by simulations at around 1 bar.

Table 3.3: Parameter set for quartz BKS potential.

Atom pair	A_{ij} (eV)	B_{ij} (\AA^{-1})	C_{ij} (eV \AA^6)	Charges
O-O	1388.773	2.760	175.000	$q_O = -1.2$
Si-O	18003.757	4.873	33.538	$q_{Si} = +2.4$

4.1.3. Short description of the software used

LAMMPS (Large-scale Atomic/Molecular Massively Parallel Simulator) is an open source classical molecular dynamics code, distributed for free and partly maintained by Sandia National

Labs (see [46] and <http://lammps.sandia.gov>). It can model the classical dynamics of an ensemble of only a few particles up to millions or billions of particles in a liquid, solid, or gaseous state. It can model atomic, polymeric, biological, metallic, granular, and coarse-grained systems using a variety of force fields and boundary conditions. LAMMPS must be used through input scripts (that can include external data files). It is written internally in C++ in a modular way so that it can be easily extended by other pieces of codes called fixes.

Fix-phonon is such a user-contributed extension, which implements a method to evaluate the phonon dispersion [39] directly from molecular dynamics simulations. The basic algorithm is to construct the dynamical matrices by observing the displacement fluctuations and not effective force constants. The implemented method enables one to evaluate the phonon dispersion under finite temperature/pressures without turning to the usual quasi-harmonic procedure. A post-processing code (called *phana*) is also provided to help analyze the binary files in which fix-phonon saves the dynamic matrices calculated from the LAMMPS runs. It is driven by menu, so that one can follow the menu step by step to perform the post-processing tasks. Details on *phana* can be found in Refs. [48] and [49] and by following the link: http://code.google.com/p/fix-phonon/wiki/Help_on_phana.

4.2. Estimation of the average angular frequency

We have calculated numerically the phonon dispersion curves and density of states for α -quartz, by running LAMMPS, fix-phonon and phana on the clusters of the “Mesocentre de calculs de Franche-Comté”. We used $10 \times 10 \times 10$ hexagonal primitive cells with 3 Si and 6 O, at constant temperature $T = 300$ K and pressure $P = 1$ bar, during a total of 6.5 million time steps of 2 fs each. The corresponding dynamic matrices were saved in binary output files every 0.5 million time steps, after an initial period of 0.5 million time steps for equilibration. An example script is given in appendix A.

The resulting phonon dispersion curves are shown on the left part of Fig.3.5 and compared with the ab-initio quasi-harmonic results of Gonze et al. [50] and experimental values also found in [50]. A fair agreement is found.

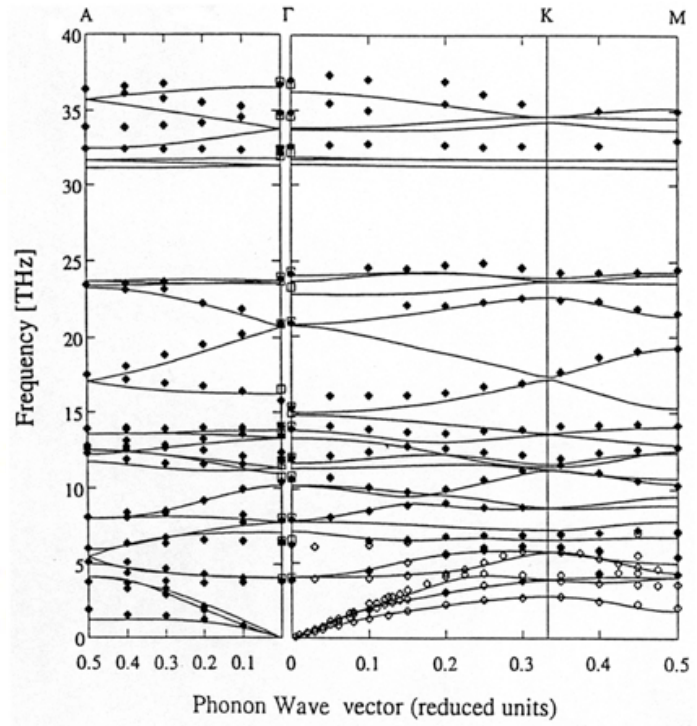
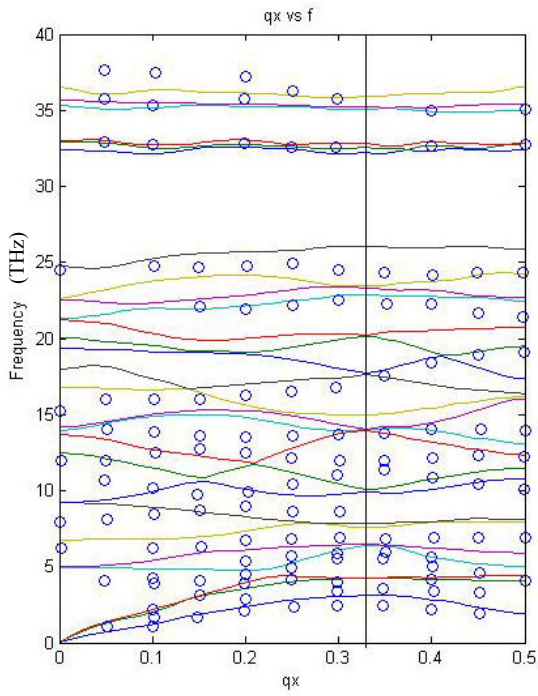


Fig.3.5: Phonon dispersion curves for α -quartz, i.e. eigenfrequencies (in THz) as a function of one of the vibration wave vector reduced coordinate, following paths along several cristallographic directions, starting from the center of the Brillouin zone (Γ), going in the $(11\bar{2}0)$ direction (ΓK), then in the $(1\bar{2}10)$ direction (KM), or in the (0001) direction (ΓA) Left: Circles are experimental values and solid lines represent the results of our calculations for 6.5 million time steps in LAMMPS. Right: Circles are experimental values and solid lines represent the results of the quasi-harmonic calculations of Gonze *et al.* [50]

Next, we turn to the PDOS curves. Fig.3.6 shows our results for 6.5 million time steps in LAMMPS. Fig.3.7 shows the same quantity as obtained by Lee and Gonze [38]. After completing the LAMMPS simulations, we found a paper by Bosak *et al.* that includes the graph of an experimental approximation of the PDOS (called X-VDOS in their paper, for Vibration Density Of States as measured by inelastic X-ray scattering) that we reproduce in Fig.3.8.

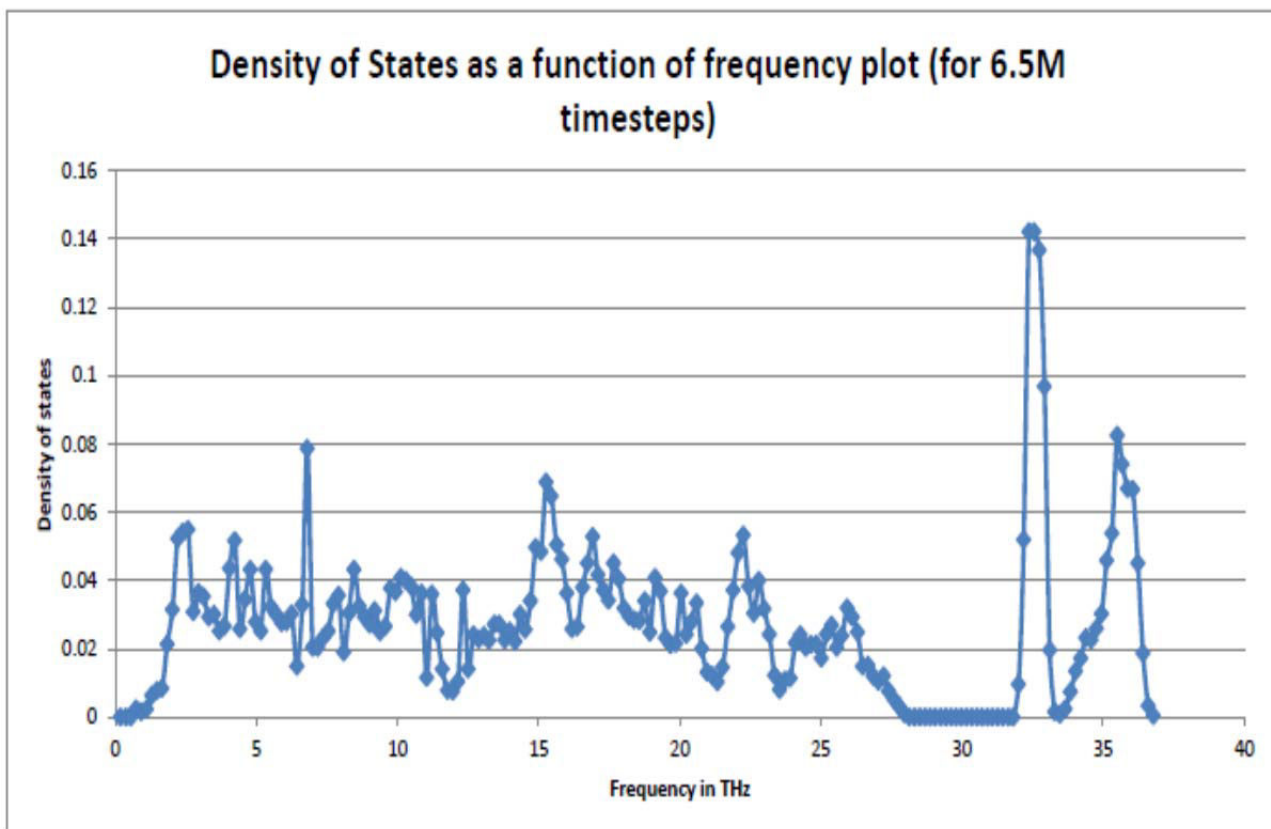


Fig.3.6: α -quartz phonon density of states vs frequency (in THz), for 6.5M time steps in LAMMPS.

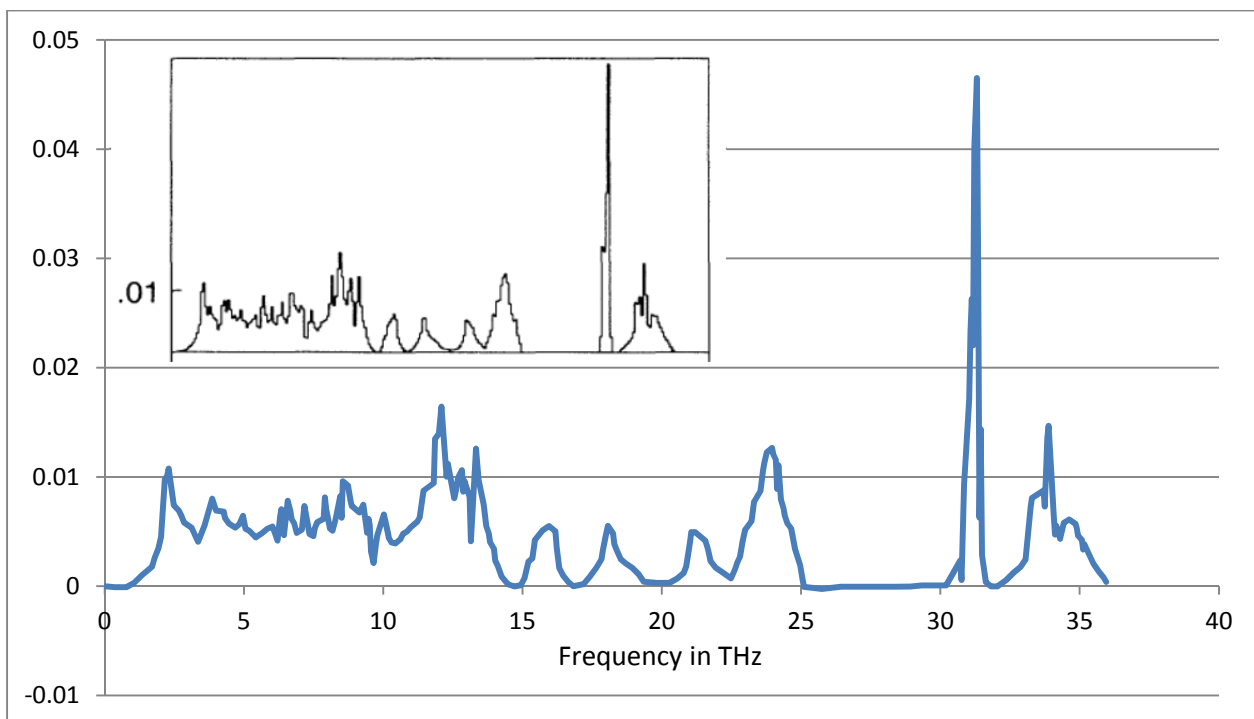


Fig.3.7: α -quartz phonon density of states vs frequency (in THz), as digitized from Fig. 1 of Ref. [38], which is recalled in the insert.

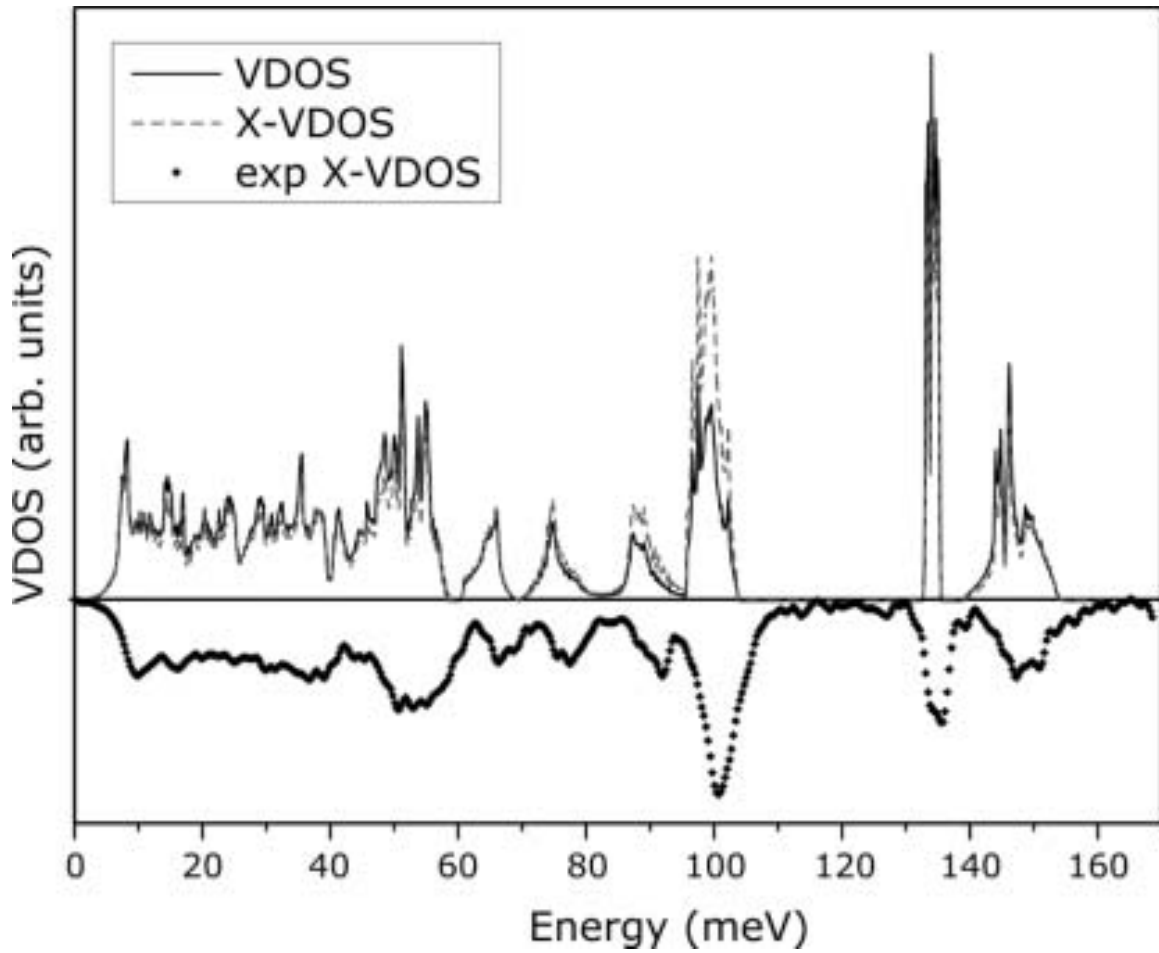


Fig.3.8: Experimental X-VDOS of *a*-quartz (room temperature) compared to the calculated X-VDOS (with the CASTEP code) and the true VDOS (as measured by neutron inelastic scattering). The areas underneath the curves are normalized to the same surface. (Fig. 1 from [51]).

Since, due to the digitization, the frequencies are not equally spaced, we have used Matlab's function for integration with the trapezoidal rule to calculate the average frequencies⁵⁵.

$$\frac{\int_0^{\infty} PDOS_{NH}(\omega)\omega d\omega}{\int_0^{\infty} PDOS_{NH}(\omega)d\omega} \text{ and } \frac{\int_0^{\infty} PDOS_H(\omega)\omega d\omega}{\int_0^{\infty} PDOS_H(\omega)d\omega} \quad (3.72)$$

The values of the average frequencies calculated for the LAMMPS simulations for different time steps are given in Table 3.4

⁵⁵ $\langle \omega \rangle_{H \text{ or } NH} = \text{trapz}(x, x.*y)/\text{trapz}(x,y)$, with x the vector filled with the frequencies and y the vector with the corresponding values of the PDOS.

Table 3.4: Average frequency for different time steps.

Nb of times steps (in 10^6)	1	1.5	2	2.5	3	3.5
$\langle\omega\rangle_{NH}$ (in THz)	18.1519	18.1546	18.1537	18.1525	18.1529	18.1519
Nb of times steps (in 10^6)	4	4.5	5	5.5	6	6.5
$\langle\omega\rangle_{NH}$ (in THz)	18.1507	18.1507	18.1512	18.1510	18.1514	18.1519

We can see that the values are pretty much constant, hence that we could have used less than 1 million time steps, while still keeping a good accuracy...

The average frequencies corresponding to the experimental curve [51] and Lee and Gonze's curve [38] (both digitized thanks to Engauge digitizer) are 17.7206 THz and 16.1601 THz respectively⁵⁶. We note that the difference between our estimation and the value derived from the experimental curve is smaller than the difference between the result extracted from the curve of Lee and Gonze and the one extracted from the experimental curve found in Ref. [51].

Hence, the average angular frequency of the "anharmonic phonons" is estimated by:

$$\langle\omega\rangle = 2\pi \times (17.7206 - 16.1601) \times 10^{12} \text{ rad/s} \approx 9.8 \times 10^{12} \text{ rad/s}$$

If we now compute β' thanks to Eq. (3.43) and numerical values from paragraph 2.3, then the new value of β' with $\langle\omega\rangle = 9.8 \times 10^{12} \text{ rad/s}$ and $\chi = 1$, is $1.7 \times 10^7 \text{ cm}^{-3}$ which is far above the experimental limit that corresponds approximately to $\beta' \approx 1 \text{ cm}^{-3}$. Hence, this result could invalidate Handel's quantum $1/f$ noise theory as applied to BAW quartz resonators but it could also invalidate our method for computing $\langle\omega\rangle$ (or the numerical values used for the other parameters in Handel's formula for β')! Indeed, the precision of our method is very probably not enough to compute quantitatively a difference between two similar quantities, but our goal was just to provide an order of magnitude so as to prove that $\langle\omega\rangle = 10^8 \text{ Hz}$ (as taken by Handel) was out of reach of what we could get with the definition (3.66).

5. Conclusions

We have reviewed Handel's theory of quantum $1/f$ noise as applied to quartz crystal resonators. We have been able to prove that Handel's main formula (3.20) for the determination of the PSD of relative frequency fluctuations is not in contradiction with experimental data though the

⁵⁶ We also found 16.561 THz from another independent (but less precise) digitization of Lee and Gonze's curve, meaning that the accuracy of the digitization process is quite important!

volume of resonator is at the numerator and not the denominator as would be expected because of the observation that thicker resonators tend to have less $1/f$ noise.

Unfortunately, we still have points of concern about the derivation of formula (3.20), in spite of two visits of P. Handel to Besançon. This causes problems to assign clear physical meaning to the quantities that are present in the expression of the β' factor (Eq. (3.43)) and therefore limit our ability to get a precise estimation of the noise floor for quartz oscillators and even more for oscillators made with other materials, in spite of our attempts at using molecular dynamics simulations to get a well-defined value of the average frequency appearing in Eq. (3.43).

We note, nonetheless that further checks of the stability of our result for $\langle\omega\rangle$ could be done by varying the parameters used to extract $\langle\omega\rangle$ (particularly replace Gonze's results with results obtained with LAMMPS/fixphonon/phana for a quadratic effective potential between all pairs of ions) and making other digitizations with even more imposed points.

As a transition to the study of the impact of dislocations on noise, in the next chapter, we note that the power dissipated in the resonator (of the order of $56 \mu\text{W}$) can be used to estimate that roughly 10^8 eV are dissipated per period of our 5 MHz oscillators. Supposing that this energy comes from the breaking of bonds along the dislocations, molecular dynamics studies could perhaps provide a relation between the concentrations of dislocation-pinning impurities and the length of dislocations per unit volume. Rough estimations show that it may not be very different from an order of magnitude of 1 cm/cm^3 that is actually measured (*cf.* chapter 1).

6. References

- [1] P. H. Handel, “ $1/f$ Noise - an 'Infrared' Phenomenon”, Phys. Rev. Lett., vol. 34, pp. 1492-1495, 1975.
- [2] P. H. Handel, “Nature of $1/f$ phase noise”, Phys. Rev. Lett., vol. 34, pp. 1495-1498, 1975.
- [3] P. H. Handel, “Quantum theory of $1/f$ noise”, Phys. Lett. vol. 53A, no. 6, pp. 438-440, 1975.
- [4] P. H. Handel, “ $1/f$ Macroscopic Quantum Fluctuations of Electric Currents Due to Bremsstrahlung with Infrared Radiative Corrections”, Zeitschrift für Naturforschung, vol. 30A, pp. 1201, 1975.
- [5] D.R. Yennie, S.C.Frautschi, H.Suura, “The infrared divergence phenomena and high-energy processes”, Ann. Phys. (New York), vol. 13, no. 3, pp. 379-452, 1961.
- [6] A. van der Ziel, “Unified presentation of $1/f$ noise in electronic devices: fundamental $1/f$ noise sources”, Proc. IEEE, vol. 76, no. 3, pp. 233-258, 1988.
- [7] M. B. Weissman, “ $1/f$ noise and other slow, nonexponential kinetics in condensed matter”, Rev. Mod. Phys., vol. 60, pp. 537-571, 1988.
- [8] L.B. Kiss, P. Heszler, “An exact proof of the invalidity of ‘Handel’s quantum $1/f$ noise model’, based on quantum electrodynamics”, J. Phys. C: Solid State Phys. vol. 19, pp. L631-L633, 1986.
- [9] P. H. Handel, “On the invalidity of the Kiss-Heszler ‘exact proof’ and correctness of the quantum $1/f$ noise theory”, J. Phys. C: Solid State Phys. vol. 21, pp. 2435-2438, 1988.
- [10] Th. M. Neiuwenhuigen, D. Frenkel and N.G. van Kampen, “Objections to Handel’s quantum theory of $1/f$ noise”, Phys. Rev. A, vol. 35, no. 6, 1987.
- [11] P. H. Handel, “ $1/f$ noise universality in high-technology applications”, in Proc. IEEE Int. Freq. Contr. Symp., Boston, June 1994, pp. 8-21.
- [12] P. H. Handel and F. L. Walls, “Analysis of quantum $1/f$ effects in frequency standards”, in Proc. IEEE Int. Freq. Contr. Symp., Boston, June 1994, pp. 539-540.
- [13] P. H. Handel, A. Tournier and B. Henning, “Quantum $1/f$ effect in resonant biochemical piezoelectric and MEMS sensors”, IEEE Trans. Ultrason., Ferroelec., Freq. Contr., vol. 52, no. 9, pp. 1461-1467, 2005.
- [14] P. H. Handel and A. G. Tournier, “Nanoscale engineering for reducing phase noise in electronic devices”, Proc. IEEE, vol. 93, no. 10, pp. 1784-1814, October 2005.
- [15] F.L. Walls, P. H. Handel, R. Besson, J.J. Gagnepain, “New model of $1/f$ noise in BAW quartz resonators”, 1992 IEEE Freq. Contr. Symp., pp. 327-333, DOI: 10.1109/FREQ.1992.269996.
- [16] P. H. Handel, “Quantum approach to $1/f$ noise”, Phys. Rev. A, vol. 22, pp. 745-757, 1980.

- [17] A. van der Ziel, "Semiclassical derivation of Handel's expression for the Hooge parameter," J. Appl. Phys., vol. 63, no. 7, pp. 2456-2457, 1988.
- [18] P. H. Handel, "Nature of $1/f$ frequency fluctuations in quartz crystal resonators", Solid State Electronics, vol. 22, pp. 876-876, 1979.
- [19] T. Parker, " $1/f$ frequency fluctuations in quartz acoustic resonators", Appl. Phys. Lett., vol. 46, no. 3, pp. 246-248, 1985
- [20] P. H. Handel, "Incoherence and negative entropy in the quantum $1/f$ effect of BAW and SAW quartz resonators", in Proc. IEEE Int. Freq. Contr. Symp., Orlando, 1997, pp. 464-469.
- [21] P. H. Handel, "Quantum $1/f$ quartz resonator theory versus experiment", in 1999 joint meeting EFTF - IEEE IFCS, Besançon, 1999, pp. 1192-1195.
- [22] M. Devel, R. Bourquin, S. Ghosh, J. Imbaud, G. Cibiel, F. Sthal, "Quartz crystal resonator noise and fluctuation-dissipation theorem considerations", Proc. IEEE Int. Freq. Cont. Symp., Baltimore, Maryland, 21-24 May 2012, pp. 425-429.
- [23] F. Sthal, M. Devel, S. Ghosh, J. Imbaud, G. Cibiel and R. Bourquin "Volume dependence in Handel's model of quartz crystal resonator noise", IEEE Transactions on Ultrasonics, Ferroelectrics, and Frequency Control, vol. 60, no. 9, pp. 1971-1977, 2013.
- [24] J.R.Norton, "Performance of ultrastable quartz oscillators using BVA resonators," Proc. European Frequency and Time Forum, Weihenstephan, Germany, March 1994, pp. 457-465.
- [25] R. J. Besson, M. Mourey, S. Galliou, F. Marionnet, F. Gonzalez, P. Guillemot, R. Tjoelker, W. Diener, A. Kirk, "10 MHz Hyperstable quartz oscillators", Proc. Joint Meeting IEEE Ann. Freq. Cont. Symp. and European Frequency and Time Forum, Besançon, France, april 1999, pp. 326-330.
- [26] J. Chauvin, P. Weber, J.P. Aubry, F. Lefebvre, F. Sthal, S. Galliou, E. Rubiola and X. Vacheret, "A new generation of very high stability BVA oscillators", Proc. Joint Meeting IEEE Ann. Freq. Cont. Symp. and European Frequency and Time Forum, Genova, Switzerland, June 2007, pp. 1261-1268.
- [27] A. Kuna, J. Cermak, L. Sojdr, P. Salzenstein and F. Lefebvre, "Lowest flicker-frequency floor measured on BVA Oscillators", IEEE Trans. Ultrason., Ferroelec., Freq. Contr., vol. 56, no. 3, pp. 548-551, 2009.
- [28] P. Salzenstein, A. Kuna, L. Sojdr and J. Chauvin, "Significant step in ultra high stability quartz crystal oscillators", Electron. Lett., vol. 46, no. 21, pp. 1433-1434, 2010.
- [29] D. S. Stevens, H. F. Tiersten, "An analysis of doubly rotated quartz resonators utilizing essentially thickness modes with transverse variation", J. Acous. Soc. Am., vol. 79, no. 6, pp. 1811-1826, 1986.

- [30] R. Bourquin, B. Dulmet, J. J. Boy, "SC-cut resonator operating in anharmonic modes with B-mode reduction", Proc. European Frequency and Time Forum, Brighton, United Kingdom, March 1996, pp. 239-243.
- [31] D. Schneuwly, Y. Schwab, "Quartz clocks", 3rd Int. Telec. Sync. Forum, London, UK, Oct. 2005.
- [32] J. Lamb, J. Richter, "Anisotropic acoustic attenuation with new measurements for quartz at room temperatures", Proc., Roy. Soc. Series A, vol. 293, pp. 479-492, 1966.
- [33] D. W. Allan, "Statistics of atomic frequency standards", Proc. IEEE, vol. 54, no. 2, Feb., pp. 136-154, 1966.
- [34] IEEE, "IEEE Standard Definitions of Physical Quantities for Fundamental Frequency and Time Metrology - Random Instabilities", in IEEE STD 1139-2008: IEEE, 2008, pp. 1-35.
- [35] E.S. Ferre-Pikal, F. L. Walls, J. R. Vig, J. F. Garcia Nava, "Experimental studies on Flicker noise in quartz crystal resonators as a function of electrode volume, drive current, type of quartz, and fabrication process", Proc. IEEE Ann. Freq. Cont. Symp., Honolulu, Hawaii, June 1996, pp. 844-851.
- [36] M. M. Driscoll, W. P. Hanson, "Measured vs. volume model-predicted flicker-of-frequency instability in VHF quartz crystal resonators", Proc. IEEE Ann. Freq. Cont. Symp., Salt Lake City, Utah, June 1993, pp. 186-192.
- [37] F. L. Walls, "The quest to understand and reduce $1/f$ noise in amplifiers and BAW quartz oscillators", in Proc. European Frequency and Time Forum, Besançon, France, 1995, pp. 227-243.
- [38] C. Lee, X. Gonze, "Ab.initio calculation of the thermodynamic properties and atomic temperature factors of SiO₂ n-quartz and stishovite", Phys. Rev. B, vol. 51, no. 13, pp. 8610-8613, 1995.
- [39] W. C. Swope, H. C. Anderson, P. H. Berens and K. R. Wilson, "A computer simulation method for the calculation of equilibrium constants for the formation of physical clusters of molecules: application to small water clusters", J. Chem. Phys., vol 76, no. 1, pp. 637-649, 1982.
- [40] D. C. Rapaport, "The Art of Molecular Dynamics Simulation", 2nd ed., Cambridge University Press, 2004.
- [41] W. Cai, "Handout 1. An Overview of Molecular Simulation", ME346 – Introduction to Molecular Simulations – Stanford University – Winter 2007.
- [42] S. Nosé, "A unified formulation of the constant temperature molecular dynamics methods", J. Chem. Phys., vol. 81, no. 1, pp. 511-519, 1984 and S. Nosé, "A molecular dynamics method for simulations in the canonical ensemble", Mol. Phys. vol. 52, pp. 255-268, 1984.

- [43] William G. Hoover, “Canonical dynamics: Equilibrium phase-space distributions”, *Phys. Rev. A*, vol. 31, no. 3, pp. 1695-1697, 1985.
- [44] B. W. H. van Beest, G. J. Kramer and R. A. van Santen, “Force Fields for Silicas and Aluminophosphates Based on *Ab Initio* Calculations”, *Phys. Rev. Lett.*, vol. 64, no. 16, pp. 1955-1958, 1990.
- [45] M. R. Farow and M. I. J. Probert, “Atomistic molecular dynamics simulations of shock compressed quartz”, *J. Chem. Phys.*, vol. 135, 044508, 2011.
- [46] S. Plimpton, “Fast Parallel Algorithms for Short-Range Molecular Dynamics”, *J. Comp. Phys.*, vol. 117, 1-19, 1995.
- [47] L.T. Kong, “Phonon dispersion measured directly from molecular dynamics simulations”, *Comp. Phys. Comm.*, vol. 182, no. 10, pp. 2201-2207, 2011.
- [48] L.T. Kong and L.J. Lewis, “Surface diffusion coefficients: Substrate dynamics matters”, *Phys. Rev. B*, vol. 77, 165422, 2008.
- [49] C. Hudon, R. Meyer, and L.J. Lewis, “Low-frequency vibrational properties of nanocrystalline materials: Molecular dynamics simulations of two-dimensional systems”, *Phys. Rev. B*, vol. 76, 045409, 2007.
- [50] X. Gonze, J.C. Charlier, D.C. Allan, M.P. Teter, “Interatomic force constants from first principles: The case of α -quartz”, *Phys. Rev. B*, vol. 50, no. 17, pp. 13035-13038, 1994.
- [51] A. Bosak, M. Krisch, D. Chernyshov, B. Winkler, V. Milman, K. Refson and C. Schulze-Briesev, “New insights into the lattice dynamics of α -quartz”, *Z. Kristallogr.*, vol. 227, no. 2, pp. 84-91, 2012.

APPENDIX A: example of LAMMPS input script

Calculation of vibrations properties of alpha quartz using BKS potential and fixPhonon

units metal

newton on

atom_style charge

dimension 3

boundary p p p

variable n equal 10

read_data quartz\$n.pos

kpace_style ewald/n 1.0e-5

pair_style buck/coul/long 10.0

pair_coeff 1 1 0.0 0.0001 0.0

pair_coeff 1 2 18003.7572 0.205205 133.5381

pair_coeff 2 2 1338.7730 0.362319 175.0000

#value for time steps

variable ts equal 2e-3 # since time unit is ps, this is 2 fs

parameters for the thermostat/barostat fix

variable r equal 57085

variable t equal 300 # temperature (in K)

variable p equal 1 # pressure (in bar(s) if units = metal)

#variable td equal 0.05 # 100 time steps

variable td equal 100*\${ts} # as advocated in LAMMPS nvt help page

variable pd equal 1000* $\{ts\}$ # 1000 time steps

initialize

velocity all create \$t \$r rot yes dist gaussian mom yes

reset_timestep 0

dump init all xyz 100000 Quartz-tilt-\$n.xyz

fixes

#fix 1 all npt temp \$t \$t \$d iso 1. 1. 1. pchain 8 drag 1.0

fix 1 all npt temp \$t \$t $\{td\}$ iso \$p \$p $\{pd\}$

#fix 1 all nvt temp \$t \$t $\{td\}$

fix 2 all phonon 10 50000 500000 map.quartz\$n.in QuartzPhonon\$n

timestep $\{ts\}$

output 1 2 3 4 5 6 7 8 9 10 11 12

thermo_style custom step temp pe ke press vol lx ly lz xy xz yz cella cellb cellc cellalpha cellbeta
cellgamma

thermo 500000

restart 2000000 restart.one restart.two

execution

run 6500000

write_restart Restart.final

Chapter 4: Investigation of $1/f$ Noise With The help of Fluctuation-Dissipation Theorem

In this chapter we use the fluctuation-dissipation theorem to investigate the origin of $1/f$ noise in quartz crystal resonators. First, we concentrate on the contribution of thickness fluctuations on the level of noise, at low frequencies. For that purpose, we solve a motion equation with both viscous and some structural damping, i.e. with a term proportional to speed and another to amplitude. We show how the fluctuation dissipation theorem allows us to recover a $1/f$ noise spectral density at low frequency. We can then numerically estimate the absolute level of $1/f$ noise as a function of the structural damping coefficient. Finally, we use the Granato-Lücke theory of dislocation motion to provide some hints on a possible physical origin of the type of structural damping that we modelled.

1. Fluctuation-Dissipation Theorem (FDT)

The fluctuation-dissipation theorem (later on called FDT for short) finds its origins in works of Einstein (First connection between a diffusion coefficient and an energy damping coefficient) [1], Callen and Welton (First demonstration using statistical mechanics) [2], Callen and Greene (extension to the macroscopic thermodynamic domain) [3] and Kubo [4] (review paper on the subject with an emphasis on the use of correlation functions, collective modes of a many-particles systems and a matrix formulation). It is a powerful tool in statistical mechanics to study the behavior of a thermodynamic system near thermal equilibrium. It uses the fact that if a statistical system in thermal equilibrium is subjected to a small external force that drives it out of equilibrium, the dissipative forces that will restore a thermal equilibrium are the same as those that occur during a spontaneous fluctuation of some thermodynamic variable of the systems. Thus, the FDT may be used to deduce the response of the statistical system to an arbitrary but small perturbation since it gives a relation between the “impedance” of a general dissipative linear system and the fluctuations of the corresponding “generalized forces” [2]. FDT is a link between an equilibrium property of the system (spectrum of fluctuations) and some quantity characterizing an irreversible loss of energy due to the interaction with some external perturbation. Furthermore, it applies both to classical and quantum mechanical systems, but in slightly different forms⁵⁷. We will use the classical form for our application.

⁵⁷ In the quantum case, autocorrelation functions must be redefined so as to take into account the fact that observables may not commute (see e.g. [4]), furthermore, in the classical case the equipartition theorem for quadratic terms in the energy is used.

1.1. Callen-Welton form of the FDT

First, we recall some definitions from [2]: “A system may be said to be *dissipative* if it is capable of absorbing energy when subjected to a time-periodic perturbation”. It may be said to be *linear* “if the power dissipation is quadratic in the magnitude of the perturbation”. Hence, for a linear dissipative system, the proportionality constant between the power and the square of the perturbation amplitude may be used to define the (generalized complex) impedance of the system as the ration of the (complex) amplitude of the perturbation (V) by the time derivative of the response of the system to the perturbation (\dot{q}). If the perturbation is not sinusoidal, then the definition applies for the Fourier components: $\hat{V}(\omega) = Z(\omega)\hat{q}(\omega)$. We will also say that the eigenstates of the dissipative quantum system are densely distributed in energy if we can replace the summation over the eigenstates by an integral on the energy, weighted by the density of states. In their conclusion Callen and Welton see this process as a loss of internal coherence in a source system caused by the random fluctuations generated by the dissipative system and acting on the source system. “The dissipation thus appears as the macroscopic manifestation of the disordering effect of the Nyquist fluctuations and, as such, is necessarily quantitatively correlated with the fluctuations”.

Callen and Welton fundamental theorem (Eq. 4.8 and 4.11 of [2]) is then:

$$\langle V^2 \rangle_{eq} = \frac{2}{\pi} \int_0^\infty R(\omega) \left[\left(n(\omega) + \frac{1}{2} \right) \hbar \omega \right] d\omega \xrightarrow{\omega \ll k_B T / \hbar} \frac{2k_B T}{\pi} \int_0^\infty R(\omega) d\omega \quad (4.1)$$

where $\langle \rangle_{eq}$ represents a statistical ensemble average of the fluctuation at equilibrium, $R(\omega) = \text{Re}(Z(\omega))$ and $n(\omega)$ is Planck’s distribution $1/[\exp(\hbar\omega/k_B T) - 1]$ ⁵⁸.

A simple change from circular frequency to frequency then allows to find the usual Johnson-Nyquist formula⁵⁹ for the one-sided spectral power density of voltage fluctuations: $S_V(f) \approx 4k_B TR$ (or $V_{RMS}^2 = 4k_B TR \times \Delta f$ in a given frequency band, if R is independent of frequency).

We note that Callen and Welton also applied their fundamental formula (that they called “generalized Nyquist relation”) to the case of Brownian motion, electric dipole radiation resistance and electric field fluctuations in vacuum (rederiving Planck’s radiation law) and to the calculations of pressure fluctuations in a gas, thanks to the definition of an acoustic radiation resistance.

1.2. Callen-Greene form of the FDT

Trying to find new ways to deal with thermodynamic irreversible processes, Callen and Greene generalized the previous formula. Their fundamental results are [3]:

⁵⁸ $n(\omega) + \frac{1}{2} = \frac{1}{2} \coth\left(\frac{\hbar\omega}{2k_B T}\right) \xrightarrow{\omega \ll k_B T / \hbar} \frac{k_B T}{\hbar\omega}$, which can be showed to be equivalent to using the equipartition theorem.

⁵⁹ In 1926, at Bell labs, J. B. Johnson discovered that the mean square of the fluctuations of the potential difference across a resistor is proportional to its resistance and to its absolute temperature and independent of the material and shape of the conductor. He also noted that “in the range of audio frequencies, at least, the noise contains all frequencies at equal amplitude”. He attributed that phenomenon to the thermal agitation of the carriers of electricity in the conductors [5]. His colleague, Harry Nyquist was able to justify a law that would describe these results. In 1928, Johnson published a detailed account of his experiment [6] and Nyquist his theory [7].

$$\langle (x_j - X_j)^2 \rangle = -\frac{2k_B}{\pi} \int \sigma_S(\omega) \frac{d\omega}{\omega^2} \quad (4.2)$$

$$\langle (x_j - X_j)^2 \rangle = \frac{2k_B T}{\pi} \int \sigma_U(\omega) \frac{d\omega}{\omega^2} \quad (4.3)$$

The first relation applies in the microcanonical case for which all the extensive parameters of the system (including total energy U) other than the one which fluctuations are computed are supposed to be constant, while the second applies in canonical case where the constraint on the energy is replaced by the condition of adiabatic insulation (no flow of heat through the frontiers of the system, which is almost the same as a condition of constant entropy S). σ_S and σ_U are generalized conductances (real part of the complex generalized admittance $Y(\omega)$ to be defined later in this paragraph). In these relations, $\langle (x_j - X_j)^2 \rangle$ is the mean square fluctuations of the j^{th} extensive thermodynamic variable x_j around its equilibrium value X_j , in the frequency interval determined by the effective range of the integral. To a fluctuation extensive parameter $x(t)$ of the system is attached a generalized force $f(t)$ which is the corresponding intensive parameter of the “driving reservoir” whose interactions with system cause the fluctuations of (t) ⁶⁰. Then, the generalized admittance is defined by⁶¹:

$$Y(\omega) = i\omega \hat{x}(\omega) / \hat{f}(\omega), \quad (4.4)$$

where $\hat{x}(\omega)$ and $\hat{f}(\omega)$ are the Fourier transforms of $x(t)$ and $f(t)$ ⁶².

These relations can be restated in terms of the fluctuations of the corresponding (intensive thermodynamic variables conjugated to the corresponding intensive variable x_j in the development of the entropy S or the internal energy U : $F_j = (\partial S / \partial X_j)_{U, X_i}$ and $P_j = (\partial U / \partial X_j)_{S, X_i}$:

$$\langle \delta F^2 \rangle = -\frac{2k_B}{\pi} \int R_S(\omega) d\omega \quad (4.5)$$

$$\langle \delta P^2 \rangle = \frac{2k_B T}{\pi} \int R_U(\omega) d\omega \quad (4.6)$$

where R_S and R_U are generalized resistances (real part of the complex generalized impedance $R = \text{Re}[Z(\omega)] = \text{Re}[1/Y(\omega)]$) corresponding respectively to the constant energy or adiabatic constraints.

⁶⁰ The driving reservoir must be big enough compared to the original system so that a change of an extensive thermodynamic variable of this original (small) system does not change appreciably the corresponding intensive variable of the driving reservoir. Then, the driving reservoir can be considered in quasi-static thermodynamic equilibrium and hence may be assigned instantaneous intensive thermodynamic characteristic variables with frequency components $\hat{f}(\omega)$ (as long as $\omega \ll 1/\tau$, with τ the highest relaxation time of the “driving reservoir”).

⁶¹ Callen and Greene proved that $Y(\omega) = i\omega \partial X / \partial F + O(\omega^2)$, and $Y(\omega) = i\omega \partial X / \partial F + O(\omega^2)$, so that a constant impressed force induces a finite and definite value of the extensive parameter x and that $Y(\omega)$ may have poles only in the upper half of complex ω -plane.

⁶² We use here the definitions $\hat{x}(\omega) = \int_{-\infty}^{+\infty} x(t) e^{-i\omega t} dt$, $x(t) = (1/2\pi) \int_{-\infty}^{+\infty} \hat{x}(\omega) e^{i\omega t} dt$, which are not the same as in the paper of Callen and Greene, which use a factor $1/\sqrt{2\pi}$ in front of both integrals.

1.3. Kubo's form of the FDT

In his 1966 review paper [4], Kubo begins by the general remark that during random interactions (collisions or impacts in the paper) between molecules or atoms, there are two effects: a “random part” corresponding to the effect of all these random interactions as a driving force to maintain the incessant irregular motion of the system and a “systematic part” corresponding to the frictional force for a forced motion (coming from inelastic interactions that redistribute part of the energy of the forced motion onto other internal degrees of freedom). The fact that the physical origin of these two effects of the microscopic forces are the same, lead to the fact that **the systematic part of the microscopic force, appearing as friction, is actually determined by the correlations of the random part of the force, conversely the random part must have its power spectrum determined by friction**. Hence, the FDT can be used in two ways: it can predict the characteristics of the fluctuation or the noise intrinsic to the system from the known characteristics of the admittance or the impedance, or it can be used as the basic formula to derive the admittance from the analysis of thermal fluctuations of the system.

Kubo used a modified Langevin equation [8] approach of Brownian motion, with a retarded (frequency or time dependent) friction coefficient $\gamma(t - t')$, to demonstrate relations involving autocorrelation functions of stationary processes that can be calculated at the atomic level and are therefore used in modern Molecular Dynamics code to estimate various macroscopic diffusion or energy loss coefficients. This modified Langevin equation is⁶³:

$$m\dot{u}(t) + \int_0^t m\gamma(t - t')u(t') dt' = K(t) + R(t) \quad t > 0 \quad (4.7)$$

Where $u(t)$ is the velocity of the particle at time t , $K(t)$ is the driving force imposed from the exterior of the system (from which only the linear effect is considered) and $R(t)$ is a random force, independent of the presence or absence of $K(t)$, such that:

$$\forall t_0, \quad \frac{d}{dt_0} \langle R(t_0)R(t_0 + \tau) \rangle = 0 \quad (\text{stationarity}) \quad (4.8)$$

$$\forall t, \quad \langle R(t) \rangle = 0 \quad \text{and} \quad \forall t > t_0, \quad \langle R(t)u(t_0) \rangle = 0 \quad (4.9)$$

If a periodic external force $K(t) = K_0 \cos \omega t$ is applied, then one can define a complex admittance $Y(\omega)$ (or mobility) of the system by:

$$\langle u(t) \rangle = \text{Re}(Y(\omega)K_0 \exp(i\omega t)), \quad \text{with} \quad Y(\omega) = \frac{1}{m} \frac{1}{i\omega + \gamma[\omega]} \quad (4.10)$$

with $\gamma[\omega] = \int_0^{+\infty} \gamma(t)e^{-i\omega t} dt$. Kubo then proves that:

$$Y(\omega) = \frac{1}{m\langle u^2 \rangle} \int_0^{\infty} e^{-i\omega\tau} \langle u(t + \tau)u(t) \rangle d\tau \quad (4.11)$$

⁶³ The total (internal) microscopic force is $F(t) = R(t) - \int_0^t m\gamma(t - t')u(t') dt'$, with $R(t)$ its random part and $-\int_0^t m\gamma(t - t')u(t') dt'$ its systematic (friction) part.

If the equipartition theorem $\langle u^2 \rangle = k_B T / m$ can be assumed, we then get:

$$Y(\omega) = \frac{1}{k_B T} \int_0^\infty e^{-i\omega\tau} \langle u(t+\tau)u(t) \rangle d\tau \equiv \frac{1}{k_B T} \Phi[\omega] \quad (4.12)$$

This is the first classical form of the FDT for one fluctuating classical dynamic variable for Kubo.

Going back to Eq. (4.7) with $K(t) = 0$, Kubo also showed that:

$$m\gamma[\omega] = \frac{1}{m\langle u^2 \rangle} \int_0^\infty e^{-i\omega\tau} \langle R(t+\tau)R(t) \rangle d\tau \approx \frac{1}{k_B T} \int_0^\infty e^{-i\omega\tau} \langle R(t+\tau)R(t) \rangle d\tau \quad (4.13)$$

This is the second classical form of the FDT for one fluctuating classical dynamic variable for Kubo.

Going back to the generalized Langevin equation, and the fact that the total internal microscopic force can be decomposed in $F(t) = m\dot{u}(t) = R(t) - \int_0^t m\gamma(t-t')u(t') dt'$, in section 8, Kubo proves that:

$$\frac{1}{\gamma[\omega]} = \frac{1}{\gamma_t[\omega]} - \frac{1}{i\omega} \quad (4.14)$$

with: $\gamma[\omega] = \frac{1}{mk_B T} \int_0^\infty e^{-i\omega\tau} \langle R(t+\tau); R(t) \rangle d\tau$ and $\gamma_t[\omega] = \frac{1}{mk_B T} \int_0^\infty e^{-i\omega\tau} \langle F(t+\tau); F(t) \rangle d\tau$ ⁶⁴.

This implies that the random force correlation is finite at low frequencies, while the total force

correlation tends to 0 as $i\omega$ (i.e. $\int_0^\infty \langle R(\tau); R(0) \rangle d\tau = \int_0^\infty \langle R(t+\tau); R(t) \rangle d\tau \neq 0$ while *stationarity*

$\int_0^\infty \langle F(t+\tau); F(t) \rangle d\tau = 0$), whereas at high frequencies both correlations give the same result. If we go back to the time domain, this means that both the correlation function of the random force R and the total force F will decay in a time interval (named τ_c by Kubo since this decay is due to random collisions of the big particle with atoms in Brownian motion) which is generally much shorter than the relaxation time $\tau_r = 1/\gamma[0] = 1/\int_0^{+\infty} \gamma(t)dt = mk_B T / \int_0^{+\infty} \langle R(t+\tau); R(t) \rangle d\tau$ characterizing the decay of the negative part of the time correlations of F (remember $\int_0^\infty \langle F(t+\tau); F(t) \rangle d\tau = 0$).

Finally let us note that, in section 9, Kubo uses a generalization of the FDT to several fluctuating variables using an impedance matrix and matrices of correlation functions to show that the friction spectral matrices that generalize $\gamma[\omega]$ and $\gamma_t[\omega]$ behave very differently around the eigen-frequencies of the matrix $\Omega_{jk} = -i\langle X_j(t); \dot{X}_k(t) \rangle$, but they approach the same limit at high frequencies because the source of both parts of the forces are always in the same fast microscopic processes.

⁶⁴ The « ; » sign in the middle of the correlation functions, comes from a definition of correlation that was generalized in section 5 and used in sections 6 and 7 to generalize the FDT for the quantum case in which operators do not necessarily commute. In classical mechanics this is the usual correlation function.

2. Investigation of 1/f Noise with the help of the FDT

2.1. Evaluation of the contribution of thickness fluctuations to frequency noise

In [9], we have applied the fluctuation-dissipation theorem (FDT) as formulated in [10] and [11] to estimate the power spectral density of thermal noise coming from fluctuations in the thickness ($2h$) of quartz resonators (Fig.4.1).

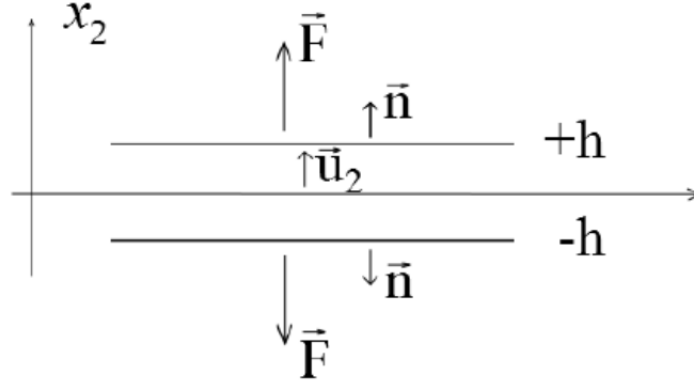


Fig.4.1: Resonator design.

In order to fulfill this task, we first describe these fluctuations by a 1D viscoelastic model of the longitudinal vibrations along the thickness of the quartz resonator. Indeed, for this mode, characterized by the mechanical displacement $u_2(x_2; t)$ inside the resonator along the x_2 axis, the strain and stress are respectively given by:

$$S_2 = \frac{\partial u_2}{\partial x_2} \quad (4.15)$$

$$T_2 = c_{22}S_2 + \eta_{22} \frac{\partial S_2}{\partial t} \quad (4.16)$$

with c_{22} is the elastic constant and η_{22} is the viscoelastic damping constant of quartz crystal.

The local version of the fundamental principle of dynamics for continuum media can then be written as:

$$\rho \frac{\partial^2 u_2}{\partial t^2} = c_{22} \frac{\partial^2 u_2}{\partial x_2^2} + \eta_{22} \frac{\partial^3 u_2}{\partial x_2^2 \partial t} \quad (4.17)$$

With ρ is the quartz mass per unit volume.

Searching for solutions of the type:

$$u_2(x_2, t) = (a \sin(kx_2) + b \cos(kx_2))e^{j\omega t} \quad (4.18)$$

with limit conditions:

$$T_2(\pm h, t) = F \cdot \frac{e^{j\omega t}}{s} \quad (4.19)$$

with F the modulus of the harmonic mechanical force applied to the surface S of the electrodes (perpendicular to x_2), gives:

$$k^2 = \frac{\rho\omega^2}{(c_{22} + j\eta_{22}\omega)} \quad (4.20)$$

$$a = \frac{F/S}{(k \cos(kh))(c_{22} + j\eta_{22}\omega)} \quad (4.21)$$

$$b = 0 \quad (4.22)$$

We can now define and compute the complex mechanical admittance of the system by [10]:

$$\bar{Y}(\omega) \equiv \frac{\frac{\partial u_2(\pm h, t)}{\partial t}}{\pm F \cdot e^{j\omega t}} = \frac{j\omega a \sin(kh)}{F} \quad (4.23)$$

The FDT then states that the spectral power density of the thickness fluctuations can then be computed by [10] and [11]⁶⁵:

$$\frac{u_2^2(\pm h, \omega)}{BW} = \frac{4k_B T}{\omega^2} \text{Re}(\bar{Y}(\omega)) \quad (4.24)$$

The connection with the spectral density of noise in the resonator in a bandwidth BW is then provided by the fact that:

$$\omega_r \propto \frac{1}{h} \Rightarrow S_y(\omega) \equiv \frac{(\delta\omega_r)^2}{\omega_r^2 BW} = \frac{u_2^2(\pm h, \omega)}{(2h)^2 BW} \quad (4.25)$$

Inserting Eq. (4.21) into (4.23), then the result into Eq. (4.24) and finally into Eq. (4.25) and introducing the volume between electrodes $V = S \times 2h$, we get:

$$S_y(\omega) = \frac{2k_B T}{hV\omega^2} \text{Re} \left(\frac{j\omega}{(c_{22} + j\eta_{22}\omega)} \cdot \frac{\sin(kh)}{k \cos(kh)} \right) \quad (4.26)$$

For quartz, $c_{22} = 8.6 \cdot 10^{10}$ Pa and $\eta_{22} = 1.4 \cdot 10^{-3}$ Pa·s [32]. Since we are interested by the low frequency noise, we can safely assume that $\omega \ll \frac{c_{22}}{\eta_{22}} \approx 6 \cdot 10^3$ rad/s. Thus, we have:

$$k \approx \sqrt{\frac{\rho}{c_{22}}} \omega \left(1 - j \frac{\eta_{22}\omega}{2c_{22}} \right) \quad (4.27)$$

If we further assume that we restrict ourselves to frequencies such that $\omega \ll \sqrt{c_{22}/\rho h^2} \approx 6 \cdot 10^6$ rad/s (for quartz $\rho = 2.65 \cdot 10^3$ kg/m³ and $h = 10^{-3}$ m for 5 MHz oscillators), we get $|kh| \ll 1$, hence $\tan(kh)/k \approx h$ and finally:

$$S_y(\omega) = \frac{2k_B T \eta_{22}}{V c_{22}^2} \quad (4.28)$$

Hence, for $V = 10^{-8}$ m³, $T = 350$ K, Fig.4.2 presents numerical estimation of the variations of $S_y(\omega)$ according ω . The fluctuations of thickness of the quartz resonator produce a white noise at low frequencies, with $S_y(\omega) = 2 \cdot 10^{-37}$ (rad/s)⁻¹, hence can be safely neglected with respect to the limiting noise source(s) (experimentally $\sim 10^{-27}$ (rad/s)⁻¹).

⁶⁵ $BW = 2\pi$ rad/s.

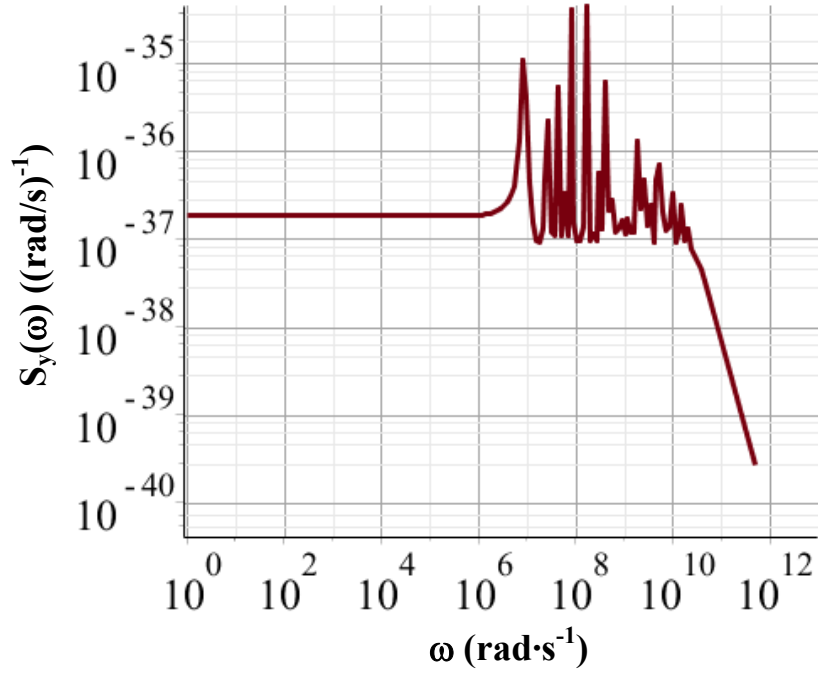


Fig.4.2: Variations of $S_y(\omega)$ in log-log scale.

The level of white noise was found to be far below what is measured; meaning that viscoelastic damping of thickness fluctuations is not the dominant noise process.

In our next calculation [12], an internal friction term φ , is added in the formulation, in order to obtain a $1/f$ spectrum at low frequencies. This gives us a complex elastic constant i.e. a frequency independent (at low frequencies) delay between stress and strain. The strain equation (4.15) is conserved as previously but the stress T_2 is now given by:

$$T_2 = c_{22}(1 + j\varphi)S_2 + \eta_{22} \frac{\partial s_2}{\partial t} \quad (4.29)$$

where φ is the internal friction coefficient [10], [11].

Then, the fundamental principles of dynamics for continuum media can be written as:

$$\rho \frac{\partial^2 u_2}{\partial t^2} = c_{22}(1 + j\varphi) \frac{\partial^2 u_2}{\partial x_2^2} + \eta_{22} \frac{\partial^3 u_2}{\partial x_2^2 \partial t} \quad (4.30)$$

By using the solution like (4.18) and using the limit condition (4.19) we have:

$$k^2 = \frac{\rho \omega^2}{(C_{22} + j(C_{22}\varphi + \eta_{22}\omega))} \quad (4.31)$$

$$a = \frac{F/S}{(k \cos(kh))(C_{22} + j(C_{22}\varphi + \eta_{22}\omega))}, \quad b = 0 \quad (4.32)$$

The complex mechanical admittance is given, as previously, by (4.23) and the power spectral density of thickness fluctuations is given by (4.24).

Inserting (4.32) into (4.23), then the result into (4.24) with the assumptions $\varphi \ll 1$ and $\omega \ll \frac{c_{22}}{\eta_{22}}$, we obtained a new expression of u_2^2 :

$$\frac{u_2^2(\pm h, \omega)}{BW} \approx \frac{4k_B T h}{S \omega c_{22}^2} (c_{22} \varphi + \eta_{22} \omega) \quad (4.33)$$

Moreover, we can consider that the circular frequency at resonance $\omega_r \sim 1/h$ (4.25), thus:

$$S_y(\omega) = \frac{2k_B T}{V c_{22}} \times \frac{1}{\omega} \left(\frac{\eta_{22} \omega}{c_{22}} + \varphi \right) \quad (4.34)$$

where V is the volume of the resonator. One can then see from the previous expression that for circular frequencies lower than $\varphi c_{22}/\eta_{22}$, the internal friction becomes dominant and gives a $1/f$ spectrum. Hence, φ could, in principle, be determined by the corner frequency between $1/f$ noise and white noise in the bare resonator (Fig.4.3) if it would not be masked by the white noise of the amplifier (cf. chapter 5). However, we recall that these results are obtained for a thickness oscillation mode (and not for the traditional shear mode) under the assumptions that neither η_{22} , nor c_{22} nor φ are frequency dependent.

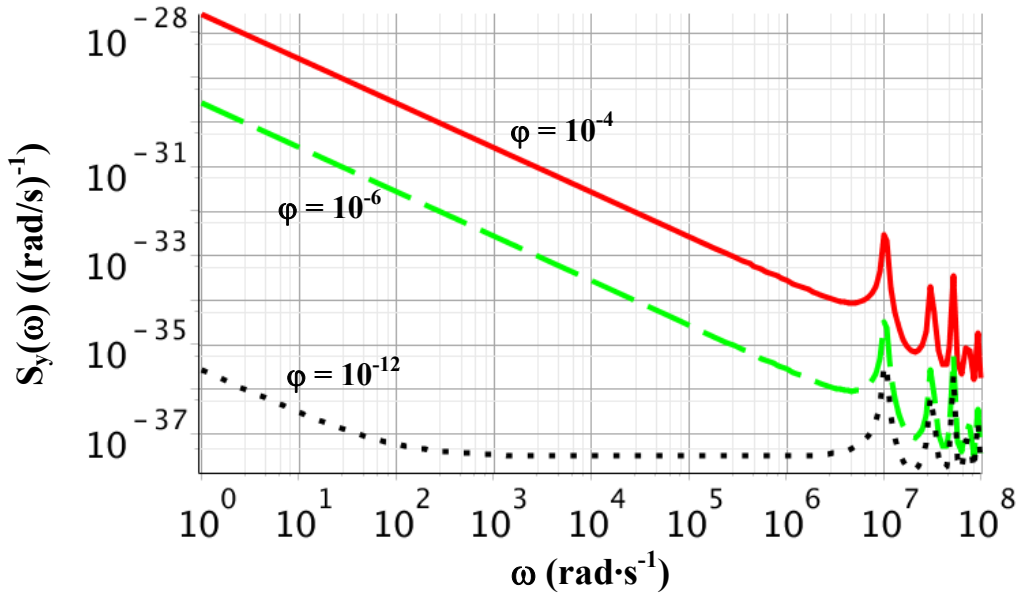


Fig.4.3: Behavior of $S_y(\omega)$ for various values of φ for a thickness oscillation mode with $\omega_r = \sqrt{c_{22}/\rho h^2} \approx 6 \cdot 10^6$ rad/s. The transition frequency between the $1/\omega$ regime and the white noise regime is proportional to φ . At low frequencies $S_y(\omega)$ is also proportional to φ , whereas at resonance and above the influence of φ can be completely neglected with respect to the traditional $\eta_{22}\omega/c_{22}$ viscoelastic damping term.

For $1/f$ (flicker) noise, the standard deviation of the difference of the average fractional frequencies measured for two consecutive samples is given by the expression [13]:

$$\sigma_{y_flicker} = \sqrt{2 \ln(2) S_y(1\text{Hz})} \quad (4.35)$$

This is the square root of the Allan variance [14]. It is commonly used to compare the short-term stabilities of various resonators, since it is the noise floor at low frequencies in terms of relative frequency fluctuations.

Provided the corner frequency is bigger than 1 Hz, $\sigma_{y_flicker}$ would be given by⁶⁶:

$$\sigma_{y_flicker} = \sqrt{2 \ln(2) \frac{2k_B T}{V c_{22}} \varphi} \quad (4.36)$$

We note that φ could depend upon the temperature and that no assumptions were made about this possible dependence.

To numerically evaluate $\sigma_{y_flicker}$, we consider numerical values typical for a 5 MHz oscillator equipped with an SC-cut quartz crystal resonator. Due to the rotations for the SC cut, the 2 axis is not the usual one, so that the constants must be evaluated in the rotated basis⁶⁷:

$$c_{22} = 115 \text{ GPa}, \eta_{22} = 1.36 \cdot 10^{-3} \text{ Pa} \cdot \text{s}, T = 350 \text{ K and } V = 0.104 \text{ cm}^3.$$

This gives:

$$\sigma_{y_flicker} \approx 1.06 \cdot 10^{-12} \sqrt{\varphi} \quad (4.37)$$

Unfortunately, in present measurements, the white noise of the amplifier is masking the white noise of the resonator, so that we cannot estimate the maximum possible value of φ from our measurements.

Hence, using a damping force proportional to strain and independent of frequency, naturally allows to get a $1/f$ noise spectrum at low frequencies. Indeed, we could get the noise limit of measured resonators, a few 10^{-14} ([15], [16], [17]), with $\varphi > 10^{-4}$. However, this would mean that the effective value of Q at the resonance would be dominated by internal damping (addition of losses: $1/Q_{eff} = (1/Q_{viscous} + \varphi)$ and lower than what is measured by at least 2 orders of magnitude. We therefore conclude that internal damping of thickness fluctuations by any force proportional to strain and independent of frequency, may not be the dominant noise mechanism for the best SC-cut quartz resonators. However, other modes may be more noisy...

2.2. Tentative physical explanation of the internal friction coefficient φ

In this paragraph, we consider whether the imaginary part of the complex spring constant φ in the equation (4.34), referred as internal friction coefficient, can be explained by the modified Granato-Lücke theory [18] of the energy loss due to some kinds of dislocation motion at the low frequency range.

⁶⁶ $\int S_y(\omega) d\omega = \int S_y(f) df$ so that $S_y(f) = \frac{2k_B T}{V c_{22}} \times \frac{1}{f} \left(\frac{\eta_{22} 2\pi f}{c_{22}} + \varphi \right)$, since $df/f = d\omega/\omega$. Furthermore, at 1 Hz $\varphi \gg \frac{\eta_{22} 2\pi f}{c_{22}}$, so that $S_y(1 \text{ Hz}) \approx \frac{2k_B T}{V c_{22}} \varphi$.

⁶⁷ These values are private communications from Roger Bourquin.

In 1952 Koehler proposed a mathematical model for the equation of motion of a pinned down dislocation loop [19]. In 1956, Granato and Lücke proposed a more complete theory of the mechanical damping due to both viscous and hysteretic motions of a pinned dislocation loop under the influence of an externally applied stress (cf. Fig.4.4 from [20]).

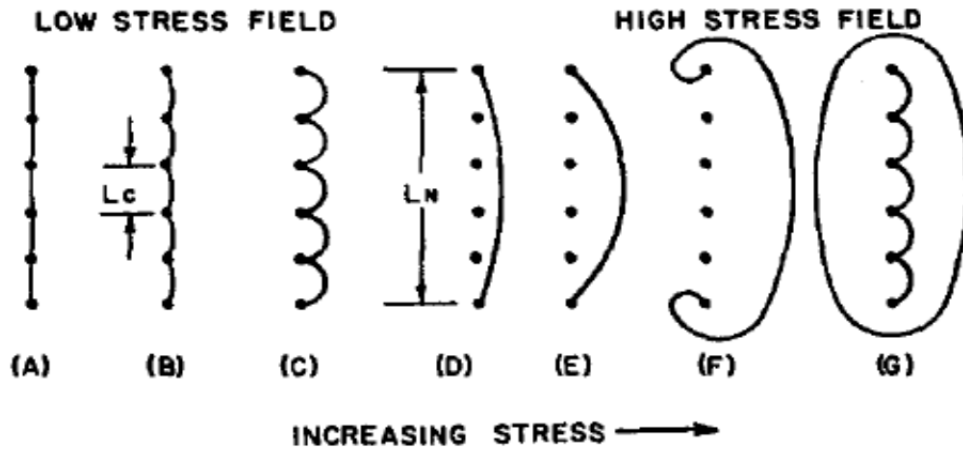


Fig.4.4: Motion of a pinned dislocation loop under the influence of externally applied stress (A. Granato and K. Lucke, "Theory of mechanical damping due to dislocations", J. Appl. Phys. Vol. 27, No-583, 1956. (page.584)).

For zero applied stress, the (network) length (L_N) is pinned down by the impurity particles (A). For a very small stress (B) loops of characteristic length L_c bend down continuously between the pinning impurities, until the breakaway stress is reached and a fast transition occurs from (C) to (D). Further increase of the stress make the resulting line of length L_N bend (E) since it is assumed that the pinning at the extremities of L_N is much stronger than the pinning at the intermediate impurities such that no breakaway of network lengths occurs and in this interval the effective modulus is determined by the network length L_N . Now, further increment of the stress (D-E) causes the creation and expansion of a new closed dislocation loop (F-G) as in the Franck-Read source mechanism. The dislocation strain in this process is irreversible since a decrease of stress after (D) will not make the system go through (C) and (B).

After simplification, Granato and Lucke obtained an analytical expression for the logarithmic decrement of the weakly damped mechanical oscillations in the material⁶⁸:

⁶⁸ The logarithmic decrement Δ is the natural logarithm of the ratio of two successive maxima of weakly damped oscillations, when no external forces are applied to maintain the oscillations. For high quality factors, $\Delta = \pi / \sqrt{Q^2 - 1/4} \approx \pi/Q$. The logarithmic decrement is also equal to the product of the damping factor and the pseudo-period of the weakly damped oscillations. The quality factor is 2π the ratio of the energy stored in an oscillatory system to the energy lost by the system during one oscillation cycle: $Q = 2\pi E/\Delta E$. If $\ddot{x} + 2\beta\dot{x} + \omega_0^2 x = 0$ and $\beta < \omega_0$, $x = A \exp(-\beta t) \cos(\omega t + \varphi_0)$ with $\omega = \sqrt{\omega_0^2 - \beta^2}$, $\Delta = \ln(x(t)/x(t+T)) = \beta T = 2\pi\beta/\omega$, so that $Q = \omega_0/2\beta$. β is the damping coefficient, reciprocal to the relaxation time τ , so that the period of the weakly damped oscillations is equal to the relaxation time multiplied by the logarithmic decrement: $T = \tau\Delta$. For forced oscillation the resonance circular frequency: $Q = 2\pi E/\Delta E$ is $\omega_r = \sqrt{\omega_0^2 - 2\beta^2} = \omega_0\sqrt{1 - 1/2Q^2}$.

$$\Delta = \frac{\Delta_0 \Lambda L_N^2}{\pi} \left(\frac{L_N}{L_c} \right) \left[\frac{\Gamma}{\sigma_0} - 1 + \dots \right] \exp \left(- \frac{\Gamma}{\sigma_0} \right) \quad (4.38)$$

where $\Delta_0 = 8Ga^2/\pi^3C$ where G is the shear modulus, a is Burger's vector and πC is the loop tension.

Λ = Total length of movable dislocation line per unit volume.

L_N = Network length, i.e. characteristic distance between two strongly pinning impurities.

L_c = Characteristic distance between two weakly pinning impurities.

$\Gamma = \pi f_m/4aL_c$, where f_m is the maximum value of the binding force.

σ_0 = Amplitude of the applied stress $\sigma = \sigma_0 \exp[-\alpha x] \exp[i\omega(t - x/v)]$.

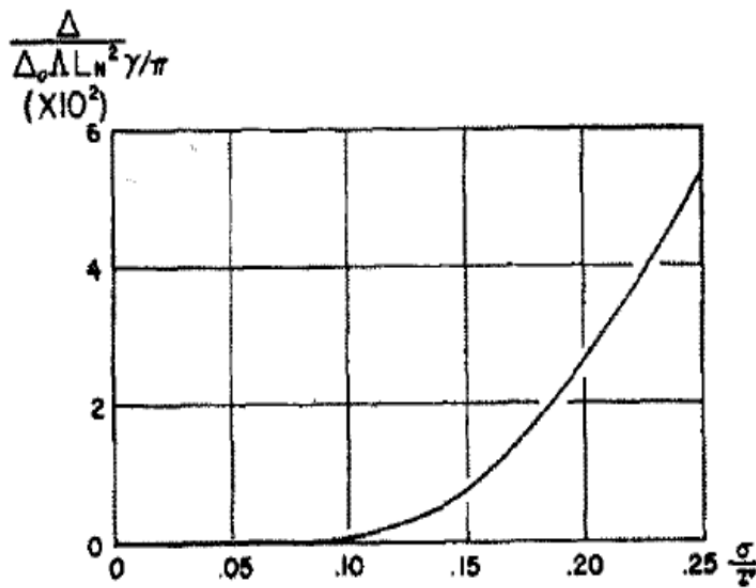


Fig.4.5: The stress-amplitude dependence of the decrement (A. Granato and K. Lucke, "Theory of mechanical damping due to dislocations", J. Appl. Phys. Vol. 27, No-583, 1956. (page.584)).

Eq. (4.38) shows that the logarithmic decrement is frequency independent as our internal friction coefficient term φ in the equation (4.34). However it is also strain amplitude dependent. This dependency is even exponential (cf. Fig.4.5). However, in 1961, Swartz and Weermann proposed a modified Koehler-Granato-Lücke theory [18] in order to account for other experimental observations that "an amplitude independent damping exists which is independent of frequency and which varies with the impurity content inversely to a power less than four". They supposed first that the pinning force F of the impurity atom which arises from elastic interactions depends on the orientation of the dislocation line. Second, they supposed that, once a dislocation has broken away from its pinning points, its motion is not necessarily limited by its line tension, but that the distance it moves may be determined by the stress field of neighboring impurity atoms. With these

assumptions, they found an expression of the decrement for the impurity spacing controlled dislocation motion that, in the small stress amplitude limit, is given by:

$$\Delta = \frac{\beta N b L_N}{\pi c^{1/3} \epsilon} \quad (4.39)$$

where:

- β is a parameter having value between 1 to 2 for impurity limited motion. We have taken the value of β as 1.5 for our calculation.
- $N =$ Total length of dislocation line in a unit volume of material = $2 \times$ surface dislocation density [21]. This value used to be between 600 cm/cm^3 and 200 cm/cm^3 for high quality quartz [22] but is now of the order of 6 cm/cm^3 judging from an X-ray image of the surface of one of the oscillators used nowadays at FEMTO-ST.
- $b =$ mean length of a Burger's vector $\approx 3 \times 10^{-8} \text{ cm}$.
- $L_N =$ Network length $= \sqrt{3/N}$ (according to Ref. [18]).
- $c =$ Atom fraction of impurity which must be lower than 1 ppm to get Q values as high as a few 10^6 .
- $\epsilon =$ Fractional difference between the radius of impurity and host atoms. Using covalent radii from the database of the software "kalzium", we estimate that for Lithium impurities and Si host atoms, ϵ could be of the order of 20%.

George A. Alers, in his paper [23] (see the paragraph "**Results**"), measured the decrement of quartz experimentally. He found that the decrement due to the internal friction below 170°C is of the order of 3×10^{-5} . If we take $N=200 \text{ cm/cm}^3$ and $c = 10^{-4}$ in Eq. (4.39), then we get:

$$\Delta = \frac{1.5 \times 200 \times 3 \cdot 10^{-8} \times \sqrt{3/200}}{3.14 \times (10^{-4})^{1/3} \times 0.2} \approx 3.8 \cdot 10^{-5}$$

which is quite similar to the experimental value.

However, in our case $N = 6 \text{ cm/cm}^3$ and $c \leq 10^{-6}$, we find:

$$\Delta \geq \frac{1.5 \times 6 \times 3 \cdot 10^{-8} \times \sqrt{3/6}}{3.14 \times (10^{-6})^{1/3} \times 0.2} \approx 3.0 \cdot 10^{-5}$$

Unfortunately, we will see in the next chapter that the values of logarithmic decrement we measure are an order of magnitude smaller.

Finally, we recall that, previously, we saw that $1/Q_{eff} = 1/Q_{viscous} + \varphi$, with $1/Q_{viscous} = \frac{\eta_{22}\omega}{c_{22}}$. Therefore at low frequencies $1/Q_{eff} \approx \varphi$. Hence, we attempt to identify Δ with $\pi\varphi$ at low frequencies, in a first approximation in spite of the fact that we are not in the dominantly viscous regime, since we saw in a previous footnote that $\Delta \approx \pi/Q$ in that regime. This would give

$Q_{eff} \approx 10^5$ and $\varphi \approx 10^{-5}$ in the low frequency regime, which would be an interesting order of magnitude to attribute at least some non negligible part of the $1/f$ noise to the fluctuations of thickness. However, this would also mean that at resonance $\frac{1}{Q_{eff}} = \frac{1}{Q_{viscous}} + \varphi \approx 4 \cdot 10^{-7} + 10^{-5} \approx 10^{-5} = \varphi$, hence that the viscous damping would not be dominant at resonant frequency which is contradictory to experimental facts.

3. Conclusions

We have seen that it is possible to find $1/f$ noise through the fluctuation-dissipation theorem, by adding a complex part to the elastic constant in the usual differential equation characteristic of a viscously damped harmonic oscillator. This corresponds to a frequency independent energy loss in the limit of small frequencies. The hysteretic motion of the dislocations described by a modified Koehler-Granato-Lücke model [18] could a priori describe such a loss mechanism. Indeed, it could provide an explanation for the experimental observations that the logarithmic decrement generally decreased when the dislocation density decreased when quartz were not as good as now and that sometimes a slightly higher concentration of impurity could improve the quality factor. However, numerical estimations seem to provide values that are at least an order of magnitude too high.

4. References

- [1] A. Einstein, “Investigations on the theory of brownian movement”, edited with notes by R. Fürth, translated by A. D. Cooper, Dover, 1951, translation of A. Einstein, “Über die von der molekularkinetischen Theorie der Wärme geforderte Bewegung von in ruhenden Flüssigkeiten suspendierten Teilchen”, Ann. d. Physik, 4th serie, vol. 17, no. 8, pp. 549-560, 1905.
- [2] H. B. Callen and T. A. Welton, “Irreversibility and generalized noise”, Phys. Rev., vol. 83, no. 1, pp. 34-40, 1951.
- [3] H. B. Callen and R. F. Greene, “On a theorem of irreversible thermodynamics”, Phys Rev., vol. 86, no. 5, pp. 702–710, 1952.
- [4] R. Kubo, “The fluctuation-dissipation theorem”, Reports on Progress in Physics, vol. 29, no. 1, pp. 255-284, 1966.
- [5] J. B. Johnson, Summary 57 in the “Proceedings of the American Physical Society: Minutes of the Philadelphia Meeting December 28, 29, 30, 1926”, published in Phys. Rev., vol. 29, pp. 367-368, 1927.
- [6] J. B. Johnson, “Thermal agitation of electricity in conductors”, Phys. Rev., vol.32, no. 1, pp. 97-109, 1928.
- [7] H. Nyquist, “Thermal agitation of electric charge in conductors”, Phys. Rev., vol.32, no. 1, pp. 110-113, 1928.
- [8] P. Langevin, “Sur la théorie du mouvement brownien”, CR Acad. Sciences, vol. 146, pp. 530-533, 1908.
- [9] M. Devel, R. Bourquin, S. Ghosh, J. Imbaud, G. Cibiel, F. Sthal, “Quartz crystal resonator noise and fluctuation-dissipation theorem considerations”, Proc. IEEE Int. Freq. Cont. Symp., Baltimore, Maryland, 22-24 May, pp. 425-429, 2012.
- [10] P. R. Saulson, “Thermal noise in mechanical experiments”, Phys. Rev. D, vol. 42, no. 8, pp. 2437–2445, 1990.
- [11] G. I. Gonzalez and P. R. Saulson, “Brownian motion of torsion pendulum with internal friction”, Phys. Lett. A, vol. 201, pp. 12-18, 1995.
- [12] S. Ghosh, F. Sthal, J. Imbaud, M. Devel, R. Bourquin, C. Vuillemin, A. Bakir, N. Cholley, P. Abbe, G. Cibiel, “Theoretical and experimental investigations of $1/f$ noise in quartz crystal resonators”, Proc. IEEE-UFFC Joint Int. Freq. Cont. Symp., Prague, Czech Republic, 21-25 July, pp. 737-740, 2013.
- [13] F. Sthal, J. Imbaud, X. Vacheret, P. Salzenstein, G. Cibiel, S. Galliou, “Computation method for the short-term stability of quartz crystal resonators obtained from passive phase noise”,

- IEEE Transactions on Ultrasonics, Ferroelectrics and Frequency Control, vol. 60, no. 7, pp. 1530-1532, 2013.
- [14] D. W. Allan, "Statistics of atomic frequency standards", Proc. IEEE, vol.54, no. 2, pp. 136-154, 1966.
- [15] J. R. Norton, "Performance of ultrastable quartz oscillators using BVA resonators", Proc. European Frequency and Time Forum, Weihenstephan, Germany, March, pp. 457-465, 1994.
- [16] R. J. Besson, M. Mourey, S. Galliou, F. Marionnet, F. Gonzalez, P. Guillemot, R. Tjoelker, W. Diener, A. Kirk, "10 MHz Hyperstable quartz oscillators", Proc. Joint Meeting IEEE Ann. Freq. Cont. Symp. and European Frequency and Time Forum, Besançon, France, April, pp. 326-330, 1999.
- [17] P. Salzenstein, A. Kuna, L. Sojdr and J. Chauvin, "Significant step in ultra high stability quartz crystal oscillators", Electron. Lett., vol. 46, no. 21, pp. 1433-1434, 2010.
- [18] J. C. Swartz and J. Weertman, "Modification of Koehler-Granato-Lucke damping theory", J.Appl.Phys, vol. 32, no. 10, pp. 1860-1865, 1961.
- [19] J. S. Koehler, "Imperfections in Nearly Perfect Crystals", John Wiley and Sons, Inc., New York, p. 197, 1952.
- [20] A. Granato and K. Lucke, "Theory of mechanical damping due to dislocations", J. Appl. Phys. vol. 27, no. 6, pp. 583-593, 1956.
- [21] G. Schoeck, "Correlation between Dislocation Length and Density", J. Appl. Phys., vol. 33, no. 5, pp. 1745-1747, 1962.
- [22] J-J Boy, PHD thesis, University of Franche-Comté, 1994.
- [23] G. A. Alers, "Internal friction of Quartz", J. Appl. Phys, vol.24, no. 3, pp. 324-331, 1953.

Chapter 5: Experimental observations

The Centre National d'Etudes Spatiales (CNES), Toulouse, France and the FEMTO-ST Institute, Besançon, France, have initiated a program of investigations on the origins of noise in bulk acoustic wave resonators. Several European manufacturers of high quality resonators and oscillators are involved in this partnership [1]. For this program, quartz crystal resonators have been cut from a quartz crystal block supplied specifically for this study on $1/f$ noise. This crystal block was grown from a seed which originated from a previous synthetic crystal which was grown from a natural seed. This kind of synthetic crystal is usually used to grow new generations of quartz crystal blocks [2]. In this chapter, the blank realization and the topology of the resonator prototype are exposed. The resulting resonators are SC-cut with a 5 MHz resonant frequency. A comparison of these resonators is given in terms of motional parameters and Q factors. The results are presented according to the position of the resonators inside the mother crystal block. Then, we report the noise measurements made on these quartz crystal resonators using an advanced phase noise measurement system [3]. Attempts to correlate these noise results using cryogenic temperature characterization of the resonators and time measurements of the acoustic attenuation will be presented.

1. Resonator Realization

1.1. *Crystal block and blank cutting*

The C2 crystal block is presented in Fig.5.1. This crystal block is obtained from a seed cut in a previous synthetic crystal which was grown using a natural seed. Its dimensions were approximately 220 mm along the Y-axis, 36 mm along the Z-axis and 110 mm along the X-axis. Two Y-cut slices have been cut before and after an oriented block used to achieve quartz bars (see red marks in Fig.5.1). The Y-cut slices have been used to make X-ray topographies for dislocations evaluation (cf. chapter 1). The crystal bars are cut in order to get the doubly rotated SC-cut. Fourteen quartz bars pre-oriented on the ϕ angle have been achieved. The length of the bars is about 70 mm. Fig.5.2 shows a side view of 5 bars and the position of the fourteen bars in the initial crystal block. Taking into account the width of the cutting saw, about 24 resonators can be obtained in each bar (Fig.5.3). At the end of the technical step, about 160 resonators have been achieved.



Fig.5.1: Quartz C2 crystal block.



Fig.5.2: Quartz crystal bars and their positions in the crystal.

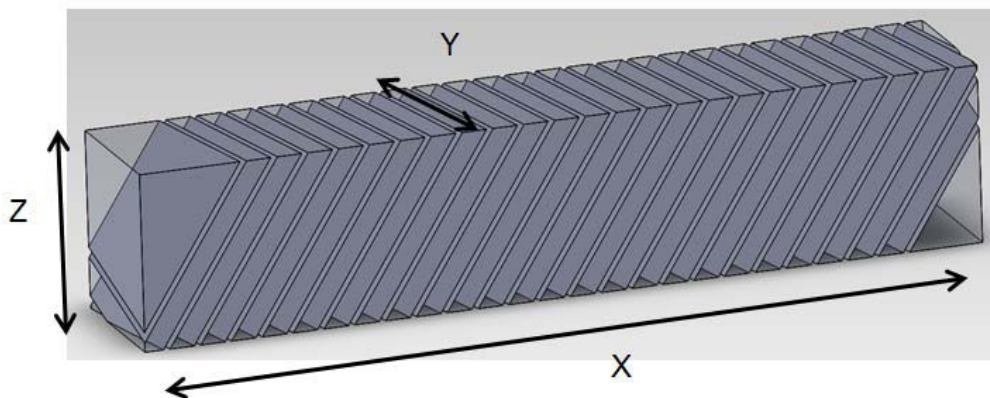


Fig.5.3: SC-cut plates obtained in the quartz crystal bar.

In bar 11 to 14, the position of all resonators is known along the bar. Resonators from bar 1 to 11 are not precisely localized along the bar.

1.2. Final 5 MHz SC-cut resonators

The prototype of the resonator is a typical 5 MHz SC-cut resonator. The diameter of the resonator is 14 mm for a thickness of 1.09 mm. As seen in the third chapter of this thesis, a plano-convex shape allows the energy trapping for the 3rd overtone of the slowest thickness shear mode (C-mode). Electrodes diameter is 8 mm. The enclosure is HC40 (Fig.5.4).

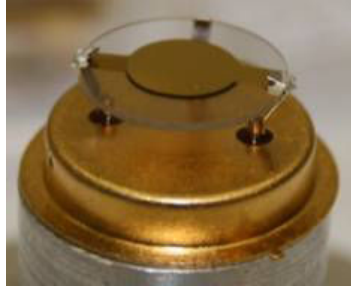


Fig.5.4: Quartz resonator.

A radius of curvature of 130 mm has been chosen to optimize this energy trapping according to the Tiersten-Stevens model [4]. In theory, the ratio of the vibration amplitude at the center of the resonator to the one at its edge is higher than 10^6 . The mode shape pattern obtained by X-ray topography is presented in Fig.5.5. It shows the optimized energy trapping of the (300) C-mode vibration. The temperature turn over point of the resonator is chosen between 80 °C and 85 °C by adjusting the cutting angles φ and θ .

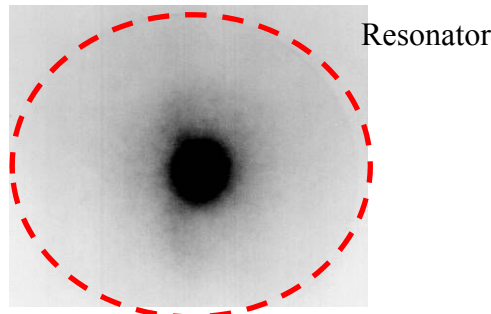


Fig.5.5: X-ray topography of the resonator in its (300) vibration mode [5].

1.3. Resonator parameters

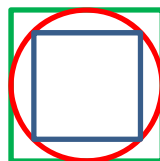
To compute an estimation of the motional parameters, we used Tiersten's formulation [4], valid for the case of square electrodes, for the squares that are internally and externally tangent to the circular electrodes (cf. drawing below). The theoretical interval of values for the motional parameters are then calculated to be (with $Q = 2.5 \cdot 10^6$):

$$69 \Omega < R_m < 79 \Omega$$

$$5.47 \text{ H} < L_m < 6.24 \text{ H}$$

$$0.159 \text{ fF} < C_m < 0.183 \text{ fF}$$

$$0.94 \text{ pF} < C_{0_th} < 1.9 \text{ pF}$$



The red circle represents the diameter of real electrodes. The squares allow setting limits on the parameter results.

Motional parameters of a batch of about forty resonators were measured using an impedance analyzer. The link between parameters is given by the classical formula $Q = 2\pi f L/R = 1/(RC2\pi f)$. The following figures (Fig.5.6 to Fig.5.9) respectively show the motional resistance, the resonant frequency, the turnover temperature and the unloaded quality factor, for each individual resonator, as a function of the resonator number. Lines indicating the average value, and the $\pm\sigma$ and $\pm 2\sigma$ distances with respect to this average value (σ is the standard deviation) are also indicated.

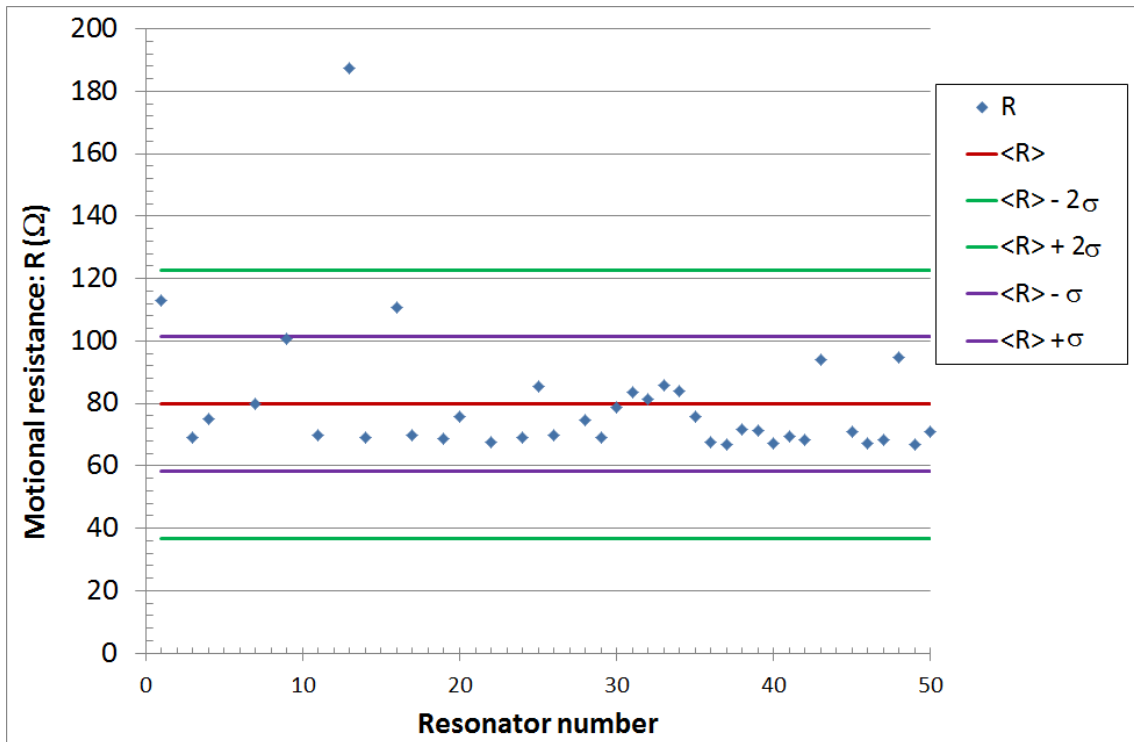


Fig.5.6: Motional resistances of measured resonators.

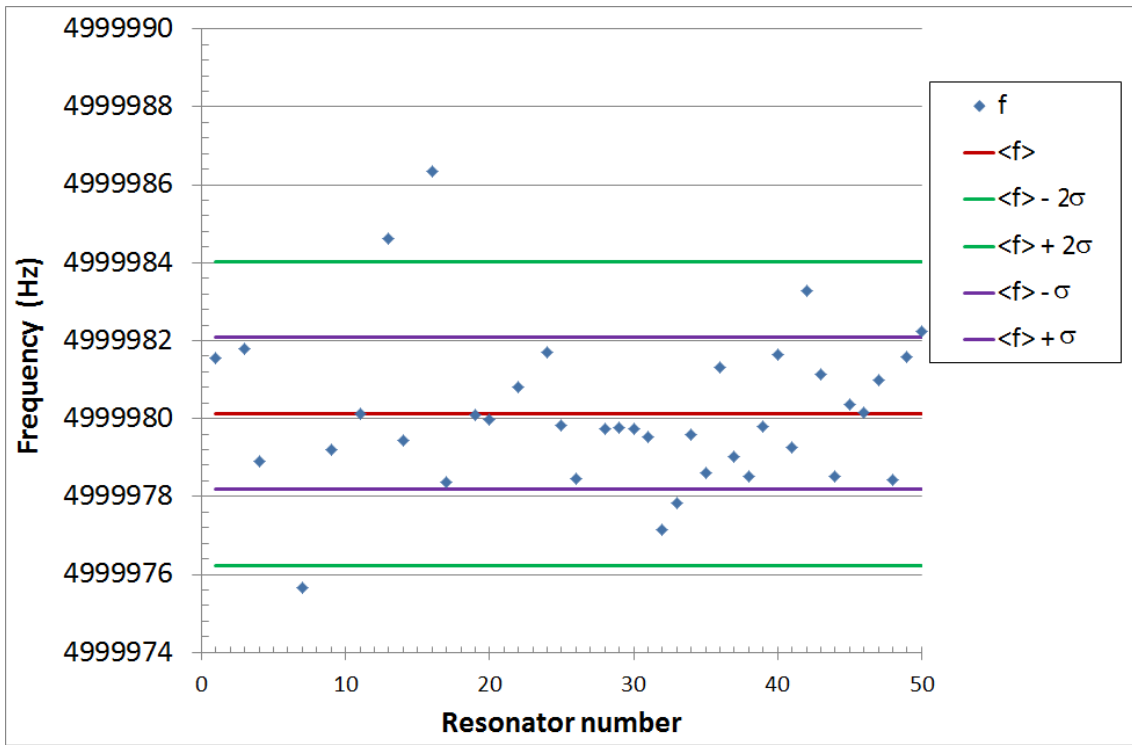


Fig.5.7: Resonant frequency of the measured resonators.

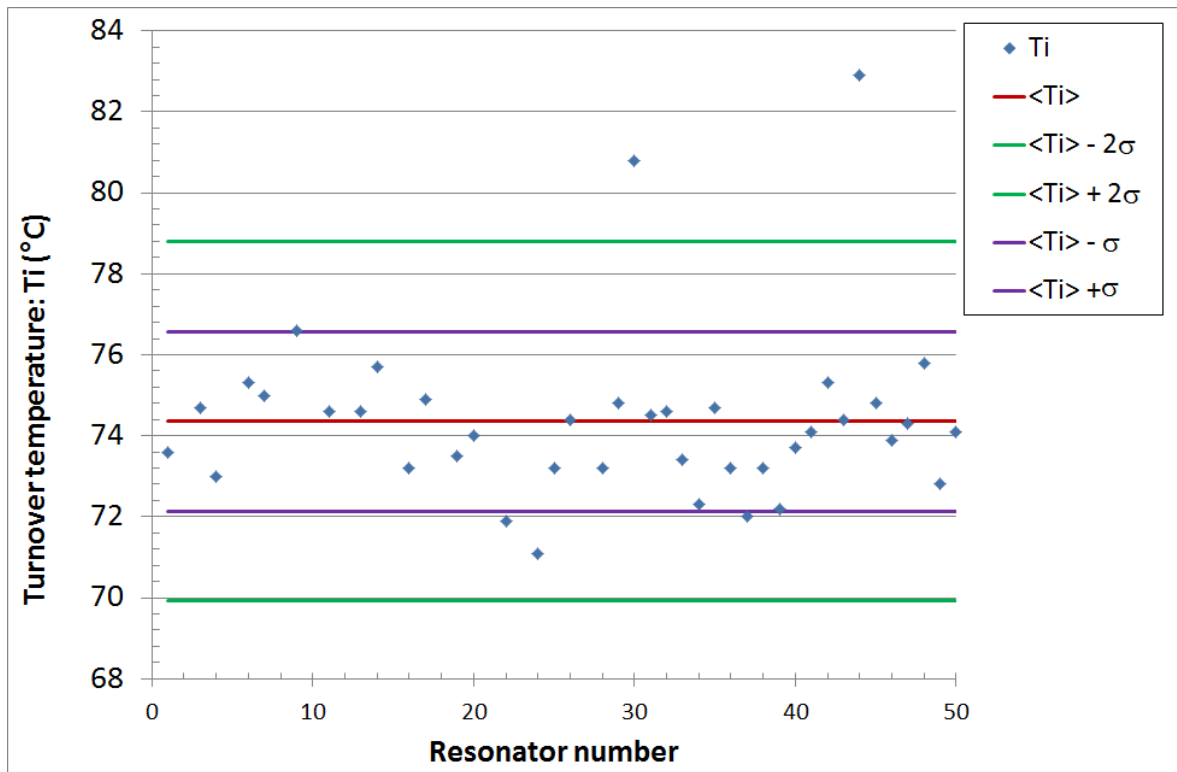


Fig.5.8: Turnover temperature of the measured resonators.

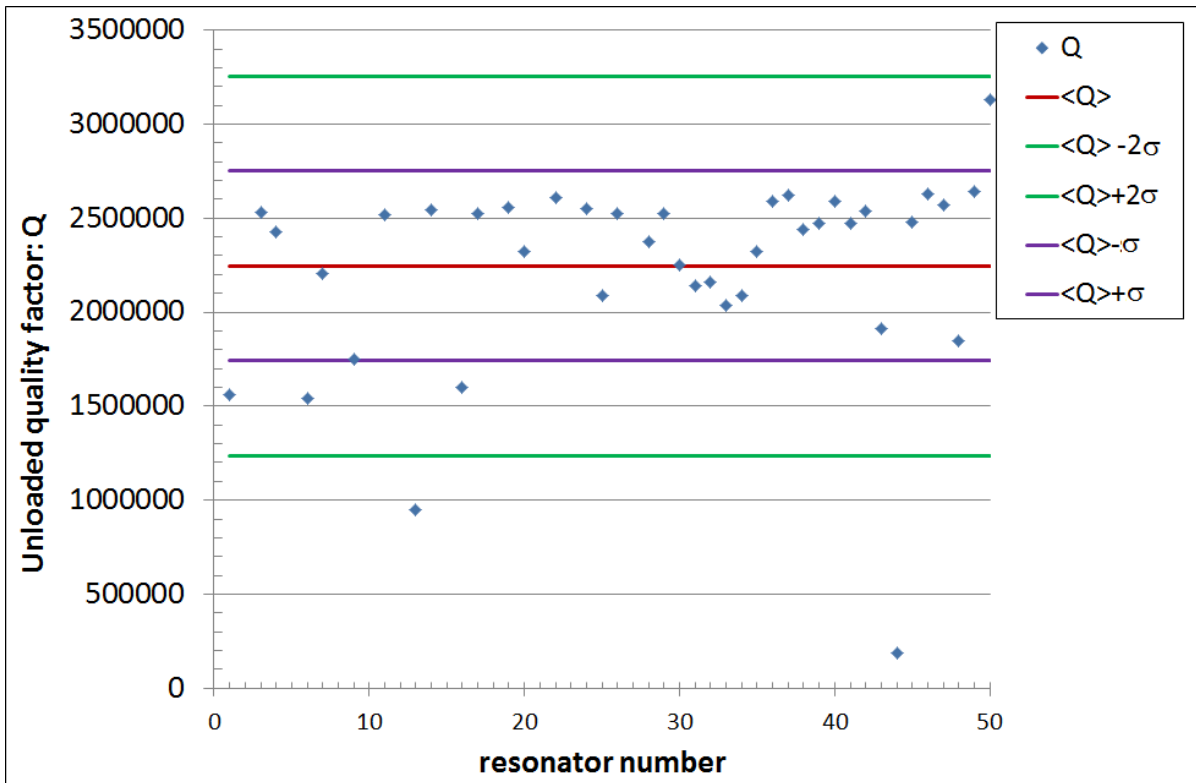


Fig.5.9: Unloaded quality factor of the measured resonators.

A projection on the Y axis of these pictures would show that in the four cases, the data points are approximately Gaussian distributed. This kind of repartition proves the very high quality of the batch of resonators. Indeed, the values of the unloaded quality factor (Q) are as high as expected for this kind of quartz crystal resonators.

2. Resonator noise measurements

2.1. Measurement set-up

The passive technique using carrier suppression is used to characterize the inherent phase stability of the ultra-stable resonators [6]. The general idea of this passive method, presented in Fig.5.10, consists in reducing the noise of the source as much as possible.

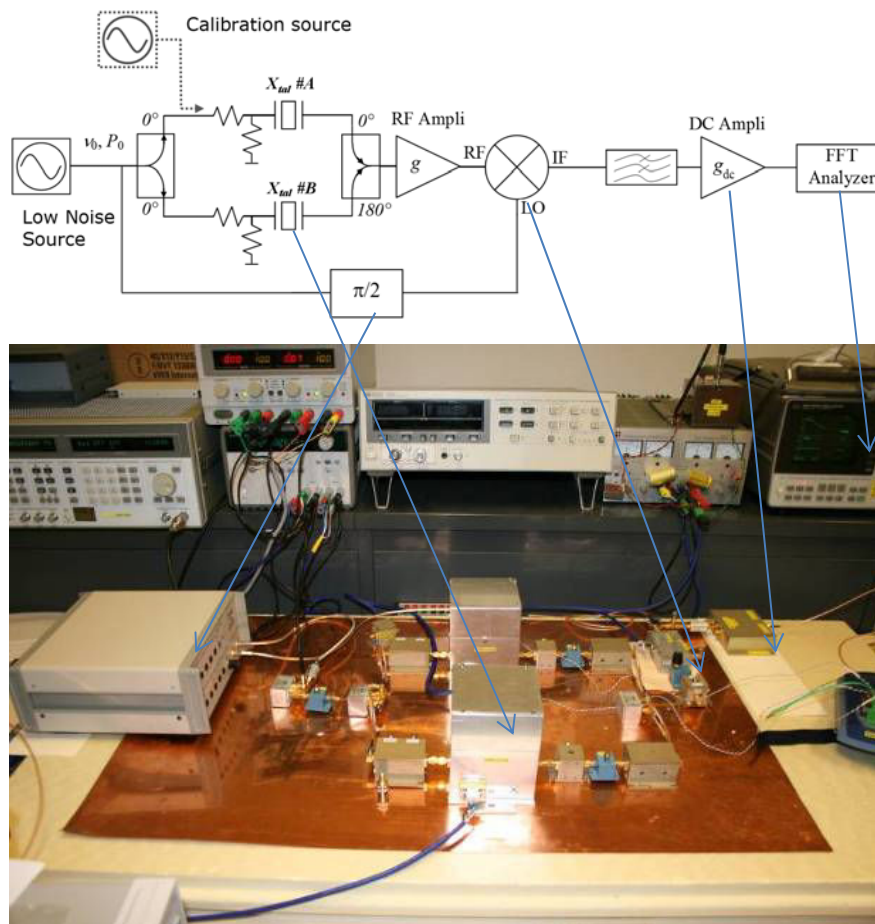


Fig.5.10: Resonator noise measurement set-up.

An oscillator is always noisier than the resonator alone. The reason is that the random noises of the resonator and of the sustaining electronics are added in the output signal. Therefore we can state that the noise of the best oscillator used as source is always higher than the noise of the best resonator alone. Thus, the direct feeding of the driving source signal through only one resonator does not permit the extraction of information about the resonator noise from the total output noise. To perform the resonator noise measurement, the source signal can be subtracted when passing through two identical arms with two resonators considered as quasi-identical. Then, the contribution of the source is reduced while the characteristic noise of both resonators is preserved. This is due to the non-correlation of the intrinsic noise of each resonator. When the carrier suppression is achieved, the resulting signal is free of the source noise. Hence, the sum of both resonators noises is measured. This signal is then strongly amplified and mixed with the source signal in order to be transposed to the low frequency domain. Finally, it is processed by a fast Fourier spectrum analyzer (FFT). With this method, the measured noise for the two resonators is above the noise level of the driving source. Calibration of the measurement system is obtained by injecting a known sideband on one of the arms of the bridge. The result of the measurement bench is corrected using the calibration factor determined from this sideband.

The noise results are usually given in term of $\mathcal{L}(f)$, the one-sided power spectral density (PSD) of the phase fluctuations. Fig.5.11 shows the phase noise of resonator #9, measured with an excitation power of 56 μ W factor in vacuum.

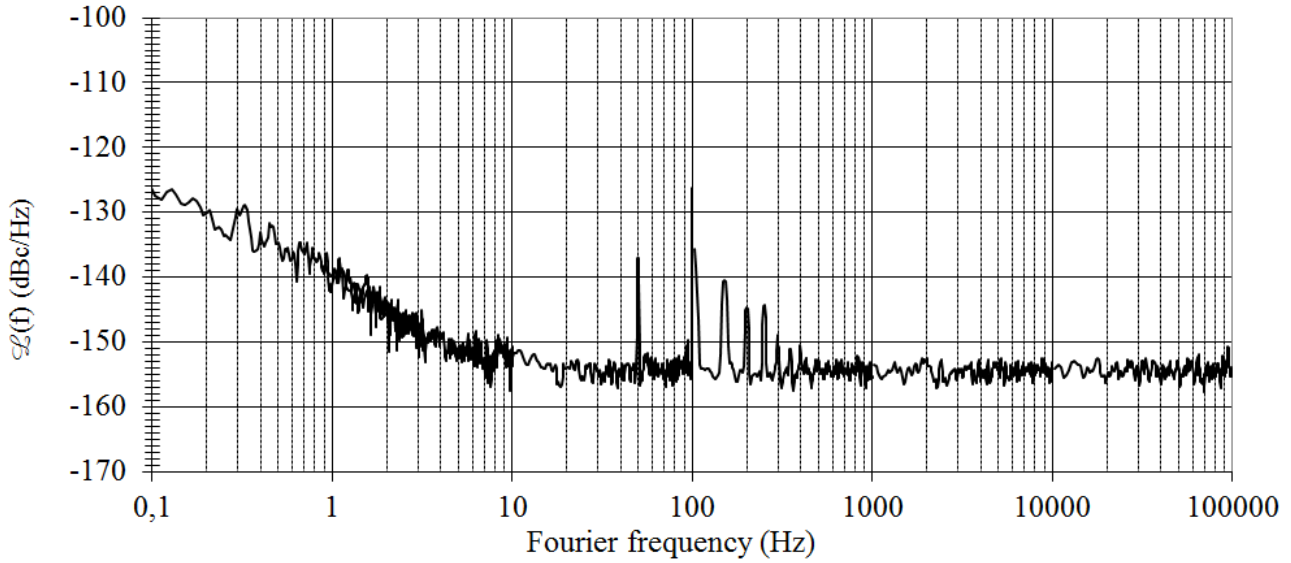


Fig.5.11: Typical phase noise measurement.

For this same resonator (#9) and excitation power, Fig.5.12 shows the transfer function. These curves are used in the conversion of the resonator's flicker frequency noise into the measured phase noise. Around the null phase, F_L can be obtained by inverting the slope of the phase curve [6]:

$$F_L = \frac{1}{\left. \frac{\Delta\phi}{\Delta f} \right|_{\pm 1^\circ}} \quad (5.1)$$

The measurement of this slope should be done in the same context as in the noise measurement. $F_L(\#9)$ is equal to 1.65 Hz, which corresponds to a quality factor over 60% of the unloaded quality factor.

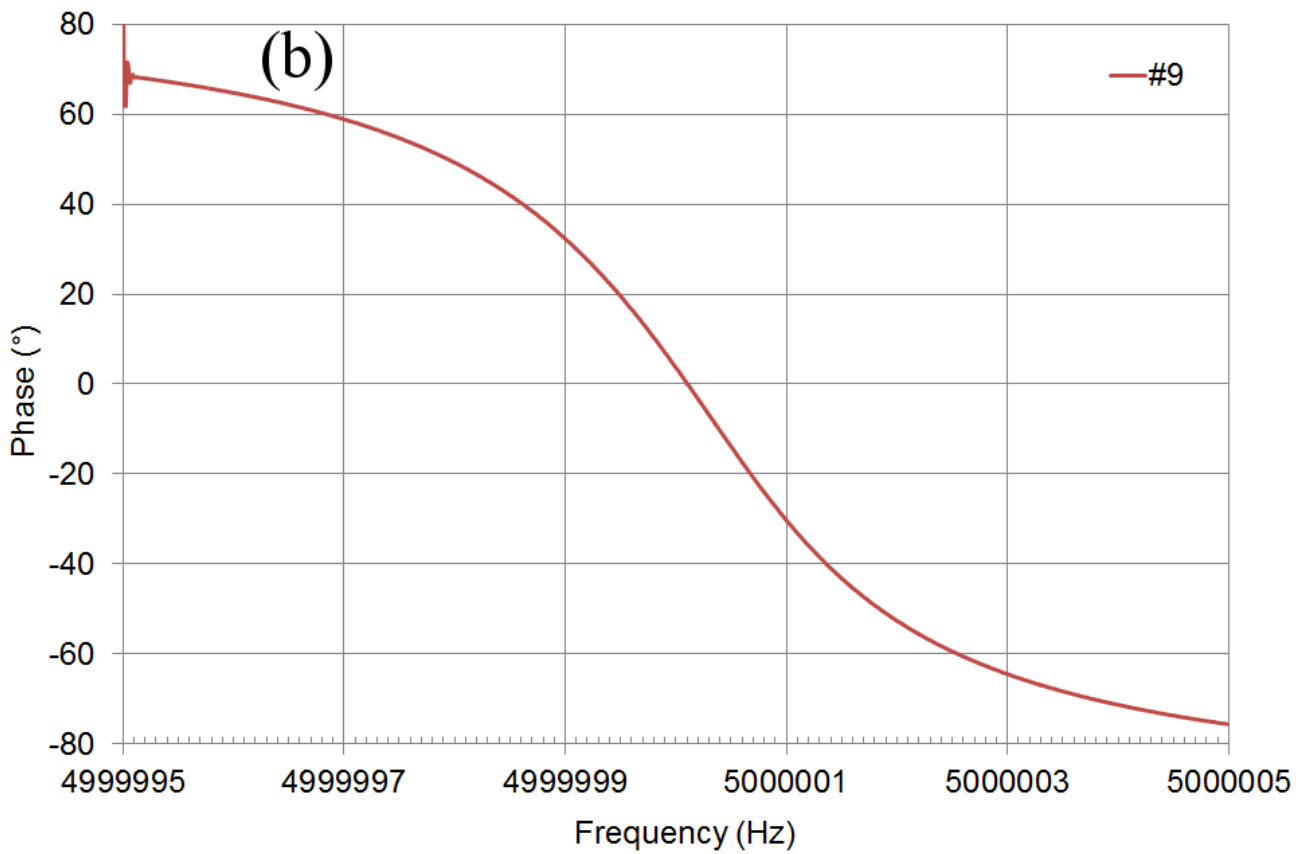
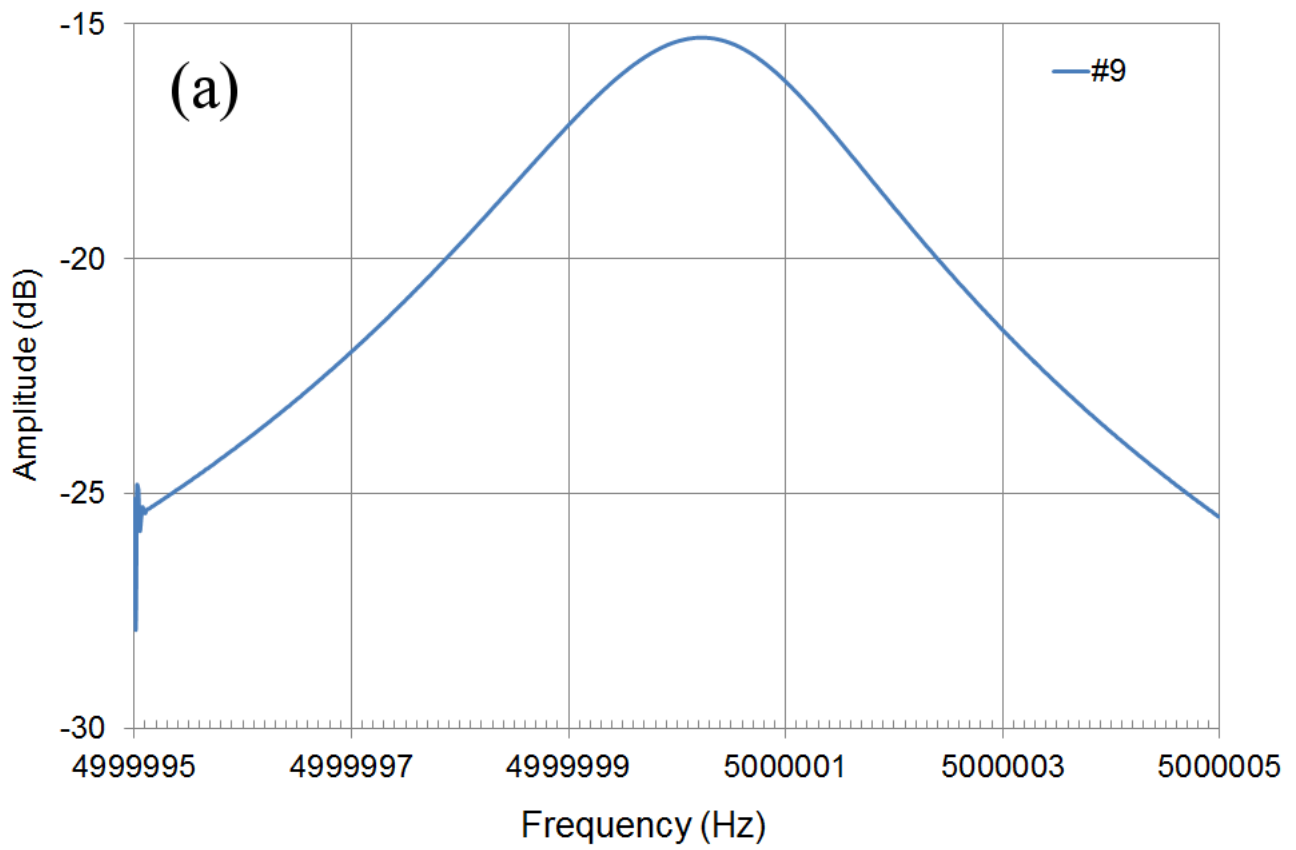


Fig. 5.12: Transfer function: a) amplitude b) phase.

If the two resonators can be considered reasonably identical, then, half of the total noise is attributed to each resonator. In that case, $\mathcal{L}(1\text{Hz})$ is equal to $S_{\phi}(1\text{Hz})$ which can be used to compute the PSD of relative frequency fluctuations $S_y(f)$, using [6]:

$$S_y(1\text{Hz}) = \left[\frac{F_L^2 + 1}{f_{res}^2} \right] S_{\phi}(1\text{Hz}) \quad (5.2)$$

with f_{res} the resonant frequency of the resonator. Finally, for $1/f$ (flicker) noise, the standard deviation of the difference of the average fractional frequencies measured for two consecutive samples is given by the equation [6]:

$$\sigma_{y_floor} = \sqrt{2\ln(2) \cdot S_y(1\text{Hz})} \quad (5.3)$$

This is the square root of the Allan variance [7]. It is commonly used to compare the short-term stabilities of various resonators, since it is the noise at low frequencies floor in terms of relative frequency fluctuations (see Chapter 1).

2.2. Noise results

As example, Fig.5.13 gives the short-term stability floors of resonators obtained in bar 14. Error bars are given according accuracies of the measurements (error on $F_L = \pm 0.1$ Hz and $\pm 2\text{dB}$ on the measured spectrum). They span approximately two orders of magnitude. The best resonators have a short-term stability (Flicker floor) below $8 \cdot 10^{-14}$, whereas the worst are above 10^{-12} . Although the positions of the blanks are known, no clear correlation between the noise results and the blanks positions (e.g. center or edges) can be found for this bar. Same behavior is observed in bar 11 to 13.

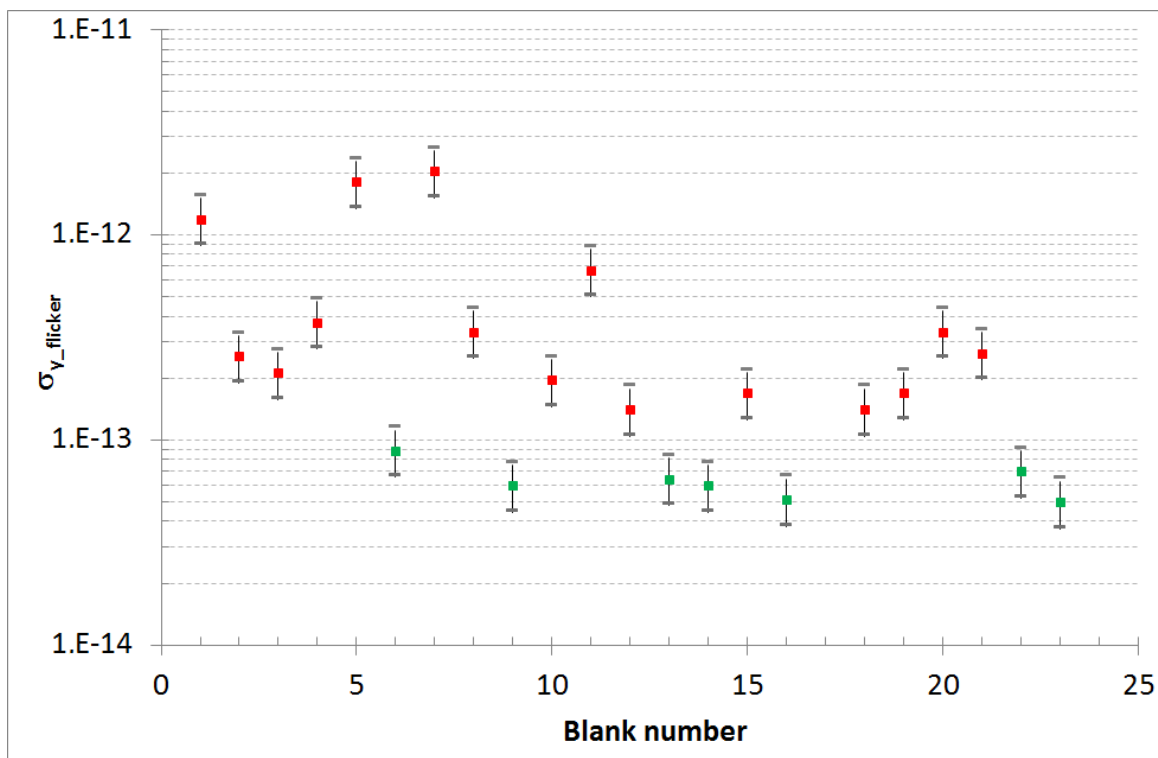


Fig.5.13: Noise measurements from resonator cut in bar 14 [2].

3. Low temperature measurements

During the last 65 years of low temperature experiments, it has been established that BAW quartz crystal resonators show very high Q-factors at cryogenic temperatures [9]-[16] and that Q factors of the resonators at low temperature could be correlated with noise at room temperature. Hence, we have carried such measurements in order to find a correlation between noise results at ambient temperature and acoustic defects in the active volume of the resonator.

3.1. Cryogenic set-up

A cryogenerator is a machine that is used to produce low temperatures. The Fig.5.15 represents the general view of a cryogenerator and measurement devices [15]. In our experiment, a two-stage pulse-tube cryocooler is used at the cryogenic system's core. Usually, the cryocooler absorbs up to 1 W at temperatures lower than 10K, typically 4.2K. The core of the experimental system is a cold head, where a device under test (DUT) is mounted on and enclosed in a vacuum chamber. The DUT is attached to a temperature-controlled copper block.

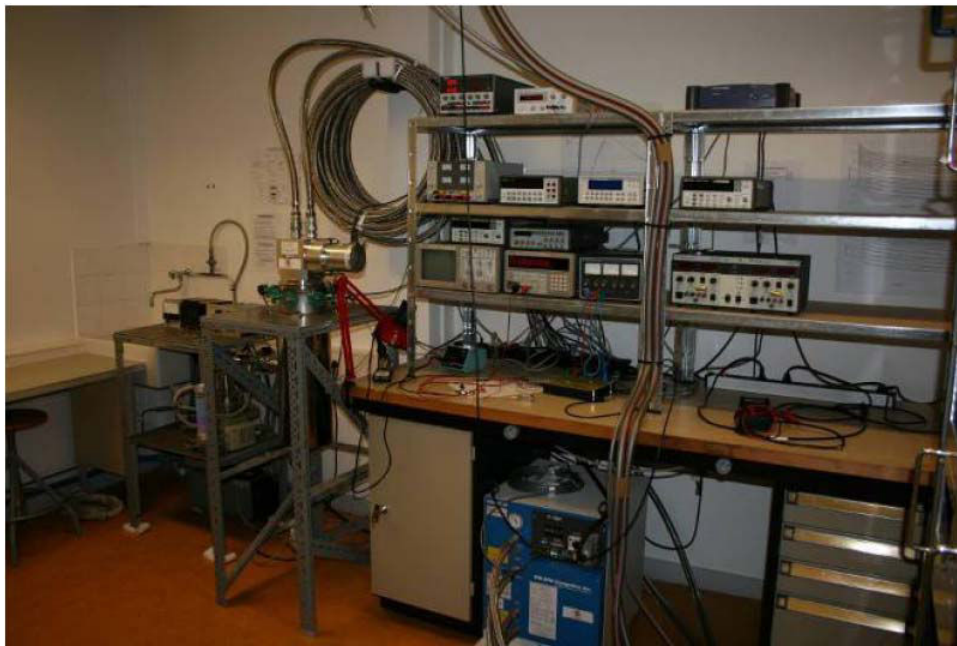


Fig.5.15: General construction of the cryogenic system [15].

A M Series Helium Compressor serves as the central source of ultrahigh purity helium gas in a closed circuit system. Our system is built on an F-70H helium compressor from Sumitomo Heavy Industries (SHI) which is compatible with a pulse tube. The pressure produced by the compressor is approximately 16.5 Bar and it consumes an electric power of 6.7 to 7.2 kW. External refrigeration by cold water is needed to maintain the compressor at a temperature of 15°C, to prevent the thermal emission.

A two-stage pulse-tube cryocooler (see Fig.5.16) is used at the cryogenic system's core. The cryocooler head used in our system is the helium pulse tube RP-082A from SHI. As described by

M. Goryachev [16], the cryocooler is shielded with two protection screens (a vacuum chamber and an anti-radiation shield). The air pressure inside the chamber is lower than 10^{-5} Pa. This shield is at room temperature and is made with a light-reflecting material. Both primary and secondary pumps are cut off from the chamber during the whole measurement time. The anti-radiation shield is attached to the first cryocooler stage and its temperature is about 50K. Its inner and outer surfaces are covered with a specially fabricated light-reflecting paper comprising several layers of metalized mylar sheets to reduce radiation losses of the second stage.

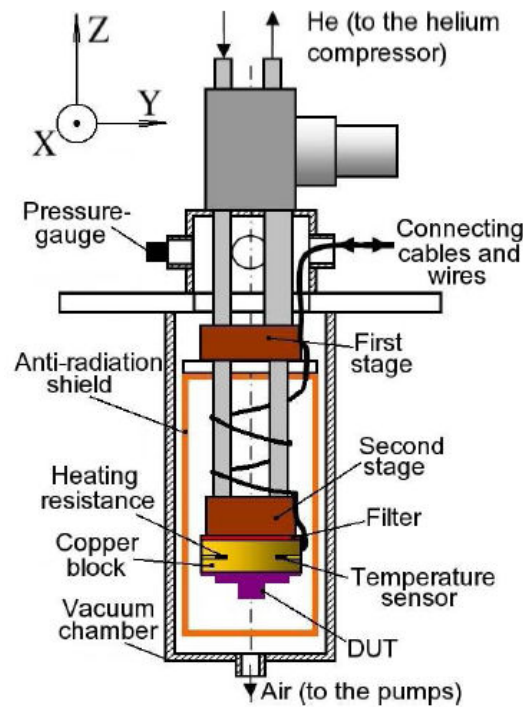


Fig.5.16: Schematic diagram of the pulse tube cryocooler [16].

Three resonators can be inserted inside final head. At controlled temperature the resonators are connected to a network analyzer in order to measure their impedance responses Fig.5.17. Classical calibration of the analyzer is made using load inserted in the head at 4K in order to suppress the length effect of the cables.

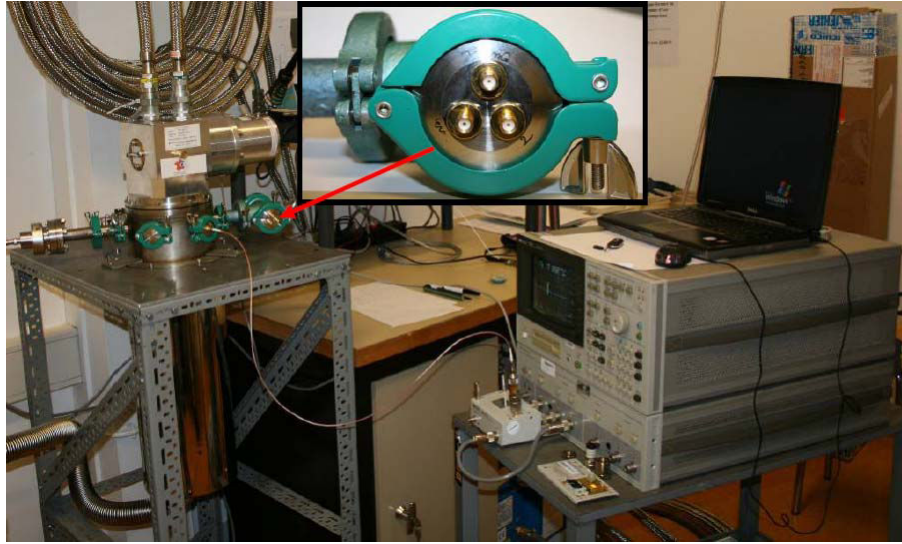


Fig.5.17: Resonator impedance measurements [15].

3.2. Measurement results

Ten resonators have been tested at 4 K. The tested resonators *a* to *l* have different noise levels. Table 5.1 gives theoretical expectations for the resonant frequencies at cryogenic temperature for each modes that we observed, computed using a formula found in Ref. [4]. Theoretical computation is done using Eq. (126) from [4] to get the theoretical values. Then, the experimental values are searched near these theoretical values on the network analyzer.

Table 5.1: Theoretical values of resonant frequencies of the designed resonator for A, B and C modes (overtones and anharmonic modes of C300 modes (Temperature = 4 K)).

C Mode	C300	C320	C302	C340	C322	C304	C500	C700
Res. Freq. (MHz)	4.993	5.117	5.127	5.242	5.251	5.267	8.287	11.583
B Mode	B300	B500	B700	B1100	B1300	B1500		
Res. Freq. (MHz)	5.487	9.112	12.736	20.161	23.631	27.244		
A mode	A300	A500	A900	A1100	A1300	A1500		
Res. Freq. (MHz)	9.362	15.569	27.988	34.177	40.385	46.587		

A sum-up of Q-factors for the different modes is given in Table 5.2. The observed modes are both thickness shear and longitudinal modes. Q-factor of C-modes at different overtone ranks and anharmonic modes of C300 have been measured. Only overtones of B-modes and A-modes have been tested.

Table 5.2: Q-factor at cryogenic temperature of selected resonators (a to l in Fig.5.14).

Q-factor	resonator	a	b	c	d	e	h	i	j	k	l
(10 ⁶)	σ_{y_floor}	7.11E-14	2.30E-12	1.81E-12	6.26E-14	6.25E-14	2.27E-12	2.12E-13	5.96E-14	3.36E-13	1.68E-13
	Blank	B12-L13	B12-L17	B14-L5	B14-L6	B13-L3	B13-L11	B14-L3	B14-L9	B14-L8	B14-L15
390K	C300	2.62	2.66	2.16	2.04	2.35	1.12	2.25	2.59	2.32	2.54
	C300	43.57	43.57	21.79	33.52	23.78	1.74	43.57	43.57	29.05	43.57
	C320	11.16	8.93	5.95	3.95	6.60	2.23	2.41	5.58	4.06	6.87
	C302	2.60	1.99	2.24	7.21	1.65	1.99	1.32	3.31	3.44	2.35
	C340	0.69	1.59	0.06		0.91					0.22
	C322	0.44	0.45		0.19	0.91		2.56		0.98	0.49
	C304		0.56		0.07			1.99	0.42		0.43
	C500	36.16	48.22	36.16	48.22	31.51	0.44	36.16	72.33	12.05	72.33
	C700	40.43				39.67	10.11	40.44	50.55	20.22	67.40
3.8K	B300	31.92	23.94	23.94	19.16	0.32	2.94	23.94	15.96	19.16	31.93
	B500	31.80	53.01	39.76	53.02	52.07	3.04	39.76	79.53	17.67	
	B700	37.04	31.75	37.05	55.58	51.98	3.71	44.46	74.10	10.59	74.11
	B1500	27.01				54.16		19.81			
	A300	5.45	16.34	0.38	0.38	19.79	5.56	2.59	0.30	3.99	1.95
	A500	67.90	90.55	54.33	36.72	53.31	9.06	90.55	54.35	2.56	45.30
	A900										
	A1100		298.15	119.26			596.64	198.78	298.25	23.86	298.29
	A1300	1.57					21.76				
	A1500						18.07				

White cells correspond to unfound modes or computation of the Q-factor aborted due to failed calibration. Like at room temperature, the evolution of the Q-factors seems to be independent of the noise level (see Fig.5.18).

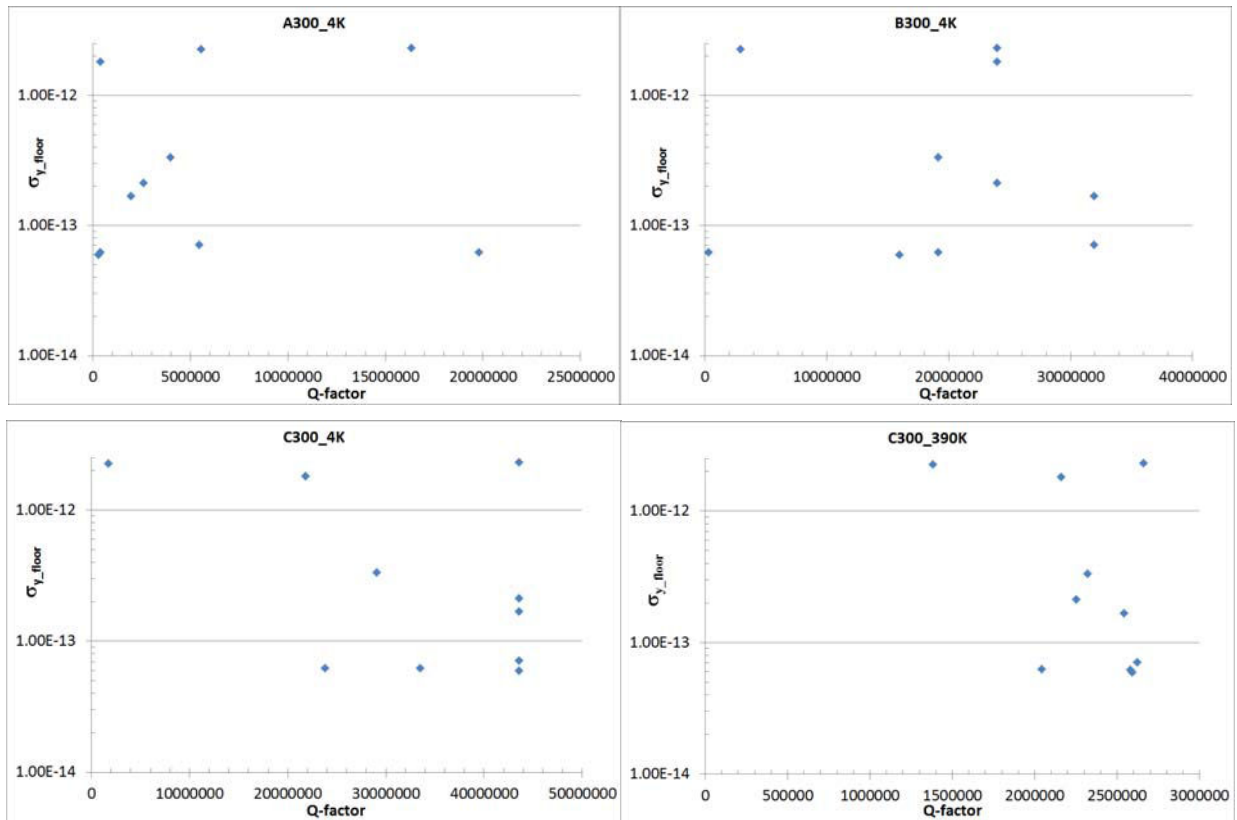


Fig.5.18: Resonator noise as a function of Q-factor of the resonators for different modes of vibration (Temperature 4K).

Results for anharmonic modes of C300 are presented in Fig.5.19. Q factors could not be measured for some of the tested resonators.

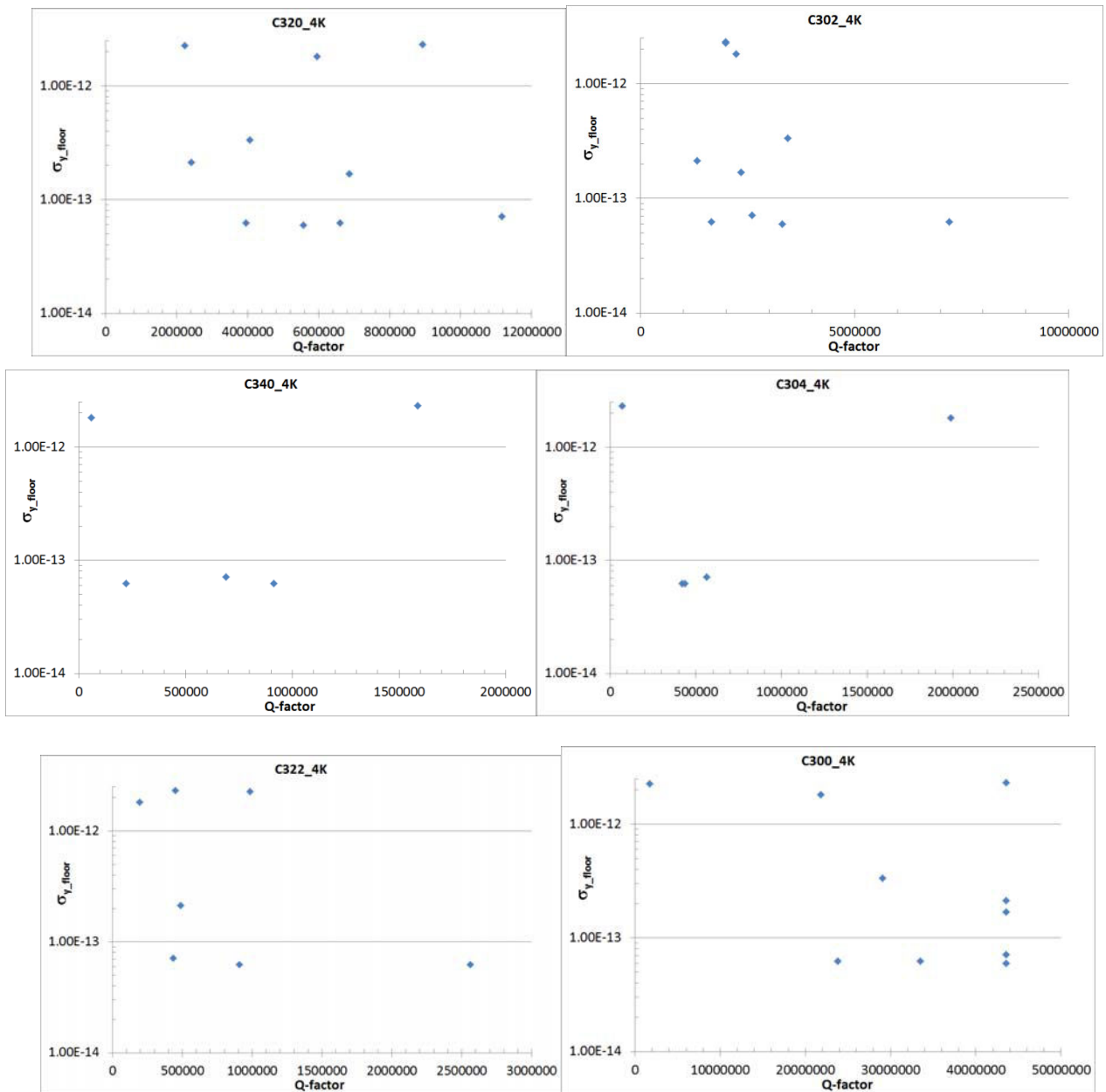


Fig.5.19: Resonator noise as a function of Q-factor of the resonators for anharmonic modes of C300 (Temperature 4K).

Fig.5.20 presents noise results according to Q-factor of overtones of C300 mode, C500 and C700.

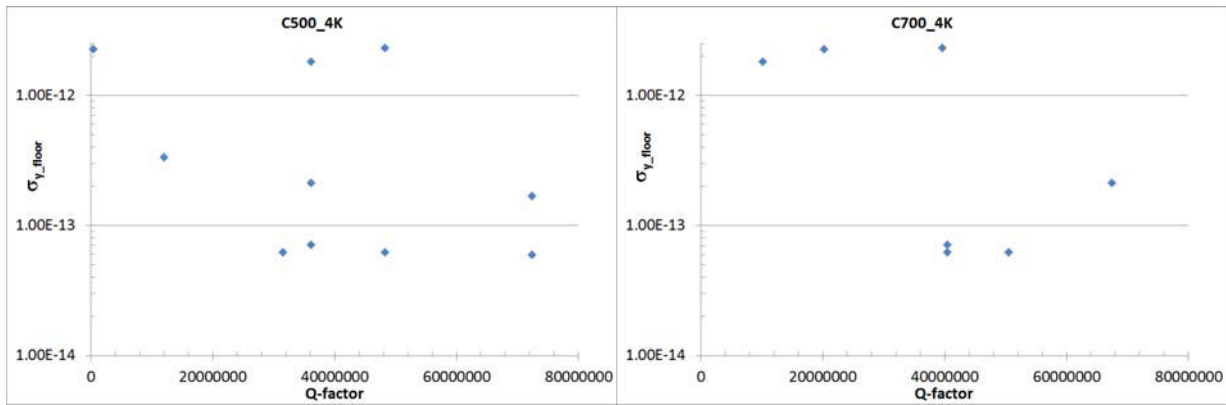


Fig.5.20: Resonator noise as a function of Q -factor of the resonators for overtone modes of C300.

Unfortunately, no clear tendency appears to give a relationship between inherent noise of resonators and behavior at low temperature which could have been related to internal defects inside the resonant volume.

4. Exploration of $1/f$ noise origin using time measurements

4.1. Time measurement setup

Resonators are put at their turnover temperature in the specific double oven of the noise measurement system. The tested resonator is driven by a synthesizer at its resonant frequency (Fig.5.21) during 2 s, by a sinusoidal signal. The excitation amplitude is limited in order to avoid the classical amplitude-frequency effect (frequency of the resonator is non-linearly dependent of the electrical power applied in the resonator). Then, the output of the synthesizer is stopped. The synchronization of the quartz signal is obtained using the TTL output of the synthesizer. High speed oscilloscope HDO6000 (courtesy of Lecroy) has been used to get the quartz signal. This kind of oscilloscope has 12 bits of vertical resolution. This vertical resolution allows 4096 voltage steps instead of traditional 256 steps for an 8 bits oscilloscope. The maximum sampling rate is 2.5 GS/s. The memory depth of this oscilloscope is 250 Mpts. In our case, the frequency of resonators is about 5 MHz. Thus the period of quartz signal is 200 ns. We store the signal during 0.5 s or 0.2 s, with a sampling rate of 2 ns and 800 ps respectively, corresponding to data files with 250 million points.

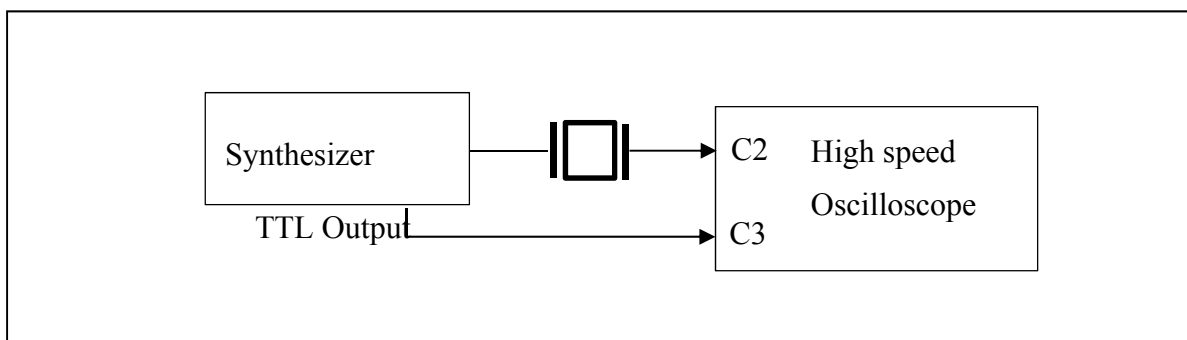


Fig.5.21: Time measurement setup [8].

Table 5.3 presents the characteristics of the tested resonators obtained with the resonator noise measurement set-up detailed in paragraph 2 above. The quality factor has the same order of magnitude for resonator *a* to *g* around $2 \cdot 10^6$. The resonator *h* has a Q factor about two times lower than the other resonators. The Allan standard deviation is below $8 \cdot 10^{-14}$ for resonator *a*, *d*, *e* and *f* and higher than 10^{-12} for resonators *b*, *g* and *h*. These resonators were chosen so as to represent at least one good and one bad resonator for each industrial provider participating in the CNES contract. The detailed origin of these resonators is hidden here due to confidentiality requirements in the contract.

Table 5.3: Resonators selected for time measurements.

<i>Resonator</i>	<i>Q</i> (10^6)	$\sigma_{y, floor}$
<i>a</i>	2.62	$7.1 \cdot 10^{-14}$
<i>b</i>	2.65	$2.3 \cdot 10^{-12}$
<i>c</i>	2.16	$1.8 \cdot 10^{-12}$
<i>d</i>	2.04	$6.3 \cdot 10^{-14}$
<i>e</i>	2.35	$6.3 \cdot 10^{-14}$
<i>f</i>	2.30	$7.8 \cdot 10^{-14}$
<i>g</i>	2.24	$1.1 \cdot 10^{-12}$
<i>h</i>	1.12	$2.3 \cdot 10^{-12}$

4.2. Results

The synchronization signal is presented in Fig.5.22a. The fall edge corresponds to the shutdown of the synthesizer output. Then, the quartz crystal vibrates freely. Fig.5.22b shows the signal obtained with the resonator *a*. The duration of the recording is 0.5 s. The sample rate is 800 ps. That corresponds to 250 samples per period. A zoom of this figure is given in Fig.5.22c. Such zoom allow to find the value of the first maximum to be provided as initial guess in latter fits.

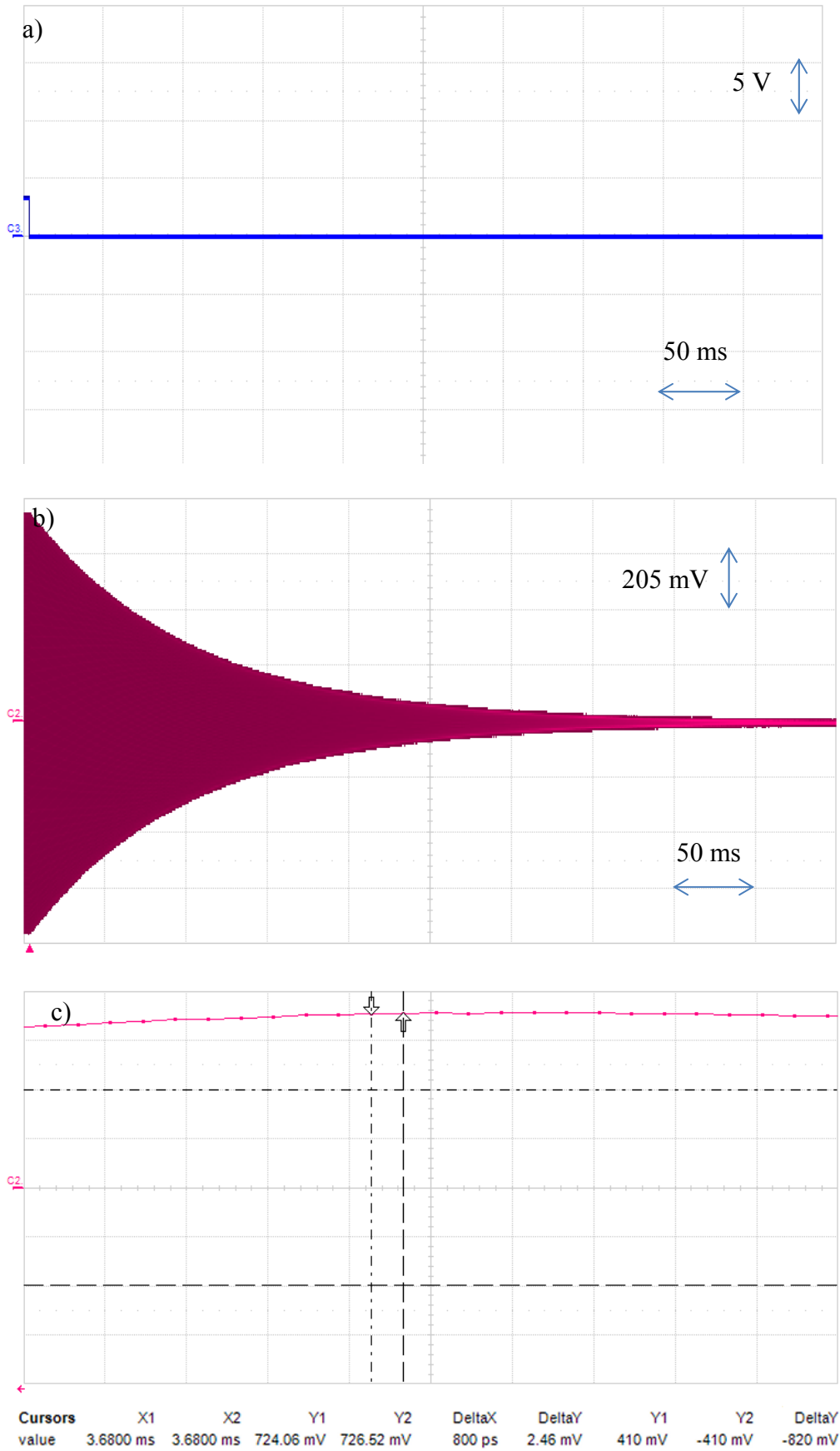


Fig.5.22: a) Synchronization signal, b) Attenuation of resonator a, c) Zoom on a maximum value of resonator a.

The result of resonator h is shown in Fig.5.23. The lower Q factor is representative of the faster attenuation of the signal.

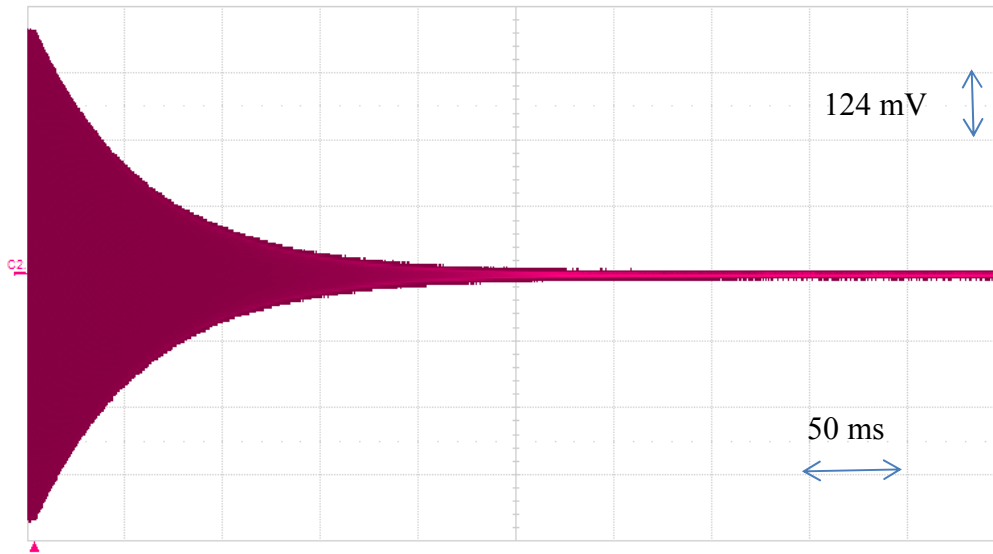


Fig.5.23: Attenuation signal of resonator h .

4.3. Mathematical treatments

The characteristic time of the exponential envelop is related to the loaded quality factor of the resonator by:

$$\tau = \frac{2Q_L}{\omega} = \frac{Q_L}{\pi f} \quad (5.4)$$

During the time measurement, the load applied on the resonator is given by the input impedance of the oscilloscope. This impedance is classically represented by a resistor of about 1 M Ω in parallel with an input capacitor which is given by Lecroy to be of the order of 15 pF. As a result, the loaded Q factors of the resonators are about 60 % of the unloaded Q. It is approximately the same working condition than in an oscillator or in the passive measurement system. A Spice-OrCAD[®] simulation is in good agreement with the time results (Table 5.4). Q_{L_th} is the computed value of the loaded Q obtained by the electrical simulation.

Table 5.4: Loaded Q -factor measured from the logarithmic decrement of weakly damped oscillations, for several very good and not so good resonators.

Res.	$Q (10^6)$	σ_{y_floor}	τ (s)	$\sigma_\tau (10^{-6} \text{ s})$	$Q_L(\tau) (10^6)$	$Q_{L_th} (10^6)$
<i>a</i>	2.62	$7.1 \cdot 10^{-14}$	0.09604	4.3	1.51	1.56
<i>b</i>	2.65	$2.3 \cdot 10^{-12}$	0.09665	3.6	1.52	1.56
<i>c</i>	2.16	$1.8 \cdot 10^{-12}$	0.09471	4.3	1.49	1.41
<i>d</i>	2.04	$6.3 \cdot 10^{-14}$	0.08248	2.6	1.30	1.39
<i>e</i>	2.35	$6.3 \cdot 10^{-14}$	0.09318	4.1	1.46	1.53
<i>f</i>	2.30	$7.8 \cdot 10^{-14}$	0.09301	3.3	1.46	1.52
<i>g</i>	2.24	$1.1 \cdot 10^{-12}$	0.08977	3.7	1.41	1.51
<i>h</i>	1.12	$2.3 \cdot 10^{-12}$	0.05599	1.3	0.88	0.92

In all the damped oscillations curves it is clear that the signal envelop exhibits the exponential decay characteristic of the underdamped oscillations of a simple harmonic oscillator with viscous damping. Hence, all the attenuation curves were fitted using the NonlinearModelFit function of Mathematica®, with the following model function ($f_0 = 5 \cdot 10^6$ Hz):

$$A_0 + A_1 \exp(-t/\tau) \sin(2\pi(f_0 - \Delta f)t + \varphi_0) \quad (5.5)$$

For practical considerations (amount of RAM), we down-sampled the 250 Mpts randomly by a factor of 10 before actually fitting the data. (25 points on average per period).

As we can see from Fig.5.24, the residuals look quite similar for these 4 resonators (randomly down-sampled by a factor 10), with quite steep variations.

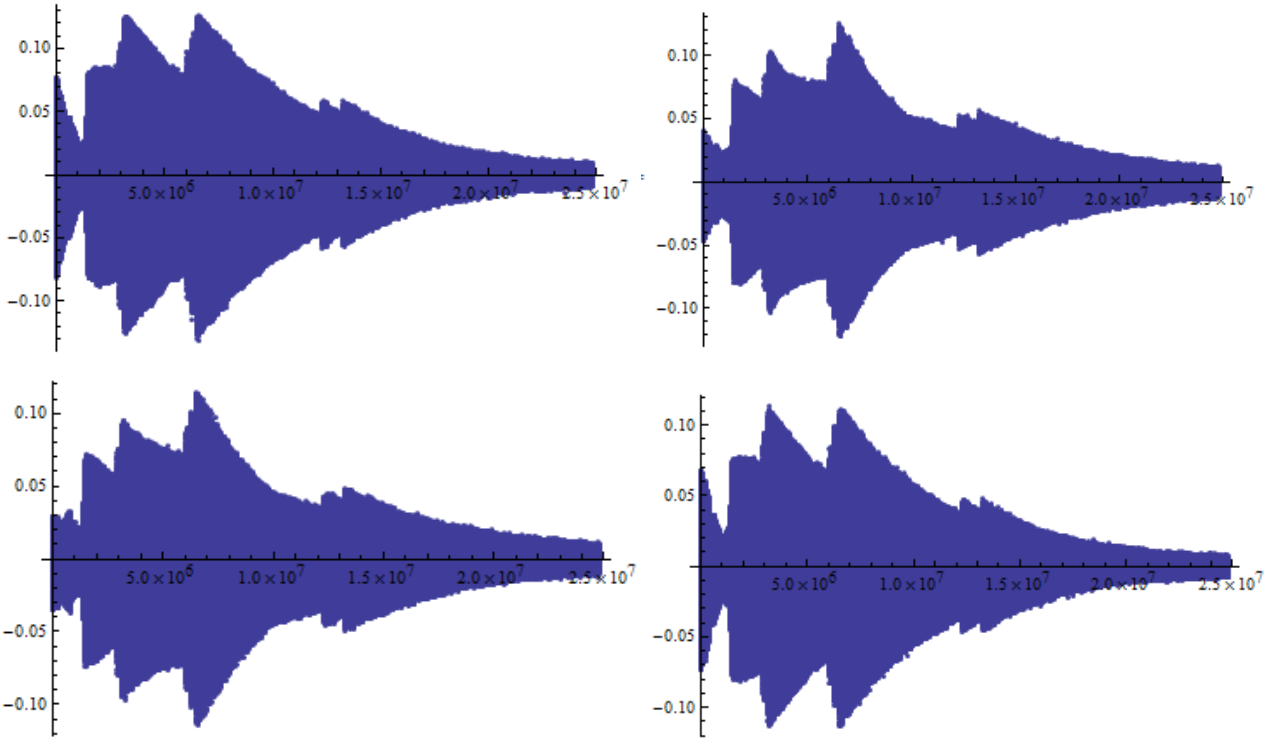


Fig.5.24: Residuals of the fit (in mV) as a function of the number of the residual for resonator *a* (top left), *b* (top right), *f* (bottom left), *g* (bottom right). The upper (or lower) envelope could be described by piecewise linear functions giving some hint at solid friction, as discussed in the conclusions.

Zooms on these variations show that there are no discontinuities but an enhanced probability for higher residuals (Fig.5.25).

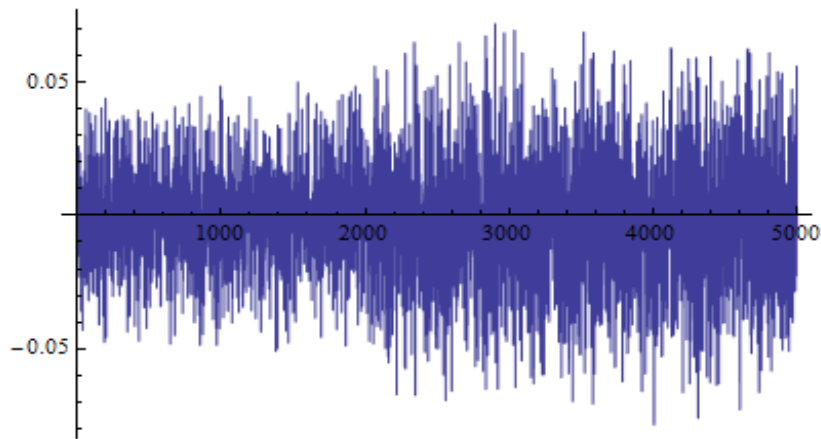


Fig.5.25: Zoom of Fig.5.24. Zoom on the residuals of the fit as a function of the number of the residual used in the figure, for resonator *f*.

Bad and good resonators (*a* and *g*, *b* and *f*) give similar shapes of the residuals that cannot authorize any distinguish between resonators.

5. Conclusions

In spite of systematic campaigns of measurements, we have not been able to find some systematic tendency in the data that would allow classifying the resonators in good and bad ones without needing to make the long measurement of the $1/f$ noise level. Correlations of the quality

with position in the original bars and with optically detected defects in these bars have not provided clear results. Cryogenic experiments do not seem to provide any additional information with respect to room temperature measurements, for this classification.

First attempts at fitting the underdamped transient oscillations of very good and bad ultra-stable oscillators by a classical exponentially damped sinusoid show residues with envelopes that can be approximated by piecewise linear functions (as can be found in the oscillations of a pendulum damped by solid friction instead of viscous friction) that could indicate the equivalent of “solid (internal) friction”. Further studies using different fitting procedures and Matlab® are under way, to assess the fact that it could be artefacts of the Plot function of Mathematica® or not.

6. References

- [1] F. Sthal, S. Galliou, J. Imbaud, X. Vacheret, P. Salzenstein, E. Rubiola, G. Cibiel, “About Quartz Crystal Resonator Noise: Recent Study”, Proc. ICNF, Pisa, Italie, 15-19 June, pp. 607-610, (2009).
- [2] F. Sthal, J. Imbaud, S. Ghosh, M. Devel, C. Vuillemin, P. Abbe, A. Bakir, N. Cholley, D. Vernier, G. Cibiel, “Noise of quartz resonators according to their origin in the mother crystal”, 22nd International Conference on Noise and Fluctuations (ICNF), 24-28 June 2013.
- [3] S. Ghosh, F. Sthal, J. Imbaud, M. Devel, R. Bourquin, C. Vuillemin, A. Bakir, N. Cholley, P. Abbe, D. Vernier, G. Cibiel, “Theoretical and experimental investigations on $1/f$ noise of quartz crystal resonators”, Proc. IEEE Joint UFFC, EFTF and PFM Symp., Prague, Czech Republic, 21-25 July, pp. 737-740, 2013.
- [4] D.S. Stevens, H.F. Tiersten, “An analysis of doubly rotated quartz resonators utilizing essentially thickness modes with transverse variation”, J.A.S.A., vol. 79, no. 6, pp. 1811-1826, 1986.
- [5] J. Imbaud, J.J. Boy, J.P. Romand, J. Frayret, D. Picchedda, G. Cibiel and F. Sthal, “Analyses of very high-Q quartz crystal aimed to high quality 5 MHz resonators achievement”, 24th European Frequency and Time Forum, Noordwijk, NL, 13-16 April, 01_03_Imbaud.pdf, 2010.
- [6] F. Sthal, J. Imbaud, X. Vacheret, P. Salzenstein, G. Cibiel, S. Galliou, “Computation method for the short-term stability of quartz crystal resonators obtained from passive phase noise measures”, IEEE Transactions on Ultrasonics, Ferroelectrics and Frequency Control, vol. 60, no. 7, pp. 1530-1532, 2013.
- [7] IEEE, “IEEE Standard Definitions of Physical Quantities for Fundamental Frequency and Time Metrology - Random Instabilities”, in IEEE STD 1139-2008: IEEE, pp. 1-35, 2008.
- [8] S. Ghosh, F. Sthal, M. Devel, G. Cabodevila, J. Imbaud, R. Bourquin, P. Abbe, A. Bakir, D. Vernier, G. Cibiel, “Exploration of $1/f$ noise origin using time measurements”, European Frequency and Time Forum, Neuchâtel, Switzerland, 23-26 June, 2014.
- [9] A. W. Warner, “Ultra-precise quartz crystal frequency standards”, IRE Transactions on Instrumentation, IEEE, vol. 1-7, no. 3, 1958.
- [10] N. Smagin, “Résonateur à quartz d’une qualité d’environ $120 \cdot 10^6$ à 2K”, Izmeritel Tekh SSR no. 9, 1960.
- [11] J.-J. Gagnepain, “Mécanismes non-linéaires dans les résonateurs à quartz”, PHD Thesis, Université de Franche-Comté (UFC), France, Mars 1972.

- [12] G. Mossuz, “Etude et réalisation d’un oscillateur à quartz à très basse température”, PHD Thesis, Université de Franche-Comté (UFC), France, Juillet 1975.
- [13] G. Robichon, J. Gros Lambert, J.-J. Gagnepain, “Frequency stability of quartz crystal at very low temperature: preliminary results”, Proc. 38th IEEE Freq. Contr. Symp., pp. 201-205, 1984.
- [14] A. El Habti, “Etude de résonateur et d’oscillateurs à quartz à très basse températures”, PHD Thesis, Université de Franche-Comté (UFC), France, Janvier 1993.
- [15] J. Imbaud, “Evaluation des potentialités des matériaux du type langasite pour la réalisation d’oscillateurs ultra-stables. Etude et réalisation préliminaires d’un oscillateur cryogénique”, PHD thesis, Université de Franche-Comté (UFC), France, Nov. 2008.
- [16] M. Goryachev, “Résonateurs à ondes acoustiques et oscillateurs à température de l’hélium liquide”, PHD thesis, Université de Franche-Comté (UFC), France, Nov. 2011.

Conclusion and perspectives:

Conclusion

This work is one more step in the quest of a usable model for $1/f$ noise origin in bulk acoustic wave resonators. The general overview of piezoelectricity, basic crystallography of alpha quartz, defects of quartz crystal, different types of crystal cuts, quartz crystal resonators and oscillators with their time and frequency definitions, given in chapter 1, shows the difficulties and the large knowledge necessary to enter in this research domain.

Due to the existence of a very large bibliography, the background research on $1/f$ noise, presented in the second chapter, is focused on the different theories and the models of $1/f$ noise that could be applicable to quartz crystal resonators. It can be observed that this topic has remained active for the last 80 years. One of the two well-known model that provide a prediction for the amplitude of $1/f$ noise in quartz crystal resonators, proposed by Michel Planat, is studied in detail and shows its limits in terms of order of magnitude comparing with experimental results. However, we think we traced the origin of the problem in the use of the classical density of vibration modes in Planat's model. Thus, the modes corresponding to frequencies of the type nf with n integer are counted both in the partition function and in the density of modes. Using an adapted density of modes with only the lowest frequency in each direction may avoid this double counting and lower the theoretical limit for the spectral power density of noise, but the $1/f$ behavior could disappear. Since, in our opinion, this is very likely, we did not attempt to find such an adapted density of modes.

The third chapter presents the other model providing a prediction for the amplitude of $1/f$ noise in quartz crystal resonators, namely Handel's theory of quantum $1/f$ noise. P. H. Handel has been continuously improving a universal theory of $1/f$ noise since 1975. He has tried to implement his theory in electrical, electronic and frequency control systems and has published numerous papers on this topic, with successes concerning the optimization of several electronic devices. Somehow, his theory explains the origin of $1/f$ noise in many areas of engineering and physics. Although criticized by many, Handel's quantum model for $1/f$ noise remains the only model giving a quantitative estimation of the level of intrinsic $1/f$ noise in quartz crystal resonators that is compatible with the best experimental results. During this work, we reconsidered the volume dependence in this model. We first argue that an acoustic volume, representing the volume in which the vibration energy is trapped, should be used instead of the geometrical volume between the electrodes. Then, we show that because there is an implicit dependence of the quality factor of the resonator with its thickness, the net effect of Handel's formula is not an increase of noise

proportionally to the thickness of the resonator, as could be naïvely expected, but a net decrease when thickness increases. Finally, we show that a plot of $Q^4 S_y$ versus the acoustic volume, instead of the usual S_y plot, could be useful to compare the quality of acoustic resonators having very different resonance frequencies. Nevertheless, in spite of a careful inspections of Handel's derivations of his formula (semi-classical or quantum), there are some points in Handel's theory which remains difficult to understand for us, especially as concerns the connection between Bremsstrahlung radiation by electron, the loss of a vibration quanta from the main mode and the polarization of the material, which are specific to quartz devices. Indeed, some numerical values used in Handel's formula of sensitivity limit for the betterment of the short term stability, seem hard for us to justify since the physical meaning and/or definition of the corresponding quantity is not clear. Attempts to correct the numerical values of the parameters to obtain a more accurate value of the sensitivity limit in Handel's theory have been done, with a limited success in spite of our using some molecular dynamics simulations to try to give a clear interpretation and numerical value to the average frequency used by P. H. Handel. However, the physical picture of $1/f$ noise coming from loss of a quanta from the main mode at random uncorrelated times and locations still seems appealing.

The 4th chapter investigates the origin of $1/f$ noise by adding an internal friction term to the classical equation of motion (already including viscoelastic damping), for the thickness oscillations of the quartz resonator. If this term is frequency independent and linear in the vibration amplitude, the fluctuation dissipation theorem allows us to recover a $1/f$ power spectrum for the frequency fluctuations. There are many possible reasons behind the physical origin of internal friction coefficient such as anelasticity, hysteretic dislocation motion or maybe motion of kinks along the dislocation, and many other physical aspects can be taken into account. However, it is not so evident to get a term frequency independent and linear in the vibration amplitude in the small frequencies limit. The possibility to explain this internal friction coefficient through the hysteretic dislocation motion thanks to modified Koehler-Granato-Lücke theory has been explored, but numerical applications seem to show that it is still not the dominant mechanism in our quartz resonators.

The 5th chapter is devoted to the presentation of experimental results achieved in parallel to the previously exposed theoretical studies. Numerous specific resonators, provided by industrial partners, have been measured and compared by the passive noise measurement technique. For this program, quartz crystal resonators have been cut from a quartz crystal block supplied specifically for this study on $1/f$ noise. The results, in terms of noise level, span approximately two orders of magnitude but the best ones are almost at the state of the art, thus increasing considerably our stock

of excellent resonators. The best items have a short-term stability (Flicker floor) below $8 \cdot 10^{-14}$, whereas the worst are above 10^{-12} . Although the positions of the resonators have been followed, no clear correlation between the noise results and the blanks positions in the mother crystal block has been put in evidence. To understand the dispersion of these noise results, some investigation of Q-factor at cryogenic temperature is proposed in order to correlate it with the measured noise. First results show that no clear tendency appears to give a relationship between inherent noise of resonators and behavior at low temperature which could be related to internal defects inside the resonant volume. Another way has been explored during this work: The possibility of finding the $1/f$ noise by high speed time measurements of the weakly damped free oscillations. The results are not so easy to extract due to the big number of data and still need work.

We hope to have shown that this work gives answers to several points evocated in the past but also brings some new interesting questions.

Perspectives

At the beginning of this work, investigations of other quartz homeotypic materials (for example: Languasite, langatate, gallium orthophosphate, *cf.* chapter 1) were envisaged. However, up to now, it is difficult to find enough ultra-stable resonators made in this other materials to make systematic studies at a level of noise that can compete with those obtained for quartz resonators. Nonetheless, they can have an important role in the near future to produce high quality crystal resonators that could work at temperature much higher than the quartz resonators. These materials have a more complex crystallography than quartz and will be very interesting to study in order to extend the models proposed in this work. Moreover, the molecular dynamics simulations could be very useful to have a better understanding of these materials (none have been published up to now), especially to go further with Handel's model.

The research on the investigations of the origin of $1/f$ noise is difficult because, owing to the very low level of noise reached, usual approximations always have to be questioned and sometimes rejected. A lot of new developments of this kind can be found in the papers concerning gravitational wave detectors such as VIRGO or LIGO, which could serve as inspiration for our studies. Furthermore, there are many mathematical models able to give rise to a $1/f^\alpha$ power spectrum (less for a pure $1/f$ spectrum), but finding how they could be restated in terms of physical processes taking place in the quartz resonators is not evident. Nonetheless, there are some promising research

lines that can be proposed for future research on the dominant origin of $1/f$ noise for BAW quartz crystal resonators:

- 1) Study of phonon generation and energy localization for quartz crystal resonators by calculating the quantum mechanical energy of the radiated phonon created by moving edge dislocations [1].
- 2) A collaboration with Pr. Moncef (University of Monastir, Tunisia) has been started to try to parameterize efficient potential energy functions for molecular dynamics studies of quartz homeotypic materials such as GaPO₄ or some members of the langasite family.
- 3) The nucleation of kink-antikink pairs along dislocations are thermally activated with possibly several different activation energies. This could lead to $1/f$ noise by the mechanism studied in paragraph 1 of chapter 2. Maybe this could be studied taking inspiration from works by Fabio Marchesoni and his collaborators (see e.g. [2]).
- 4) Some studies using a limited amount of radiation to increase slightly the amount of point defects in quartz could be attempted to control whether their hardening influence could be interpreted by the modified Koehler-Granato-Lucke theory of Swartz and Weertman [4] or possibly more recent theories on this subject.
- 5) The two tests proposed by Niemann et al. could be done on our data to assess whether the proposed power-law intermittency model developed in their paper could apply to the noise data from our resonators.
- 6) The exploitation of the residuals of the fits by a classical exponentially damped sinusoid, (or a better function to be developed) of the free weakly damped oscillations of the resonators shall be finished in order to try to find some characteristics of these residuals that would help classify the quality of the resonators without having to make the full passive noise measurements.

On the experimental side, in parallel to this work, an important set of resonators have been built during these three years by the very best industrial specialists. A study of each resonator by a reverse engineering process could give lots of information. X-ray and optical observations can be done to localize and quantify internal defects inside the resonators. The comparison between resonators with different noise results in spite of the same design would be very useful not only for understanding the physical origin of $1/f$ noise, but also improve fabrication yields or at least to find faster and earlier ways to classify the best, good and bad resonators and oscillators during production.

P. H. Handel explored many kinds of systems with his quantum $1/f$ theory, some with success. The physical ideas behind his theory should be retained to investigate more resonators using vibration as the “heart of signal”. For example, micromechanical resonators (MEMS) or even nanomechanical resonators (NEMS)⁶⁹ have a recent and interesting development in the time and frequency domain. These resonators will provide a large range of different frequencies (from 100 kHz to almost 5 GHz) and a lot of different structures. This is very exciting for future studies trying to bring these devices to their intrinsic noise limits.

References

- [1] C.S. Coffey, “Phonon generation and energy localization by moving edge dislocations”, *Physical Review B*, Vol. 24, No. 12, pp. 6984-6990, 1981.
- [2] F. Marchesoni, “Internal friction by pinned dislocations: theory of the Bordoni peak”, *Phys. Rev. Lett.*, vol. 74, no. 15, pp. 2973-2976, 1995.
- [3] M. Niemann, H. Kantz, and E. Barkai, “Fluctuations of $1/f$ noise and the low-frequency cutoff paradox”, *Phys. Rev. Lett.*, vol. 110, no. 14, pp. 140603, 5 pages, 2013.
- [4] J. C. Swartz and J. Weertman, “Modification of Koehler-Granato-Lucke damping theory”, *J.Appl.Phys*, vol. 32, no. 10, pp. 1860-1865, 1961.

⁶⁹ For example, the most sensitive mass measurement (resolution of the order of the mass of a single proton or hydrogen atom!!!) was obtained by studying the change of oscillation frequencies of a clamped-clamped carbon nanotube in the team of Adrian Bachtold (see e.g. J. chaste et al., *Nature Nanotechnology*, vol. 7, pp. 301–304, 2012).

Résumé

Depuis quelques décennies, la technologie de contrôle de la fréquence a été au cœur de l'électronique des temps modernes grâce à son vaste domaine d'applications dans les systèmes de communication, les ordinateurs, les systèmes de navigation ou de défense militaire. Les dispositifs temps-fréquence fournissent des stabilités de fréquence et des puretés spectrales élevées dans le domaine de la stabilité court-terme. L'amélioration de la performance de ces dispositifs reste un grand défi pour les chercheurs. La réduction du bruit afin d'augmenter cette stabilité court-terme et d'éviter les commutations non souhaitées entre les canaux est donc très souhaitable. Il est communément admis que la limitation fondamentale à cette stabilité court-terme est due au bruit flicker de fréquence des résonateurs. Dans ce manuscrit, un premier chapitre rappelle quelques faits de base sur l'acoustique, la cristallographie et les définitions du domaine temps-fréquence nécessaires à l'étude des résonateurs et oscillateurs ultra-stables. Le deuxième chapitre est consacré à un résumé de la littérature sur le bruit de fréquence en $1/f$. Ensuite, le troisième chapitre concerne nos études sur le modèle quantique de bruit en $1/f$ du Pr. Handel, qui, bien que critiqué par beaucoup, est encore le seul qui fournit une estimation de l'amplitude de plancher de bruit en $1/f$ et qui n'est pas infirmé par les données expérimentales. Dans le quatrième chapitre, une autre approche, basée sur le théorème de fluctuation-dissipation, est utilisée afin de mettre des contraintes numériques sur un modèle de bruit en $1/f$ causé par une dissipation interne (ou de structure) proportionnelle à l'amplitude, et non à la vitesse. Le dernier chapitre est consacré aux résultats expérimentaux. Le design et les paramètres du résonateur ultra-stable utilisé lors de cette étude sont décrits. Les mesures de bruit de phase sur plusieurs lots de résonateurs sont données. Les mesures des paramètres de résonateur ont été effectuées à basse température afin de les corrélérer avec les résultats de bruit. Afin d'évaluer rapidement la qualité des différents résonateurs, une autre approche dans le domaine temporel a été testée. Elle utilise des oscillations pseudo-périodiques transitoires mettant les oscilloscopes numériques actuellement disponibles à leurs limites de capacité. Enfin, les conclusions et perspectives sont présentées.

Mots-clés : bruit $1/f$, résonateurs acoustiques, quartz, bruit de phase, mesures passives, théorème de fluctuation-dissipation; stabilité court-terme.

Summary

Since a few decades, frequency control technology has been at the heart of modern day electronics due to its huge area of applications in communication systems, computers, navigation systems or military defense. Frequency control devices provide high frequency stabilities and spectral purities in the short term domain. However, improvement of the performance of these devices, in terms of frequency stability, remains a big challenge for researchers. Reducing noise in order to increase the short term stability and avoid unwanted switching between channels is thus very desirable. It is commonly admitted that the fundamental limitation to this short-term stability is due to flicker frequency noise in the resonators. In this manuscript, a first chapter recalls some basic facts about acoustic, crystallography and definitions of time and frequency domain needed to explore ultra-stable resonators and oscillators. The second chapter is devoted to a summary of the literature on flicker frequency noise. Then, the third chapter concerns our studies on Handel's quantum $1/f$ noise model, which although criticized by many, is still the only one that provides an estimation of the floor amplitude of $1/f$ noise that is not invalidated by experimental data. In the fourth chapter, another approach, based on the fluctuation-dissipation theorem, is used in order to put numerical constraints on a model of $1/f$ noise caused by an internal (or structural) dissipation proportional to the amplitude and not to the speed. The last chapter is devoted to experimental results. An ultra-stable resonator used during this study is described. Phase noise measurements on several batches of resonators are given. Measurements of resonator parameters have been done at low temperature in order to correlate them with noise results. Another approach with a procedure that use transient pseudo periodic oscillations and put to their limits the capacities of presently available digital oscilloscopes, is presented, in order to assess rapidly the quality of various resonators. Finally, conclusions and perspectives are given.

Keywords: $1/f$ noise, acoustic resonators, quartz crystal, phase noise, passive measurements, fluctuation-dissipation theorem; short-term stability.

The logo for SPIM (École doctorale SPIM) features the letters 'S', 'P', 'I', and 'M' in a stylized, white, sans-serif font. The 'S' is the largest and most prominent, followed by 'P', 'I', and 'M' in descending order of size. A yellow horizontal bar is positioned to the left of the 'S'.